

Stony Brook University



OFFICIAL COPY

The official electronic file of this thesis or dissertation is maintained by the University Libraries on behalf of The Graduate School at Stony Brook University.

© All Rights Reserved by Author.

**Development of Selective Inhibitors
of the Mammalian Target of Rapamycin**

A Dissertation Presented

by

Jun Yong Choi

to

The Graduate School

in Partial Fulfillment of the

Requirements

for the Degree of

Doctor of Philosophy

in

Chemistry

Stony Brook University

May 2009

Copyright by

Jun Yong Choi

2009

Stony Brook University

The Graduate School

Jun Yong Choi

We, the dissertation committee for the above candidate for the
Doctor of Philosophy degree, hereby recommend
acceptance of this dissertation.

Dale G. Drueckhammer, Professor of Chemistry - Dissertation Advisor

Richard Z. Lin, Professor of Medicine - Dissertation Co-advisor

Nancy S. Goroff, Associate Professor of Chemistry - Chairperson of Defense

Iwao Ojima, Distinguished Professor of Chemistry - 3rd member of Defense

Lisa M. Ballou, Research Assistant Professor - Outside member
of Medicine

This dissertation is accepted by the Graduate School

Lawrence Martin
Dean of the Graduate School

Abstract of the Dissertation

**Development of Selective Inhibitors
of the Mammalian Target of Rapamycin**

by

Jun Yong Choi

Doctor of Philosophy

in

Chemistry

Stony Brook University

2009

The mammalian target of rapamycin (mTOR) is a Ser/Thr protein kinase that regulates cell proliferation, size, and survival. Signaling through mTOR is hyperactivated in many human cancers and thus is an attractive target for cancer treatment. Rapamycin and its analogs selectively inhibit mTOR function and are under clinical development as anti-cancer agents.

mTOR exists in the cell as two distinct multiprotein complexes called mTORC1 and mTORC2. Rapamycin and its analogs bind to a domain of mTOR distinct from the kinase domain to block mTORC1 function, but do not affect the activity of mTORC2. Evidence indicates that compounds that inhibit both forms of mTOR, as might be achieved by directly targeting the kinase domain, should have better anticancer activity than rapamycin and its analogs.

The kinase domain of mTOR is highly homologous to the phosphatidyl inositol 3-kinases (PI3Ks) and related protein kinases. Many PI3K inhibitors are known, and most also inhibit mTOR. Two such compounds LY294002 and PI103 were used in this project as lead compounds for the development of inhibitors targeting mTOR. As the 3-D structure of mTOR has not been solved, homology modeling was performed based on a known PI3K structure to predict modifications to LY294002 to increase potency and selectivity toward mTOR. Two regions of the LY294002 structure were identified for variation, one in the region of a unique cysteine in the active site of mTOR and the other in the region of a Trp to Lys change in mTOR vs. PI3K that provides additional space in the active site for expansion of the inhibitor. A series of inhibitors have been prepared modified in each of these regions. The results of inhibition studies support the predictions based on homology modeling.

Flexible alignment of PI103 and LY294002 was used to predict the binding mode of PI103 to mTOR. Based on this alignment and the homology model, areas of PI103 were chosen for modification to increase activity toward mTOR. Compounds have been prepared and are awaiting testing. A pharmacophore model was developed based on known PI3K inhibitors and was used for virtual screening of databases of available compounds. Selected compounds have been tested as inhibitors of PI3K, resulting in the identification of new types of inhibitors of this class of enzymes. These compounds may serve as new leads for the development of more potent and selective inhibitors of mTOR.

Dedicate to my wife, Young-Ui,

daughter, Athena,

son, Ethan,

Mom, Dad and in-laws

Table of contents

List of Symbols.....	ix
List of Figures.....	xii
List of Tables.....	xv
List of Schemes.....	xvi
Chapter 1. Introduction.....	1
1.1 Mammalian target of rapamycin (mTOR).....	1
1.2 Phosphatidyl inositol 3 kinase (PI3Kinase).....	3
1.3 Hypothesis and purpose.....	4
1.4 The mTOR-involved signaling pathway.....	7
1.4.1 mTOR Complex 1 and Complex 2.....	7
1.4.2 The TSC1-TSC2 complex.....	12
1.4.3 S6 Kinase (S6K).....	17
1.4.4 Eukaryotic initiation factor 4E binding protein (4E-BP).....	22
1.5 mTOR as a drug target for many diseases.....	24
1.5.1 Human genetic diseases related to mTOR.....	24
1.5.2 Cancers related to mTOR signaling.....	26
1.5.3 Other diseases related to mTOR signaling.....	27
1.6 Computer aided molecular design.....	29
1.6.1 Homology modeling.....	30
1.6.2 Flexible alignment.....	35
1.6.3 Virtual screening and pharmacophore searching.....	37

Chapter 2.	Defining a lead compound and its biological effects on mTOR	
	signaling	43
2.1	LY294002 analogs.....	43
2.2	A selective inhibitor, C401	48
2.3	Effect of C401 on mTOR and PI3K activities <i>in vitro</i>	52
2.4	Effect of C401 on mTOR signaling in cancer cells.....	56
2.5	Computational and experimental details.....	61
Chapter 3.	Design, synthesis, and bioassay of selective inhibitors toward mTOR ...	72
3.1	Homology modeling and strategies.....	72
3.1.1	Sequence alignment and template refinement.....	72
3.1.2	Homology modeling.....	74
3.1.3	Strategies for the design of selective inhibitors.....	78
3.2	Chemical probes based on C401 for the selective inhibition of mTOR.....	80
3.2.1	Synthesis of potential inhibitors exploring the Trp to Lys mutation in mTOR.....	80
3.2.2	Enzyme inhibition assays of C-9 modified analogs.....	82
3.2.3	Synthesis of potential inhibitors targeting Cys2243 of mTOR.....	84
3.2.4	Enzyme inhibition assays of morpholine modified analogs.....	87
3.2.5	Synthesis and bioassay of enantiomerically pure compounds.....	89
3.3	Modification of other non-selective inhibitors of mTOR to increase selectivity.....	91

3.3.1	Flexible alignment.....	91
3.3.2	Redesign of non-selective inhibitors.....	94
3.3.3	Synthesis of redesigned inhibitors.....	95
3.3.4	Bioassay of redesigned inhibitors.....	98
3.4	Computational and experimental details.....	100
Chapter 4.	Generating novel lead compounds.....	129
4.1	SAR data-inspired approach.....	129
4.1.1	Design of novel lead compounds.....	140
4.1.2	Synthesis of designed lead compounds.....	142
4.2	Virtual database screening approach.....	145
4.2.1	Pharmacophore searching.....	145
4.2.2	Bioassay of hits.....	150
4.2.3	Further strategies with hits from virtual screening.....	153
4.3	Computational and experimental details.....	156
	References.....	166
	Appendix 1.....	186
	Appendix 2.....	197
	Appendix 3.....	198
	Appendix 4.....	199

List of Abbreviations

4E-BP1	Eukaryotic initiation factor 4E binding protein 1
AcOH	acetic acid
ADP	adenosine diphosphate
ATM	ataxia-telangiectasia mutated protein kinase
ATP	adenosine triphosphate
ATR	ATM- and Rad3-related protein kinase
B3LYP	Becke 3 parameter hybrid functions and Lee, Yang, and Parr correlation functions
Bn	benzyl
DBU	1,8-diazabicyclo[5,4,0]undec-7-ene
DFT	density functional theory
DMF	dimethyl formamide
DMSO	dimethylsulfoxide
DNA-PK	DNA dependent protein kinase
ESP	electrostatic potential
GST	glutathione-S-transferase
MMFF	merck molecular force field
MOE	molecular operation environment
MsCl	methanesulfonyl chloride
mTOR	mammalian target of rapamycin

mTORC1	mTOR complex 1
mTORC2	mTOR complex 2
NaOAc	sodium acetate
nBuLi	n-butyl lithium
PARP	poly (ADP-ribose) polymerase
PDB	protein data bank
PDGF	platelet-derived growth factor
PDK1	phosphoinositide-dependent kinase 1
Ph	phenyl
PI3K	phosphatidyl inositol 3-kinase
PIKK	phosphatidylinositol kinase related kinase
PIP2	phosphatidylinositol (3,4) biphosphate
PIP3	phosphatidylinositol (3,4,5) triphosphate
Red-Al	sodium bis(2-methoxyethoxy)aluminum hydride
RHF	restricted Hartree Fock
S6K	ribosomal protein S6 kinase
SAR	structure activity relationship
t-AmOH	tert-amyl alcohol
TEA, NEt ₃	triethylamine
THF	tetrahydrofuran
TLC	thin layer chromatography
TMEDA	tetramethylethylenediamine

TS transition state

TSC tuberous sclerosis complex

ZINC ZINC is not commercial; a free database of commercially available
compounds for virtual screening

List of Figures

- Figure 1.1** The structures of rapamycin, LY294002, C401, and PI103
- Figure 1.2** The schematic domain structure of mTOR
- Figure 1.3** Overview of PI3K/mTOR-mediated signaling pathway
- Figure 1.4** Schematic components in mTOR complex
- Figure 1.5** Schematic of the TSC1 and TSC2 proteins
- Figure 1.6** Two plausible mechanisms of controlling mTORC1 activity through TSC1-TSC2 and Rheb
- Figure 1.7** Upstream signaling pathways regulate the TSC1-TSC2 complex
- Figure 1.8** Schematic representations of S6K1 and S6K2
- Figure 1.9** The proposed model for the process of translation initiation through mTORC1, S6K1, and eIFs
- Figure 1.10** Schematic representation of 4E-BP1
- Figure 2.1** The initially proposed compounds to explore the effects of a morpholine ring, imidazole, pyridine, acyclic functional groups, and carbonyl oxygen of chromone ring toward mTOR
- Figure 2.2** The major interactions of LY294002 in the active site of PI3K γ
- Figure 2.3** Electrostatic potential (up) and ESP charges (down) of compounds **II** (left) and **III** (right)
- Figure 2.4** Effect of **C401** on mTOR activities *in vitro*
- Figure 2.5** Effect of **C401** and LY294002 on PI3Kinase activities *in vitro*
- Figure 2.6** Effect of **C401** and LY294002 on autophosphorylation of the p85 α subunit of p110 α /p85 α
- Figure 2.7** Effect of **C401** on mTOR signaling in Rat-1 cells
- Figure 2.8** Effect of **C401** on mTOR signaling in M059J glioblastoma cells
- Figure 2.9** Effect of **C401** on the proliferation of TSC1-/- MEFs
- Figure 2.10** Effect of **C401** on the cytoplasmic nucleosome level, or apoptosis
- Figure 3.1** Multiple sequence alignment of protein enzymes in PIKK family

- Figure 3.2** Comparison of homology model of p110 α (in blue) with its recently solved X-ray structure (in red)
- Figure 3.3** Active site residues (tube structure) and LY294002 (space filling model) in the kinase domains of PI3K γ (left) and mTOR (right)
- Figure 3.4** Strategies for the design of selective inhibitors
- Figure 3.5** The design of selective inhibitors by modifying the lead compound
- Figure 3.6** The %enzyme activities of mTOR (left) after treating with 1 μ M concentration and of PI3Kinase (right) after treating with 25 μ M concentration of **C303**, **C309**, and **C321**
- Figure 3.7** The % enzyme activity of mTOR at 0.1 μ M and 1 μ M **C401** (blue bar) and **C413** (red bar)
- Figure 3.8** The result of 'Flexible Alignment' of PI103 (tube structure) toward LY294002 (line)
- Figure 3.9** The schematic overview of interactions between the ammonium group of Lys833 and the phenolic oxygen (left) and the chromone oxygen (right)
- Figure 3.10** The redesigned compounds based on previous knowledge and the result of flexible alignment
- Figure 3.11** The % enzyme activity of PI3Kinase and mTOR at 0.1 μ M **C601** and **C701**
- Figure 4.1** Core ring fragments used in the development of PI103 by Hayakawa *et al.*
- Figure 4.2** Optimized geometries of **4.2_1**, **4.2_2**, **4.2_3**, **4.2_6** by DFT calculation
- Figure 4.3** Electrostatic potentials of **4.2** in Table 4.1
- Figure 4.4** Optimized geometries of **4.1_1** and **4.1_3** by DFT calculation
- Figure 4.5** Designed compounds **C802**, **C803**, and **C901**
- Figure 4.6** The flowchart of pharmacophore searching
- Figure 4.7** The loose query
- Figure 4.8** The structure of compound B and the refined tight query
- Figure 4.9** Hits from the pharmacophore search of the ZINC compound library
- Figure 4.10** % inhibition of mTOR at 10 μ M
- Figure 4.11** % inhibition of PI3K α at 10 μ M

Figure 4.12 Overlap of **Hit_5** with the pharmacophore query

List of Tables

Table 1.1	Comparison of mTORC1 and mTORC2
Table 2.1	Bioassay of four DNA-PK inhibitors against enzymes in the PIKK family
Table 2.2	Inhibition of protein kinases by C401
Table 4.1	Inhibition of p110 α by tricyclic derivatives
Table 4.2	The free energies of activation between R and P conformers of compounds in Table 4.1
Table 4.3	Inhibition of p110 α by 4-morpholine-4-yl-2-phenyl-quinazolines
Table 4.4	The free energies of activation between R and P conformers of compounds 4.1_1 and 4.1_3

List of Schemes

- Scheme 2.1** Synthesis of 2-methylthio-chromone (**2.3**)
- Scheme 2.2** Acid catalyzed addition-elimination reaction for attaching various amine groups
- Scheme 2.3** Based catalyzed addition-elimination reaction for attaching imidazole and 2-methyl imidazole groups
- Scheme 2.4** Metal-exchange of 3-bromopyridine by nBuLi to attach to the 2-position of chromone ring
- Scheme 2.5** Synthesis of **C201**
- Scheme 2.6** Synthesis of **C401**
- Scheme 3.1** Synthetic plan for chemical probes targeting Trp of PI3Kinase
- Scheme 3.2** Synthesis of chemical probes targeting Trp of PI3Kinase
- Scheme 3.3** Synthetic plan for chemical probes targeting Cys of mTOR
- Scheme 3.4** Synthesis of morpholine modified analogs
- Scheme 3.5** Synthesis of morpholine modified analogs
- Scheme 3.6** Synthesis of enantiomerically pure compounds
- Scheme 3.7** Synthetic plan for the syntheses of **C601** and **C701**
- Scheme 3.8** Synthesis of **C601**
- Scheme 3.9** Synthesis of **C701**
- Scheme 4.1** Synthesis of **C801** and **C802**
- Scheme 4.2** Synthesis of **C901**
- Scheme 4.3** Schematic procedure for synthesis of **Hit_5** analogs identified by pharmacophore searching

Acknowledgments

In my opinion, people around us affect our life and thinking because we are in community. The chances of meeting people neighboring us is pretty low because there are 6.7 billion people in the world at this time. The chances become much lower when we think about generation. Some people guide us to ups, while others lead us to downs. In terms of this concept, I am very lucky because people that I have been acquainted with have led me in paths of bright prospects. People I describe here have made who I am. I am clearly sure that I am able to complete my Ph.D. course with their advise, guide, help, and caring, which are irreplaceable with anything.

I would like to thank my mom, dad, wife, daughter, son, and in-laws. My mom and dad always say, "Do your best whatever you do" and "Be nice to your friends". These lessons have been mottos in my life, and I have tried to keep their instructions in mind. The teaching has led me to work hard and given me strong mind to complete Ph.D. course. My wife, Young-Ui, has been a great advisor, supporter, counselor, or friend for the last five years. She has pointed out my demerits and encouraged my merits. With her devoted supports such as taking care of our kids and me, I can concentrate on my study and research in Stony Brook. The responsibility for my lovely daughter, Athena, and son, Ethan, have led me to work hard. In-laws always encourage my wife to support me well and try to soothe wife's feeling. With big hands from all members in my family and in-laws I can successfully finish my Ph.D. course.

The advices, comments, and guides from Professor Dale Drueckhammer, Professor Richard Lin, and Assistant Professor Lisa Ballou are gratefully acknowledged. I am absolutely sure I cannot finish my dissertation and defense without their helps. They are not just advisors, but also, I have felt, friends, brothers and sister, or daddy and mommy. Studying abroad is not easy since we need to overcome homesick brought by unexpected happenings and events. Whenever I missed cares by my mom and dad, they have been greatly on behalf of my parents. Furthermore, as we talked about my research projects, they have tried to let me understand their knowledge, and they have an open-ear for my ideas. Scientific discussion with them has enlarged and deepened my knowledge about organic synthesis, computational chemistry/biology, biology, and medicine. There is no doubt that this knowledge will be a great companion for my future career next time.

Committee member, a chairperson of defense, Associate Professor Nancy Goroff, and 3rd member of defense, Distinguished Professor Iwao Ojima are highly thanked. In last several committee meetings with them, their comments, questions, and corrections were very helpful not only for my knowledge but also for my presentation skills.

Assistant Professor Robert Rizzo is very thanked for kind discussion about computational modeling and calculations in his classes.

I am grateful to Ms. Elzbieta Selinger for her time and effort for bioassay of mTOR and cell experiments. I am also grateful to Dr. James Marecek for his kind discussion about NMR data and for sharing his lab facilities such as a hydrogenation reactor, a melting point apparatus, and a high-pressure evaporator. I thank to Chem. lab

members including Diana, Lilly, Haeung, Ana, and Peter and former lab members such as Donghoon, Yimin, Haidong, Chen, Yonglian, Kevin, and Qi. I also thank to Bio. Lab members including Ya-ping, Chia-Yen, and Moha. For providing some lab facilities, I would like to thank Professor Nicole S. Sampson and her lab members including Younjoo, Eunjung, Siyeon, Yoojin, XinXin, Jin, Suzanne, Airong, Natasha and to thank Professor Kathlyn A. Parker and her lab members such as Keunsoo and Jungyong. Dr. Ojima's lab members are thanked such as Pat, Shi, Jin, Ray, Stephen, Joseph, Gary, Kunal, Edison, Corey, Chih-Wei, and ICB&DD staff members such as Seung-Yup, Bela, and Ilaria are thanked. I also thank Professor Frank W. Fowler, Professor Joseph W. Lauher, and Dr. Susan Oatis. Chemistry staff members such as Katherine, Heidi, Charmine, Jeffrey, Francis, and Michael are thanked. Some of my friends including Sunny, Jongsik, Kunwoo, Yoon-Hyeun, Kun-eeek, Kyunghwan, Sungjong, Tae-Jin, Jaechul, and Jongkhak are thanked.

My master's degree advisors, Professor Chankyung Kim, Professor Bon-Su Lee, and Professor Hai Whang Lee, are gratefully acknowledged for their concerns, help, and teaching of basic knowledge and skills about quantum calculations and molecular modeling during master's course.

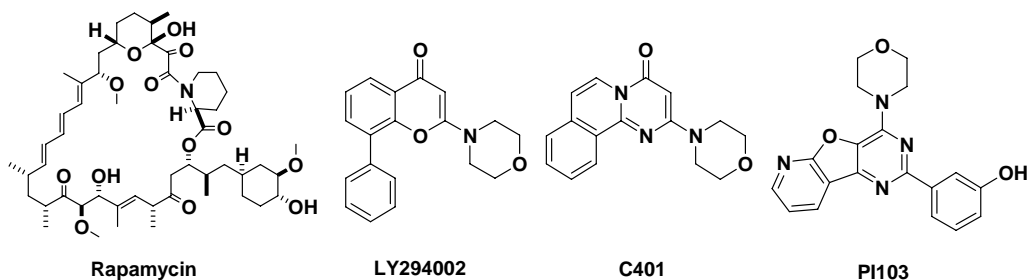
I could never successfully complete my Ph.D. course without helps by the above people. I am absolutely sure that with comments, advises, and guides I am well prepared, and I am ready for the long journey for achieving my goal in the future.

Chapter 1. Introduction

1.1 Mammalian target of rapamycin (mTOR)

The mammalian target of rapamycin (mTOR) is a Ser/Thr protein kinase that regulates cell proliferation, size and survival.¹⁻⁵ Many genetic defects found in human cancers cause mTOR signaling to be hyperactivated. This has brought attention to mTOR as an attractive target for cancer treatment. The natural product rapamycin,^{6, 7} a macrocyclic antibiotic produced by the bacterium *Streptomyces hygroscopicus* (Figure 1.1), and its analogs (CCI-779,^{8, 9} RAD001,¹⁰⁻¹² and AP23573,^{13, 14} also called rapalogs) inhibit mTOR function by an unknown mechanism. Rapamycin has been used as an immunosuppressant agent in organ transplant patients while its analogs are under clinical development as anti-cancer agents.

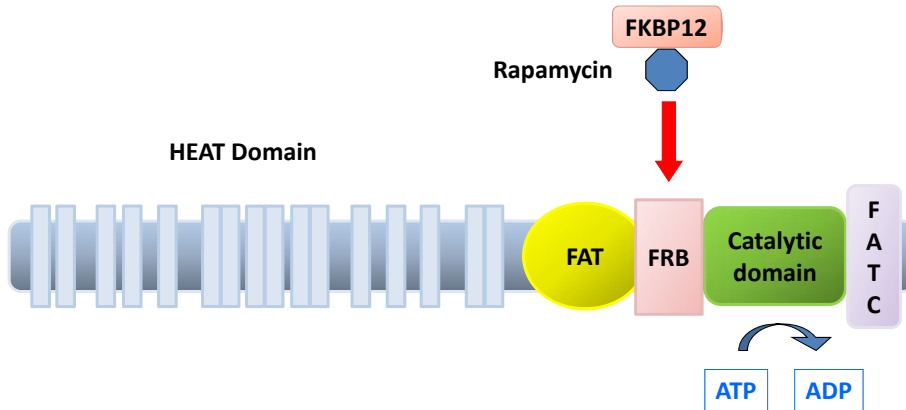
Figure 1.1 The structures of rapamycin, LY294002, **C401**, and PI103



mTOR has five domains; the HEAT, FAT, FRB, catalytic, and FATC domains (Figure 1.2). The signaling mechanism of activated mTOR starts with the binding of adenosine

triphosphate (ATP) to the active site of the catalytic domain. The ATP-mTOR complex activates downstream targets such as S6K1 and 4E-BP1 by phosphorylating Thr389 of S6K1, and then adenosine diphosphate (ADP) is released from the active site of the catalytic domain. By this phosphorylation, enzymes inside the cell are activated, and cell signals are transmitted for protein synthesis, cell growth, proliferation, and differentiation. To inhibit mTOR activity rapamycin or rapalogs first bind to the FK506-binding protein (FKBP12), and then this rapamycin-FKBP12 protein complex binds to the FRB domain, causing deformation of the catalytic domain to prevent ATP from binding to the active site.¹⁵ Therefore rapamycin and rapalogs have attracted interest as possible drugs for the treatment of mTOR related cancers.

Figure 1.2 The schematic domain structure of mTOR. The protein consists of HEAT (huntingtin, EF3, a subunit of PP2A and TOR) motifs, FAT (FRAP-ATM-TRRAP) domain, FRB (FKBP12-rapamycin-binding) domain, a catalytic kinase domain, and FATC (FAT C terminus) domain.



1.2 Phosphatidyl inositol 3-kinases (PI3Ks)

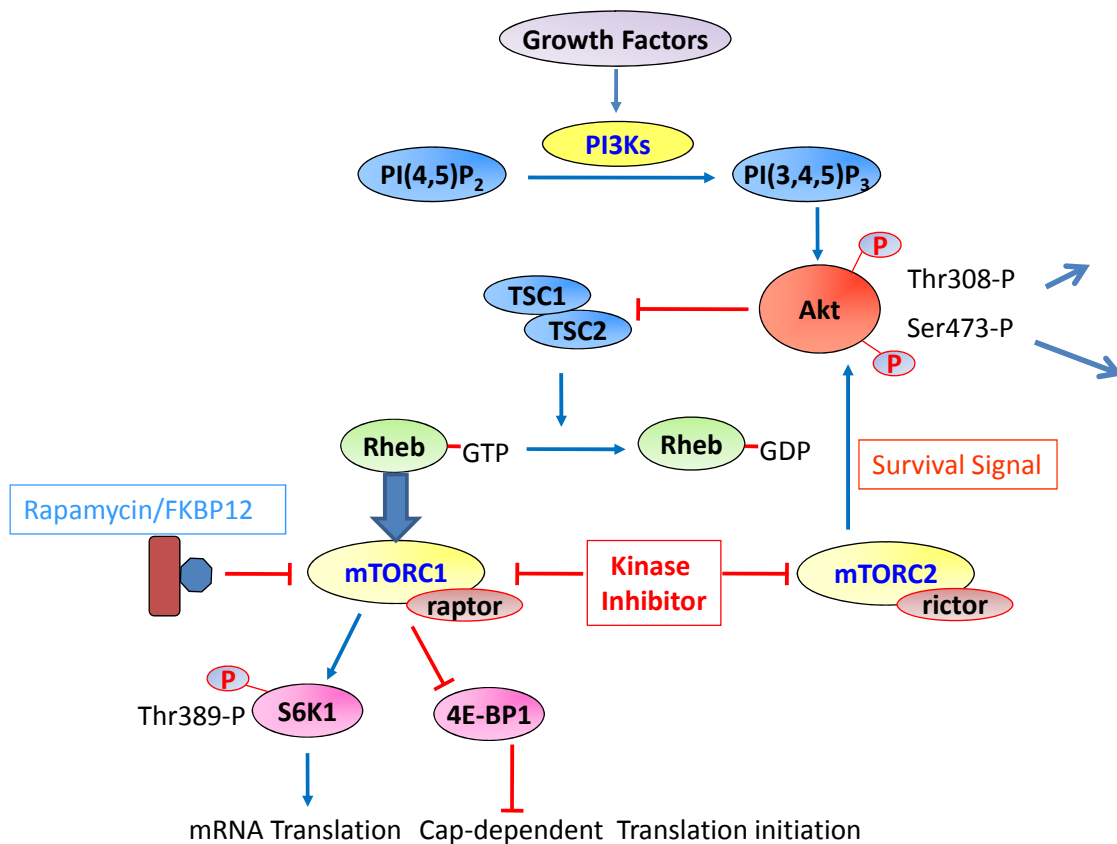
The phosphatidyl inositol 3-kinases (PI3Ks) are a family of enzymes that mediate intracellular signaling and play an important role in various cellular functions including apoptosis, proliferation, and vesicular trafficking.¹⁶⁻¹⁸ PI3Ks phosphorylate the 3-hydroxyl position of phosphatidylinositol lipids to produce phosphatidylinositol 3-phosphates, which bind to the pleckstrin homology (PH) domain of protein kinase B (PKB). This causes translocation of PKB to the cell membrane and subsequent phosphorylation of PKB, playing an important role in cancer progression.

The PI3Ks are subdivided into four classes: IA, IB, II, and III. Class IA PI3Ks, including p110 α , p110 β , and p110 δ as catalytic subunits, form complexes with p85 regulatory subunits. Class IB PI3Ks, having p110 γ as the catalytic subunit, form a complex with p101 and p84 regulatory subunits. In many human cancers the PI3KCA gene, encoding PI3K p110 α , is amplified and mutated, resulting in increased levels of p110 α and its activity. It is believed that PI3K α would be an effective drug target for treatment of some cancers. In contrast, other class I PI3Ks (β , γ , and δ) appear to have distinct biological roles different from those of PI3K α in various pathophysiological processes; PI3K β plays a role in the thrombotic process,¹⁹ PI3K γ plays a role in the inflammatory process mediated by neutrophils,²⁰⁻²² and PI3K δ plays a role in lymphocyte-mediated immune responses.²³ Therefore, production of selective PI3K α inhibitors for cancer treatment is important to avoid side effects caused by inhibition of other PI3K isoforms.

1.3 Hypothesis and purpose

A number of different physiological signaling pathways regulate mTOR, and the best characterized positive effector is the PI3K/Akt pathway (Figure 1.3). Recently, it was reported that mTOR forms two distinct multiprotein complexes, called mTORC1 and mTORC2.²⁴⁻²⁷ The mTORC1 complex contains mTOR, Raptor,^{24, 25} and mLST8,²⁸ while the mTORC2 complex contains mTOR, Rictor,^{26, 27} mLST8, and mSIN1.²⁹⁻³¹ The roles of mTORC1 and mTORC2 are totally different in the signaling pathway. Constitutive activation of mTORC1 is commonly seen in many human cancers, but the roles of mTORC2 in cancer are still ambiguous and need more studies for further characterization. Interestingly, rapamycin only inhibits mTORC1, and there is no inhibition of mTORC2 by rapamycin and its analogs. Because of this phenomenon rapamycin and rapalogs inhibit only one part of mTOR functions. This results in the critical disadvantage that when the mTORC1 complex is inhibited by rapamycin, mTORC2 sends a survival signal to Akt by phosphorylating S473, and then this phosphorylated Akt activates other kinases to enhance cell survival.²⁷ Therefore, rapamycin and its analogs may need to be co-administered with inhibitors of the Akt pathway to kill mTOR related cancers.

Figure 1.3 Overview of PI3K/mTOR-mediated signaling pathway. Growth factors such as insulin activate PI3K, causing increased production of the second messenger phosphatidylinositol (3,4,5) triphosphate (PI(3,4,5)P₃). Akt is activated upon binding to PI(3,4,5)P₃, which allows phosphoinositide-dependent protein kinase 1 (PDK1) to phosphorylate T308 of Akt. The TSC1/TSC2 complex inhibits mTORC1 by stimulating the GTPase activity of Rheb (Ras homolog enriched in brain), converting it to the inactive GDP-bound state. The phosphorylated Akt inhibits the TSC1/TSC2 complex and allows Rheb to remain in the active GTP-bound form, which causes activation of mTORC1. mTORC1 phosphorylates the translation repressor 4E-BP1 and S6 kinase (S6K1) at T389, leading to its activation.



Therefore, our hypothesis is that direct kinase inhibitors that can bind to the active site of the catalytic domain of mTOR where ATP binds can show broader anti-cancer activities than rapamycin and rapalogs. mTORC1 and mTORC2 possess the

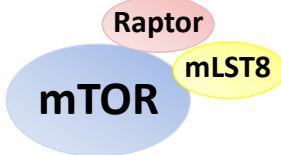
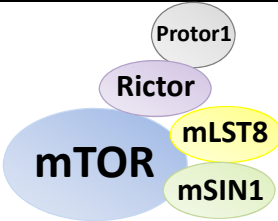
common mTOR component. The fact that the kinase catalytic domain of mTOR can be blocked by kinase inhibitors is good rationale for our hypothesis. However, the disadvantage of direct kinase inhibitors is that they may also bind to the active site of the catalytic domain of PI3Kinases, as the catalytic domain of mTOR is highly homologous to that of PI3Kinases. This may result in severe side effects such as increased glucose levels. Therefore, the goal of this research is to find direct selective inhibitors that can bind to the active site of the catalytic domain of mTOR but that cannot bind to the active site of PI3Kinases and other related kinases.

1.4 The mTOR signaling pathway

1.4.1 mTOR Complex 1 and Complex 2⁵

mTOR has emerged as an essential regulator in many fundamental biological processes, such as cell growth, cell survival, cell proliferation, cell motility, protein synthesis, and transcription in response to growth factors, nutrients, energy levels, and cellular stress. mTOR forms two multiprotein complexes, mTORC1 and mTORC2, which have very different physiological functions (Table 1.1).²⁴⁻²⁷

Table 1.1 Comparison of mTORC1 and mTORC2

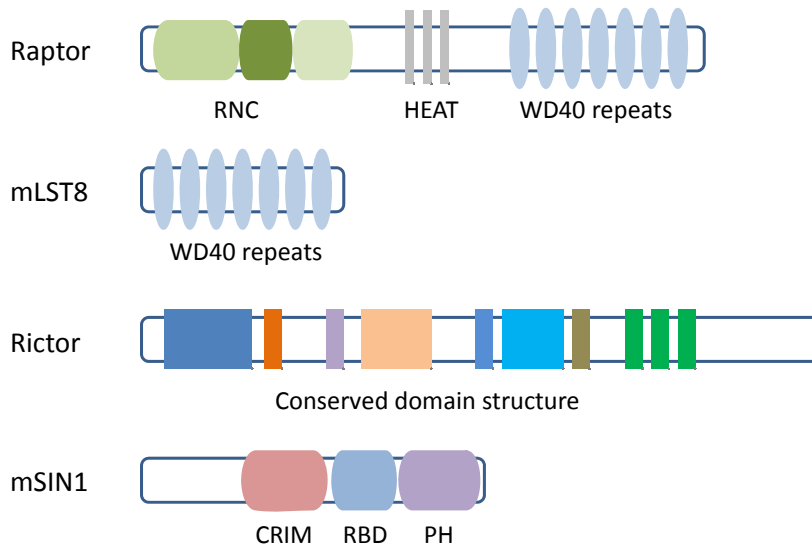
	mTORC1	mTORC2
Components		
Known Substrates	4E-BP1, S6K1, PRAS40	Akt, PKC α
Biological processes	Cap-dependent translation Ribosome biogenesis Autophagy Hypoxic adaptation	Growth factor signaling/survival Cytoskeletal reorganization
Inhibitors	FKBP12-Rapalog complex PI103 LY294002	PI103 LY294002

Components of mTOR complex

The mTOR Complex 1 (mTORC1) includes mTOR, Raptor^{24, 25} and mLST8²⁸ and is inhibited by rapamycin. Raptor is a 149 kDa non-enzymatic subunit of mTORC1, which is essential for mTOR-mediated phosphorylation. Its role is to recruit substrates (S6K1 and 4E-BP1) by binding through their corresponding TOS (TOR signaling) motifs. This binding gives a positive stimulation of mTOR activity in nutrient-stimulated signaling.

Interestingly, negative regulation of mTOR activity can also be caused by the tight association of Raptor with mTOR. Under nutrient starvation conditions the binding of Raptor to mTOR is enhanced to inhibit mTOR activity, while the binding is severely reduced in rapamycin treatment. Raptor contains three domains (Figure 1.4); a highly conserved amino-terminal region RNC (Raptor N-terminal conserved domain), three HEAT repeats, and seven WD40 (about 40 amino acids with conserved W and D forming four anti-parallel beta strands) repeats. The RNC domain has a high propensity to form α -helixes and its mutations disrupt the association with mTORC1. Similar to the RNC domain, mutations in WD40 also affect the interaction with mTORC1, supporting the idea that multiple regions on Raptor and at least the HEAT repeats of mTOR are required for the interaction. mLST8 is another mTORC1 component, which consists entirely of seven WD40 repeats. It is a positive regulator and binds to the kinase domain of mTOR. This binding strongly enhances the activity of mTOR, the opposite effect from the stable interaction of Raptor with mTOR.²⁸ However, it has been shown that loss of mLST8 does not critically affect mTORC1 function.³²

Figure 1.4 Schematic components in mTOR complex (modified from a Ref 1)



The mTOR Complex 2 (mTORC2) includes mTOR, Rictor, mLST8, and mSIN1 and is insensitive to rapamycin inhibition.^{26, 27} Rictor and mSIN1 are unique components of mTORC2, while mTOR and mLST8 are found in both mTORC1 and mTORC2. Rictor, a 190 kDa subunit of mTORC2, has seven conserved domains, and their functions are still unknown, but they possibly mediate substrate binding and mTORC2 assembly. In contrast to mTORC1, mTORC2 is not inhibited by rapamycin and is not affected by nutrient depletion conditions, resulting in unchanged activity of S6K1 and 4E-BP1 by loss of mTORC2 activity (or hyperactivity) in cells. Furthermore, Rictor knockout mice die around E10.5 (embryonic day 10.5), which indicates it has a critical role in physiological and developmental process.³³ In addition to Rictor, another unique and functionally essential component of mTORC2 is mSIN1.²⁹⁻³¹ The role of mSIN1 is similar to that of Rictor. mSIN1 stabilizes Rictor (and *vice versa*) and stabilizes the interaction between mTORC2 and Rictor by binding to Rictor and cooperatively building the structural motif

with Rictor for mTORC2. The phosphorylation status of Akt on S473 and its functions are dramatically decreased in knockout mSIN1. mSIN1 has three domains; the CRIM (conserved region in the middle), RBD (Raf-like Ras binding domain), and PH (Pleckstrin homology) domains.³⁴ It was reported that mSIN1 interacts with activated Ras protein through its RBD domain by binding and co-localizing, and suppresses Ras signaling in cells.³⁴ mSIN1 binds to PI and other lipids through the PH domain as most enzymes having a PH domain are capable of binding to lipids. Recently, it was revealed that mSIN1 has at least five isoforms and three of them (isoforms 1, 2, and 5) assemble individually into mTORC2 to form three distinct mTORC2s.²⁹ Interestingly, the activities of only two of the three mTORC2s (containing mSIN1.1 and mSIN1.2) are insulin sensitive, while all three mTORC2s phosphorylate Ser473 of Akt *in vitro*. The other component of mTORC2 is mLST8. In contrast to the effect of mLST8 toward mTORC1, its role toward mTORC2 is significant and similar to that of Rictor. For example, mLST8-knockout mice die around E10.5. This mutation disrupts only mTORC2 assembly and decreases the phosphorylation status of Akt on S473, while S6K1 and 4E-BP1 are not affected.³² Thus, loss of mLST8 causes an impaired mTORC2, indicating its essential role, but a functional mTORC1, indicating its dispensable role in that complex. Very recently, a novel Rictor-binding component of mTORC2 was identified, termed Protor-1 (protein observed with Rictor-1)(Table 1.1).³⁵ It is a specific component of Rictor in mTORC2, but not of Raptor in mTORC1. The expression of Protor-1 is regulated by Rictor and mSIN1, but it is not essential for the assembly of other components into mTORC2. Further research is required to characterize its role related to mTORC2 functions.

Upstream regulators and downstream targets of mTOR

A connection between the extracellular growth factor signals (insulin-PI3K-Akt) and the intracellular TSC1/2-mTORC1-S6K1/4E-BP1 regulation was established by the discovery of direct phosphorylation of TSC2 on multiple sites by Akt.³⁶⁻³⁹ PI3K is activated by the growth factor-initiated intracellular signaling pathway through cell surface receptors, with activation leading to the conversion of PIP2 to PIP3.^{40, 41} PIP3 recruits Akt via its PH domain to the plasma membrane, which stimulates phosphorylation of Akt on Thr308 by PDK1.^{42, 43} Consequently, TSC2 is phosphorylated by the activated Akt, but the mechanism is still unclear (more details of the signaling pathway from Akt to S6K1/4E-BP1 through TSC1/TSC2 will be described in the following sections). In addition to phosphorylation of TSC2 by Akt, Akt can phosphorylate 40 kDa PRAS40 (proline-rich Akt substrate or AKT1S1 (Akt1 substrate 1)) on T246, and then the stimulated PRAS40 negatively affects mTORC1 activity.⁴⁴ Therefore, PRAS40 is a direct regulator of PI3K-Akt signaling, bypassing TSC1/2-Rheb. There is still debate whether PRAS40 is an mTOR binding partner or a substrate^{44, 45}, but clearly it directly inhibits mTORC1 function through the insulin-PI3K-Akt-mTORC1 pathway without effecting TSC1/2-Rheb activity.⁴⁶ (Downstream targets of mTORC1 such as S6K1 and 4E-BP1 will be further described in the following sections.)

Akt has another role as a downstream target of mTORC2 in cells. Ser473 in the C-terminal hydrophobic motif of Akt is directly phosphorylated by mTORC2, and phosphorylation on Thr308 by PDK1 is triggered by the priming phosphorylation on Ser473.²⁷ Akt belongs to the AGC (cyclic AMP-dependent protein kinase, cyclic GMP-

dependent protein kinase and protein kinase C) kinase family. PKC is one member of this family, which also includes S6K1. The distinct feature of the AGC family is the highly conserved hydrophobic motif in the kinase domain, supporting the result of phosphorylation of S6K1 and Akt by mTOR. Furthermore, most members of the AGC family are similar to Akt, supporting the idea that mTORC2 phosphorylates other kinases in the AGC family. Phosphorylations of PKC α , PKC δ , and PKC ϵ on their hydrophobic motif are reported to be regulated by mTORC2,^{32, 47} but more experiments are needed to define whether other isoforms (10 isoforms) of PKC and which other AGC family members are stimulated by mTORC2.

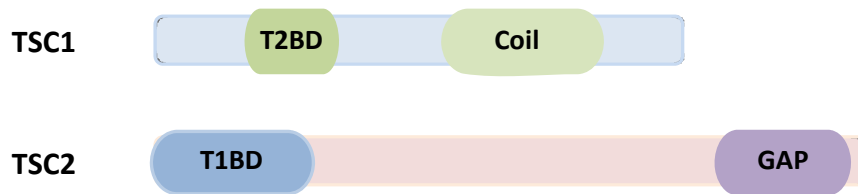
Other potential substrates of mTOR are the signal transducer and activator of transcription 3 (STAT3)⁴⁸ and p53.⁴⁹ mTOR phosphorylates Ser727 in the Ser/Pro motif of STAT3 and Ser15 of p53. These phosphorylation events are related to transcriptional regulation and caspase activation, respectively.^{48, 49}

1.4.2 The TSC1-TSC2 complex⁵⁰

In the benign tumor disease tuberous sclerosis complex (TSC), one or both of the tumor suppressor genes, *TSC1* and *TSC2*, is mutated.⁵⁰ The *TSC1* and *TSC2* genes encode the proteins hamartin and tuberin respectively.⁵¹⁻⁵³ These two proteins form a complex that negatively controls mTOR activity through regulation of Rheb. The TSC1-TSC2 complex plays a significant role in growth-factor, nutrient and stress signals that control protein synthesis, cell growth and other cellular processes.

There is no homology between TSC1 (140 kDa) and TSC2 (200 kDa) proteins and they have very little homology with other proteins. Each protein is comprised of two domains (Figure 1.5). The acronyms T2BD and T1BD refer to TSC2-binding domain and TSC1-binding domain, respectively. The predicted coiled-coil domain and GAP domain homologous with that in Rap1GAP are represented as Coil and GAP respectively. TSC1 and TSC2 proteins are physically associated, but only the activity of the GAP domain of TSC2 is directly related to its tumor suppressor activity.⁵⁴ However, TSC1 is necessary to stabilize TSC2 and prevent its ubiquitin-mediated degradation. TSC2 degradation is sometimes caused by missense mutations in TSC1 or TSC2, leading to destabilization of the complex.

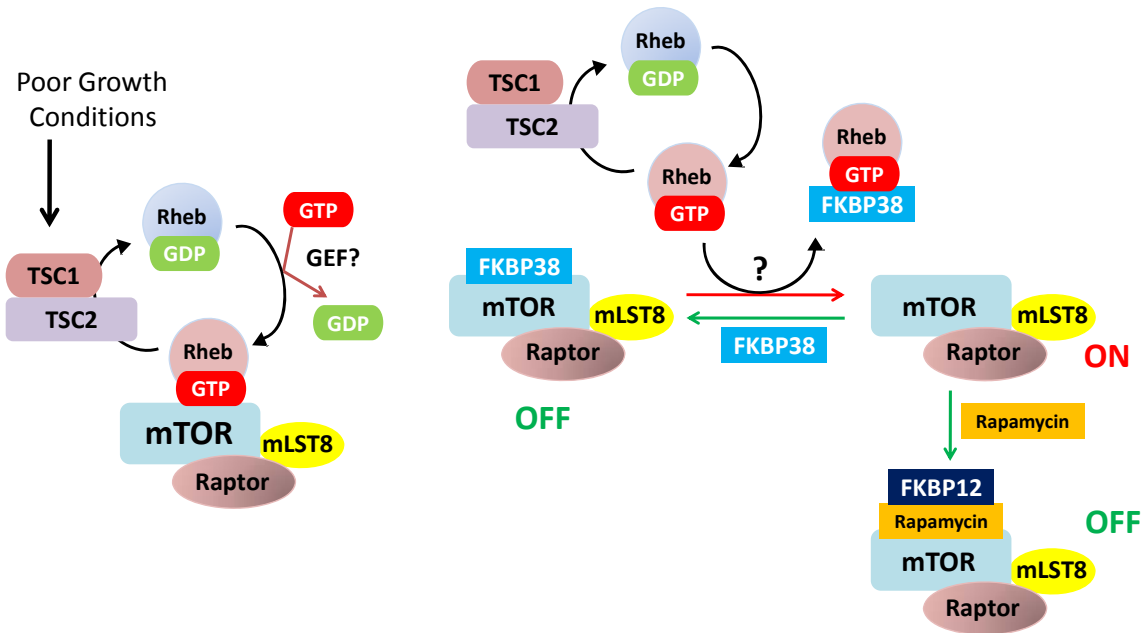
Figure 1.5 Schematic of the TSC1 and TSC2 proteins (modified from ref ⁵⁰)



Rheb, a member of the Ras superfamily, is the small G-protein target of the TSC2 GAP domain. The intrinsic GTPase activity of Rheb is stimulated by the GAP domain of TSC2 within this complex to trigger the conversion of Rheb-GTP into Rheb-GDP. Under normal growth conditions, mTORC1 is activated by direct binding of the accumulated Rheb-GTP. Under poor growth conditions (i.e. serum or amino acid withdrawal) the

TSC1-TSC2 complex is stimulated, leading to accumulation of the Rheb-GDP state resulting in inactivation of mTORC1. A recent report shows that FKBP38 (An FKBP12 homologue also known as FKBP8) associates with mTORC1 preferentially under poor growth conditions by binding the FRB domain of mTOR.⁵⁵ However, Rheb-GTP stimulates mTORC1 activity through binding to FKBP38 and triggers its release from mTORC1 (Figure 1.6).

Figure 1.6 Two plausible mechanisms for controlling mTORC1 activity through TSC1-TSC2 and Rheb



The TSC1-TSC2 complex regulates growth by inhibition or activation in response to multiple upstream signals such as growth factor signaling, cytokine signaling, energy- and oxygen-sensing pathways, and other unknown pathways.⁵⁰ The PI3K-Akt pathway and ERK-RSK (Extracellular-Signal-Regulated kinase/p90 Ribosomal protein S6 Kinase) are directly related to the TSC1-TSC2 complex in cells in response to growth factors

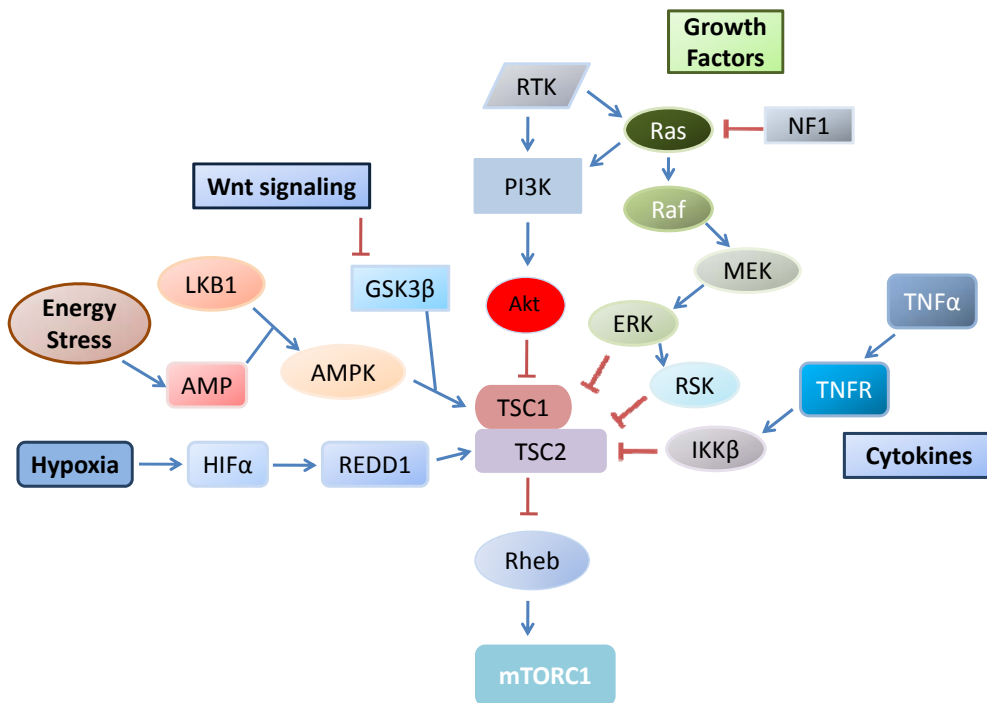
(Figure 1.7). Akt directly phosphorylates TSC2 at Ser939 and Thr1462 (and three other predicted phosphorylation sites), which inhibits the function of the TSC1-TSC2 complex. The molecular mechanism of this inhibition is still unclear, but one enticing mechanism involves association with 14-3-3 proteins.⁵⁶ A binding site for 14-3-3 proteins on TSC2 is created through phosphorylation of Ser939 and Thr1462 and/or Ser981 by Akt. Binding of 14-3-3 proteins may contribute to Akt-induced inhibition of TSC2. Furthermore, activated ERK and its downstream target RSK stimulate mTORC1 activity by inhibiting the TSC1-TSC2 complex through multisite phosphorylation of TSC2. ERK and RSK are the downstream effectors of the Ras/Raf/MEK signaling pathway controlled by growth factors (Figure 1.7). Phosphorylation of Ser540 and/or Ser664 by ERK causes dissociation of the TSC1-TSC2 complex.

Recently it was reported that mTORC1 signaling is stimulated by the pro-inflammatory cytokine TNF α (tumor necrosis factor α) through IKK β (inhibitory κ B kinase β). IKK β phosphorylates TSC1 on Ser487 and Ser511, resulting in deactivation of the TSC1-TSC2 complex.⁵⁷ The mechanism is proposed to involve rapid dissociation of the complex, leading to increased degradation of TSC1, though this mechanism is not proven.

mTORC1 signaling for protein synthesis is very sensitive to energy (ATP) starvation. Direct phosphorylation of TSC2 by AMPK (AMP-dependent protein kinase) enhances the activity of the complex under energy depletion.⁵⁸ Energy depletion results in the intracellular level of AMP being increased. Binding of AMP to AMPK stimulates its subsequent activation by the tumor suppressor, LKB1. Two residues on TSC2, Ser1387

and Thr1271, are phosphorylated by AMPK, leading to increased energy-generating catabolic processes and decreased energy-depleting anabolic processes. Further (or subsequent) phosphorylation on TSC2 is accomplished by GSK3 β (glycogen synthase kinase 3 β , a downstream component in Wnt signaling) after the AMPK-priming phosphorylation.

Figure 1.7 Upstream signaling pathways regulate the TSC1-TSC2 complex (modified from Ref 50)



Under oxygen depleted state (i.e. hypoxia), mTORC1 signaling is blocked through the regulation of the TSC1-TSC2 complex by REDD1, which is a transcriptional target of HIF α (hypoxia-inducible factor α).⁵⁹ The molecular mechanism of TSC1-TSC2 activation by REDD1 is its binding to 14-3-3 proteins through a motif surrounding Ser137.⁶⁰ 14-3-3

proteins are bound to two phosphorylated sites on TSC2 (Ser939 and Thr1462) by Akt and then are moved to the site of Ser137 on TSC2, phosphorylated by REDD1. Therefore, this movement of 14-3-3 proteins suggests that REDD1 activates the TSC1-TSC2 complex by removing Akt-induced inhibition. Hypoxia can also cause activation of the TSC1-TSC2 complex through AMPK-mediated phosphorylation, because oxygen starvation leads to a decrease in aerobic ATP production through mitochondrial oxidative phosphorylation.

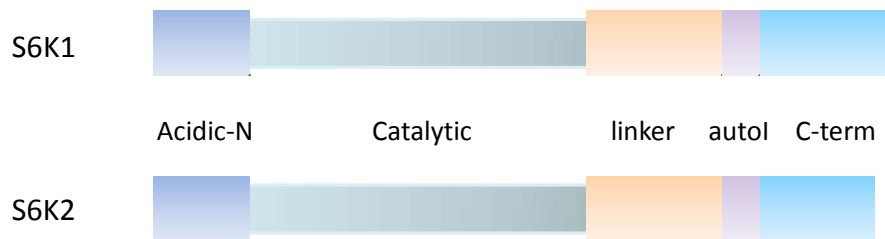
As described, the TSC1-TSC2 complex is a critical upstream regulator of Rheb and mTORC1 to promote cell growth. However, its role in controlling mTORC2 is currently not clearly known. The TSC1-TSC2 complex has numerous phosphorylation sites targeted by several aforementioned proteins and still unrevealed ones. The characterization of these proteins and the understanding of their linkage with TSC1-TSC2/Rheb/mTORC1 (or mTORC2) will be promising research fields in the near future.

1.4.3 S6 Kinase (S6K)⁶¹

A ribosomal protein S6 kinase (S6K, 70 kDa, also known as p70^{S6K}) is one of the downstream effectors of mTORC1, and stimulates protein synthesis in response to growth factors and nutrients.^{62, 63} The synthesis of ribosomal RNA (rRNA)^{64, 65} and cell cycle progression^{66, 67} are also reported to be regulated by S6K. In animal studies, the loss of S6K causes a decrease in cell size followed by a reduction of animal size accompanied by type 2 diabetes.⁶⁸ S6K is categorized as a member of the aforementioned AGC kinase family due to its homologous catalytic domains.⁶⁹ Two types of S6K are present; S6K1 and S6K2. They are highly homologous (70% sequence

identity), and have a conserved domain structure including an acidic N-terminal, and catalytic, linker and autoinhibitory domains, resulting in presumably similar regulation by mTOR.

Figure 1.8 Schematic representations of S6K1 and S6K2



The PI3K-mTORC1 pathway, as previously described, is one of the main regulators of S6K1 activity. The mechanism involves the binding of Raptor in mTORC1 to S6K1 (also 4E-BP1, described below) through the TOS motif, followed by recruiting of S6K1 to mTOR for phosphorylation. The Ras/MEK/ERK and c-MYC pathways are also known as effectors of cell growth by deactivating TSC1/2, resulting in activation of mTORC1-S6K1. Independent of the PI3K-mTORC1 pathway, S6K1 is also activated by forming a complex with the atypical PKC isoforms λ and ζ and PDK1 and also by the Cdc42-PLD1 (phospholipase D1)-PA (phosphatidic acid) cascade,^{70, 71} but details at this process are not fully characterized.

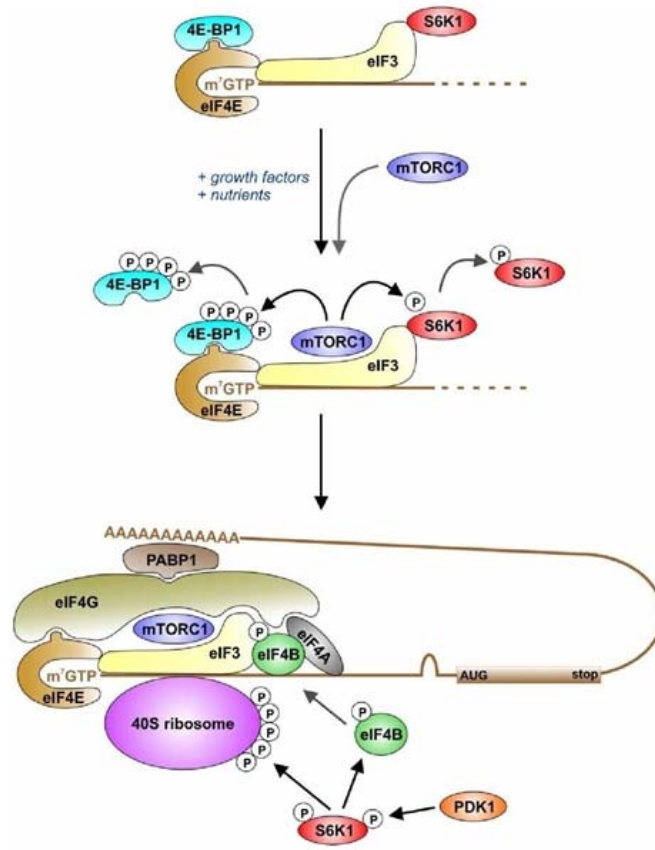
In contrast to regulation of S6K1 by the PI3K-mTOR pathway, S6K1 also inhibits PI3K signaling in a feedback loop by shutting off insulin/IGF signaling through activation of the insulin receptor substrate (IRS-1).⁷²⁻⁷⁴ Under basal conditions, or upon

extracellular ligand binding, insulin receptors or IGF-1 receptors are phosphorylated, followed by triggering the cytoplasmic binding of IRS-1 to these receptors. This binding leads to activation of the PI3K-Akt-mTORC1 pathway. However, continuous activation of mTORC1 by loss of TSC1/2 or prolonged input of nutrients aberrantly overstimulates S6K1. This abnormal S6K1 disrupts the association of IRS-1 with its receptors through direct phosphorylation of IRS-1 on S307 and S527, thereby nullifying the ability of IRS-1 to activate PI3K. Therefore, chronic activation of mTORC1 resulting in activation of S6K1 imposes a feedback inhibitory effect on IRS-1 to diminish IRS-dependent processes including cell survival.

S6K1 plays a major role in cell growth via enhanced protein synthesis, in contrast to the minimal effect of S6K2.⁶¹ Thus many S6K1 substrates are involved in regulation of translation such as the 40S ribosomal subunit protein (rpS6),^{75, 76} eIF4B,⁷⁷ eEF2K,⁷⁸ and CBP80.⁷⁹ rpS6 was the first identified substrate of S6K1. Phosphorylation of rpS6 by S6K1 increases protein synthesis through the regulation of translation efficiency of ribosomes (production of translation factors) as well as ribosome biogenesis (synthesis of ribosomal proteins). A model of translation pre-initiation complex assembly and initiation of protein translation through mTORC1, S6K1, and eukaryotic initiation factors (eIFs) was proposed (Figure 1.9).^{80, 81} An eIF3 translation pre-initiation complex bound to mRNA is associated with inactive S6K1 (but not S6K2) under basal conditions. Under growth factor and nutrient stimulation, mTORC1 is recruited to the complex. mTORC1 then phosphorylates S6K1 (on T389) and 4E-BP1 followed by their dissociation from the eIF3 complex. The released S6K1 (T389 phosphorylated) becomes further activated by

binding with PDK1 and phosphorylation on T229. The fully activated S6K1 then phosphorylates its substrates rpS6 and eIF4B (on S422). eIF4B is the essential regulatory subunit of eIF4A, which is an mRNA helicase. The activated eIF4B is recruited to the translation pre-initiation complex, leading to the binding of eIF4G scaffold to the mRNA cap structure for the assembly of the translation initiation complex with 5' mRNA. Finally the initiation of mRNA translation occurs.⁸⁰

Figure 1.9 The proposed model for the process of translation initiation through mTORC1, S6K1, and eIFs (modified from Ref 80).



S6K1 also regulates the elongation step of translation by phosphorylation of eEF2 kinase (eEF2K, eukaryotic translation elongation factor 2 kinase) on S366, leading to the inactivation of eEF2K, followed by activation of eEF2.⁷⁸ The activated eEF2 interacts with the ribosome and mediates the translocation step of elongation. Phosphorylation of eEF2 on Thr56 by eEF2K prevents association with the ribosome and thus inactivates the ribosome. Furthermore, S6K1 has been shown to play a role in cap-dependent mRNA splicing by phosphorylating CBP80, a subunit of the Cap Binding Complex (CBC, an RNA-binding protein).⁷⁹ In addition to translational efficiency

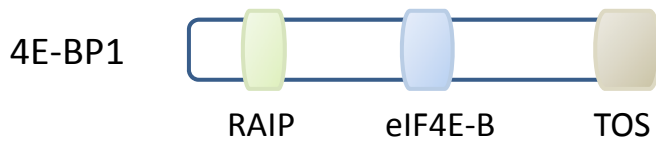
(promoting protein synthesis) by S6K1, translational capacity (ribosome biogenesis) of cells can be regulated via the mTORC1-S6K1 pathway. The rate-determining step of ribosome biogenesis is rRNA gene transcription. S6K1 relieves the inhibition of rRNA resulting from overexpression of PTEN, a negative regulator of PI3K.⁸² Schmelzle and Hall have reported that the activity of S6K1 is also related to the regulation of G1 to S phase cell cycle progression,⁸³ but the mechanism of the S6K-mediated cell cycle is not clear.

1.4.4 Eukaryotic initiation factor 4E binding protein (4E-BP)

4E-BP has three isoforms: 4E-BP1, 4E-BP2 and 4E-BP3. The role of 4E-BP1 is assembly of the translation complex cooperatively with S6K1, while the role of other isoforms is not clear. 4E-BP1 suppresses eIF4E through association, and it is another downstream effector of mTORC1. 4E-BP1 has a short sequence of amino acids (118), containing a binding motif for interaction with eIF4E called the eIF4E-binding domain, and two regulatory domains, the RAIP motif and the TOS motif. The RAIP motif, a novel regulatory motif of four amino acids, lies within the first 24 residues of 4E-BP1. This motif is necessary for efficient phosphorylation and optimal regulation of 4E-BP1, as the N-terminal truncated 4E-BP1, which does not have the first 24 residues, binds to eIF4E but fails to become phosphorylated to be released from eIF4E.⁸⁴ The TOS motif is positioned near the C-terminus of 4E-BP1 (FEMDI, the last five residues), and may function as a docking site of mTOR.⁸⁵

4E-BP1 is directly associated with eIF4E (a 7-methyl-guanosine mRNA cap binding protein). This interaction prevents a scaffold protein eIF4G from binding to eIF4E, which inhibits formation of the translation pre-initiation complex (eIF4F, the eIF4E/4G/4A complex is referred to as eIF4F) thereby repressing translation⁸⁶ (Figure 1.9). Upon stimulation with growth factors or nutrients, 4E-BP1 is phosphorylated and inactivated by mTORC1 recruited to eIF3. eIF4E is thus released from phosphorylated 4E-BP1. This dissociation enables eIF-4G to bind to eIF-4E and make an active complex with eIF-3, eIF-4A and eIF-4B activated by S6K1, resulting in initiation of cap-dependent translation.

Figure 1.10 Schematic representation of 4E-BP1



1.5 mTOR as a drug target for many diseases

1.5.1 Human genetic diseases related to mTOR^{87, 88}

Tuberous sclerosis complex (TSC) is a genetic disorder that causes tumors to form in many different organs, primarily in the brain, eyes, heart, kidney, skin and lungs. Two genes have been identified that can cause tuberous sclerosis complex;⁵¹⁻⁵³ the TSC1, or hamartin gene (located on chromosome 9) and the TSC2, or tuberin gene (located on chromosome 16). The major function of these proteins is to antagonize the mTOR pathway. Both genes are regarded as tumor growth suppressors, in which loss or defection results in TSC. TSC is transmitted either through genetic inheritance (one-third of TSC cases) or as a spontaneous genetic mutation (the remaining two-thirds) where the cause is not clearly understood. Most people with TSC have dermatologic signs such as hypomelanotic macules, forehead fibrous plaques, facial angiofibromas or shagreen patches. The most severe effects of TSC are neurological disabilities including developmental delay, mental retardation and autism.

Peutz-Jeghers syndrome, also known as Hereditary Intestinal Polyposis Syndrome, is characterized by benign hamartomatous polyps, with increased risk of malignant tumors, in the intestine and abnormal mucocutaneous pigmentation.⁸⁹ This syndrome is caused by mutation in the *LKB1* tumor suppressor gene, which encodes a serine/threonine kinase that phosphorylates and activates AMPK (5'-AMP-activated protein kinase).^{90, 91}

Cowden, Bannayan-Riley-Ruvalcaba and proteus syndromes, and Lhermitte-Duclos disease, caused by *PTEN* mutations, are all autosomal dominant hamartoma

disorders.^{92, 93} By converting PIP3 to PIP2, PTEN plays a role as a tumor suppressor. Loss of PTEN causes increased Akt activity, resulting in down-regulation of tuberlin's function.

Von Hippel-Lindau disease (VHL) is caused by mutations in the VHL tumor suppressor gene. This genetic disorder is characterized by the aberrant growth of certain tumors such as Haemangioblastomas (tumors of the central nervous system) found in the brain, the spinal cord, the retina, and other areas of the nervous system.⁹⁴ The protein encoded by this gene is part of a multiprotein complex involved in the ubiquitination and degradation of a hypoxia-inducible-factor (HIF), which is a transcription factor in the regulation of gene expression by oxygen. Patients with this disease have balance, walking and vision problems, headaches, dizziness, high blood pressure, and weakness of the limbs.

Neurofibromatosis type 1 (NF1) is caused by mutations in the *NF1* gene, on chromosome 17, responsible for control of cell division. NF1 is characterized by the development of neurofibromas, a type of peripheral nerve sheath tumor.^{95, 96} The *NF1* gene encodes neurofibromin, which is a negative regulator of the Ras signal transduction pathway. In mutated *NF1*, Ras is hyperactivated, causing constitutive activation of mTOR. The most common complications in patients with NF1 are cognitive deficits and learning disability, bone deformations and hamartomatous lesions of the iris.

Polycystic kidney syndrome is caused by mutations in the *PKD1* gene that encodes polycystin-1 (PC-1). This syndrome is characterized by progressive cyst development in both kidneys, which become enlarged with multiple cysts. Another protein, NEK1, is known to cause this syndrome by interacting with tuberlin. The

symptoms caused by this disease include renal function abnormalities, hypertension, renal pain, and renal insufficiency.

1.5.2 Cancers related to mTOR signaling

As mentioned above, mutations in tumor suppressor genes such as *TSC1*, *TSC2*, *LKB1*, *PTEN*, *VHL*, *NF1* and *PKD1* lead to some cancers. PI3K plays a role as a protooncogene, for which increased activity induces cell transformation and progression, particularly in ovarian and gastrointestinal cancers.^{97, 98} Furthermore, abnormal activities of upstream elements such as epidermal growth factor, ErbB2, or insulin-like growth factor 1 receptor cause persistent activity of PI3K in a wide variety of cancer cell types.^{1, 3} In addition, mutations in the *PTEN* gene are also commonly found in human cancers such as prostate, breast, lung, bladder, melanoma, endometrial, thyroid, brain, and renal carcinomas. Akt,⁹⁹ Rheb,¹⁰⁰ eIF4E, and S6K¹⁰¹ are frequently overexpressed and amplified in many cancers, although reported mutations in mTOR are rare.⁸⁸

Tumor angiogenesis, a physiological process involving the growth of blood vessels that provides tumor cells with nutrients and oxygen and the transition of tumors from a dormant state to a malignant state,¹⁰² is related to the function of mTOR. Antiangiogenic effects can be obtained by treatment with rapamycin, causing a decrease in concentration of vascular endothelial growth factor (VEGF), which is the major contributor to angiogenesis, and the suppression of VEGF-induced vascular endothelial proliferation, survival and migration.¹⁰³

Renal cell carcinoma, the most common type of kidney cancer arising from the renal tubule, can be treated by inhibition of mTOR.^{94, 104} mTOR inhibition causes loss of VHL tumor suppressor activity and consequently triggers HIF activity in most renal cell carcinomas. Inhibition of mTOR signaling presents clinical advantages in patients with poor prognostic features by downregulating HIF.¹⁰⁵ In sporadic bladder cancers, ovarian and gall bladder carcinoma, non-small-cell carcinoma of the lung, and breast cancer, the TSC protein complex is also mutated or its expression is reduced. Recently, it was reported that loss of expression or phosphorylation of tuberin (TSC2) is frequently observed in endometrial carcinoma.¹⁰⁶

1.5.3 Other diseases related to mTOR signaling

Alzheimer's disease is reported to be linked to mTOR through translation of tau mRNA and degradation of tau protein.¹⁰⁷ The tau protein, which is a microtubule-associated protein (MAP) abundant in neurons in the CNS, is found frequently in the brains of patients with Alzheimer's disease. An activated PKN, a serine/threonine kinase, phosphorylates tau. This phosphorylation destabilizes microtubules, causing the self-assembly of tangles of paired helical filaments and straight filaments, which is involved in the etiology of Alzheimer's disease. Therefore, inhibition of mTOR signaling can cause a reduced concentration of tau, and lower the toxicity caused by tau accumulation, for Alzheimer treatment.¹⁰⁸

Type 2 diabetes is a metabolic disorder characterized by insulin resistance (or insensitivity to insulin), and by inhibition of insulin-receptor substrate (IRS) proteins by

phosphorylation of IRS1.¹⁰⁹ The retained activation of mTOR is related to the insensitivity of IRS to insulin by the inhibition of the association of IRS with insulin receptor through the negative feedback loop by activated S6K. Furthermore, chronic activation of mTOR in β -cells is observed by chronic hyperglycemia (high blood sugar), leading to the degradation of IRS2 followed by the reduction of cell mass and insulin secretion.¹¹⁰ Patients with Type 2 diabetes have problems with obesity, hypertension, elevated cholesterol, and metabolic syndrome. As a result, inhibitors negatively controlling mTOR could be potential drugs for managing Type 2 diabetes.

Cardiac hypertrophy (heart enlargement) is also reported to be related to the hyperactivation of the PI3K-mTOR cascade, and to be prevented by inhibition of mTOR.¹¹¹ It is also reported that the IGF/mTOR pathway has a key role of controlling the regulation of lifespan and aging.¹¹²

In summary, many human diseases are directly or indirectly linked to the dysregulation of mTOR, such as rare genetic diseases, many cancers, neurological disorders, and metabolic and cardiovascular diseases. Since an abnormally hyperactivated mTOR pathway is the critical etiology of these diseases, inhibitors targeting the persistent activity of mTOR might be potentially effective drugs for these diseases.

1.6 Computer aided molecular design

Computer based approaches for molecular design have been widely used over the last two decades in many research fields.^{113, 114} With greatly increased computer speed and graphics, molecular modeling is an indispensable tool in medicinal chemistry and drug discovery. Computer modeling can aid scientists in rational drug design and reduce the level of experimental effort. Two general approaches to drug discovery are structure-based drug design (SBDD, structure refers to the structure of a protein target) and ligand-based drug design (LBDD).

SBDD methods include Molecular Dynamics (MD),¹¹⁵ Monte Carlo (MC)¹¹⁶ calculations, homology modeling, and receptor based virtual screening (Docking). SBDD has become popular largely due to the rapidly increasing number of crystal structures of enzyme and receptor proteins. The basic assumption of SBDD is that potent inhibitors must possess significant structural and chemical complementarities to their targets.

LBDD includes QSAR (Quantitative Structure Activity Relationship), CoMFA (Comparative Molecular Field Analysis, or 3D-QSAR), ligand-based pharmacophore searching, and ADMET test (Absorption, Distribution, Metabolism, Excretion, and Toxicity).¹¹⁷⁻¹¹⁹ These approaches may be applied when the structures of several ligands, or even a single ligand, and their biological activities are known, even if the 3D structure of the biological target is unknown. This approach is sometimes called chemoinformatics. Molecular properties of each ligand are calculated as a series of “descriptors” representing chemical or geometric characteristics. The mathematical relationship between these values and biological activities or toxicities is derived by statistical

analysis such as PLS (partial least squares)^{120, 121} and PCA (principal component analysis)^{122, 123} and by computational techniques such as GA (genetic algorithms)^{124, 125} and RP (recursive partitioning).¹²⁶ Based on statistical correlations predictive models are identified and used to predict the desired properties (activities or toxicities) of unknown ligands.

1.6.1 Homology modeling

Homology modeling, or comparative modeling, is a class of methods for generating 3D model of a protein of interest (target) from its amino acid sequence, based on related proteins of already known structures as a template. The fundamental assumption of this method is that proteins of similar amino acid sequence will have similar tertiary structures and share common structural properties. Small or medium changes in sequence typically result in only small changes in the 3D structure.¹²⁷ Thus, if there is sequence similarity between proteins, structural similarity can usually be assumed.¹²⁸ In general, 30% sequence identity is required for generating useful models. In parallel with the availability of high-resolution experimental data by X-ray crystallography and NMR spectroscopy, the contribution of homology modeling to drug discovery has been greatly increased. Homology modeling contributes to lead identification and optimization, but also to target identification and validation. Generating homology models is not time-consuming, and such models can assist medicinal chemists to make hypotheses of how to design biologically meaningful compounds in the early conceptual step in drug discovery research.

The procedure of homology modeling can be generally divided into four sequential steps: template selection, target-template alignment, model construction, and model assessment. The template assignment process identifies proteins having known 3D structure for which the amino acid sequence is closely related to that of the unknown target structure. In the Molecular Operation Environment (MOE), a two step MOE-SearchPDB is performed to assign the template.¹²⁹ A Fast Scan that uses a generalized version of the Fasta methodology¹³⁰ is used to create an initial list of candidates. For further analysis the list includes any family containing at least one high-scoring sequence based on the determined expectation value (E-Value). The list is systematically reduced by comparing the calculated Z-Score value, which is an estimate of the statistical significance of an alignment score and represents the likelihood that sequences are related.

After defining the template protein(s), the protein sequences are aligned to identify the correspondences between the residues in the template and target sequences. The MOE-Align program aligns protein sequences using sequence-only information (residue identities), but also protein sequences using sequence-derived information (predicted secondary structure) and structure-based information in multiple sequence alignment.¹³¹ In a modified version of the original alignment methodology,¹³¹ alignments are processed by optimizing a function based on residue similarity scores and gap penalties imposed by introducing and extending gaps in one sequence with respect to another. For the alignment between two sequences, simple pairwise sequence alignment can be applied using 'dot-matrix', 'dynamic programming', and

'word' methods.¹³² These methods are useful to find the best-matching piecewise (local) or global alignments and they are often used in applications that do not require extreme precision. However, these methods have difficulty with low homology sequences where the number of repetitions differs in the two sequences to be aligned.

Multiple sequence alignment is commonly used to incorporate more than two sequences to be aligned at a time.¹³³ This alignment is very important and useful since biological inferences can be made by identifying conserved sequence regions within a group of evolutionarily related sequences, such as defining the catalytic active sites of enzymes in conjunction with structural and mechanistic information and building evolutionary relationships by making phylogenetic trees.¹³³ Furthermore, this alignment can give more reliable results than pairwise alignment. Due to the large computational cost in alignment of a large number of sequences, most multiple alignments are performed using heuristic methods rather than global optimization. In the MOE program this alignment consists of four steps; initial pairwise build-up, round-robin realignment, randomized iterative refinement, and structure-based realignment. In initial pairwise build-up, a progressive or tree-based method is used to calculate the initial estimate of the alignment. The progressive method, which is sensitive to the sequence order, aligns sequence 1 and 2, then aligns sequence 3 to the previous resulting alignment, and continues until all sequences have been processed.¹³⁴

In the tree-based method, which is sequence order insensitive but requires more computational time, all alignment scores between each pair of sequences are pre-calculated. The alignment is then built by aligning the sequence or sequences with the

highest pairwise score. The pairwise score between two groups is defined as the maximum of all scores between their respective sequences. After initial pairwise alignment is employed, a single round-robin series of realignment is used to refine the initial estimate in a round-robin realignment step. Re-alignment is performed with the remaining sequences after extraction of each sequence in succession from the global alignment. A series of realignments is employed in randomized iterative refinement where two groups are formed randomly from the group of previously aligned sequences, and a two-way alignment of the subset is processed. The resulting new alignment is accepted if it improves the alignment score, otherwise it is rejected, and then the process is repeated. In structure-based realignment, to consider the tertiary structures of sequences defined by the coordinates of the alpha carbons, a new similarity matrix is constructed using the relative alpha carbon coordinates after a multi-body superposition of structures. Sequences having these alpha carbons are re-aligned with this matrix, and then steps 1 through 3 are repeated with the structured sequences re-introduced as an indivisible unit among the unstructured sequences.¹³⁴

Given a template and an alignment, in the model construction step an all-atom 3D model for the protein sequence (target) is built and refined. Ligands, prosthetic groups or other molecular entities can be included in models, and they can also be built as multimers. Model building includes three steps: initial partial geometry specification, building the intermediate models, and choosing and refining the final model.¹³⁵ First, an initial partial geometry for each sequence is obtained from regions of template. If residue identity is conserved between the template and the target, all coordinates are

copied; otherwise, only backbone coordinates are transferred. In the second step, by applying a Boltzmann-weighted randomized modeling procedure with specialized logic for the proper handling of insertions and deletions, an ensemble of independent models of the target structure is built. Some lists of molecular data including 'indel', 'sidechain', and 'outgap' lists are taken for handling the missing atoms and residues from the Protein Data Bank and a rotamer library generated by systematic clustering of high-resolution PDB data. 'Indel' means the backbone fragments which can span insertions in the target sequence, 'sidechain' means sidechain conformations for residues with unmodeled sidechain atoms, and 'outgap' means a backbone fragment extending beyond the N-terminus or C-terminus of the template (usually omitted). After data collection, independent models are generated in the sequence of loop modeling, missing sidechain building, and constructing outgaps. After building intermediate models with all of the backbone segment and sidechain conformations, hydrogens are added, and the model is minimized to remove steric strains and scored. In the last step, the final model is chosen as the best-scoring model based on the following approaches; by averaging the position of all intermediate models, by using the electrostatic solvation energy, by using a knowledge-based residue packing quality function, and by measuring the effective atomic contact energy. Once the final model is selected, it is examined to verify the consistency of the model's stereochemistry with known crystal structures.

Homology models and 3D crystal structures are applicable in many research areas such as protein-protein interaction prediction, ligand docking, virtual screening, structure-based prediction of small molecules' metabolism and toxicity, and functional

annotation of genes. A significant limit of homology modeling is its low accuracy, particularly in loop regions on the protein surface, because these are normally more variable even between evolutionarily related proteins. However, the critical active site regions of the protein tend to be more highly conserved through closely related proteins, leading to them being more accurately modeled. Furthermore, with the aid of molecular dynamics simulations, particularly replica exchange methods developed by Simmering et al.,¹³⁶⁻¹³⁸ the bottleneck of homology modeling (prediction of loop regions) has become significantly diminished. This method has become a useful technique at the initial step of many research applications to predict 3D structures of targets and to make hypotheses for further research.

1.6.2 Flexible alignment^{139, 140}

The flexible alignment of small molecules is a very useful computational technique for deducing structural requirements of ligands for biological activity by pharmacophore elucidation¹⁴¹ and for pharmacophore generation to search a database for ligands that match the pharmacophore.¹⁴² The pharmacophore approach assumes that if two ligands have similar biological activity and bind in similar modes, then the bound conformations of the two ligands align well and inferences can be made about the nature of the receptor.¹³⁹ The binding mode of ligands can be derived from the alignment with the template ligand(s), for which binding modes are known. In addition, a collection of essential molecular features required for binding to a biological target can be derived from the alignment.

Flexible alignment aligns ligands, maximizing their overlap within a set of pre-determined features including a) the strain energy of each molecule is small, b) molecules have a similar shape, c) molecules have similar Log P (octanol/water) values, d) molecules have comparable molar refractivities, e) aromatic atoms overlap, f) hydrogen bond donors and acceptors overlap, g) acidic groups and basic groups overlap, h) atoms of similar partial charge overlap, and i) hydrophobic areas overlap. A collection of alignments along with a score that quantifies the quality of the alignment in terms of both internal strain and overlap of molecular features is obtained in this method. It has been found that steric features such as volume and aromatic groups and electronic features such as H-bond donors and acceptors are the most important, while other features including log P, molar refractivity, hydrophobicity, and exposed surface area do not significantly improve alignments.¹³⁹ Each feature can be weighted to emphasize one over the others.

The procedure of the flexible alignment consists of five steps to search the conformational space of each molecule and the alignment space of the collection for optimal alignments: Initialize, Perturb, Optimize, Compare, and Filter.¹³⁹ In the 'Initialize' step, the values of the adjustable parameters are set. In the 'Perturb' step, all rotatable bonds except terminal and ring bonds are set to random dihedral angles, and all molecules are oriented randomly by choosing three atoms randomly from each molecule, and are superposed. An objective function, $-kT \log \mathbf{F} + \mathbf{U}$, is minimized with respect to the coordinates of all of the atoms in the 'Optimize' step (\mathbf{F} is the similarity function, and \mathbf{U} is the average potential energy of the molecules). In the 'Compare' step,

the new configuration that has not been seen before is taken, and then the search is repeated until the iteration meets the predefined value. The list of configurations is pruned in the 'Filter' step by removing all configurations in which the average potential energy (of the alignment) is greater than the minimum observed average potential energy plus some predefined threshold.

1.6.3 Virtual screening and pharmacophore searching

Recently, the use of virtual screening (VS) has dramatically increased as a cost-effective complement to high-throughput screening (HTS) for novel lead generation in modern medicinal chemistry. In HTS, a large number of compounds must be submitted to experimental screening to obtain only a low number of hits. VS has the advantage of identifying a relatively small subset of compounds to be submitted to experimental screening. Successful VS depends on an understanding of the chemical and structural details of target active sites and target-ligand interactions. In parallel with experimental data such as X-ray and NMR structures and SAR (structure activity relationship) results, knowledge about pharmacophores, encoded into a 3D query that can be matched against a molecular database, has led to further utilization of VS. Three approaches are commonly employed in VS, depending on the presence or absence of target structures or ligands and their activities: structure-based VS (SBVS), ligand-based VS (LBVS), and pharmacophore-based VS (PBVS).

Structure-based virtual screening: When the structure of the biological target is available by crystal or NMR structure analysis or sophisticated homology modeling, SBVS

can be employed.^{143, 144} The procedure involves target and database preparation, docking a large number of molecules into the active site of the target, producing a predicted binding mode for each compound, scoring the binding affinity, and then selecting hits for experimental testing. In the database and target preparation step, an initial database having externally available compounds from chemical vendors and/or having readily synthesizable virtual compounds is screened by applying several physical and chemical filters to remove irrelevant compounds without the physical properties or chemical functionality consistent with most known drugs. Other filtering methods are further applied to exclude compounds containing specific chemical substructures associated with poor chemical stability or toxicity. Target structures can be prepared by adding hydrogens and charges and by determining the appropriate protonation states of ionizable residues in the docking site followed by relaxation to remove steric repulsion.

The next step of SBVS is docking each molecule in the prepared database into the active site of the prepared target. In this step, each possible ligand pose is scored and then the predicted binding mode is taken. Conformational flexibility of each molecule is considered usually by pre-computing all possible conformers of each molecule in a database followed by docking all calculated conformers. Flexibility of the target structure is also considered in docking methods, but since it increases complexity and computational cost, most screening by docking is done by fixing a protein target in its crystal structure conformation. Recently in some programs, protein mobility is taken into account by enabling the motion and relaxation of sidechains nearby a docked ligand or by using an ensemble of protein structures.¹¹⁹ After generating binding poses of each

compound, scoring functions are used to rank and select the best for the compound with respect to other. Binding affinity of compounds toward a target is predicted and a list of compounds is chosen for testing based upon the ranking order. Furthermore, post-analysis can be employed to minimize the number of false positives in the selected list and to increase the true hits by using consensus-scoring methods.

Ligand-based virtual screening: LBVS is frequently performed if only ligand information (structure and activity) is available. The similarity-based searching method, which includes fingerprint-based searching and descriptor-based searching, is the most commonly used LBVS method. The rationale for similarity-based searching is based on the Similar Property Principle, which states that structurally similar molecules are likely to exhibit similar properties. LBVS is a rather crude approach, but in cases where there is just a single bioactive lead molecule and no evidence about which parts are responsible for the observed activity, LBVS can serve as a precursor and complement to more sophisticated approaches.^{145, 146} The steps of similarity searching involve calculating the similarity between the known target (reference) structure and molecules in a database, ranking the molecules, and then testing the top-ranked molecules. 2D fingerprints including SMILES or BIT STRINGS, which encode the presence (1) or absence (0) of substructural fragments, are applied to annotate compounds in a database for the measurement of structural similarity with a target structure. Furthermore, a vast number of compounds in a database can be grouped on the basis of their annotation. Descriptors based on physicochemical properties and topological index are also used in

similarity searching as representors of molecules using a fixed-length string of real numbers (or dataprint).

Pharmacophore-based virtual screening: A pharmacophore is a set of steric and electrostatic features of a ligand that are necessary to recognize the binding site of a target and that are closely related to its biological activity. PBVS is a screening technique to identify novel lead compounds that share features with the pharmacophore model (or query). The procedure of PBVS typically consists of four steps: generating the pharmacophore query, pre-treating the compound library, screening, and selecting hits or refining the original query by post-analysis.¹⁴⁷

Pharmacophore-based VS starts with generating pharmacophoric structural features (the pharmacophore model) represented as labeled points in space by analyzing a set of reference ligands or, if available, the 3D structure of a target. The commonly used structural features are hydrogen bond acceptor (Acc), hydrogen bond donor (Don), cations (Cat), anions (Ani), aromatic center (Aro), and hydrophobic areas (Hyd). In addition to these features, the direction of a hydrogen bond, planar preference of an aromatic ring, and volume constraints can also be specified in a pharmacophore query. The pharmacophore can be recognized automatically from a set of bioactive and bioinactive compounds in the MOE/Pharmacophore Elucidation program. Furthermore, by using the Pharmacophore Query Editor in MOE, a pharmacophore can be constructed interactively, by a process in which users can adjust position tolerance radius, and assign features as “essential” or “optional” to specify pharmacophore mapping.¹⁴⁸ Logic terms including AND, OR, and NOT can be used to define a feature, for example a

feature marked “(Acc|Don)!Ani” means “H-bond acceptor or H-bond donor but not anion”. The success of interactive building of a pharmacophore can be enhanced by an accumulated knowledge on a target as well as a series of bioactive/inactive ligands.

Each compound in a database is assigned an annotation, encoding the structural features in that compound. Flexibility of molecules can be considered during screening by creating a structural ensemble from a seed molecule in a database. Multiple conformations of each molecule are enumerated by 2D-to-3D conversion followed by 3D structure calculation. In addition to ligand flexibility, inherent flexibility of a protein can be taken into account by uniformly adjusting the size of all excluded volumes or by developing a dynamic pharmacophore model from a result of MD simulation. All possible conformations of each compound in a database are screened through the built pharmacophore model to find biologically active compounds. Hits are submitted to experimental screening, and then with the knowledge of hits and their biological activity, the pharmacophore model is further refined for the next search.

As compared to LBVS, the strength of PBVS is that it is capable of finding compounds with similar experimental results to a target ligand but with different chemical scaffolds. This merit is reliable because the definition of pharmacophoric features is conceptual and abstract rather than atomic (in LBVS). Consequently, different functional groups can be mapped into the same space of a predefined feature. Therefore, a pharmacophore model can serve as a bridge to reach unidentified diverse small molecules from already known ligands. Major concerns in SBVS are the accuracy of scoring functions for guiding docking and predicting the correct binding mode of ligands

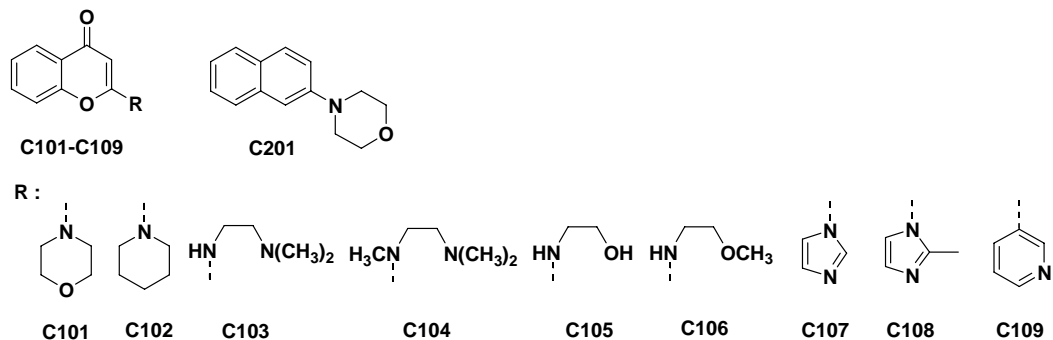
and their binding free energies. These difficulties are simplified in PBVS by introducing a tolerance radius for each pharmacophoric feature to handle flexibility. Some other molecular characteristics such as physico-chemical, and ADMET properties are not accounted for in pharmacophore models, thus the analysis of these properties needs to be performed either prior to or after searching for further development of hits.

Chapter 2. Defining a lead compound and its biological effects on mTOR signaling

2.1 LY294002 analogs

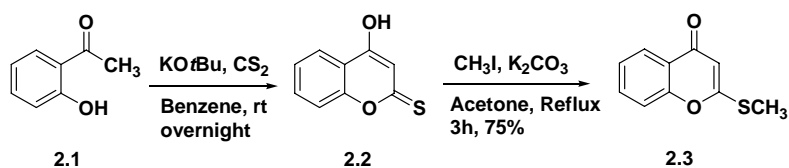
LY294002 (Figure 1.1), which is a synthetic compound developed by Eli Lilly as an inhibitor of PI3Kinase, was used as a lead compound for our initial study because it also inhibits mTOR. The potency of this inhibitor toward PI3Kinase and mTOR is similar; IC₅₀ values of LY294002 are 1.4 μM and 2.5 μM toward PI3Kα and mTOR, respectively.^{149, 150} It was reported that the compound without the phenyl ring attached to the 8-position of the chromone ring is 3-fold less active against PI3Kinase than LY294002.¹⁴⁹ Furthermore, the morpholine ring, particularly the oxygen in the ring, attached to the 2-position of the chromone ring was found to be necessary for inhibition of PI3Kinase.¹⁴⁹ Inhibitors **C103 – C106** having other flexible amine groups rather than a morpholine ring at the 2-position of the chromone ring and compound **C102** were proposed to further explore variations on the morpholine moiety. Compounds **C107 - C109** having piperidine, imidazole, 2-methyl imidazole, and pyridine rings at the 2-position of the chromone ring were suggested by computer modeling to place the nitrogen atoms in position to hydrogen bond to the backbone N-H that forms an H-bond to the morpholine oxygen of LY294002. Furthermore, **C201**, 4-naphthalen-2-yl-morpholine, was proposed to examine the importance of the carbonyl oxygen of the chromone ring toward mTOR.

Figure 2.1 The initially proposed compounds to explore the effects of a morpholine ring, imidazole, pyridine, acyclic functional groups, and carbonyl oxygen of chromone ring toward mTOR



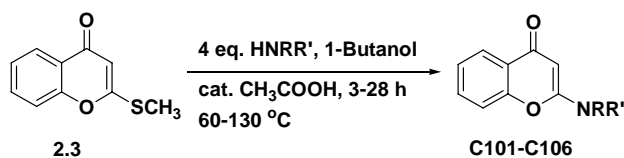
The synthesis of 2-methylthio-chromone (**2.3**) started with the condensation reaction of 2'-hydroxy acetophenone (**2.1**) with carbon disulfide and potassium t-butoxide, leading to compound **2.2**.^{149, 151} The yellow solid was precipitated by addition of dilute acid (H₂SO₄), and was washed with petroleum ether to give a pale yellow solid. **2.2** was converted to 2-methylthio-chromone (**2.3**) by potassium carbonate and iodomethane at reflux. The resulting product (**2.3**) was recrystallized to give needle-like crystals.

Scheme 2.1 Synthesis of 2-methylthio-chromone (**2.3**)



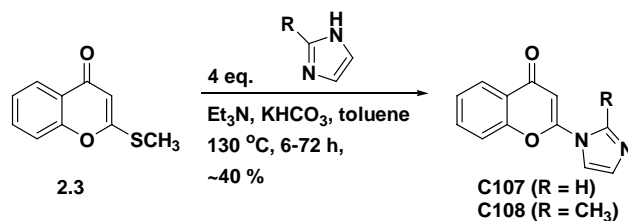
Various primary and secondary amine groups including morpholine, piperidine, N,N-dimethylethylenediamine, N,N,N'-trimethylethylenediamine, ethanolamine, and 2-methoxyethylamine were attached to the 2-position of the chromone ring by the acid-catalyzed addition-elimination reaction (Scheme 2.2). For secondary amines, high temperature (120 °C) and long reaction time (up to 6 hours) were needed, while 60 °C for 3 hours or less was sufficient for primary amines.

Scheme 2.2 Acid catalyzed addition-elimination reaction for attaching various amine groups

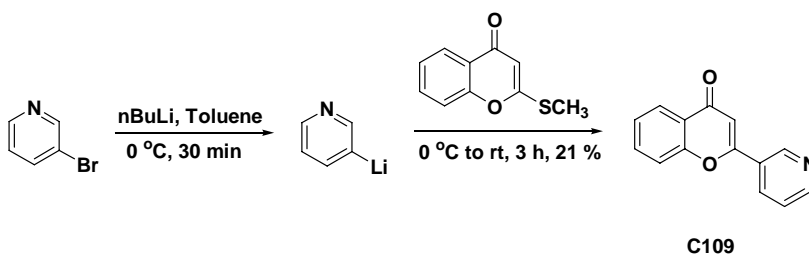


Imidazole and 2-methyl imidazole groups were introduced by a base catalyzed addition-elimination reaction (Scheme 2.3). The methyl thiol group was also substituted with pyridine (the 3-position of pyridine was attached to the 2-position of the chromone ring) by metal-exchange of 3-bromopyridine by n-BuLi followed by an addition-elimination reaction (Scheme 2.4).

Scheme 2.3 Base catalyzed addition-elimination reaction for attaching imidazole and 2-methyl imidazole groups

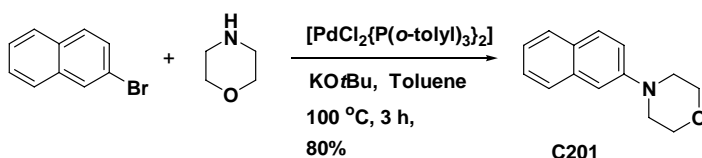


Scheme 2.4 Metal-exchange of 3-bromopyridine by nBuLi to attach to the 2-position of the chromone ring



A Buchwald-Hartwig reaction¹⁵²⁻¹⁵⁴ was applied for connecting the morpholine ring to the 2-position of naphthalene to examine the effect of the carbonyl group in the chromone ring toward PI3Kinase and mTOR (Scheme 2.5).

Scheme 2.5 Synthesis of **C201**

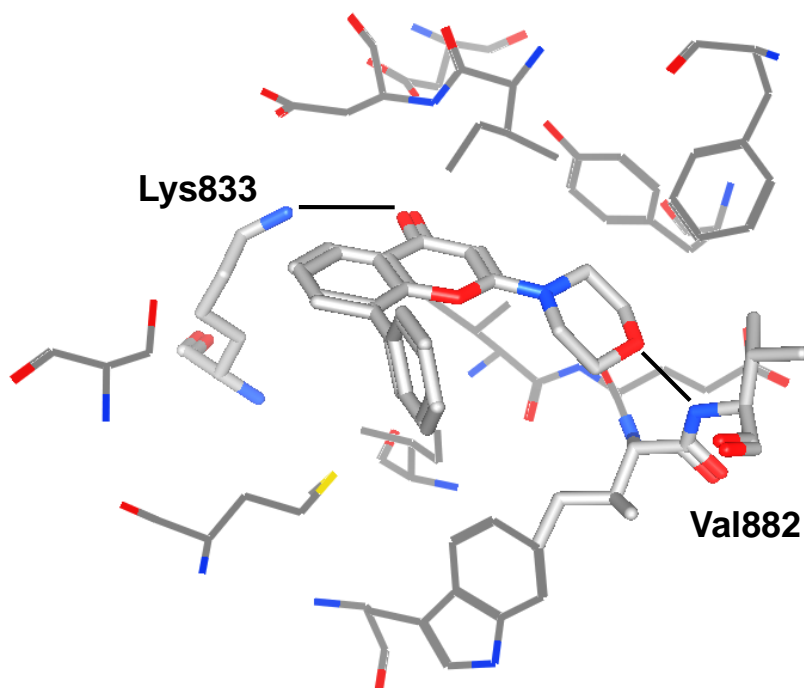


All of the compounds (**C101-C109** and **C201**) were tested against PI3Kinase and mTOR by Dr. Lisa Ballou and Ms. Elzbieta Selinger in Prof. Richard Lin's lab in the Stony

Brook University School of Medicine. Interestingly, all of the compounds having the morpholine ring replaced with an acyclic amine showed almost no inhibition (less than 10% at 10 μ M) against PI3Kinase as well as mTOR. This result suggests that flexible morpholine analogs decrease the inhibition against PI3Kinase and mTOR due to the increased degree of freedom. In addition, the loss of the carbonyl oxygen of the chromone ring and oxygen in the morpholine ring resulted in complete loss of inhibition, with both **C108** and **C109** exhibiting <10% inhibition of mTOR at 10 μ M.

These results can be rationalized from the crystal structure of PI3Kinase with LY294002.^{155, 156} In this structure, it can be seen that the major binding components of LY294002 toward PI3Kinase are two hydrogen bond interactions: one between the carbonyl oxygen of the chromone ring and the ammonium ion of Lys833, and another between the oxygen in the morpholine ring and the amide backbone N-H of Val882 (Figure 2.2). Abraham has also reported that the lysine and the valine of those H-bonds are highly conserved in the phosphatidylinositol kinase related kinase (PIKK) family including PI3Kinase, mTOR, DNA-PK (DNA-dependant protein kinase), ATM (ataxia telangiectasia-mutated), and ATR (ATM and Rad3-related).¹⁵⁷ Therefore, we can conclude that the carbonyl oxygen in the chromone ring and the oxygen in the morpholine ring are critical for the inhibition of PI3Kinase as well as mTOR. In addition, the rigidity of the morpholine ring appears necessary for tight binding to the active site of PI3Kinase and mTOR.

Figure 2.2 The major interactions of LY294002 in the active site of PI3K γ . The residues within 4.5 Å from LY294002 in the crystal structure (PDB ID : 1E7V) are presented. The major interactions of LY294002 and amino acids are marked by black lines. The amino acids of Lys833 and Val882 and LY294002 are shown as tube structures, and the other amino acids in the active site are shown as line drawings. For clarity, hydrogens are omitted.

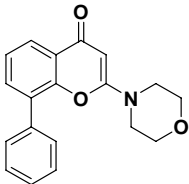
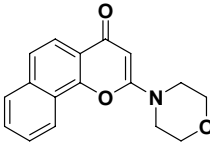
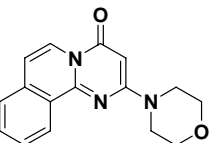
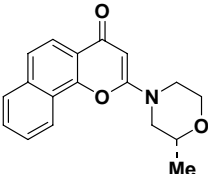


2.2 A selective inhibitor, C401

While this project was underway, the synthetic compound 2-(morpholine-1-yl)pyrimido[2,1-*a*]isoquinoline-4-one (**C401** in Figure 1.1) was reported as a DNA-PK inhibitor by Griffin *et al.*^{150, 158} More than 100 compounds were synthesized and tested against DNA-PK in that paper. Among them four compounds were selected and tested against enzymes in the PIKK family. As shown in Table 2.1 with compound III (**C401** in Figure 1.1) inhibits mTOR moderately but not PI3Kinase with IC₅₀ values of 5.2 μM and more than 100 μM against mTOR and PI3Kinase, respectively. Interestingly, the overall

shape of compounds **II** and **III** are very similar (benzochromone ring vs. pyrimidoisoquinoline ring), but the inhibition properties are totally different. Compound **II** shows moderate inhibition against both PI3Kinase and mTOR, but compound **III** only inhibits mTOR (in red in Table 2.1).

Table 2.1 Bioassay of four DNA-PK inhibitors against enzymes in the PIKK family. This table is adopted from the original reference and compound names are modified.

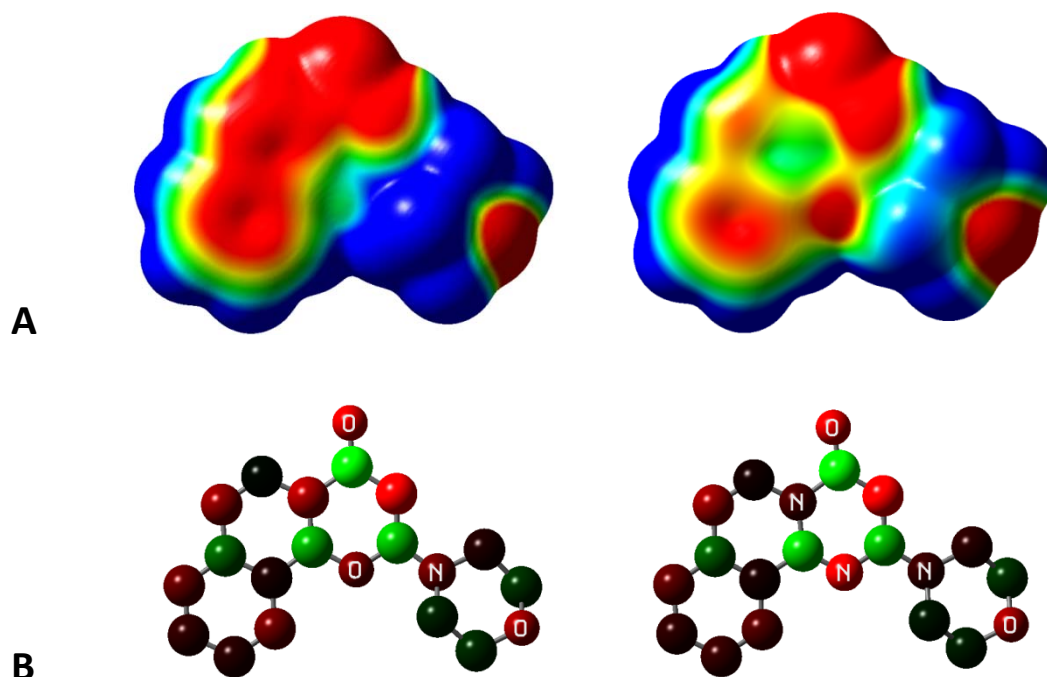
PIKK	I	II	III	IV
				
DNA-PK	1.5±0.2	0.23±0.01	0.28±0.02	0.19±0.01
PI3Kα	2.3±0.8	13±3.0	>100	2.4±0.7
ATM	>100	>100	>100	>100
ATR	>100	>100	>100	>100
mTOR	2.5±0.2	6.4±0.1	5.3±0.8	4.8±1.4

The reason for the loss of inhibition against PI3Kinase in compound **III** (**C401**) is not clear, but the altered electrostatic potential due to the presence of nitrogen atoms replacing oxygen and carbon atoms accounts for this phenomenon. In addition, decreased hydrogen bonding ability of the carbonyl oxygen in the pyrimido ring, caused by the heteroatom substitution, may also contribute.

To examine the electrostatic difference between compounds **II** and **III**, density functional theory (DFT) calculations^{159, 160} were performed with Gaussian 03W¹⁶¹ software. The initial structures of compounds **II** and **III** were built using GaussView.¹⁶²

The structures were initially optimized at the RHF/6-31G(d) level¹⁶³, and further optimized at B3LYP/6-311G(d).^{164, 165} Frequency calculations were performed to confirm the stationary point of each structure.¹⁶⁶ Total density of each compound was calculated by the 'cube' utility in GaussView to measure the density. Electrostatic potential (ESP)¹⁶⁷ of each compound was mapped to the calculated total density (Figure 2.3).

Figure 2.3 Electrostatic potential (up) and ESP charges (down) of compounds II (left) and III (right). Red, green, and blue colors in ESP represent negative, neutral, and positive potentials, respectively. Red, black, and green colors in ESP charges represent negative, neutral, and positive charges, respectively. For clarity hydrogen atoms are omitted and carbon atoms are not labeled.



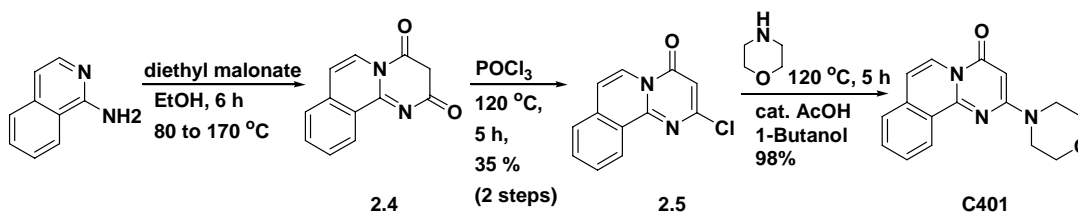
The major difference in electrostatic potential between compounds **II** and **III** is the negative potential in the ring fragments. The negative potential in compound **II** is delocalized through the benzochromenone ring, but it is localized on the pyrimido-isoquinoline ring of compound **III**. Charges were calculated by fitting to the electrostatic potential at points according to the Merz-Singh-Kollman scheme.^{168, 169} The charges of N1 and N5 of compound **III** are -0.61 and -0.18, while those of the corresponding O1 and C5 of compound **II** are -0.31 and -0.43, respectively. These values imply that negative charges are localized to N1 of compound **III**, while those are well distributed through the ring fragment, or slightly localized to C5 of compound **II**.

It is still not clear why compound **III** has selectivity between mTOR and PI3K, but compound **II** has no selectivity. As mentioned, the overall shape and pharmacophore of these compounds are the same, as the carbonyl oxygen can interact with Lys833 of PI3K and the morpholine oxygen can interact with Val882 (Figure 2.2). These two residues are highly conserved in PIKK family enzymes. Somehow the different ring systems having N1 and N5 in compound **III** vs. O1 and C5 in compound **II** leads to different properties, resulting in different inhibition profiles.

C401 was synthesized according to the reported¹⁵⁸ procedure to verify its selectivity between mTOR and PI3Kinase *in vitro* and to test the cellular effect of mTOR inhibition. From the reaction of 2-aminoisoquinoline with diethyl malonate, the pyrimido-[2,1-*a*]isoquinoline template (**2.4**) was synthesized, and subsequently converted into the 2-chloro derivative (**2.5**) by reaction with phosphorus oxychloride.

The morpholine group at the 2-position was introduced by displacement of chloride, as shown in Scheme 2.6.

Scheme 2.6 Synthesis of **C401**



2.3 Effect of **C401** on mTOR and PI3K activities *in vitro*

Dr. Ballou and Ms. Selinger, in Prof. Richard Lin's lab, carried out *In vitro* kinase assays were performed to confirm that **C401** selectively inhibits mTOR over PI3K. **C401** was shown to inhibit immunoprecipitated epitope-tagged mTOR and endogenous mTOR in Raptor immunoprecipitates, giving results consistent with those of Griffin *et al.* In both cases, 5 μM or 10 μM **C401** gave inhibition of 67% or 78%, respectively (Figure 2.4). However, at these concentrations **C401** showed almost no inhibition of the p110 α /p85 α or p110 β /p85 α PI3K complexes as shown in dose response curves (closed symbols in Figure 2.5). By contrast, LY294002 gave almost complete inhibition of both PI3Ks at these concentrations (open symbols in Figure 2.5). Inhibition of the protein kinase activity of p110 α was also tested by examining autophosphorylation of p85 α in the PI3K complex. There was no effect on this autophosphorylation by **C401** at 25 μM , while

LY294002 inhibited this reaction at 5 μM (Figure 2.6). Therefore, these results confirm that **C401** exhibits selective inhibition toward mTOR over PI3Kinase, in contrast to non-selective inhibition by LY294002.

Figure 2.4 Effect of **C401** on mTOR activities *in vitro*. mTOR kinase activity in AU1 or Raptor immunoprecipitates was assayed in the presence of the indicated concentrations (in μM) of compound **401**.



Figure 2.5 Effect of **C401** and LY294002 on PI3Kinase activities *in vitro*. PI3K activity of p110 α /p85 α (circles) or p110 β /p85 α (squares) was assayed in the presence of increasing concentrations of **C401** (closed symbols) or LY294002 (open symbols).

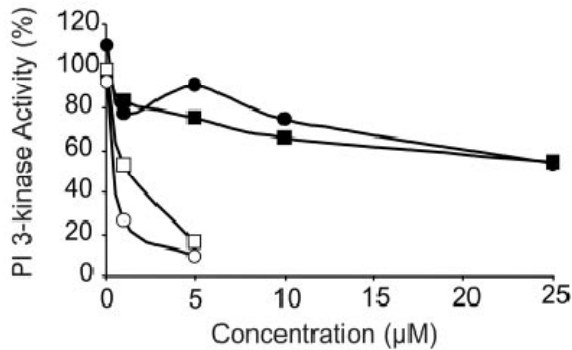
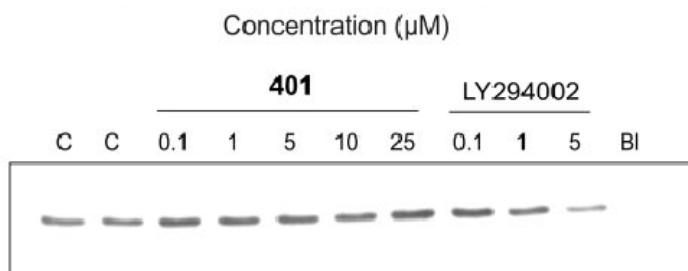


Figure 2.6 Effect of **C401** and LY294002 on autophosphorylation of the p85 α subunit of p110 α /p85 α . Autophosphorylation of the p85 α subunit of p110 α /p85 α was assessed in the presence of the indicated concentrations (in μ M) of **C401** and LY294002. C, vehicle control; BI, enzyme blank.



There are more than 300 different protein kinases involved in cell signaling that use adenosine triphosphate (ATP) as a substrate. Therefore, we examined whether compound **C401** inhibits other protein kinases. **C401** was tested against 40 different protein kinases at 5 μ M concentration. At this concentration most of these enzymes were inhibited less than 20% by **C401**, except MAPKAPK2 (MAP kinase-activated protein kinase 2), PIM1, and STK6 (Serine/threonine Kinase 6, or Aurora A) which showed inhibition of 40%, 44%, and 44%, respectively (in red in Table 2.2). While these inhibition values are higher than those of the other kinases, these protein kinases are not directly related to the PI3K/mTOR signaling pathway, and thus may not interfere with studies of cellular effects of mTOR inhibition.

Table 2.2 Inhibition of protein kinases by **C401**. Protein kinases were assayed with 5 μ M **C401** and 100 μ M ATP (SelectScreen™ Profiling Service, Invitrogen). Values show an average of duplicate measurements.

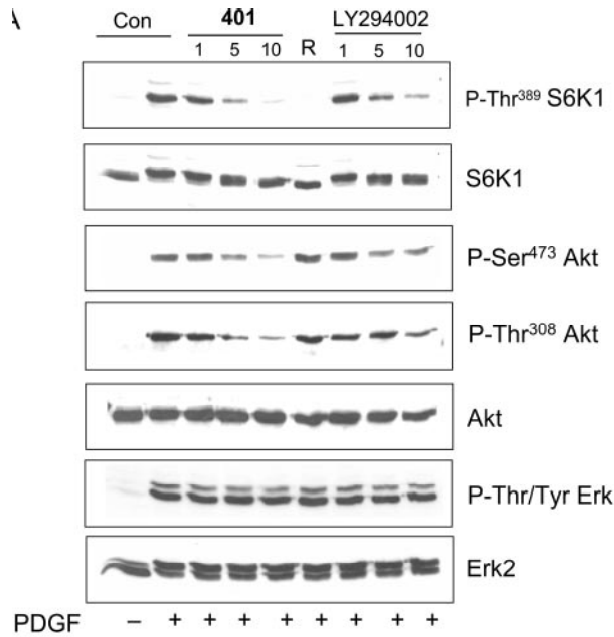
Kinase	%inhibition	Kinase	%inhibition
ABL1	-5	LCK	-3
AKT1 (PKB alpha)	5	MAP2K1 (MEK1)	-8
BTK	9	MAP4K4 (HGK)	3
CDK1/cyclin B	3	MAPK14 (p38 alpha)	17
CHEK1 (CHK1)	-9	MAPK3 (ERK1)	-3
CSNK1G2 (CK1 gamma 2)	2	MAPKAPK2	40
CSNK2A1 (CK2 alpha 1)	3	MET (cMet)	19
DYRK3	5	NTRK1 (TRKA)	-17
EGFR (ErbB1)	-3	PDGFRB (PDGFR beta)	-4
EPHA2	-13	PHKG2	-6
ERBB2 (HER2)	3	PIM1	44
FGFR1	0	PRKACA (PKA)	-11
FLT3	36	PRKCB1 (PKC beta I)	8
GSK3B (GSK3 beta)	0	RET	-4
IGF1R	-8	ROCK1	13
INSR	-3	RPS6KA3 (RSK2)	7
IRAK4	-5	SRC	-14
JAK3	2	STK6 (Aurora A)	44
KDR (VEGFR2)	0	SYK	14
KIT	13	TEK (Tie2)	12

2.4 Effect of C401 on mTOR signaling in cancer cells

S6K1 and Akt are two effectors of mTOR signaling (Figure 1.3). Thr389 in the hydrophobic motif of S6K1 is phosphorylated by mTORC1. Similarly, mTORC2 phosphorylates Akt at Ser473 in the hydrophobic motif and facilitates PDK1 phosphorylation of Thr308 in the T loop.²⁷ Therefore, examining the phosphorylation state of S6K1 Thr389 and Akt Ser473 is an efficient way for measuring intracellular mTORC1 and mTORC2 activity, respectively.

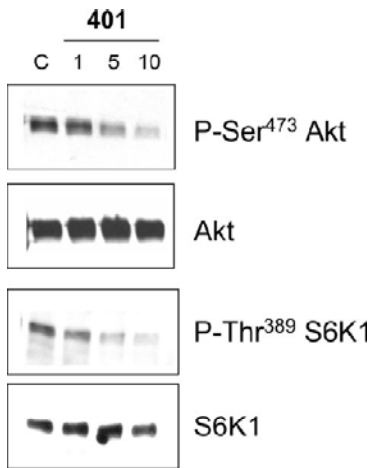
Serum-starved Rat-1 fibroblasts were pretreated with **C401**, LY294002, and rapamycin and then stimulated with PDGF to test the effect of **C401** on growth factor-activated mTOR signaling. The phosphorylation of S6K1 and Akt was analyzed on Western blots probed with antibodies that recognize S6K1 phospho-Thr389 or Akt phospho-Ser473. As predicted, **C401** decreased the phosphorylation of both sites (Thr389 S6K1 and Ser473 Akt). LY294002 also showed similar ability for targeting mTOR by reducing the phosphorylation of both sites (Figure 2.7). However, rapamycin affected only the mTORC1 site (Thr389 S6K1), and there was no decreased phosphorylation of Ser473 Akt by rapamycin.

Figure 2.7 Effect of **C401** on mTOR signaling in Rat-1 cells. The indicated concentrations of **C401** or LY294002 are in μM , and (R) represents 10 nM rapamycin.



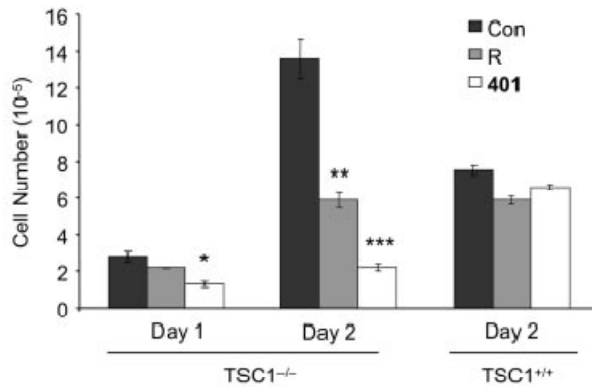
Since **C401** is also a potent inhibitor of DNA-PK ($\text{IC}_{50} = 0.28 \mu\text{M}$), it is possible that the inhibition of DNA-PK directly or indirectly gives effects on Akt and S6K1 phosphorylation. This possibility was tested in M059J glioma cells, which lack DNA-PK. The phosphorylation of Ser473 Akt and Thr389 S6K1 were decreased at the same doses that were effective in Rat-1 cells by the treatment of M059J cells with **C401** (Figure 2.8). Therefore, the inhibitory effect of **C401** on phosphorylation of these mTOR sites is not due to DNA-PK inhibition.

Figure 2.8 Effect of **C401** on mTOR signaling in M059J glioblastoma cells. The indicated concentrations of **C401** are in μM .



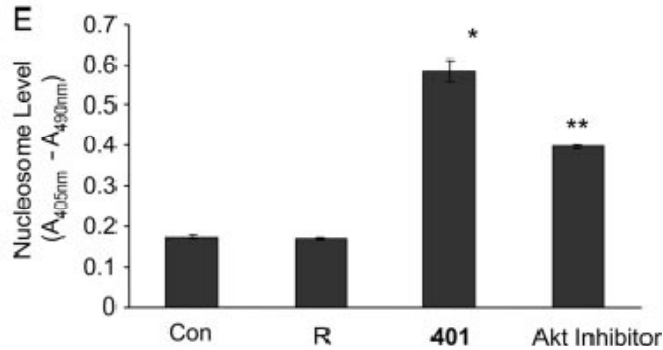
We also examined whether rapamycin and **C401** differentially affect the proliferation of TSC1^{-/-} cells by measuring cell growth and apoptosis in mouse embryo fibroblasts (MEFs) derived from TSC1-null mice. The cell number was slightly decreased after treatment with rapamycin for 1 day, as compared to the control cells (gray bars in Figure 2.9), and a moderately decreased cell number was found after 2 days. By contrast, proliferation was strongly inhibited in cells exposed to **C401** for 1 day (54%) or 2 days (84%) (white bars in Figure 2.9). This growth inhibition by **C401** is not caused by general toxicity, as there was only a slight decrease in cell number in TSC1^{+/+} MEFs treated for 2 days in the presence of the drugs (Figure 2.9).

Figure 2.9 Effect of **C401** on the proliferation of TSC1^{-/-} MEFs. Cells were treated with 0.1% dimethyl sulfoxide (**Con**), 100 nM rapamycin (**R**), or 10 μM **C401**. * represents a statistically significant difference between **C401** and control on day 1. ** and *** represent statistically significant differences between rapamycin and control and **C401** and control, respectively, on day 2.



The level of nucleosomes in the cytoplasm of drug-treated TSC1^{-/-} MEFs was measured to determine whether apoptosis causes the decreased cell number induced by **C401**. Whereas the nucleosome level was not changed in cells treated by rapamycin, treatment with **C401** significantly increased apoptosis (Figure 2.10). An Akt1/2 inhibitor also induced an increase in apoptosis of TSC1^{-/-} MEFs, suggesting that the cytotoxic effect of **C401** might be due in part to suppression of mTORC2/Akt signaling.

Figure 2.10 Effect of **C401** on the cytoplasmic nucleosome level, or apoptosis. The cytoplasmic nucleosome level was determined as a measure of apoptosis. Akt inhibitor was used at 5 μ M. * and ** shows statistically significant differences between **C401** and control and Akt inhibitor and control, respectively.



All of these results prove our initial hypothesis that inhibition of mTOR kinase activity by a small molecule inhibitor is more effective than rapamycin at killing $TSC1^{-/-}$ MEFs that exhibit hyperactivated mTOR signaling. However, the inhibition of mTOR by **C401** is moderate, and at high concentration (25 μ M) **C401** also inhibits PI3Kinase (~50%). Therefore, it is important to optimize **C401** to have more potency against mTOR without inhibiting PI3Kinase even at high concentration.

2.5 Computational and experimental details

The Gaussian 03W program package (Revision-C.02) was used for optimization and frequency calculation of geometries. Input files were generated using GaussView 3.09. This program was also used to generate Cubes for measuring total density and electrostatic potential surfaces and to visualize EPS atomic charges.

Geometry optimization and frequency calculation: The initial structures of compounds **II** and **III** were built using GaussView. The geometries were initially optimized at the RHF/6-31G(d) level. The stationary point of each optimized structure was confirmed by frequency calculation, and no imaginary frequency was found for either optimized structure. The geometries were further optimized at the B3LYP/6-31G(d) followed by the B3LYP/6-311G(d) level. Frequency calculations of the final optimized geometries were performed at the B3LYP/6-311G(d) level, and no imaginary frequency was obtained. The 'Formchk' utility, which converts the data in a Gaussian checkpoint file into a formatted form for visualization, were employed to the final checkpoint files of compound **II** and **III**. Two formatted checkpoint files were obtained (C400-dft.fch and C401-dft.fch of compound **II** and **III**, respectively).

Generating cubes and surfaces: Cube for total SCF density of compound **II** was generated from the formatted checkpoint file in GaussView and saved as C400-dft.cube. Electron density from total SCF density was obtained by setting the isovalue at the default value (0.0004). Electrostatic potential was mapped to the total density. Mapped-electrostatic potential of compound **III** was generated by performing the same procedure with C401-dft.fch file. The maximum and minimum values of each compound

for visualization were changed to 1.0E-2 and -1.0E-2 from the automatically generated values because with automatically generated values the difference of ESP between compound **II** and compound **III** cannot be examined clearly.

Calculation of electrostatic potential-derived charges: To obtain charges fit to the electrostatic potential at each atomic point, the final generated checkpoint file of compound **II** was employed and charge calculation was performed. The same method (B3LYP) and same basis set (6-311G(d)) were applied. The ESP charge type was loaded to the structure by coloring atoms by ESP charges. The ESP charges of compound **III** was calculated by the same procedure. The charge range for coloring was slightly changed to -0.70 to 0.70 from the automatically generated ranges to compare the difference between compound **II** and compound **III** directly.

4-Hydroxy-2-thio-1-benzopyran (2.2): To a suspension of potassium *tert*-butoxide (7.0 g, 62 mmole) in benzene (40 mL) at room temperature was slowly added a solution of 2'-hydroxyacetophenone (1.36 g, 10 mmole) and carbon disulfide (1.82 g, 24 mmol) in benzene (20 mL). The yellow viscous mixture was stirred overnight, and then poured into water (300 mL). The organic layer was removed and the aqueous phase was washed with ether (100 mL \times 2). The aqueous phase was cooled and acidified slowly with 10% ice-cold sulfuric acid and stirred. The precipitate was collected by filtration and washed well with petroleum ether to give **(2.2)** as a yellow solid (0.94 g, 5.3 mmol, 53% yield); $^1\text{H-NMR}$ (300 MHz, DMSO) δ , 7.89 (d, 1 H, $J = 7.4$ Hz), 7.74 (t, 1 H, $J = 7.8$ Hz), 7.56 (d, 1 H, $J = 9.0$ Hz), 7.44 (t, 1 H, $J = 7.6$ Hz), 6.66 (s, 1 H), 3.42 (s, 1 H).

2-Methylthio-1-benzopyran-4-one (2.3): To a stirred suspension of $K_2CO_3 \cdot 1\frac{1}{2}H_2O$ (1.90 g, 11.5 mmol) in acetone (10 ml) was added compound **2.2** (0.95 g, 5.3 mmol) in acetone (5 ml) and 1.5 mL of CH_3I . The bath temperature was set to 75 to 80 °C to achieve reflux. After 3 hours, the reaction mixture was filtered while hot. The filtrate was evaporated and 50 mL of chloroform was added. The resulting solution was washed with water (2 × 20 ml) and brine (30 ml). It was dried with $MgSO_4$ followed by evaporation to a solid. This solid was recrystallized with toluene and petroleum ether. The transparent needle like crystals (75% yield) were collected; TLC R_f = 0.47 (Hexane/EtOAc 1:2); mp 110 °C (ref, 109.5 – 110.5 °C); 1H -NMR (400 MHz, $CDCl_3$) δ , 8.15 (dt, 1 H, J = 7.6 Hz, 0.8 Hz), 7.63-7.59 (m, 1 H), 7.39-7.35 (m, 2 H), 6.20 (s, 1 H), 2.53 (s, 3 H); ^{13}C -NMR (100 MHz, $CDCl_3$) δ , 175.63, 169.92, 156.73, 133.32, 125.80, 125.25, 123.47, 117.18, 107.38, 13.75.

2-(Morpholin-4-yl)-4H-1-benzopyran-4-one (C101)¹⁷⁰: To a stirred solution of compound **2.3** (0.34 g, 1.8 mmol) in 1-butanol (10 ml) was added morpholine (0.25 ml, ca. 3 mmol) in 1-butanol (5 ml) and a catalytic amount of acetic acid (2 drops). The reaction mixture heated at 130 °C. After 12 hours the mixture was evaporated to a solid and the product was recrystallized with ethyl acetate. The product was further purified with column chromatography by eluting with chloroform/ethyl acetate (1/1); TLC R_f = 0.06 (Hexane/EtOAc 1:2); 1H -NMR and ^{13}C -NMR are consistent with those in the literature; 1H -NMR (300 MHz, $CDCl_3$) δ , 8.10 (dd, 1 H, J = 7.8 Hz, 1.6 Hz), 7.51 (td, 1 H, J =

7.8 Hz, 1.3 Hz), 7.32-7.23 (m, 2 H), 5.45 (s, 1 H), 3.78 (t, 4 H, $J = 5.0$ Hz), 3.46 (t, 4 H, $J = 5.0$ Hz); ^{13}C -NMR (100 MHz, CDCl_3) δ , 177.06, 162.54, 153.55, 132.23, 125.40, 124.70, 122.77, 116.22, 87.16, 65.83, 44.52.

2-(Piperidin-1-yl)-1-benzopyran-4-one (C102): To a stirred solution of compound **2.3** (0.20 g, 1.1 mmol) in 1-butanol (7 ml) was added piperidine (0.20 ml) in 1-butanol (3 ml) and a catalytic amount of acetic acid (3 drops). The reaction mixture was heated at 120 °C. The reaction was stopped after 4 hours, though TLC still showed some unreacted **2.3**. The solvent was removed by rotary evaporation. The product mixture was redissolved in chloroform (50 ml) and washed with water (20 mL \times 2) and dried over MgSO_4 . The product was purified by column chromatography, eluting with chloroform and ethyl acetate (1/1) to give the title compound (0.22 g, 0.96 mmole, 87% yield) as a colorless solid; ^1H -NMR (300 MHz, CDCl_3) δ , 8.11 (dd, 1 H, $J = 7.8$ Hz, 1.2 Hz), 7.49 (t, 1 H, $J = 8.6$ Hz), 7.31-7.23 (m, 2 H), 5.50 (s, 1 H), 3.48 (s, 4 H), 1.67 (s, 6 H); ^{13}C -NMR (100 MHz, CDCl_3) δ , 176.85, 162.24, 153.63, 131.86, 125.33, 124.42, 116.14, 86.69, 85.78, 45.83, 25.11, 24.01.

2-(2-Dimethylamino-ethylamino)-1-benzopyran-4-one (C103): To a stirred solution of compound **2.3** (0.20 g, 1.0 mmol) in 1-butanol (7 ml) was added *N,N*-dimethylethylenediamine (1.0 ml) in 1-butanol (3 ml) and a catalytic amount of acetic acid (2 drops). The reaction mixture was heated at 70 °C. After 3 hours the reaction was

stopped and the mixture was evaporated. The sticky product mixture was dissolved in water (50 ml) and dilute aqueous HCl was added. The resulting solution was extracted with ether (20 ml). The water layer was basified with aqueous NaOH and the product mixture was extracted with chloroform (50 × 2 ml). The resulting solution was dried over MgSO₄ and evaporated. The product was further purified by column chromatography on silica gel to give the title compound (0.22 g, 0.95 mmol, 95% yield); ¹H-NMR (300 MHz, CDCl₃) δ, 8.02 (dd, 1 H, *J* = 7.8 Hz, 1.5 Hz), 7.42 (td, 1 H, *J* = 7.6 Hz, 1.3 Hz), 7.20 (td, 1 H, *J* = 7.6 Hz, 0.3 Hz), 7.11 (d, 1 H, *J* = 7.8 Hz), 6.36 (s, 1 H), 5.30 (s, 1 H), 3.21 (qd, 2 H, *J* = 10.5 Hz, 5.4 Hz), 2.53 (t, 2 H, *J* = 6.0 Hz), 2.22 (s, 6 H); ¹³C-NMR (100 MHz, CDCl₃) δ, 176.62, 163.17, 153.56, 131.83, 125.27, 124.19, 122.99, 116.04, 85.73, 85.21, 56.56, 44.82, 38.69.

2-[(2-Dimethylamino-ethyl)-methyl-amino]-1-benzopyran-4-one (C104): The procedure was the same as that of **C103** except the temperature was 110 °C and reaction time was 28 h. The yield of this product is 48% (0.12 g); ¹H-NMR (300 MHz, CDCl₃) δ, 8.09 (dd, 1 H, *J* = 8.0 Hz, 1.6 Hz), 7.47 (td, 1 H, *J* = 7.9 Hz, 1.3 Hz), 7.29-7.21 (m, 2 H), 5.35 (s, 1 H), 3.51 (t, 2 H, *J* = 7.0 Hz), 3.02 (s, 3 H), 2.49 (t, 2 H, *J* = 7.0 Hz), 2.24 (s, 6 H); ¹³C-NMR (100 MHz, CDCl₃) δ, 176.38, 162.52, 153.52, 131.82, 125.35, 124.47, 122.77, 116.05, 85.95, 56.61, 47.99, 45.55, 36.32.

2-(2-Hydroxy-ethylamino)-1-benzopyran-4-one (C105): To a stirred solution of compound **2.3** (0.20 g, 1.0 mmol) in 1-butanol (7 ml) was added 2-methylaminoethanol (1.0 ml) in 1-butanol (3 ml) and a catalytic amount of acetic acid (3 drops). The reaction mixture was heated at 60 °C. After one and one half hours reaction was stopped and the solvent was evaporated. The product was purified with column chromatography (eluent, chloroform/methanol (2/1)). The slightly impure product was further purified by preparative TLC using the same solvent to give **C105** (20.6 mg, 0.10 mmol, 10% yield); TLC $R_f = 0.51$ (CHCl₃/MeOH : 2/1); ¹H-NMR (300 MHz, CD₃OD) δ , 8.01 (d, 1 H, $J = 8.1$ Hz), 7.62 (t, 1 H, $J = 7.6$ Hz), 7.42-7.34 (m, 2 H), 5.46 (s, 1 H), 3.74 (t, 2 H, $J = 5.7$ Hz), 3.45 (t, 2 H, $J = 5.4$ Hz).

2-(2-Methoxy-ethylamino)-1-benzopyran-4-one (C106): To a stirred solution of compound **2.3** (0.20 g, 1.0 mmol) in 1-butanol (7 ml) was added 2-methoxyethylamine (1.0 ml) in 1-butanol (3 ml) and a catalytic amount of acetic acid (1 drops). The reaction mixture was heated at 70 °C. After 7 hours the reaction was stopped and the solvent was evaporated. The sticky product was dissolved in water (40 ml) and extracted with ether (30 ml) and chloroform (40 mL \times 2). The combined organic layers were washed with brine (20 ml), dried over MgSO₄, and evaporated to give **C106** (0.21 g, 0.90 mmol, 90% yield); ¹H-NMR (300 MHz, CDCl₃) δ , 8.06 (dd, 1 H, $J = 7.8$ Hz, 1.8 Hz), 7.42 (td, 1 H, $J = 7.9$ Hz, 1.4 Hz), 7.22 (td, 1 H, $J = 7.6$ Hz, 0.8 Hz), 6.54 (s, 1 H), 5.39 (s, 1 H), 3.54 (t, 2 H, J

= 5.4 Hz), 3.38 (t, 2 H, $J = 5.3$ Hz), 3.31 (s, 3 H); ^{13}C -NMR (100 MHz, CDCl_3) δ , 176.59, 163.53, 153.51, 131.83, 125.19, 124.30, 122.95, 116.14, 85.44, 69.85, 58.62, 41.19.

2-(Imidazol-1-yl)-1-benzopyran-4-one (C107): A mixture of imidazole (0.20 g, 2.9 mmol), triethylamine (0.65 g, 6.46 mmol), a catalytic amount of KHCO_3 (0.10 g) and the reactant **2.3** (0.21 g, 1.1 mmol) was stirred in benzene (15 ml) at room temperature overnight. The temperature was increased to 120 °C and more KHCO_3 (ca. 0.2g) was added. After 6 hours the reaction was stopped, though some of the reactant **2.3** remained. The solvent was evaporated and the mixture was redissolved in dichloromethane (100 ml). The resulting solution was washed with water (20 mL \times 2) and brine (30 ml) and dried over MgSO_4 . The product (0.07 g, 0.33 mmol, 30% yield) was purified by column chromatography, eluting with ethyl acetate/hexane (4/1); ^1H -NMR (300 MHz, CDCl_3) δ , 8.28 (dd, 1 H, $J = 7.8$ Hz, 1.8 Hz), 8.28 (s, 1 H), 7.80 (td, 1 H, $J = 7.9$ Hz, 1.5 Hz), 7.60 (d, 1 H, $J = 7.5$ Hz), 7.58-7.51 (m, 2 H), 7.33 (s, 1 H), 6.45 (s, 1 H); ^{13}C -NMR (100 MHz, CDCl_3) δ , 196.06, 177.67, 154.21, 153.33, 134.78, 134.29, 134.27, 131.82, 126.21, 126.00, 125.99, 123.38, 117.56, 115.83, 97.07.

2-(2-Methyl-imidazol-1-yl)-1-benzopyran-4-one (C108): A mixture of 2-methyl imidazole (0.12 g, 1.7 mmol), triethylamine (0.48 g, 4.8 mmol), KHCO_3 (0.27 g, 2.7 mmol) and the reactant **2.3** (0.19 g, 1.0 mmol) was stirred in toluene at 130 °C. After 72 hours, the reaction was stopped; the reactant wasn't completely consumed. The mixture was

evaporated and redissolved in methylene chloride (50 mL). The resulting solution was washed with water (20 mL \times 2) and brine (20 ml) and dried over MgSO₄. The product (ca. 40%) was purified by column chromatography, eluting with ethyl acetate/methylene chloride (10/1); ¹H-NMR (300 MHz, CDCl₃) δ , 8.22 (dd, 1 H, J = 8.0 Hz, 1.4 Hz), 7.74 (td, 1 H, J = 7.8 Hz, 1.5 Hz), 7.51-7.46 (m, 2 H), 7.27 (d, 1 H, J = 1.8 Hz), 7.06 (d, 1 H, J = 1.8 Hz), 6.31 (s, 1 H), 2.66 (s, 3 H); ¹³C-NMR (100 MHz, CDCl₃) δ , 177.96, 154.59, 134.38, 129.13, 126.21, 126.01, 123.23, 118.40, 117.60, 102.19, 15.58.

2-(Pyridin-3-yl)-1-benzopyran-4-one (C109): nBuLi (2.5 M in hexane, 2.20 ml, 5.5 mmol) was slowly added to the round bottom flask filled with toluene (6 ml) at 0 °C. 3-bromopyridine (0.79 g, 0.48 ml, 5 mmol) in toluene (2 ml) was slowly added. A yellow solid was precipitated and it gradually turned to a red-brown color. After 30 minutes, the reactant **2.3** (0.20 g, 1.0 mmol) in toluene (3 ml) was slowly added to the reaction mixture. The temperature was slowly increased to room temperature. After 3 hours, the reaction was stopped, filtered, and evaporated. The product mixture was dissolved in ethyl acetate (80 ml), washed with water (20 mL \times 2) and brine (30 ml) and dried over MgSO₄. The product was purified with column chromatography, eluting with ethyl acetate/hexane (3/1) to give **C109** (0.05 g, 0.22 mmol, 22% yield); ¹H-NMR (300 MHz, CDCl₃) δ , 8.78 (d, 1 H, J = 3.6 Hz), 8.74 (s, 1 H), 7.80 (t, 1 H, J = 3.9 Hz, 1.9 Hz), 7.59 (t, 1 H, J = 7.7 Hz), 7.49 (t, 1 H, J = 6.3 Hz), 7.45-7.38 (m, 2 H), 7.27 (t, 1 H, J = 7.4 Hz), 6.40 (s, 1 H).

4-(Naphthalen-2-yl)-morpholine (C201)¹⁵³: A solution of 2-bromonaphthalene (0.42 g, 2.0 mmol), morpholine (0.60 g, 6.9 mmol), dichlorobis(tri-*o*-tolylphosphine)-palladium(II) (0.04 g), and potassium *tert*-butoxide (0.24 g) in toluene (15 ml) was stirred at 100 °C for 3 hours. The reaction mixture was poured into ether (50 ml) and washed with water (10 mL × 2) and brine (15 ml). The product was purified by column chromatography (10/1 = hexane/ethyl acetate) to obtain **C201** (0.35 g, 1.6 mmol, 80% yield); ¹H-NMR is consistent with that in the literature; ¹H-NMR (300 MHz, CDCl₃) δ, 7.76 (m, 3 H), 7.42 (t, 1 H, *J* = 7.2 Hz), 7.34-7.24 (m, 3 H), 3.93 (t, 4 H, *J* = 5.1 Hz), 3.27 (t, 4 H, *J* = 4.6 Hz).

2-Chloropyrimido[2,1-*a*]isoquinoline-4-one (2.5)¹⁵⁸: 2-Aminoisoquinoline (0.72 g, 5.0 mmol) was dissolved in diethyl malonate (1 ml) with heating, and the reaction mixture was stirred at 80 °C for 30 minutes. Ethanol (5 ml) was added, and the solution was refluxed (heated to 170 °C) for 6 hours. A Dean Stark apparatus was installed, and ethanol was removed by stirring at 150 °C. The residual pale solid was collected and washed with ethyl acetate to get the title compound **2.4** as a pale brown solid, which was used for the next step without further purification. **2.4** was dissolved in POCl₃ (5 ml) and the solution was heated at 120 °C for 5 hours. The reaction mixture was cooled and poured carefully into ice water. Saturated Na₂CO₃ solution was added to adjust the pH to 7. The product (**2.5**) was extracted with dichloromethane, and the organic layer was dried with MgSO₄ and evaporated. The crude product was purified by chromatography

on silica gel, eluting with ethyl acetate/hexane (1/4) and 10% dichloromethane, to provide the title compound as a white solid (0.40 g, 1.73 mmol, 35% yield). TLC R_f = 0.45 (Hexane/EtOAc 1:1); mp 198 °C (lit. mp = 197 – 199 °C); $^1\text{H-NMR}$ (400 MHz, CDCl_3) δ , 9.02 (d, 1H, J = 8.0 Hz), 8.76 (d, 1H, J = 7.6 Hz), 7.88-7.73 (m, 3H), 7.37 (d, 1H, J = 7.6 Hz), 6.60 (s, 1H) (lit. $^1\text{H-NMR}$ (CDCl_3) δ , 6.12-6.17 (1H, m, Ar-H), 6.81 (1H, s, CH), 7.24-7.45 (5H, m, Ar-H); $^{13}\text{C-NMR}$ (100 MHz, CDCl_3) δ , 158.15, 157.96, 149.78, 134.27, 133.54, 129.17, 127.61, 126.61, 125.98, 121.57, 116.06, 105.40; MS (ESI), m/z = 231.0 ($\text{M}+1$)⁺ (lit. MS (ESI+) m/z 231.5 (M^+)).

2-(Morpholine-1-yl)pyrimido[2,1-*a*]isoquinoline-4-one (C401)¹⁵⁸: To solution of **1.9** (1 eq.) in 1-butanol (10 ml) was added morpholine (~ 4 eq.) and three drops of acetic acid. The solution was stirred under reflux for overnight. As the reaction was completed, it was cooled and the solvent was evaporated. To the resulting solid was added dichloromethane and water. The organic layer was dried with MgSO_4 and evaporated. The crude product was purified by chromatography on silica gel, eluting with ethyl acetate/hexane (2/1) and 10% dichloromethane, to provide the title compound as a white solid (98% yield); mp 210 °C; $^1\text{H-NMR}$ is consistent with that in the literature; $^1\text{H-NMR}$ (300 MHz, CDCl_3) δ , 8.81 (d, 1 H, J = 7.8 Hz), 8.66 (d, 1 H, J = 7.5 Hz), 7.75-7.57 (m, 3 H), 7.05 (d, 1 H, J = 7.8 Hz), 5.64 (s, 1 H), 3.84-3.71 (m, 8 H); $^{13}\text{C-NMR}$ (100 MHz, CDCl_3) δ , 160.37, 159.63, 149.10, 134.33, 132.35, 127.96, 126.89, 126.38, 126.17, 122.03, 112.43, 82.22, 66.52, 44.63; MS (ESI), m/z = 282.0 ($\text{M}+1$)⁺.

Chapter 3. Design, synthesis, and bioassay of selective inhibitors of mTOR

3.1 Homology modeling and strategies

One of the bottlenecks of this research is the absence of the 3D structure of the catalytic domain of mTOR. The crystal structure of the complex of the catalytic domain of PI3Kinase with LY294002 has been solved.¹⁵⁵ However, PI3Kinase is not our target, but rather the goal is to develop mTOR inhibitors that do not inhibit PI3Kinase. To address this limitation, homology modeling was performed using the Molecular Operating Environment software package¹²⁹ to develop a computer model of the 3D structure of the catalytic domain of mTOR. The catalytic domains of enzymes in the PIKK family are highly homologous. Thus a computational model of mTOR may be generated using the known PI3Kinase structure as a template. Furthermore, the calculated 3D structure of the catalytic domain of mTOR and the crystal structure of PI3Kinase can be compared for the design of selective inhibitors for mTOR over PI3Kinase.

3.1.1 Sequence alignment and template refinement

The human sequences of mTOR, DNA-PK, PI3K α , PI3K γ , ATM, and ATR were chosen from the Swiss-Prot Database. The crystal structure of the LY294002 complex of PI3K γ (PDB ID : 1E7U in PDB bank), the only PIKK family member for which a 3D structure is available, was used as a template for the model building. MOE was first used to refine the PI3K γ -LY294002 template by filling in missing residues (disordered loop

regions not resolved in the crystal structure) while predicting the best conformation of these regions by a rotamer library and PDB structure matching. The sequences of mTOR, DNA-PK, PI3K α , PI3K γ , ATM, and ATR were loaded into MOE, and the sequence alignment was performed with **MOE-Align**, which aligned the target sequence to the sequences of enzymes in the PIKK family. The mTOR sequence was 13.3% identical with the PI3K γ template in the multiple alignment. The DNA-PK, ATM, ATR sequences also exhibited 12 to 15% identities with PI3K γ , while PI3K α was 36.8% identical in this alignment. By using multiple sequence alignment instead of one-by-one (target by template) sequence alignment, conserved residues within the PIKK family can be effectively considered, leading to a more reasonable result. In one-by-one sequence alignment, the results were dependent on the parameter options set in **MOE-Align** because the algorithm of the scoring function in sequence alignment is based only on sequence identity without considering conservation of residues throughout the family. However, multiple sequence alignment gave consistent results with different parameter options, suggesting the result does not depend on the parameter options.

The highly conserved amino acids among the PIKK family are well aligned (highlighted in yellow in Figure 3.1) in the multiple sequence alignment. The amino acids highlighted in green represent significant residue differences in the PIKK family in the active site of the catalytic domain. These differences may be exploited for the design of selective inhibitors of mTOR.

Figure 3.1 Multiple sequence alignment of protein enzymes in PIKK family. This figure shows the aligned amino acids near the active site of the catalytic domain. For the full sequence alignment see the appendix.

```

PI3-K $\gamma$  808 KKPLWLEFKCAD -PTALSNETI G I I F KHGDDLRLQDMLI L QI L
PI3-K $\alpha$  776 KRPLWLNWENPDIMS ELLFQNE I I F KNGDDLRLQDMLTL QI I
mTOR 2167 QRPRKLTLMGSN - - - - -GHEFVFL LKGHEDLRLQDERVMQLF
DNA-PK 3733 RRPKR I I I RGH D- - - - - EREHPFLV KGGEDLRLQDQRVEQLF
ATM 2697 NLPK I I DCVGS D- - - - - GKERRQLV KGRDDLRLQDAVMQQVF
ATR 2307 QKPK I I S LKGS D- - - - - GKFYI MMC KPKDDLRLKDCRLMEFN

PI3-K $\gamma$  849 RI MESIWETESL - - - - DLCLLPYGC I STGDKI GMI EI VKDA
PI3-K $\alpha$  818 RI MENIWQNQGL - - - - DL RMLPYGC I SI GDCVGLI EVVRNS
mTOR 2203 GLVNTLLANDPTSLRKNLSIQR YAVI PLSTNS GLI GWVPHC
DNA-PK 3769 QVMNGI LAQDS ACSQRALQLRTYSVV P MTSRLGLI EWLENT
ATM 2733 QMCNTLLQRNTETRKRK LTI CTYKVV PLSQRS GVL E WCTGT
ATR 2343 SLI NKCLRKDAESRRRE LHI RTYAVI PLNDECGI I E WVNNT

```

3.1.2 Homology modeling

After the sequence alignment, the **MOE-Homology module** was used to build the mTOR structure based on the result of the sequence alignment with the PI3Ky template structure. In this process, ‘outgaps’ of the mTOR sequence were ignored, and ‘indel’ data (backbone fragments which can span insertions in the target sequence) and sidechain data were collected from the Protein Data Bank and a rotamer library. 1000 intermediate models were generated and the final structure was constructed by averaging the coordinates of these 1000 models, followed by minimization using the Amber99 force field with an RMS gradient of 0.1. In the aligned sequence, there are two large ‘indels’ (K1815-T1844, and R2266-D2298 in mTOR, see the Figure in appendix), and these backbones could not be built properly. However, the former is fairly distant from the active site. The latter is somewhat near the active site, but it is not a component of the active site and forms a long loop in the outer region of the active site.

Structural models for the LY294002 complexes of DNA-PK and PI3K α were constructed by the same approach. ATM and ATR were not further characterized since they are not generally inhibited by compounds having structures related to that of LY294002. More recently, the crystal structure of PI3K α (the p110 α /p85 α complex) having no inhibitor, or ATP bound, was solved and published.^{171, 172} The crystal structure and homology model of PI3K α were compared. The overall shape and amino acid sequences are almost the same, and the residue sequences and positions in the active site are identical to each other (Figure 3.2). The RMSD value of all atoms between the homology model and the crystal structure is 5.7 Å, which is somewhat large. The major deviation comes from amino acids in the loop regions, but these regions are not important for our research. The active site region of each structure (Gly750 to Val850 of p110 α) was further compared, and the RMSD value of all atoms is 2.1 Å. Except for the loop turn (right part of the right figure) the two structures are highly overlapping with each other. This analysis supports the idea that the homology model of mTOR is similar to its unsolved X-ray structure. The overall structure and the core part such as the active site of each structure should be highly similar, with high deviation in the outer loop regions.

Figure 3.2 Comparison of homology model of p110 α (in blue) with its recently solved X-ray structure (in red); the overall shape (left) and the active site part (right)

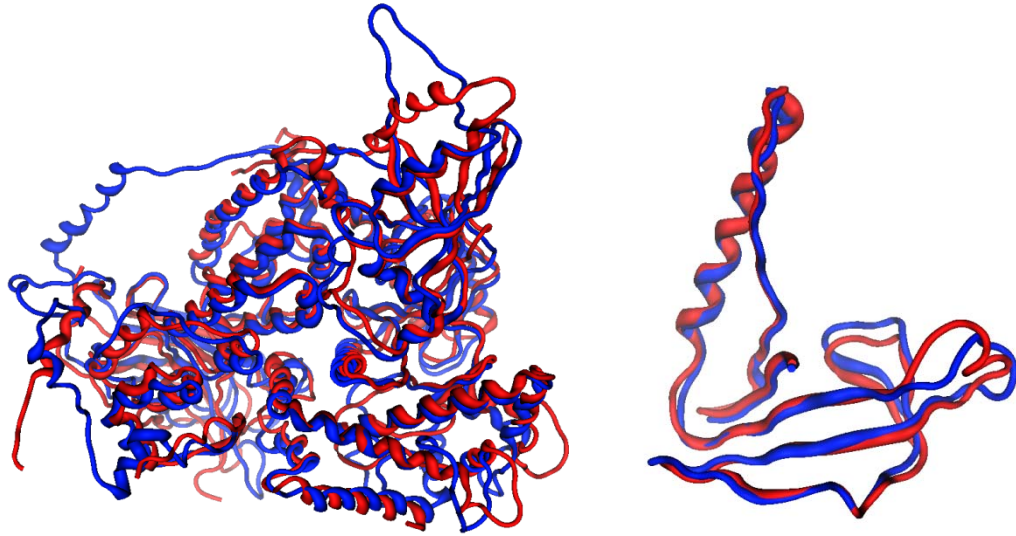
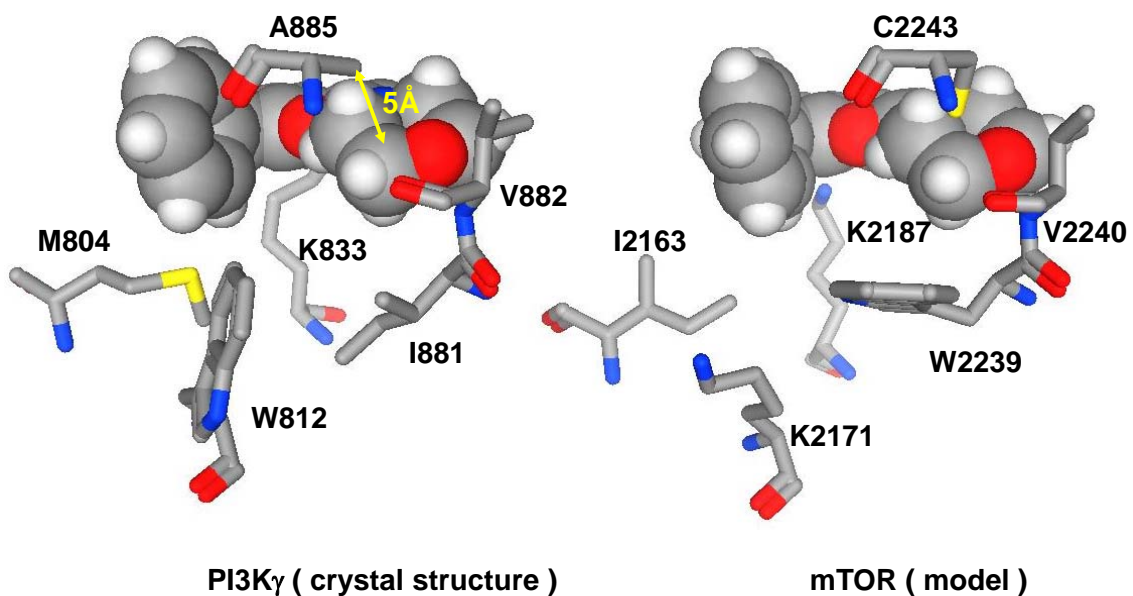


Figure 3.3 shows active site residues represented by tube structures and LY294002 represented by a space filling model in the catalytic domain of PI3K γ (left) and the model of mTOR (right). Highly conserved residues (K833 and V883 of PI3K γ , and K2187 and V2240 of mTOR) in the PIKK family form interactions with the carbonyl oxygen of the chromone ring and the oxygen in the morpholine ring. This is consistent with the inhibition by LY294002 of both PI3Kinase and mTOR.

Figure 3.3 Active site residues (tube structure) and LY294002 (space filling model) in the kinase domains of PI3K γ (left) and mTOR (right). The mTOR structure was derived from homology modeling based on the crystal structure of PI3K γ using the MOE software package. Carbons are gray, oxygens are red, nitrogens are blue, sulfurs are yellow and hydrogens are white (hydrogens of the protein are omitted for clarity).



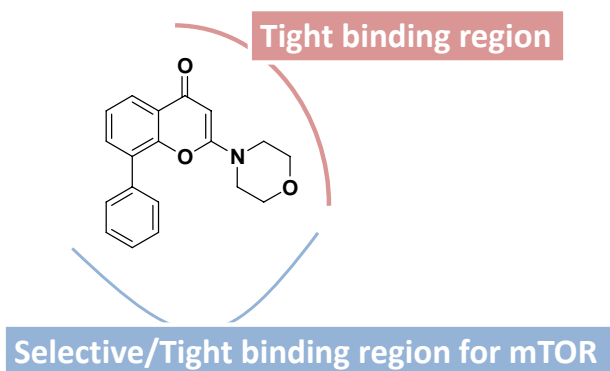
The results reveal two interesting differences in active site residues between these kinases. The bulky and rigid side chain indole of W812 in PI3K γ is very close to the carbon-8 phenyl group of LY294002. The equivalent residue in mTOR is K2171, which has a more flexible side chain. The model suggests that the active site of mTOR might have enough space in this area to accommodate a group that is bulkier than the phenyl ring at the 8-position of LY294002. The other difference in active site residues is that A885 of PI3K γ corresponds to S855 of PI3K α , C2243 of mTOR, and T3810 of DNA-PK. mTOR is the only member of this kinase family that has cysteine at this position (see also Figure 3.1). The methyl group of A885 in PI3K γ is about 5 Å away from the 2-position of

the methylene carbon in the morpholine moiety of LY294002. Thus, C2243 in mTOR provides a potential site for covalent modification by a group on the morpholine moiety of inhibitors that react with the thiol, and they could give especially high selectivity for mTOR.

3.1.3 Strategies for the design of selective inhibitors

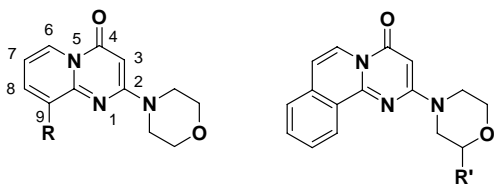
Based on the results of initial studies with LY294002 analogs and of homology modeling, strategies for the design of selective inhibitors were made (Figure 3.4). Since the lysine and valine in PI3Kinase and mTOR are highly conserved and their interactions with the carbonyl oxygen in the chromone ring and with the oxygen in the morpholine ring are major factors for the binding of LY294002, these two oxygen atoms and their relative geometries (distance and rigidity) were taken as the 'minimum requirement' for the binding toward PI3Kinase as well as mTOR. Homology modeling suggests two distinct residue differences that may be exploited for selectivity as described in the previous section. The phenyl ring attached to the 8-position of the chromone ring and the methylene carbon of the morpholine ring closest to A885/C2243 lie in the active site regions nearest these amino acid differences.

Figure 3.4 Strategies for the design of selective inhibitors



Our hypothesis for the design of selective inhibitors for mTOR over PI3Kinase is that sterically bulky groups at the 9-position of 2-morpholine-4-yl-pyrido[1,2-*a*]pyrimidin-4-one can increase the steric repulsion with W812 of PI3Kinase, thus leading to decreased inhibition of PI3Kinase. Inhibition of mTOR by these compounds may be retained because of the flexible lysine residue of mTOR at the equivalent position. The other hypothesis is that functional groups attached to the 2-position of the morpholine ring in **C401**, that can target the thiol group of C2243 in mTOR, may increase the selectivity and potency toward mTOR vs. the PI3Kinases and DNA-PK (Figure 3.5).

Figure 3.5 The design of selective inhibitors by modifying the lead compound. The R group is for the steric repulsion with Trp of PI3Ks, and the R' group is for the targeting Cys2243 of mTOR.

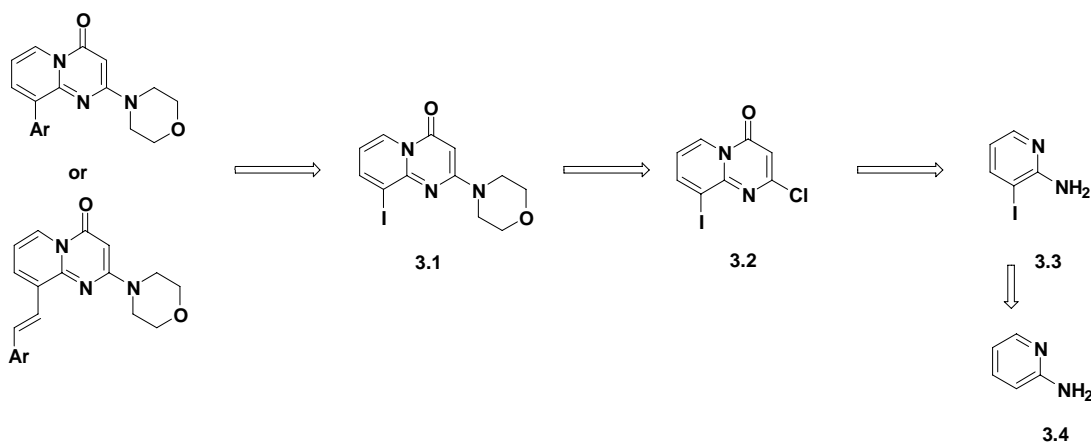


3.2 Chemical probes based on C401 for the selective inhibition of mTOR

3.2.1 Synthesis of potential inhibitors exploring the Trp to Lys mutation in mTOR

The synthetic approach involved connecting a versatile intermediate (**3.1**) and bulky aryl groups (Scheme 3.1) by using Suzuki coupling and Heck reaction methodology. A morpholine ring would be attached to the intermediate (**3.2**) obtained by the cyclization of diethyl malonate with 2-amino-3-iodopyridine (**3.3**), which is not commercially available, but was synthesized from 2-aminopyridine.

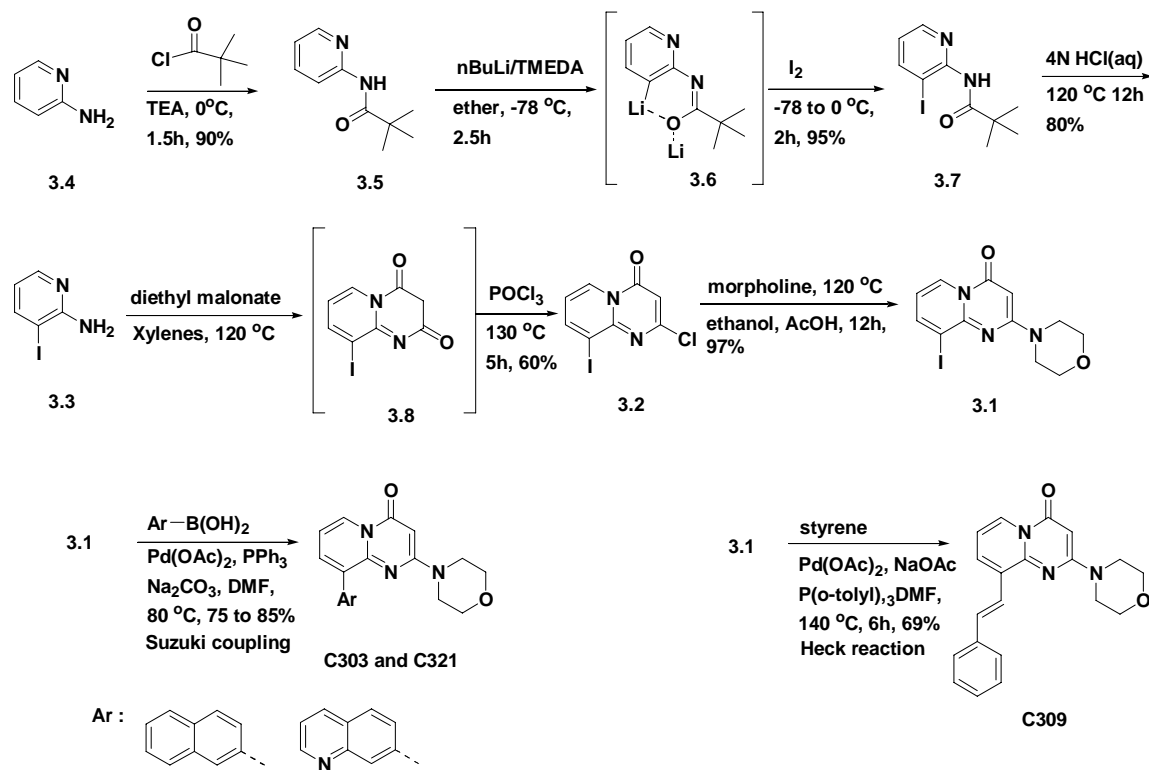
Scheme 3.1 Synthetic plan of chemical probes targeting Trp of PI3Kinase



The synthetic procedure for making 2-amino-3-iodopyridine (**3.3**) has been reported (Scheme 3.2).¹⁷³ Commercially available 2-aminopyridine was reacted with trimethyl acetyl chloride at 0 °C to protect the amine group as a pivaloylamino derivative. This compound was subjected to lithiation by butyllithium/TMEDA chelate at -78 °C, and then the reaction mixture was stirred at 0 °C for 2 hours. The lithiation

occurred at position 3 selectively (**3.5**). The reaction mixture was cooled to $-78\text{ }^{\circ}\text{C}$ again followed by addition of iodine, and the temperature was increased to $0\text{ }^{\circ}\text{C}$ slowly to obtain ortho iodo(pivaloylamino)pyridine (**3.7**). The amine was deprotected by heating in acidic aqueous solution to get the desired product **3.3**. The obtained compound reacted with diethylmalonate at $150\text{ }^{\circ}\text{C}$ to make the cyclized compound **3.8**, which was treated with phosphorous oxychloride without purification to give 2-chloro-9-iodo-pyrido[1,2-*a*]pyrimidin-4-one (**3.2**). Morpholine was attached to the 2-position of compound **3.2** by an acid catalyzed addition elimination reaction to give **3.1**. Aryl groups were introduced to the 9-position of compound **3.1** by Suzuki coupling¹⁷⁴⁻¹⁷⁶ with several aryl boronic acids to give products such as **C303** and **C321**. In addition, Heck reactions¹⁷⁷ were used to introduce arylalkene groups at the 9-position to give products such as **C309**.

Scheme 3.2 Synthesis of chemical probes targeting Trp of PI3Kinase. Compound **3.1** was modified by reacting with different arylboronic acids (Suzuki coupling) and arylalkenes (Heck reactions) to form the various 9-substituted compounds.

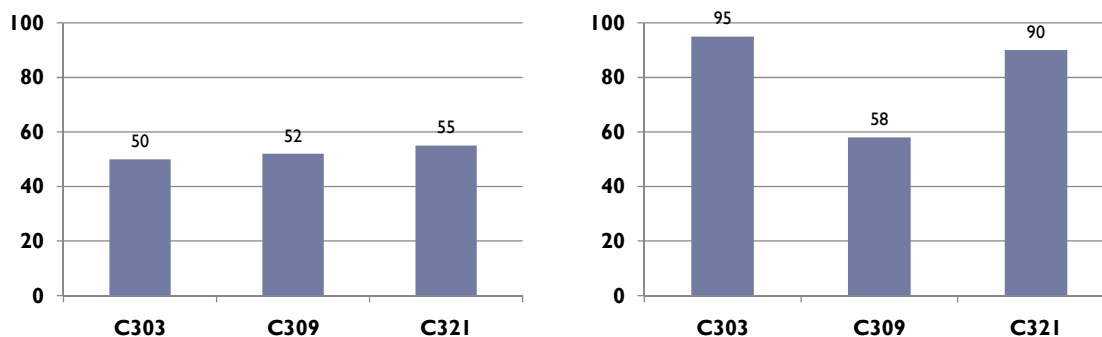


3.2.2 Enzyme inhibition assays of C-9 modified analogs

C303, **C309**, and **C321** having a naphthyl ring, a styrene group, and a quinoline ring at the 9-position of the pyridopyrimidinone ring respectively were tested against mTOR at 1 μ M concentration (left in Figure 3.6) and PI3Kinase at 25 μ M concentration (right in Figure 3.6). The enzyme activity of mTOR at 1 μ M concentration of each compound is about 50%, which is slightly more potent than that of the lead compound **C401**. This result shows that inhibitors having sterically bulky groups at the 9-position of the pyridopyrimidinone ring retain their inhibition potency against the mTOR, with activity similar to the lead compound **401**. It implies that the sterically bulky groups of

these inhibitors do not cause decreased inhibition against mTOR. The enzyme activity of PI3Kinase treated with 25 μ M **C309** is 58%, which is similar to that with 25 μ M **C401**, while they are 95% and 90% after treating with **C303** and **C321** respectively. It shows that **C309** having the relatively flexible bulky group (styrene) inhibits the PI3Kinase at high concentration (25 μ M) as **C401** does, even though the bulky Trp residue of PI3Kinase might be expected to cause steric repulsion. In contrast, even at high concentration no inhibition was observed with **C303** and **C321** having more rigid aromatic groups. The results may be explained by the steric repulsion of the naphthyl group and the quinoline group of **C303** and **C321**, respectively, interacting with the indole ring of Trp of PI3Kinase, while this steric repulsion is less with the more flexible group of **C309**.

Figure 3.6 The % enzyme activities of mTOR (left) after treating with 1 μ M concentration and of PI3Kinase (right) after treating with 25 μ M concentration of **C303**, **C309**, and **C321**.

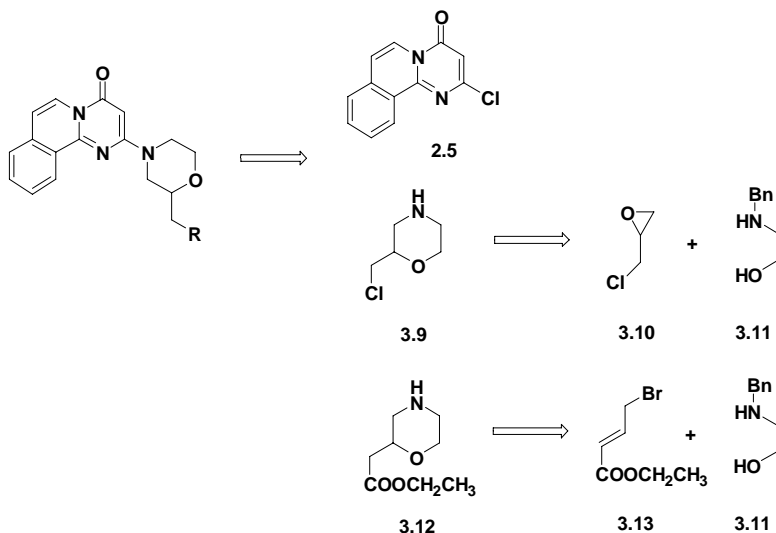


The above biological results support the hypothesis that Trp780 of PI3K α (Trp812 of PI3K γ) and Lys2171 of mTOR are in equivalent positions of the active site, as predicted by sequence alignment and homology modeling. Thus, mTOR can tolerate more bulky groups at the 9-position while PI3K cannot.

3.2.3 Synthesis of potential inhibitors targeting Cys2243 of mTOR

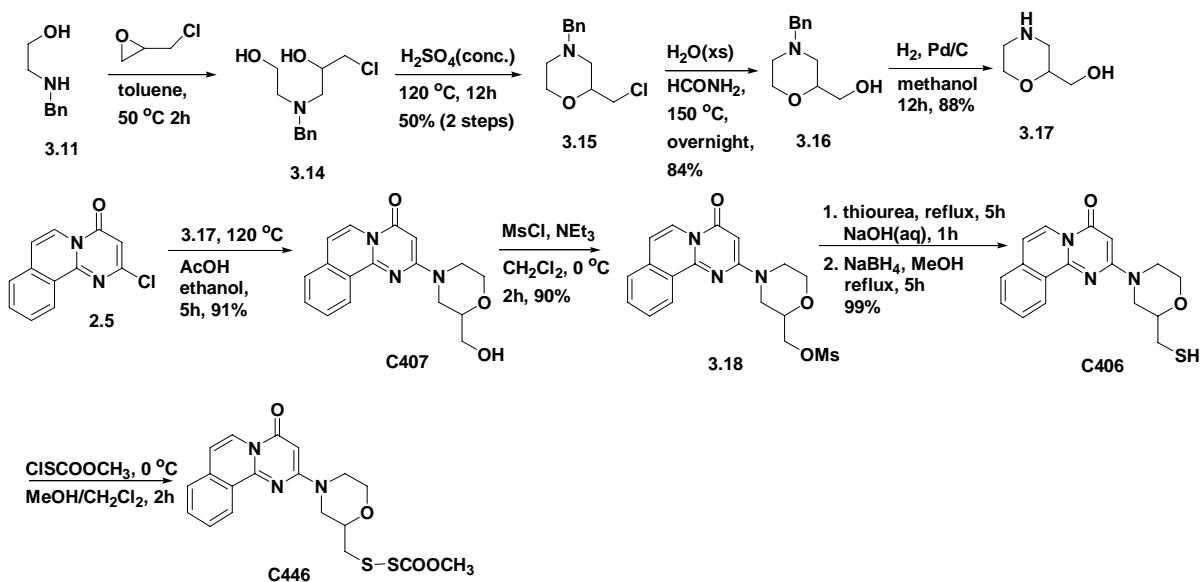
The synthetic approach to introduce thiol reactive groups into the morpholine moiety involved reacting 2-chloro-pyrimido[2,1-*a*]isoquinolin-4-one (**2.5**) with the appropriate morpholine derivatives (Scheme 3.3). The morpholine derivatives were obtained by cyclization of the initial alkylation product of **3.10** and **3.11** with concentrated acid followed by N-benzyl deprotection. Similarly, one-carbon elongated morpholine derivatives were made using ethyl 4-bromocrotonate (**3.13**) instead of epichlorohydrin (**3.10**).

Scheme 3.3 Synthetic plan of chemical probes targeting Cys of mTOR



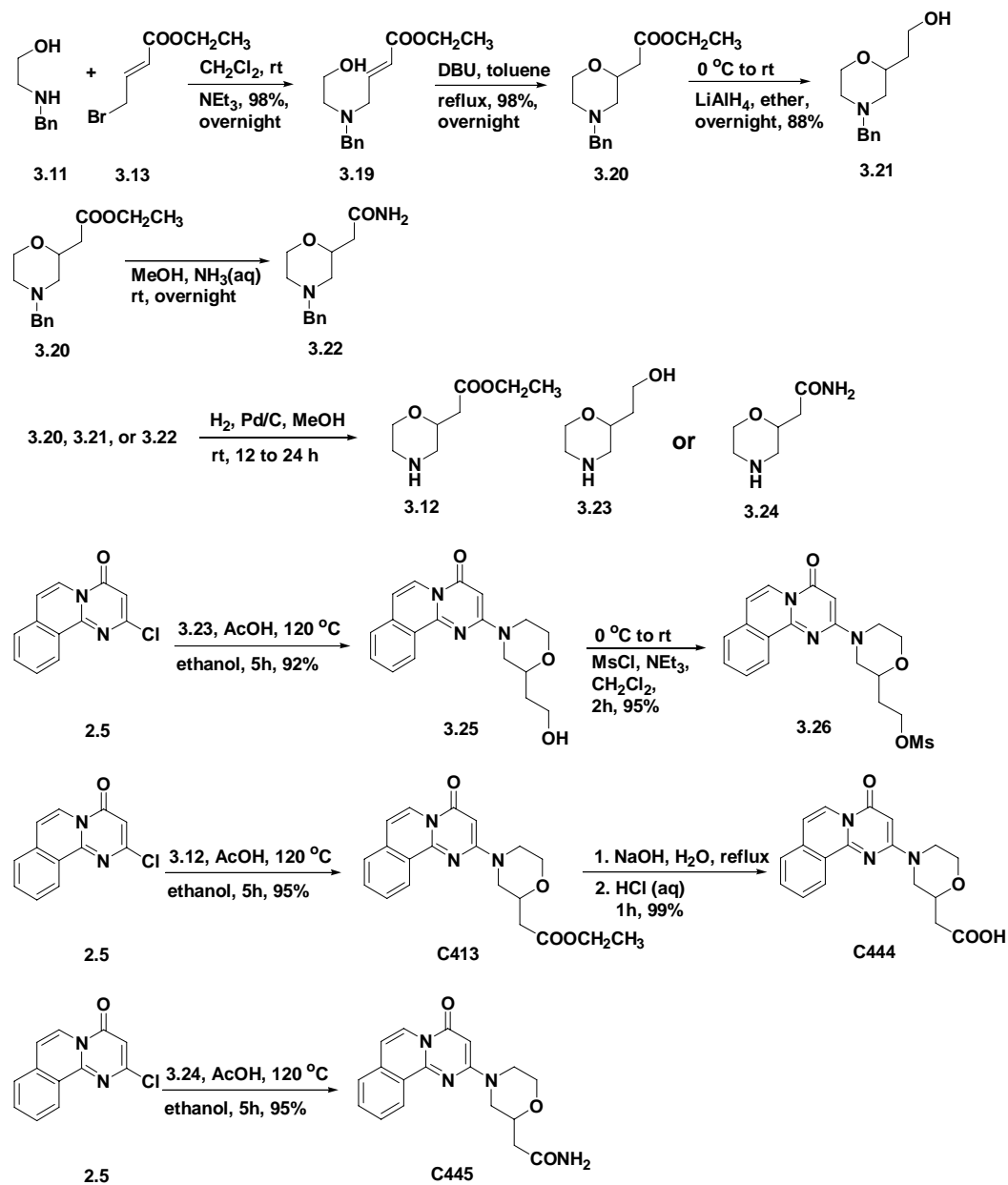
The details of the synthesis are shown in Scheme **3.4**. N-benzyl-ethanolamine (**3.11**) was converted into the chloromethyl-morpholine derivative **3.15** via epoxide ring opening of epichlorohydrin **3.10** by the amine followed by treatment with concentrated sulfuric acid for the acid-catalyzed dehydration of the resulting intermediate diol (**3.14**). The chloromethyl N-benzyl morpholine derivative (**3.15**) was hydrolyzed to the corresponding hydroxyl compound **3.16** using aqueous formamide at high temperature. Catalytic hydrogenation in methanol was performed for N-debenzylation to give the morpholine derivatives (**3.17**). The resulting secondary amine reacted with 2-chloropyrimidoisoquinolinone **2.5** via an acid-catalyzed addition-elimination reaction to make compound **C407**, which was converted into the corresponding mesylate (**3.18**) using standard conditions for mesylation. The mesylate was reacted with different nucleophiles to introduce different substituents into the morpholine moiety. A disulfide derivative of **C406** was made by reaction of **3.18** with thiourea, which was reduced with sodium borohydride to give **C406**. The methoxycarbonylsulfonyl group was attached to the thiol group of **C406** to make **C446**, which will be further converted to **C447** with sodium thiosulfate.¹⁷⁸

Scheme 3.4 Synthesis of morpholine modified analogs



Reaction of N-benzylethanolamine **3.11** with ethyl 4-bromocrotonate **3.13** in dichloromethane and triethylamine gave allylic amine **3.19**, which was treated with DBU in toluene under reflux to form morpholine derivative **3.20** (Scheme 3.5). The ester was reduced to the alcohol to give **3.21**. Both **3.20** and **3.21** were N-debenzylated to the corresponding morpholine derivatives **3.12** and **3.23**, respectively, by hydrogenolysis. The two products reacted with compound **2.5** to give compounds **3.25** and **C413**, respectively. Compound **3.25** was converted to the mesylate **3.26** which reacted with nucleophiles as with **3.18** in Scheme 3.4. The carboxylic acid derivative of **C413** was made by hydrolysis of **C413** to give **C444**. Amide **C445** was made by the reaction of compound **2.5** and morpholine acetamide **3.24**, which was obtained from the ammonolysis of **3.20** followed by debenzylation.

Scheme 3.5 Synthesis of morpholine modified analogs



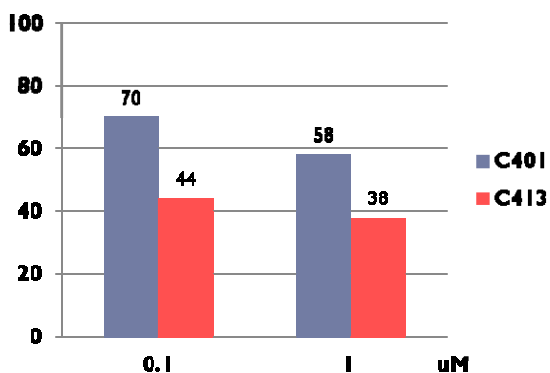
3.2.4 Enzyme inhibition assays of morpholine modified analogs

Enzyme activities of mTOR were determined in the presence of 0.1 μM and 1 μM

C413. These results were compared with those of the lead compound, **C401** (Figure 3.7).

At 0.1 μM and 1 μM , the enzyme activity of mTOR was decreased to 44% and 38% respectively, compared to 70% and 58% with **C401**. This result implies that the added ester group at the 2-position of the morpholine ring can contribute to inhibition of mTOR by interacting with the thiol group of Cys in the active site, as predicted by homology modeling. We also tested compound **C444** having a carboxylic acid group instead of the ester group at the 2-position of the morpholine ring, in order to examine whether the carboxylic acid contributes to the high potency toward mTOR via hydrolysis of the ester under the assay conditions. Compound **C445** with an amide group at the equivalent position, was also tested. Compound **C444** exhibited no inhibition of mTOR at 1 μM and 10 μM , suggesting that the ester group itself at the 2-position of the morpholine ring and not a carboxylic acid causes the increased inhibition of mTOR. Furthermore, the inhibition of mTOR by the amide **C445** was dramatically decreased, with 75% enzyme activity observed at 1 μM **C445** vs. only 38% with 1 μM **C413**. The IC_{50} value for **C413** must be less than 0.1 μM since the enzyme activity at 0.1 μM **C413** is 44%. Furthermore, the ester **C413** has a chiral center on the morpholine ring, so enantiomerically pure **C413** might be even more potent.

Figure 3.7 The % enzyme activity of mTOR at 0.1 μM and 1 μM of **C401** (blue bar) and **C413** (red bar)



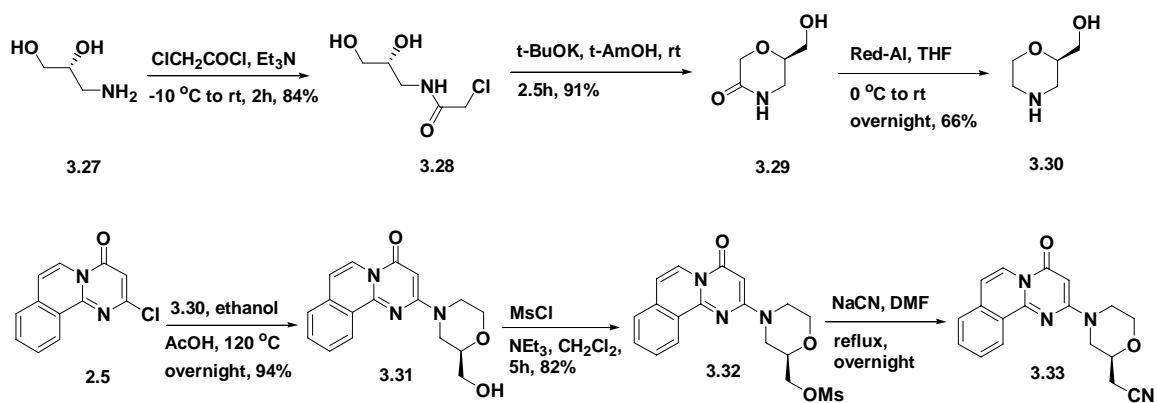
3.2.5 Synthesis of enantiomerically pure compounds

Homology modeling predicts that the R-enantiomer of **C413** places the ester group close to the thiol group of C2243. To prepare this single isomer, (R)-2-(hydroxymethyl)morpholine (**3.30**) was made, following the procedure for the synthesis of the (S)-enantiomer.¹⁷⁹ Commercially available (R)-3-amino-1,2-propanediol was reacted with chloroacetyl chloride in $\text{CH}_3\text{CN}/\text{CH}_3\text{OH}$ to provide the amide (**3.28**) (Scheme **3.6**). Morpholinone (**3.29**) was obtained by addition of the amide (**3.28**), without protection of the primary alcohol, to a solution of t-BuOK in t-amyl alcohol. Compound **3.29** was reduced to (R)-2-(hydroxymethyl)morpholine (**3.30**) with Red-Al as a reducing agent, and was attached to compound **2.5**. The resulting alcohol (**3.31**) was converted to the mesylate (**3.32**). The mesylate group was replaced with a cyano group to form compound **3.33**, and then the cyano group was converted to an ester group by

alcoholysis with $\text{CH}_3\text{CH}_2\text{OH}/\text{H}_2\text{SO}_4$ to obtain the desired enantiomerically pure product

(R)-C413.

Scheme 3.6 Synthesis of enantiomerically pure compounds



3.3 Modification of other non-selective inhibitors of mTOR to increase selectivity

The results of homology modeling, syntheses, and bioassays described in the previous section suggest that Trp812 of PI3K γ (and the equivalent Trp of α , β , and δ isoforms) and Cys2243 of mTOR may be critical residues for the selective inhibition of mTOR over PI3Kinase by **C303**, **C321**, and **C413**. The next step was to apply these ideas to improving the selectivity toward mTOR of other known potent but non-selective PIKK inhibitors. Most inhibitors of the PIKK family are very non-selective, due to the highly homologous catalytic domains of PI3Kinase, mTOR, and other PIKKs. PI103 (Figure 1.1) is non-selective but very potent inhibitor against both mTOR and PI3Kinase (IC₅₀ values against mTOR and PI3K α are 20 nM and 5 nM respectively).¹⁸⁰⁻¹⁸² This compound may serve as a better lead compound for improving selectivity toward mTOR by exploiting the greater active site space in mTOR due to the Lys vs. Trp residue and the unique C2243 thiol in the active site of mTOR, as revealed by homology modeling.

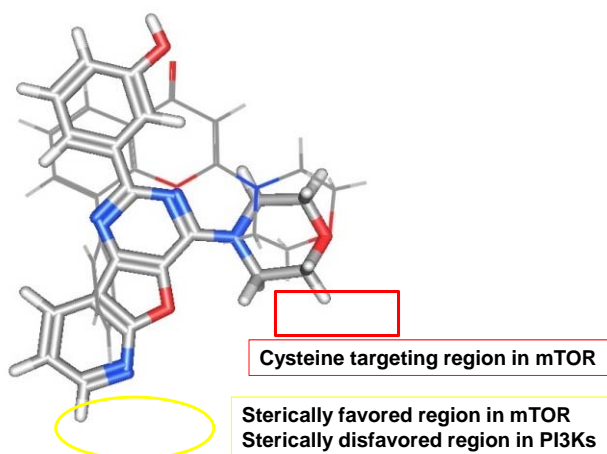
3.3.1 Flexible alignment

No crystal structure of the complex of PI3Kinase or mTOR with PI103 has been solved. Therefore, 'Flexible Alignment' of PI103 with LY29400, for which the binding mode toward PI3K γ is known, was performed using MOE software. This alignment modeling provided a prediction of the binding orientation of PI103 in the active sites of PI3Kinase and mTOR by finding common features between PI103 and LY294002.

In this calculation, the structure of LY294002 was fixed to be used as the exactly bound shape of LY294002 in the active site of PI3Kinase. The MMFF94 force field was

selected. After calculation, three possible overlapped structures were obtained. By examining scoring values of S (the alignment score of the configuration) or F (the total mutual similarity score), the best plausible overlapped result was taken (Figure 3.8). This result is very similar to that predicted by Shokat *et al.*¹⁸²

Figure 3.8 The result of 'Flexible Alignment' of PI103 (tube structure) toward LY294002 (line).



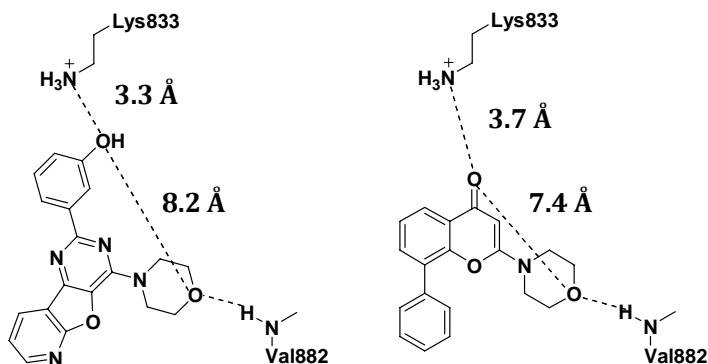
The oxygen atoms in the morpholine ring of LY294002 and PI103 are matched to each other, and the carbonyl oxygen in the chromone ring and the hydroxyl oxygen in the phenol ring of PI103 occupy the same area. These two oxygen atoms in LY294002 are essential binding components toward PI3Kinase and mTOR by forming hydrogen bonds with the ammonium group of lysine and an amide backbone (-NH-) of valine, which are highly conserved in the PIKK family. The alignment suggests the phenolic oxygen and the morpholine oxygen of PI103 are very important for inhibition of PI3Kinase and mTOR by interacting with the same residues. This result is also supported

by Structure Activity Relationship (SAR) data as the absence of the phenolic oxygen or the morpholine ring dramatically decreased inhibition against PI3Kinase.^{180, 181}

No explanation for the greatly increased inhibition of PI103 toward PI3Kinase and mTOR as compared with that of LY294002 has been provided in the literature.^{180, 181}

One possibility is that the overall shape of the PI103 molecule is simply a better fit with the kinase active sites. An alternate possibility is that the greater distance between the phenolic oxygen and the morpholine oxygen in PI103 (8.2 Å) vs. 7.4 Å in LY294002 is a better match with the distance between their H-bond partners in the active site (Figure 3.9)

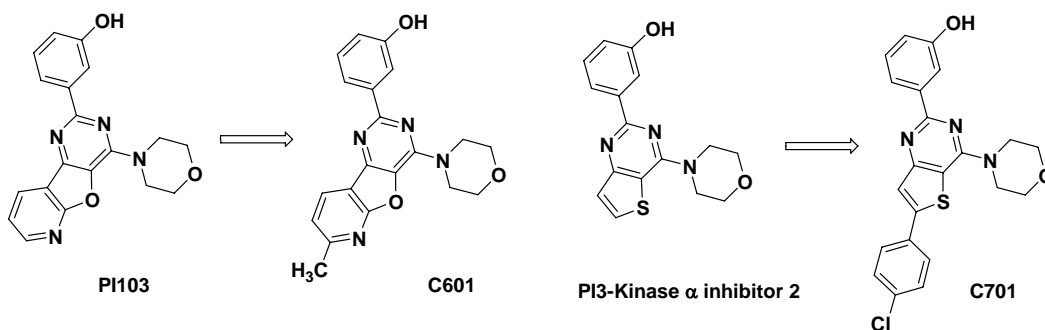
Figure 3.9 The schematic overview of interactions between the ammonium group of Lys833 and the phenolic oxygen (left) and the chromone oxygen (right). The binding mode of PI103 was predicted by the flexible alignment of PI103 toward LY294002-PI3K γ crystal structure. The distances in LY294002 structure (right) are measured from the crystal structure, and the distance in PI103 (left) are the estimated values based on the result of flexible alignment.



3.3.2 Redesign of non-selective inhibitors

Based on homology modeling and the flexible alignment described above, structures related to PI103 were designed in an effort to increase selectivity toward mTOR. Relatively small functional groups such as a methyl or chlorine substituent at the 2-position of the 9-oxa-1,5,7-triaza-fluorene core fragment might increase the steric repulsion with Trp of the PI3Kinase (Figure 3.10). More bulky groups such as a phenyl or a naphthyl ring might also be introduced, but they could cause steric repulsion with Lys or other residues in the active site of mTOR. A 4-chlorophenyl ring at the 6-position of the thienopyrimidine core might similarly increase selectivity toward mTOR. Furthermore, the ester substituent and other modifications to the morpholine ring that are found to increase inhibition potency toward mTOR by apparently interacting with the C2243 thiol group might also be introduced into the morpholine moieties of PI103 and a compound called PI3-Kinase α inhibitor 2.

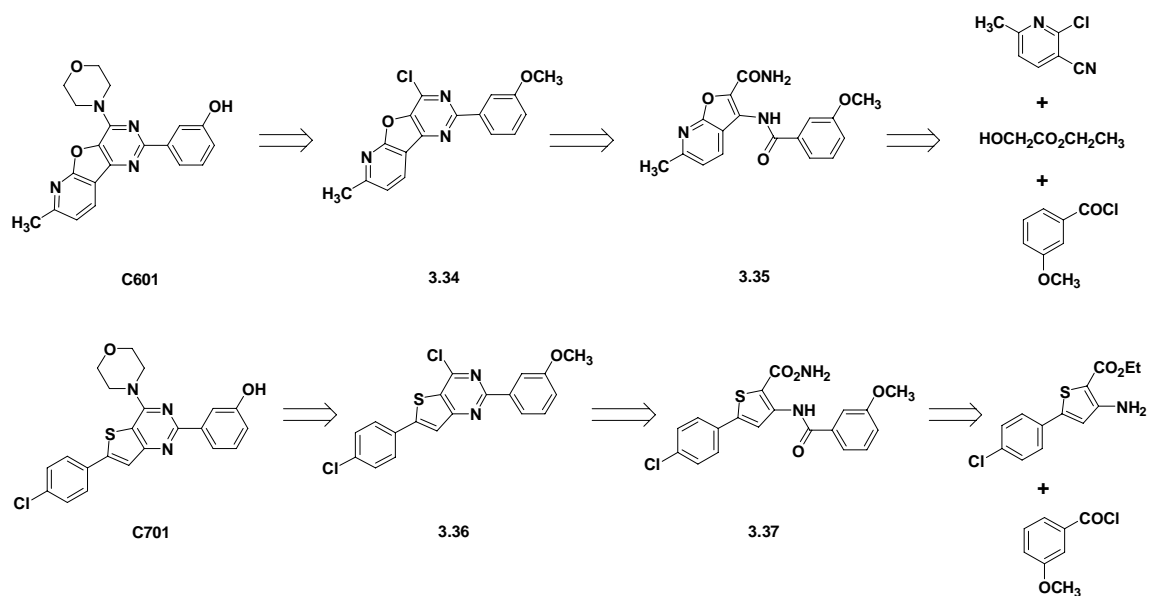
Figure 3.10 The redesigned compounds based on previous knowledge and the result of flexible alignment



3.3.3 Synthesis of redesigned inhibitors

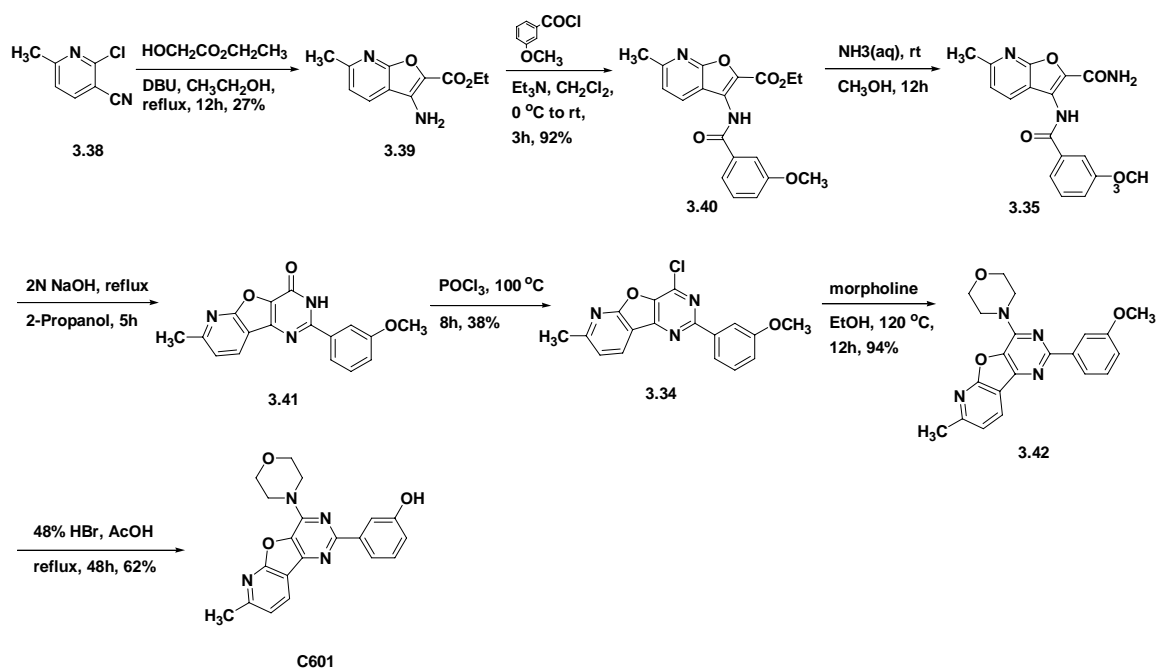
The syntheses of **C601** and **C701** were performed by slight modification of procedure for making PI103 (Scheme 3.7).^{180, 181} The synthetic procedure for compounds **C601** and **C701** involves connection of the morpholine ring with the oxa-triaza-fluorene (**3.34**) and thienopyrimidin (**3.36**) core fragments, followed by demethylation. Compounds **3.34** and **3.36** are prepared by the 6-membered heterocyclic ring formation reaction, under basic conditions, from furopyridine derivative (**3.35**) and thiophene derivatives (**3.37**), respectively. The furopyridine ring fragment has been made by the reaction of 2-chloro-6-methyl-nicotinonitrile and ethyl glycolate, which reacts with 3-methoxy benzoylchloride to form **3.34**. Compound **3.36** was made by reaction of 3-methoxybenzoyl chloride with the commercially available thiophene derivative.

Scheme 3.7 Synthetic plan for the syntheses of **C601** and **C701**



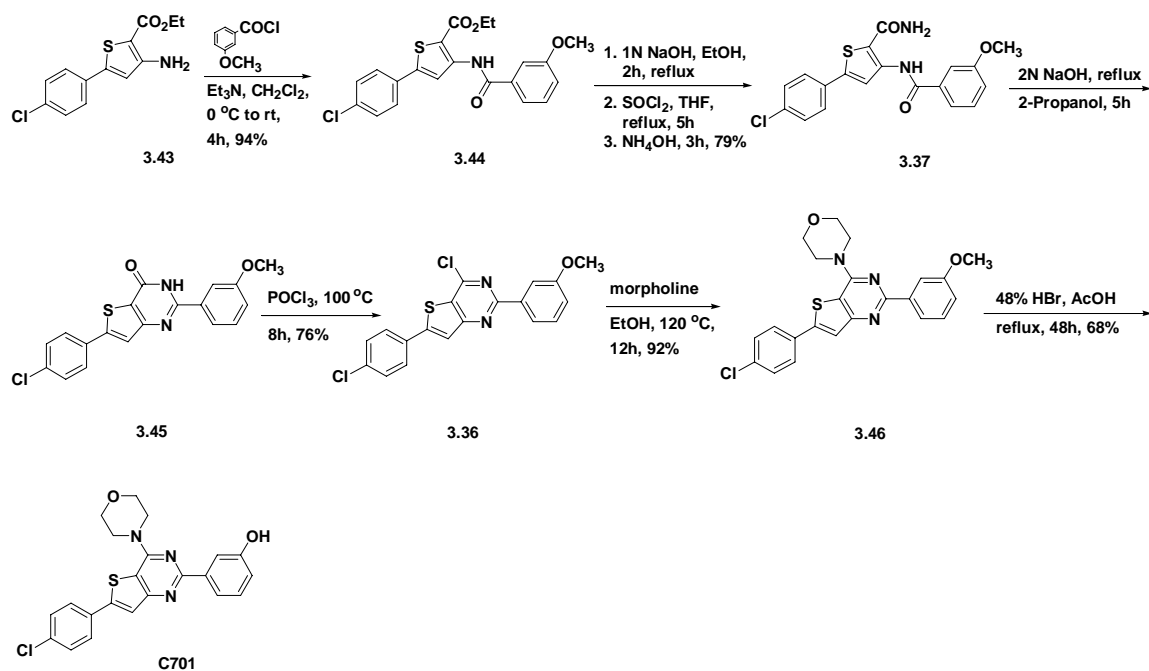
In the presence of DBU, 2-chloronicotinitrile (**3.38**) was treated with ethyl glycolate to afford a bicyclic acid ester (**3.39**), (Scheme 3.8). Acylation of the resulting product was performed with 3-methoxy-benzoyl chloride to form compound (**3.40**). Treatment with aqueous ammonium hydroxide afforded amide **3.35**, which cyclized using 2-propanol and aqueous sodium hydroxide to form compound **3.41**. Chlorination with phosphorous oxychloride gave the intermediate (**3.34**). Substitution with morpholine followed by demethylation with hydrobromic acid gave the desired product (**C601**).

Scheme 3.8 Synthesis of C601



Compound **C701** was synthesized by a similar procedure (Scheme 3.9). The thiophene derivative **3.43** was acylated with 3-methoxybenzoyl chloride to form compound **3.44**. The product reacted with aqueous ammonium hydroxide in an attempt to form amide **3.37**, but only starting material was obtained. Therefore, the ester was hydrolyzed, converted to the acid chloride with SOCl_2 and subsequently treated with aqueous ammonium hydroxide to get the desired amide (**3.37**). Cyclization with 2-propanol and aqueous sodium hydroxide formed compound **3.45**. The resulting product was chlorinated with phosphorous oxychloride to form compound **3.36**, followed by substitution with morpholine to get compound **3.46**. Compound **3.46** was demethylated with hydrobromic acid to afford the desired final product, **C701**.

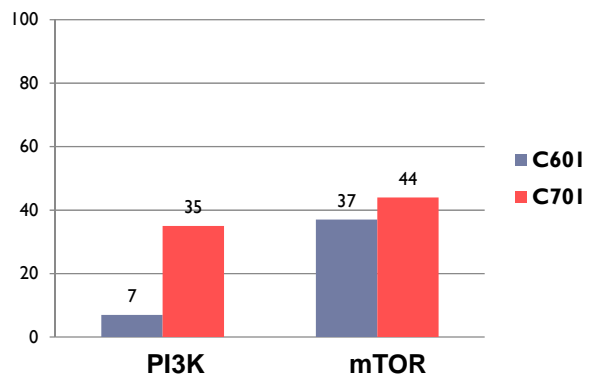
Scheme 3.9 Synthesis of **C701**



3.3.4 Bioassay of redesigned inhibitors

Enzyme activities of mTOR and PI3Kinase with **C601** and **C701** were measured as described in Section 2.3. Figure 3.11 shows the activities of PI3Kinase and mTOR at 0.1 μM **C601** or **C701**. The methyl group at the 2-position of PI103 in compound **C601** did not significantly decrease the inhibition of PI3Kinase. Compound **C601** was still very potent against both PI3K α and mTOR with 7% and 37% observed activity of PI3K α and mTOR, respectively, at 0.1 μM inhibitor. By contrast, compound **C701** which has an additional *p*-chlorophenyl ring relative to PI3-Kinase α inhibitor 2, shows dramatically decreased inhibition against PI3Kinase, with 35% activity observed at 0.1 μM inhibitor while the IC_{50} for PI3-Kinase α inhibitor 2 against PI3K α is only 2 nM. This indicates that introduction of the *p*-chlorophenyl ring significantly diminishes the activity against PI3K. However, compound C701 is an even poorer inhibitor of mTOR, as shown in Figure 3.11. It is possible that the extremely high affinity of PI103 and PI3-Kinase α inhibitor 2 to PI3Kinase nullifies steric effects of an additional methyl group, or *p*-chlorophenyl ring. The flat shape of **C601** and **C701** may also not lead to effective steric repulsion toward Trp of PI3Kinase. Other larger aromatic rings and differently (ortho-, or meta-) substituted phenyl rings may be explored to further increase selectivity.

Figure 3.11 The % enzyme activity of PI3Kinase and mTOR at 0.1 μ M **C601** and **C701**



3.4 Computational and experimental details

Homology models were created using the MOE software package. The human sequences of mTOR, DNA-PK, PI3K α , PI3K γ , ATM, and ATR were chosen from the Swiss-Prot Database and their IDs are P42345, P78527, P42336, P48736, Q13315, and Q13535 respectively. The procedure consists of three steps: template selection and refinement, target-template alignment, and model building.

Template selection and refinement: The crystal structure of PI3K γ was chosen as the template in model building since it was the only solved structure at that time. Now the PI3K α structure is also available. The p110 γ -LY294002 complex structure was chosen (PDB ID : 1E7U in PDB bank) as a template from the four different inhibitor complexes, since **C401** is similar to LY294002. In an alternative procedure to choose the template structure, a MOE-SearchPDB search was performed to search for protein structures that are homologous to the query sequence, the sequence of mTOR. The sequence of mTOR was loaded into MOE-SearchPDB, and the sequences that matched well to the query sequence were searched. The best scored structure was the FRB domain of mTOR (PDB ID : 1NSG in PDB bank), which was solved already, with an E-value of 1.1E-47 and Z-score of 'good'. The E-value¹ (an expectation value) is an estimate of the number of possible false positives, and the Z-score² is an estimate of the statistical significance of an alignment score (likelihood that sequences are related). The second best score was for the p110 γ structure (PDB ID : 1E7U) with an E value of 1.9E-4 and Z-score of 7.2. The third best was the karyopherin beta2-Ran GppNHp nuclear transport complex (PDB ID :

¹ High E-values correspond to poor scores and low E-values correspond to good scores.

² The Z-scores of about 7 indicate that the sequences are very likely to be related.

1QBK) with 3.3E-3 and 8.9 as E-value and Z-score respectively. However, this sequence is matched with the HEAT repeat of mTOR (residue number 1 to 900) rather than the kinase domain.¹⁸³ The human sequence of p110 γ was loaded in the MOE-Sequence Editor and then the p110 γ -LY294002 complex structure was loaded. Sequence alignment between the full human sequence of p110 γ and the sequence from the crystal structure of p110 γ -LY294002 was performed with default values (without changing values in the program). These sequences were perfectly matched except the missing residues in loop regions of the crystal structure, which would be filled in in this procedure. The refined structure of p110 γ -LY294002 was built by running MOE-homology. One hundred homology intermediate models were generated. The final model was obtained by averaging 100 intermediates followed by minimization with the Amber99 force field.

Target-template alignment: The human sequences of mTOR, DNA-PK, PI3K α , PI3K γ , ATM, and ATR, and the refined structure of PI3K γ were loaded into MOE. Multiple alignment was performed using MOE-Align with the 'Match' substitution matrix and default values. The sequence identity of mTOR, DNA-PK, ATM, ATR, and p110 α to p110 γ are 13.3%, 15.7%, 12.6%, 13.0%, and 36.8%.

Model Building: MOE-homology was used to build homology models using the structure of p110 γ as a primary template. 'Intermediate Models' were set to 1000 and 'Final Models' was set to *Cartesian Average*, which means 1000 built structures (intermediate models) will be generated, and the final structure will be rebuilt by

averaging the coordinates of all of these 1000 models. 'Minimization' was set to *fine* for the minimization of each model with RMS gradient test of 0.1.

Model Evaluation: MOE-Protein Report was used to collect the measurements of dihedral angles, bond angles, bond lengths, and contacts of built protein structures. There are some outliers (outliers from the statistical range of specific dihedral angles such as phi, psi, omega, chi1, chi2, zeta angles and cis/trans conformation), but the outliers are far from the active site of the protein. Furthermore there is still debate about fixing outliers, because native protein structures in the PDB database also have some outliers. Therefore, instead of fixing outliers, the residues in the active sites of other proteins in the PIKK family were analyzed. This analysis showed that the residues in the active sites of other proteins in the PIKK family are homologous to each other, especially the hinge region of the active sites and lys833 (numbering in p110 γ) are conserved in other proteins in the PIKK family. In addition, we examined whether the results of the sequence alignment are dependent on the various alignment methods. The homology models were built after the alignment using other substitution matrixes such as 'blosum' and 'pam', and they gave consistent results, as the residues in the active site are the same as observed with other substitution matrixes.

Homology models of p110 α and DNA-PK were also generated through the same approach, but those of ATM and ATR were not built since these are not inhibited by LY294002 type compounds.

2,2-Dimethyl-N-pyridin-2-yl-propionamide (3.5)^{184, 185}: To a solution of 9.82 g (104.3 mmol) 2-aminopyridine (**3.4**) and 18 mL (130 mmol) triethylamine in 70 mL ether at 0 °C was added a solution of 14.4 g (120 mmol) pivaloyl chloride in 30 mL ether dropwise. After stirring for further 20 min, the reaction mixture was allowed to warm to room temperature and stirred further for 1 h. The reaction was then quenched by addition of 30 mL H₂O. The reaction mixture was diluted in ether, and the organic layer was separated, washed with 30 mL saturated NaHCO₃ solution and with brine. The organic layer was collected, dried with MgSO₄, and evaporated. The residual solid was purified with flash column chromatography on silica gel to yield the desired product as a transparent solid (16.8 g, 94.3 mmol, 90%). TLC *R*_f = 0.51 (Hexane/EtOAc 4:1); mp 71 °C (lit. mp 71 – 73 °C)¹⁸⁴; ¹H-NMR and ¹³C-NMR are consistent with those in the literature¹⁸⁵; ¹H-NMR (400 MHz, CDCl₃) δ, 8.22-8.19 (m, 2 H), 8.03 (br, 1 H), 7.64 (td, 1 H, *J* = 7.8 Hz, *J* = 2.0 Hz), 6.97 (t, 1 H, *J* = 6.1 Hz), 1.28 (s, 9 H); ¹³C-NMR (100 MHz, CDCl₃) δ, 176.91, 151.49, 147.60, 138.18, 119.55, 113.83, 39.64, 27.36; MS(ESI), *m/z* = 179.1 (M+H)⁺.

N-(3-Iodo-pyridin-2-yl)-2,2-dimethyl-propionamide (3.7)¹⁷³: To a cold (-78 °C) suspension of 2-(pivaloylamino)pyridine (1.0 g, 5.6 mmol) in a mixture of 20 mL dry ether and TMEDA (2.2 ml, 1.7 g, 14.6 mmol) was slowly added n-butyllithium (6 ml, 15 mmol). The resulting solution was reacted for 20 min at -78 °C, before being stirred for 2 h at 0 °C. A white precipitate slowly appeared, the mixture was cooled to -78 °C, and a solution of iodine (1.8 g, 7.1 mmol) in 20 mL ether was added. Stirring was continued for 2 h at -78 °C, and then the temperature was increased to 0 °C. Excess iodine was

destroyed by adding a sat. potassium thiosulfate solution. The reaction mixture was further diluted in ether and extracted. The organic layer was collected, washed with brine, dried over MgSO₄. The solvent was removed with a rotary evaporator to obtain a crude product, which was purified with flash column chromatography on silica gel to afford the desired product **3.7** (1.63 g, 5.4 mmol, 95%). TLC *R_f* = 0.23 (Hexane/EtOAc 1:1); mp 146 °C (lit. mp 148 °C); ¹H-NMR is consistent with that in the literature; ¹H-NMR (400 MHz, CDCl₃) δ, 8.35 (dd, 1 H, *J* = 4.6 Hz, *J* = 1.4 Hz), 8.08 (br, 1 H), 8.02 (dd, 1 H, *J* = 7.8 Hz, *J* = 1.4 Hz), 6.76 (dd, 1 H, *J* = 8.0 Hz, *J* = 4.8 Hz), 1.29 (s, 9 H); ¹³C-NMR (100 MHz, CDCl₃) δ, 175.77, 150.90, 147.95, 147.65, 121.54, 88.25, 39.75, 27.26; MS(ESI), *m/z* = 304.0 (M+H)⁺.

3-Iodo-pyridin-2-ylamine (3.3)¹⁷³: To compound **1.16** (0.91 g, 3.0 mmol) was added 20 mL 4 N HCl. The reaction mixture was stirred under reflux at 120 °C overnight. NaOH(aq) was added to adjust the pH to 7 after cooling to room temperature. The reaction mixture was diluted with methylene chloride and extracted. The organic layer was collected, washed with brine, dried with MgSO₄, and evaporated to afford the crude product. It was further purified with flash column chromatography on silica gel to yield the desired product **3.3** (0.53 g, 2.4 mmol, 80%). TLC *R_f* = 0.54 (Hexane/EtOAc 1:1); mp 88 °C (lit. mp 86 °C); ¹H-NMR is consistent with that in the literature; ¹H-NMR (400 MHz, CDCl₃) δ, 7.96 (dd, 1 H, *J* = 4.8 Hz, *J* = 1.6 Hz), 7.78 (dd, 1 H, *J* = 7.6 Hz, *J* = 1.6 Hz), 6.30 (dd, 1 H, *J* = 7.6 Hz, *J* = 4.8 Hz), 5.37 (br, 1 H); ¹³C-NMR (100 MHz, CDCl₃) δ, 157.64, 147.59, 146.80, 114.83, 77.74; MS(ESI) *m/z* = 220.9 (M+H)⁺.

2-Chloro-9-iodo-pyrido[1,2-*a*]pyrimidin-4-one (3.2): To a solution of 3-iodo-pyridin-2-ylamine (**3.3**) (2.19 g, 10.0 mmol) in 30 mL xylene was added triethylamine (1.7 mL, 12.2 mmol). The solution was heated to 80 °C for 30 min, and diethyl malonate (3.0 mL, 30.8 mmol) was added. After stirring for further 30 min, TLC was examined. The reactant was completely gone, and intermediate was present (TLC R_f = 0.31 (Hexane/EtOAc 1:1). To this solution was added 10 mL POCl₃, and the reaction mixture turned to a yellow suspension. Stirring was continued for 5 h at 130 °C, and cooled to room temperature. The solution was poured carefully into ice water, and the aqueous solution was adjusted to pH = 7 with saturated Na₂CO₃ solution. The crude product was extracted with methylene chloride, washed with brine, dried with MgSO₄, and concentrated with a rotary evaporator. The product was purified with flash column chromatography on silica gel to afford the desired product **3.2** as a pale yellow solid (1.84 g, 6.0 mmol, 60% yield). TLC R_f = 0.60 (Hexane/EtOAc 1:1); mp 224 – 225 °C; ¹H-NMR (400 MHz, CDCl₃) δ, 9.05 (d, 1 H, J = 6.8 Hz), 8.44 (d, 1 H, J = 7.2 Hz), 6.95 (t, 1 H, J = 7.0 Hz), 6.49 (s, 1 H); ¹³C-NMR (100 MHz, CDCl₃) δ, 159.07, 157.42, 148.58, 148.23, 128.44, 116.64, 102.99, 96.52; MS(ESI) m/z = 307.0 (M+H)⁺.

9-Iodo-2-morpholin-4-yl-pyrido[1,2-*a*]pyrimidin-4-one (3.1): To a solution of **3.2** (1.84 g, 6.0 mmol) in ethanol (20 mL) was added excess morpholine (~ 5 eq.) and catalytic amount of acetic acid (3 drops), and the solution was stirred under reflux overnight. After cooling, the solvent was removed with a rotary evaporator. The reaction mixture

was redissolved in water, and the product mixture was extracted with methylene chloride. The organic layer was washed with brine, dried with MgSO_4 , and concentrated with a rotary evaporator. The product was purified with flash column chromatography on silica gel to give **3.1** as a colorless solid (2.03 g, 5.8 mmol, 97% yield). TLC R_f = 0.23 ($\text{CH}_2\text{Cl}_2/\text{EtOAc}$ 1:1); mp 215 °C; $^1\text{H-NMR}$ (400 MHz, CDCl_3) δ , 8.87 (dd, 1 H, J = 7.2 Hz, J = 1.2 Hz), 8.18 (dd, 1 H, J = 7.2 Hz, J = 1.2 Hz), 6.60 (t, 1 H, J = 7.0 Hz), 5.54 (s, 1 H), 3.80-3.70 (m, 8H); $^{13}\text{C-NMR}$ (100 MHz, CDCl_3) δ , 160.55, 158.90, 148.08, 146.59, 128.34, 113.08, 95.63, 80.34, 66.50, 44.69; MS(ESI) m/z = 358.0 ($\text{M}+\text{H}$) $^+$.

2-Morpholin-4-yl-9-naphthalen-2-yl-pyrido[1,2-*a*]pyrimidin-4-one (C303): To a solution of **3.1** (0.14 g, 0.4 mmol) in 5 mL dry DMF were added 20 mg $\text{Pd}(\text{OAc})_2$, 60 mg $\text{P}(\text{o-tolyl})_3$, 120 mg Na_2CO_3 . 2-Naphthylboronic acid (0.17 g, 0.99 mmol) was added to this reaction mixture, and it was stirred at 80 °C for 2 h. After completion of the reaction, the cooled reaction mixture was poured into a saturated NaHCO_3 solution (20 mL). The crude product was extracted with ethyl acetate, washed with brine. The organic layer was dried over MgSO_4 and evaporated. The product was purified with flash column chromatography on silica gel to yield the desired product **C303** as a colorless solid (0.12 g, 0.33 mmol, 83% yield). TLC R_f = 0.34 ($\text{CH}_2\text{Cl}_2/\text{EtOAc}$ 1:1); mp 211 – 212 °C; $^1\text{H-NMR}$ (300 MHz, CDCl_3) δ , 8.99 (d, 1 H, J = 6.0 Hz), 8.06 (s, 1 H), 8.06-7.86 (m, 3 H), 7.82-7.75 (m, 2 H), 7.55-7.52 (m, 2 H), 7.02 (t, 1 H, J = 7.1 Hz), 5.72 (s, 1 H), 3.71-3.52 (m, 8H); $^{13}\text{C-NMR}$ (100 MHz, CDCl_3) δ , 160.42, 159.04, 149.18, 136.60, 135.55, 134.59, 133.19,

132.95, 128.76, 128.09, 127.82, 127.63, 127.19, 126.91, 126.49, 126.29, 112.51, 80.89, 66.50, 44.52; MS(ESI) $m/z = 358.1$ (M+H)⁺.

2-Morpholin-4-yl-9-quinolin-7-yl-pyrido[1,2-a]pyrimidin-4-one (C321): Compound **C321** was prepared from **3.1** and quinolin-7-ylboronic acid according to the same procedure as that for **C303**. Compound **C321** was obtained as a colorless solid (0.08 g, 0.22 mmol, 55 % yield and some unreacted reactant).

2-Morpholin-4-yl-9-styryl-pyrido[1,2-a]pyrimidin-4-one (C309): To a solution of **3.1** (0.36 g, 1.0 mmol) in 5 mL dry DMF were added 20 mg Pd(OAc)₂, 60 mg P(o-tolyl)₃, 130 mg NaOAc. Styrene (0.2 mL, 1.7 mmol) was added to this reaction mixture, and it was stirred at 140 °C for 6 h. After completion of the reaction, saturated NaHCO₃ solution (20 mL) was added to the cooled reaction mixture. The crude product was extracted with methylene chloride. The organic layer was washed with brine, dried over MgSO₄, removed by evaporation. The product was purified by flash column chromatography on silica gel to yield the desired product **C309** (0.23 g, 0.69 mmol, 69%). TLC $R_f = 0.17$ (Hexane/EtOAc 1:1); mp 204.5 – 205.5 °C; ¹H-NMR (400 MHz, CDCl₃) δ, 8.89 (d, 1 H, $J = 7.2$ Hz), 7.89 (d, 1 H, $J = 6.8$ Hz), 7.77 (d, 1 H, $J = 16.4$ Hz), 7.56 (d, 2 H, $J = 7.6$ Hz), 7.41 (t, 2 H, $J = 7.4$ Hz), 7.34-7.25 (m, 2 H), 6.93 (t, 1 H, $J = 7.0$ Hz), 5.66 (s, 1 H), 3.84-3.70 (m, 8H); ¹³C-NMR (100 MHz, CDCl₃) δ, 160.32, 158.90, 148.73, 137.01, 132.03, 131.70, 131.42, 128.84, 128.34, 126.90, 126.51, 122.56, 112.45, 81.25, 66.60, 44.68; MS(ESI) $m/z = 334.1$ (M+H)⁺.

4-Benzyl-2-chloromethyl-morpholine (3.15)¹⁸⁶: To a solution of N-benzyl-ethanolamine (14.4 mL, 100 mmol) in toluene (20 mL) (\pm)-epichlorohydrine (9.4 mL, 120 mmol) was slowly added at room temperature. The reaction mixture was stirred and heated to 50 °C for 2 h. The reaction mixture was then cooled, and the solvent was evaporated. The remaining epichlorohydrin was exhaustively removed in vacuum to give the intermediate diol as a pale green viscous oil. TLC R_f = 0.30 (Hexane/EtOAc 1:1). The diol was treated with concentrated sulfuric acid (ca. 12 mL) at room temperature, and the resulting orange mixture was stirred at 120 °C for 12 h, turning dark brown in color. After cooling the reaction mixture, ice water was added. The aqueous layer was then basified (pH 14) using 4 N aqueous sodium hydroxide solution, and the crude product was extracted with methylene chloride. The organic extracts were combined, washed with water and brine, dried with MgSO₄, and concentrated with a rotary evaporator. Purification with flash column chromatography on silica gel gave the desired product as a yellow oil (11.23 g, 49.8 mmol, 50 % yield over 2 steps); TLC R_f = 0.67 (Hexane/EtOAc 1:1); ¹H-NMR is consistent with that in the literature; ¹H-NMR (400 MHz, CDCl₃) δ , 7.37-7.24 (m, 5 H), 3.89 (d, 1 H, J = 11.6 Hz), 3.79-3.73 (m, 1 H), 3.70 (td, 1 H, J = 11.1 Hz, J = 2.7 Hz), 3.54-3.43 (m, 4 H), 2.84 (d, 1 H, J = 10.8 Hz), 2.64 (d, 1 H, J = 11.2 Hz), 2.20 (td, 1 H, J = 11.3 Hz, J = 3.3 Hz), 2.01 (t, 1 H, J = 10.6 Hz); ¹³C-NMR (100 MHz, CDCl₃) δ , 137.50, 129.06, 128.29, 127.23, 75.13, 66.80, 63.14, 55.84, 52.70, 44.89; MS (ESI), m/z = 226.1 (M+H)⁺.

(4-Benzyl-morpholin-2-yl)-methanol (3.16)¹⁸⁶: To a solution of (±)-4-benzyl-2-chloromethyl-morpholine (**3.15**) (1.1 g, 4.9 mmol) dissolved in formamide (10 mL) was added an excess of water (3 mL). The reaction mixture was stirred at 150 °C overnight. After complete consumption of the reactant indicated by TLC and mass analyses, the reaction mixture was cooled to room temperature and diluted with water before being basified (to pH = 14) using 4 N aqueous sodium hydroxide solution. Toluene was used to extract the crude product. The combined toluene extracts were washed with brine and dried with MgSO₄. The solvent was removed by a rotary evaporator, and the product was purified with flash column chromatography on silica gel to give the desired alcohol as a viscous yellow oil (0.85 mg, 4.1 mmol, 84%). TLC R_f = 0.24 (100 % EtOAc); ¹H-NMR is consistent with that in the literature; ¹H-NMR (300 MHz, CDCl₃) δ, 7.33-7.24 (m, 5 H), 3.89 (d, 1 H, J = 11.1 Hz), 3.75-3.45 (m, 6 H), 2.71-2.65 (m, 2 H), 2.27 (br, 1 H), 2.19 (td, 1 H, J = 11.8 Hz, J = 3.8 Hz), 2.00 (t, 1 H, J = 10.7 Hz); ¹³C-NMR (100 MHz, CDCl₃) δ, 137.20, 129.10, 128.13, 127.09, 75.99, 66.39, 63.85, 63.17, 54.47, 52.82; MS (ESI), m/z = 208.1 (M+H)⁺.

Morpholin-2-yl-methanol (3.17)^{179, 186}: To a solution of compound **3.16** (1.4 g, 6.8 mmol) in 30 mL methanol was added ~ 0.5 g of palladium on carbon. After removing air in the flask using a vacuum pump, hydrogen gas was added to the reaction flask using a balloon. The reaction mixture was stirred for 1 h, the flask was evacuated by vacuum and refilled with hydrogen gas. This was repeated 3 times and the reaction mixture was

stirred overnight at room temperature. Palladium on carbon was removed by filtration. The filtrate was collected and evaporated to give a viscous oil (ca. 0.70 g, 6.0 mmol, 88 % yield). After confirming the product of debenylation using $^1\text{H-NMR}$, the product was directly used for the next step; $^1\text{H-NMR}$ is consistent with that in the literature; $^1\text{H-NMR}$ (300 MHz, CDCl_3) δ , 3.80 (d, 1 H, $J = 6.6$ Hz), 3.55-3.45 (m, 4 H), 2.95 (br, 1 H), 2.81-2.55 (m, 2 H), 2.58-2.55 (m, 1 H), 0.96 (d, 1 H, $J = 6.6$ Hz).

2-(2-Hydroxymethyl-morpholin-4-yl)-pyrimido[2,1-*a*]isoquinolin-4-one (C407): To compound **2.5** (0.25 g, 1.1 mmol) in ethanol (10 mL) was added compound **3.17**. A catalytic amount of acetic acid (3 drops) was added and the reaction mixture was stirred under reflux at 120 °C for 5 h. TLC test showed that the reactant was completely gone and a new polar spot was appeared. The reaction mixture was cooled and ethanol was removed by using a rotary evaporator. The product mixture was redissolved in water and extracted with methylene chloride. The organic layer was dried with MgSO_4 and evaporated to give the title compound as a white solid. It was further purified with flash column chromatography on silica gel eluting with 5 % ethanol in ethyl acetate, and pure **C407** was obtained (0.32 g, 1.0 mmol, 91%); TLC $R_f = 0.09$ (100 % EtOAc); $^1\text{H-NMR}$ (400 MHz, $\text{DMSO-}d_6$) δ , 8.74 (d, 1 H, $J = 8.0$ Hz), 8.50 (d, 1 H, $J = 7.6$ Hz), 7.83-7.66 (m, 3 H), 7.28 (d, 1 H, $J = 7.2$ Hz), 5.69 (s, 1 H), 4.85 (s, 1 H), 4.42 (s, br, 1 H), 4.28 (s, br, 1 H), 3.96 (d, 1 H, $J = 11.2$ Hz), 3.58-3.50 (m, 4H), 3.03 (t, 1 H, $J = 12.2$ Hz), 2.79 (t, 1 H, $J = 11.2$ Hz); $^{13}\text{C-NMR}$ (100 MHz, $\text{DMSO-}d_6$) δ , 159.72, 158.14, 148.52, 134.05, 132.66, 128.28, 126.68,

126.43, 125.40, 121.51, 112.33, 81.09(81.12), 65.42, 62.20, 46.16, 43.95; MS (ESI), $m/z = 312.1$ (M+H)⁺.

Methanesulfonic acid 4-(4-oxo-4H-pyrimido[2,1-*a*]isoquinolin-2-yl)-morpholin-2-

ylmethyl ester (3.18): To a solution of **C407** (0.24 g, 0.77 mmol) in methylene chloride (50 mL) was added triethylamine (0.3 mL) at 0 °C. To this reaction mixture was slowly added methanesulfonyl chloride (0.15 mL, 1.9 mmol) at 0 °C. After 30 min the temperature was increased to room temperature. After 1 h the reactant was completely gone (by TLC) and the reaction was quenched by adding water at 0 °C. The product mixture was extracted with methylene chloride and the extracts were washed with brine. The organic layer was dried with MgSO₄ and concentrated with a rotary evaporator to give a dim yellow solid. The product was further purified with flash column chromatography on silica gel by eluting with ethyl acetate/hexane (2/1) and a white solid (0.27 g, 0.69 mmol, 90 % yield) was obtained; TLC $R_f = 0.36$ (100 % EtOAc); mp 190 – 191 °C; ¹H-NMR (400 MHz, CDCl₃) δ, 8.79 (d, 1 H, $J = 8.0$ Hz), 8.65 (d, 1 H, $J = 7.6$ Hz), 7.76-7.60 (m, 3 H), 7.08 (d, 1 H, $J = 7.6$ Hz), 5.67 (s, 1 H), 4.48 (d, 1 H, $J = 11.6$ Hz), 4.37 (d, 2 H, $J = 4.8$ Hz), 4.19 (d, 1 H, $J = 11.6$ Hz), 4.12-4.08 (m, 1 H), 3.92-3.86 (m, 1 H), 3.73 (td, 1 H, $J = 11.6$ Hz, $J = 2.8$ Hz), 3.18 (td, 1 H, $J = 12.4$ Hz, $J = 3.6$ Hz), 3.12 (s, 3 H), 3.00 (dd, 1 H, $J = 13.0$ Hz, $J = 10.6$ Hz); ¹³C-NMR (100 MHz, CDCl₃) δ, 160.26, 159.62, 149.20, 134.36, 132.53, 128.14, 126.94, 126.46, 126.08, 121.97, 112.76, 82.68, 72.96, 69.30, 66.16, 45.30, 44.10, 37.73; MS (ESI), $m/z = 390.1$ (M+H)⁺.

2-(2-Mercaptomethyl-morpholin-4-yl)-pyrimido[2,1-*a*]isoquinolin-4-one (C406): To a solution of compound **3.18** (0.11 g, 0.28 mmol) in methanol (10 mL) was added thiourea (0.1 g, 1.3 mmol). This reaction mixture was stirred under reflux for 5 h. After cooling, 1N NaOH (5 mL) was added and stirred under reflux for 1 h. After cooling, methanol was removed by a rotary evaporator. The product mixture was redissolved in water and extracted with methylene chloride. The organic layer was dried with MgSO₄ and removed by a rotary evaporator. TLC test showed one single more polar spot ($R_f = 0.24$ (100 % EtOAc)) than that of the reactant ($R_f = 0.36$, 100 % EtOAc), but it was the oxidized disulfide compound. To this disulfide compound was added methanol (10 mL) and NaBH₄ (0.2 g). This reaction mixture was stirred under reflux again for 5 h, and it became homogeneous. After cooling, 1 N HCl (0.1 mL) was added and the solvent was removed by a rotary evaporator. The product mixture was redissolved in water and extracted with methylene chloride. The organic layer was dried with MgSO₄ and removed by a rotary evaporator to give a dim yellow solid (0.10 g, 0.30 mmol, 100 % yield with some impurity, not purified by column); TLC $R_f = 0.15$ (100 % EtOAc); ¹H-NMR (300 MHz, CDCl₃) δ , 8.80 (d, 1 H, $J = 8.4$ Hz), 8.65 (d, 1 H, $J = 7.2$ Hz), 7.76-7.58 (m, 3 H), 7.06 (d, 1 H, $J = 7.2$ Hz), 5.65 (s, 1 H), 4.48 (d, 1 H, $J = 12.9$ Hz), 4.24 (d, 1 H, $J = 12.9$ Hz), 4.09-4.04 (m, 1 H), 3.71 (td, 1 H, $J = 11.6$ Hz, $J = 3.0$ Hz), 3.65-3.57 (m, 1 H), 3.16 (td, 1 H, $J = 12.3$ Hz, $J = 3.6$ Hz), 2.94 (dd, 1 H, $J = 12.9$ Hz, $J = 10.2$ Hz), 2.83-2.62 (m, 2 H), 1.69 (dd, 1 H, $J = 9.3$ Hz, $J = 7.5$ Hz).

C446 (not desired product): To a solution of C406 (0.10 g, 0.30 mmol) in methanol (10 mL) and methylene chloride (10 mL) was added methoxycarbonylsulfonyl chloride (0.1 mL, 1.1 mmol) at 0 °C. This reaction mixture was stirred at 0 °C and the temperature was slowly increased to room temperature. After 6 h, TLC test showed that all of the reactant was changed to a less polar compound. Solvents were removed with a rotary evaporator. The product was directly purified by flash column chromatography on silica gel by eluting with ethyl acetate/hexane (1/1) to give the title compound; TLC R_f = 0.57 (100 % EtOAc); $^1\text{H-NMR}$ (400 MHz, CDCl_3) δ , 8.80 (d, 1 H, J = 8.4 Hz), 8.64 (d, 1 H, J = 7.6 Hz), 7.80-7.63 (m, 3 H), 7.12 (d, 1 H, J = 8.0 Hz), 4.66 (d, 1 H, J = 13.2 Hz), 4.41 (dd, 1 H, J = 13.4 Hz, J = 1.8 Hz), 4.02 (d, 1 H, J = 11.6 Hz), 3.93-3.85 (m, 7 H), 3.76 (td, 1 H, J = 11.6 Hz, J = 2.4 Hz), 3.43-3.36 (m, 1 H), 3.13 (dd, 1 H, J = 13.2 Hz, J = 10.0 Hz), 3.08-2.90 (m, 2 H); $^{13}\text{C-NMR}$ (100 MHz, CDCl_3) δ , 169.70, 169.17, 163.47, 160.16, 148.54, 134.65, 133.09, 128.47, 127.15, 126.55, 125.92, 122.64, 113.54, 85.62, 74.00, 66.76, 55.51, 54.60, 52.06, 48.69, 41.54.

4-[Benzyl-(2-hydroxy-ethyl)-amino]-but-2-enoic acid ethyl ester (3.19): To a solution of N-benzyl ethanolamine **3.11** (7.5 mL, 50 mmol) in methylene chloride (30 mL) were added ethyl 4-bromocrotonate **3.13** (75 % purity, 9.1 mL, 50.2 mmol) and triethylamine (8 mL, 57.4 mmol) at room temperature. The reaction mixture was stirred overnight, and then diluted in methylene chloride and water. The product was extracted with methylene chloride and washed with brine. The organic layer was dried with MgSO_4 and

concentrated with a rotary evaporator to give a viscous oil. The product was further purified by flash column chromatography on silica gel by eluting with ethyl acetate/hexane (1/1) and a viscous oil (12.9 g, 49.0 mmol, 98 % yield) was obtained; TLC $R_f = 0.63$ (100 % EtOAc); $^1\text{H-NMR}$ (300 MHz, CDCl_3) δ , 7.37-7.25 (m, 5 H), 6.99 (dt, 1 H, $J = 16.8$ Hz, $J = 6.2$ Hz), 6.02 (dd, 1 H, $J = 16.8$ Hz, $J = 1.2$ Hz), 4.21 (q, 2 H, $J = 7.1$ Hz), 3.66-3.61 (m, 4 H), 3.29 (dd, 2 H, $J = 6.1$ Hz, $J = 1.3$ Hz), 2.69 (t, 2 H, $J = 5.5$ Hz), 1.31 (t, 3 H, $J = 7.5$ Hz); $^{13}\text{C-NMR}$ (100 MHz, CDCl_3) δ , 165.75, 145.11, 138.03, 128.55, 128.12, 126.98, 123.09, 60.06, 58.66, 58.10, 55.02, 54.23, 13.92 .

(4-Benzyl-morpholin-2-yl)-acetic acid ethyl ester (3.20): To a solution of compound **3.19** (12.9 g, 49 mmol) in toluene (50 mL) was added DBU (3.0 mL, 20.0 mmol) at room temperature. The reaction mixture was stirred under reflux overnight. After cooling, the reaction mixture was diluted in ethyl acetate and water. The product mixture was extracted with ethyl acetate and washed with brine. The solvent layer was dried with MgSO_4 and concentrated with a rotary evaporator to give a viscous oil. By eluting with 20 % ethyl acetate in hexane the product was further purified to give an viscous oil (12.7g, 48.2 mmol, 98 % yield); TLC $R_f = 0.60$ (1/1 EtOAc/Hexane); $^1\text{H-NMR}$ (300 MHz, CDCl_3) δ , 7.32-7.21 (m, 5 H), 4.12 (q, 2 H, $J = 7.2$ Hz), 4.02-3.94 (m, 1 H), 3.82 (dq, 1 H, $J = 11.5$ Hz, $J = 1.7$ Hz), 3.67 (td, 1 H, $J = 11.2$ Hz, $J = 2.7$ Hz), 3.48 (s, 2 H), 2.76 (dt, 1 H, $J = 11.4$ Hz, $J = 1.9$ Hz), 2.62 (dq, 1 H, $J = 11.4$ Hz, $J = 2.0$ Hz), 2.53-2.31 (m, 2 H), 2.16 (td, 1 H, $J = 11.3$ Hz, $J = 3.3$ Hz), 1.91 (dd, 1 H, $J = 10.8$, Hz, $J = 9.9$ Hz); $^{13}\text{C-NMR}$ (100 MHz, CDCl_3) δ ,

170.29, 137.37, 128.65, 127.89, 126.77, 71.95, 66.32, 62.70, 60.02, 57.50, 52.41, 38.55, 13.80; MS (ESI), $m/z = 264.1$ (M+H)⁺.

Morpholin-2-yl-acetic acid ethyl ester (3.12): To a solution of compound **3.20** (2.0 g, 7.6 mmol) in 30 mL methanol was added ~ 1.0 g of palladium on carbon. Hydrogen gas was added to the reaction flask of hydrogen reactor in Jim's lab. The reaction mixture was shaken under 55 psi overnight (about 12 h). Palladium and carbon were filtered. Filtrate was collected and evaporated to give viscous oil (1.2 g, 6.9 mmol, 91 % yield). After confirming of debenzylation using ¹H-NMR, the product was directly used for the next step; ¹H-NMR (300 MHz, CDCl₃) δ , 3.89 (q, 2 H, $J = 7.5$ Hz), 3.65-3.56 (m, 3 H), 3.35 (td, 1 H, $J = 8.0$ Hz, $J = 4.3$ Hz), 2.71-2.08 (m, 6 H), 1.68 (s, 1 H), 1.01 (t, 3 H, $J = 7.1$ Hz).

2-(4-Benzyl-morpholin-2-yl)-ethanol (3.21): LiAlH₄ (0.47 g, 12.4 mmol) was dissolved in anhydrous ether (100 mL) at 0 °C. To this solution was added a solution of compound **3.20** (3.08 g, 11.7 mmol) in anhydrous ether (50 mL) dropwise. After stirring at 0 °C for 30 min, the temperature was increased to room temperature and the reaction mixture was stirred overnight. 0.47 mL of water, 0.47 mL of 15 % NaOH, and 1.41 mL of water were sequentially added to the reaction mixture at 0 °C. The precipitated white solid was filtered off, and the filtrate was concentrated with a rotary evaporator. After flash column chromatography on silica gel by eluting with 50 % hexane in ethyl acetate, the product **3.21** was obtained (2.27 g, 10.3 mmol, 88 % yield); TLC $R_f = 0.15$ (1/1 EtOAc/Hexane); ¹H-NMR (300 MHz, CDCl₃) δ , 7.37-7.26 (m, 5 H), 3.85 (dq, 1 H, $J = 11.3$

Hz, $J = 1.6$ Hz), 3.80-3.65 (m, 4 H), 3.52 (s, 2 H), 3.41 (br, 1 H), 2.76-2.64 (m, 2 H), 2.18 (td, 1 H, $J = 11.3$ Hz, $J = 3.2$ Hz), 1.95 (dd, 1 H, $J = 11.1$ Hz, $J = 10.2$ Hz), 1.80-1.57 (m, 2 H); ^{13}C -NMR (100 MHz, CDCl_3) δ , 137.47, 129.04, 128.16, 127.07, 75.36, 66.66, 63.09, 60.45, 58.36, 52.86, 35.52.

2-Morpholin-2-yl-ethanol (3.23): Compound **3.23** was prepared from **3.21** (0.93 g, 4.2 mmol) in methanol (50 mL) according to the same procedure as that for **3.17**.

Compound **3.23** was obtained as a viscous oil (0.50 g, 3.8 mmol, 90 % yield). After confirming of debenzylation using ^1H -NMR and ^{13}C -NMR, the product was directly used for the next step; ^1H -NMR (300 MHz, CDCl_3) δ , 3.79 (d, 1 H, $J = 9.6$ Hz), 3.55-3.45 (m, 4 H), 2.95 (br, 2 H), 2.81-2.73 (m, 2 H), 2.58-2.55 (m, 2 H), 0.96 (dq, 1 H, $J = 6.5$ Hz, $J = 1.3$ Hz); ^{13}C -NMR (300 MHz, CDCl_3) δ , 137.47, 129.04, 128.16, 127.07, 75.36, 66.66, 63.09, 60.45, 58.36, 52.86, 35.52.

2-[2-(2-Hydroxy-ethyl)-morpholin-4-yl]-pyrimido[2,1- α]isoquinolin-4-one (3.25):

Compound **3.25** was prepared from **3.23** (4 eq.) and **2.5** (0.23 g, 1.0 mmol) according to the same procedure as that for **C407**. Compound **3.25** was obtained as a colorless solid (0.30 g, 0.92 mmol, 92% yield); TLC $R_f = 0.18$ (100 % EtOAc); ^1H -NMR (300 MHz, CDCl_3) δ , 8.64 (d, 1 H, $J = 7.8$ Hz), 8.54 (d, 1 H, $J = 7.5$ Hz), 7.66-7.48 (m, 3 H), 6.95 (d, 1 H, $J = 7.8$ Hz), 5.58 (s, 1 H), 4.24 (br, 2 H), 4.00 (dd, 1 H, $J = 11.6$ Hz, $J = 2.6$ Hz), 3.85-3.61 (m, 4 H),

3.18 (br, 1 H), 3.07 (td, 1 H, $J = 12.6$ Hz, $J = 3.6$ Hz), 2.81 (dd, 1 H, $J = 12.9$ Hz, $J = 10.5$ Hz), 1.88-1.75 (m, 2 H).

Methanesulfonic acid 2-[4-(4-oxo-4H-pyrimido[2,1- α]isoquinolin-2-yl)-morpholin-2-yl]-ethyl ester (3.26): Compound **3.26** was prepared from **3.25** (0.30 g, 0.92 mmol)

according to the same procedure as that for **3.18**. Compound **3.26** was obtained as a colorless solid (0.35 g, 0.87 mmol, 95% yield); TLC $R_f = 0.39$ (100 % EtOAc); mp > 250 °C; $^1\text{H-NMR}$ (300 MHz, CDCl_3) δ , 8.77 (d, 1 H, $J = 8.1$ Hz), 8.63 (d, 1 H, $J = 7.8$ Hz), 7.74-7.57 (m, 3 H), 7.05 (d, 1 H, $J = 7.5$ Hz), 5.63 (s, 1 H), 4.47-4.37 (m, 3 H), 4.18 (d, 1 H, $J = 12.9$), 4.03 (dd, 1 H, $J = 11.6$ Hz, $J = 2.2$ Hz), 3.74-3.62 (m, 2 H), 3.12 (td, 1 H, $J = 12.5$ Hz, $J = 3.6$ Hz), 3.03 (s, 3 H), 2.83 (dd, 1 H, $J = 13.1$ Hz, $J = 10.7$ Hz), 2.08-1.92 (m, 2 H); $^{13}\text{C-NMR}$ (100 MHz, CDCl_3) δ , 160.09, 159.56, 149.10, 134.27, 132.42, 128.04, 126.91, 126.37, 126.05, 121.90, 112.56, 82.33(82.31), 71.46, 66.10, 48.84, 44.17, 37.24, 37.22, 32.81 .

[4-(4-Oxo-4H-pyrimido[2,1- α]isoquinolin-2-yl)-morpholin-2-yl]-acetic acid ethyl ester (C413): Compound **C413** was prepared from **3.12** (4 eq.) and **2.5** (0.23 g, 1.0 mmol)

according to the same procedure as that for **C401**. Compound **C413** was obtained as a colorless solid (0.35 g, 0.95 mmol, 95% yield); TLC $R_f = 0.39$ (100 % EtOAc); mp 168 °C; $^1\text{H-NMR}$ (400 MHz, CDCl_3) δ , 8.68 (d, 1 H, $J = 8.0$ Hz), 8.56 (d, 1 H, $J = 7.6$ Hz), 7.67-7.50 (m, 3 H), 6.97 (d, 1 H, $J = 7.6$ Hz), 5.57 (s, 1 H), 4.35 (br, 1 H), 4.16 (q, 3 H, $J = 7.2$), 4.00-3.93 (m, 2 H), 3.67 (td, 1 H, $J = 11.6$ Hz, $J = 2.4$ Hz), 3.09 (td, 1 H, $J = 12.4$ Hz, $J = 3.6$ Hz), 2.84 (dd, 1 H, $J = 13.0$ Hz, $J = 10.6$ Hz), 2.63-2.49 (m, 2 H), 1.25 (t, 2 H, $J = 7.2$ Hz); $^{13}\text{C-}$

NMR (100 MHz, CDCl₃) δ , 170.13, 159.91, 159.36, 148.87, 134.11, 132.18, 127.77, 126.68, 126.19, 125.92, 121.80, 112.29, 82.17, 71.88, 66.07, 60.65, 48.38, 43.88, 38.39, 14.04; MS(ESI) m/z = 368.1 (M+H)⁺.

[4-(4-Oxo-4H-pyrimido[2,1- α]isoquinolin-2-yl)-morpholin-2-yl]-acetic acid (C444): To

compound **C413** (0.11 g, 0.30 mmol) were added MeOH (10 mL), H₂O (1 mL), and 1N NaOH (1 mL), and the mixture was stirred at 70 °C for 1 h. The heterogeneous reaction mixture became homogeneous. TLC test showed that all starting material was hydrolyzed. After cooling, methanol was removed with a rotary evaporator. Ethyl acetate was added to extract the unreacted reactant or any neutral compound, and then the aqueous layer was acidified (pH = ~ 2) with aqueous 1N HCl. The transparent water layer turned to a white solution. The product mixture was extracted with ethyl acetate. The organic layer was dried over MgSO₄ and solvent removed with a rotary evaporator to give the title compound as a white solid (0.10 g, 0.29 mmol, 97% yield);

¹H-NMR (300 MHz, CDCl₃) δ , 8.77 (d, 1 H, J = 8.4 Hz), 8.50 (d, 1 H, J = 7.5 Hz), 7.84-7.64 (m, 3 H), 7.29 (d, 1 H, J = 7.8 Hz), 5.63 (s, 1 H), 4.50 (br, 1 H), 4.28 (br, 1 H), 3.94 (d, 1 H, J = 12.3 Hz), 3.82 (d, 1 H, J = 4.5 Hz), 3.55 (t, 1 H, J = 11.4 Hz), 3.04 (t, 1 H, J = 11.0 Hz), 2.81 (t, 1 H, J = 12.0 Hz), 2.64-2.40 (m, 3 H); ¹³C-NMR (100 MHz, CDCl₃) δ , 171.82, 159.57, 158.20, 148.59, 134.09, 132.70, 128.29, 126.70, 126.54, 125.44, 121.52, 112.40, 81.16, 72.09, 65.60, 48.04, 43.80, 38.06.

2-[4-(4-Oxo-4H-pyrimido[2,1-*a*]isoquinolin-2-yl)-morpholin-2-yl]-acetamide (C445): To a solution of compound **3.20** (0.11 g, 0.45 mmol) in methanol was added aqueous ammonium hydroxide (NH₄OH) at room temperature. The reaction mixture was closed tightly with a septum and stirred overnight at room temperature. The completion of the reaction was confirmed by mass spectral analysis. The major amide product peak (*m/z* = 235.1) and the minor carboxylic product peak (*m/z* = 236.1) were detected. The solvent and water were removed with a rotary evaporator and the residue was further dried by connecting to a vacuum pump overnight. The product mixture (**3.22**) was redissolved in methanol and palladium on carbon (ca. 0.2 g) was added. The benzylation was performed according to the same procedure as that for **3.12** to give **3.24**. **C445** was prepared from **2.5** (0.23 g, 1.0 mmol) and **3.24** according to the same procedure as that for **C407**. Compound **C445** was obtained as a colorless solid (0.05 g, 0.15 mmol, 33% yield); TLC *R_f* = 0.12 (EtOAc/MeOH : 9/1); ¹H-NMR (400 MHz, DMSO-*d*₆) δ, 8.80 (d, 1 H, *J* = 8.0 Hz), 8.52 (d, 1 H, *J* = 8.0 Hz), 7.88-7.83 (m, 2 H), 7.70 (td, 1 H, *J* = 7.4 Hz, *J* = 2.0 Hz), 7.40 (s, 1 H), 7.31 (d, 1 H, *J* = 7.6 Hz), 6.91 (s, 1 H), 5.64 (s, 1 H), 4.46 (br, 1 H), 4.29 (br, 1 H), 3.93 (d, 1 H, *J* = 10.8 Hz), 3.84-3.79 (m, 1 H), 3.53 (td, 1 H, *J* = 11.6 Hz, *J* = 2.4 Hz), 3.09-3.02 (m, 1 H), 2.81 (dd, 1 H, *J* = 13.0 Hz, *J* = 10.6 Hz), 2.38-2.30 (m, 2 H); ¹³C-NMR (100 MHz, DMSO-*d*₆) δ, 171.24, 159.60, 158.18, 148.61, 134.11, 132.74, 128.34, 126.73, 126.55, 125.45, 121.54, 112.39, 81.10, 72.40, 65.52, 48.38, 43.86.

(R)-2-Chloro-N-(2,3-dihydroxy-propyl)-acetamide (3.28): To a solution of (R)-3-amino-1,2-propanediol (**3.27**) (3.98 g, 43.7 mmol) in a mixture of CH₃CN/methanol (80 mL/24

mL) at - 10 °C was added triethylamine (7.2 mL, 51.6 mmol). After 10 min, chloroacetyl chloride (4.4 mL, 55.3 mmol) was added dropwise at - 10 °C over 2 h. The reaction mixture was stirred overnight at room temperature. The solvent was removed with a rotary evaporator and a white solid was obtained. The product was further purified by flash column chromatography on silica gel by eluting with ethyl acetate/methanol (95/5) to give compound **3.28** as a white solid (6.14 g, 36.6 mmol, 84% yield); TLC R_f = 0.24 (EtOAc/MeOH : 9/1); $^1\text{H-NMR}$ (300 MHz, DMSO- d_6) δ , 8.07 (t, 1 H, J = 5.2 Hz), 4.78 (d, 1 H, J = 5.1 Hz), 4.54 (t, 1 H, J = 5.7 Hz), 4.05 (s, 2 H), 3.54-3.20 (m, 5 H), 3.03-2.95 (m, 1 H).

(R)-6-Hydroxymethyl-morpholin-3-one (3.29): To a solution of potassium tert-butoxide (5.51 g, 49.1 mmol) in 100 mL 2-butanol at room temperature was added **3.29** (2.80 g, 16.7 mmol) in 100 mL 2-butanol over 2 h under nitrogen. After one more hour stirring, methanol (15 mL) and H₂O (1 mL) were added. The reaction mixture was stirred for an additional 20 min. The solvent was removed with a rotary evaporator and the residue was further dried by connecting to a vacuum pump overnight. The product was purified with flash column chromatography on silica gel by eluting with ethyl acetate/methanol (4/1), and a white solid was obtained (2.00 g, 15.2 mmol, 91% yield); TLC R_f = 0.24 (EtOAc/MeOH : 4/1); $^1\text{H-NMR}$ (300 MHz, DMSO- d_6) δ , 7.91 (s, 1 H), 4.87 (br, 1 H), 3.99 (q, 2 H, J = 12.3 Hz), 3.63 (s, 1 H), 3.43 (qd, 2 H, J = 11.6 Hz, J = 5.3 Hz), 3.20-3.02 (m, 2 H).

(R)-Morpholin-2-yl-methanol (3.30): To a solution of **3.29** (1.20 g, 9.15 mmol) in anhydrous THF (90 mL) was slowly added a solution of Red-Al (bis(2-methoxyethoxy)aluminum hydride) (70 wt. % in toluene) (10 mL, 35 mmol) at 0 °C over 1 h under nitrogen. The reaction mixture was stirred overnight at room temperature. After cooling the reaction mixture, 1.2 mL of water followed by 2 mL of 4N KOH were added. The precipitated solid was removed by filtration, and the filtrate was concentrated with a rotary evaporator and the residue was further dried by connecting to a vacuum pump overnight. The product was further purified with flash column chromatography on silica gel by eluting with ethyl acetate/methanol (9/1) and a viscous oil (0.71 g, 6.06 mmol, 66% yield) was obtained; TLC R_f = 0.21 (EtOAc/MeOH : 9/1); TLC R_f = 0.51 (EtOAc/MeOH : 4/1); $^1\text{H-NMR}$ (300 MHz, DMSO- d_6) δ , 4.10 (s, 3 H), 3.68 (d, 1 H, J = 10.5 Hz), 3.44-3.16 (m, 4 H), 2.78 (d, 1 H, J = 11.4 Hz), 2.66-2.49 (m, 2 H), 2.32 (t, 1 H, J = 10.5 Hz).

(R)-2-(2-Hydroxymethyl-morpholin-4-yl)-pyrimido[2,1- α]isoquinolin-4-one (3.31):

Compound **3.31** was prepared from **3.30** (0.12 g, 0.92 mmol) and **2.5** (0.35 g, 1.52 mmol) according to the same procedure as that for **C407**. Compound **3.31** was obtained as a colorless solid (0.27 g, 0.87 mmol, 94% yield); TLC R_f = 0.51 (EtOAc/MeOH : 9/1); $^1\text{H-NMR}$ (300 MHz, CDCl₃) δ , 8.80 (d, 1 H, J = 7.8 Hz), 8.65 (d, 1 H, J = 7.5 Hz), 7.76-7.58 (m, 3 H), 7.07 (d, 1 H, J = 7.5 Hz), 5.67 (s, 1 H), 4.33 (d, 1 H, J = 16.4), 4.12-4.07 (m, 1 H), 3.83-3.62 (m, 5 H), 3.16 (td, 1 H, J = 12.4 Hz, J = 3.6 Hz), 3.00 (dd, 1 H, J = 12.9 Hz, J = 10.2 Hz).

Methanesulfonic acid 4-(4-oxo-4H-pyrimido[2,1-a]isoquinolin-2-yl)-morpholin-2-ylmethyl ester (3.32): Compound **3.32** was prepared from **3.31** (0.38 g, 1.22 mmol) according to the same procedure as that for **3.18**. Compound **3.32** was obtained as a colorless solid (0.44 g, 1.00 mmol, 82% yield); TLC R_f = 0.36 (100% EtOAc)

3-Amino-6-methyl-furo[2,3-*b*]pyridine-2-carboxylic acid ethyl ester (3.39): To compound 2-chloro-6-methyl-3-pyridinecarbonitrile (**3.38**) (1.14 g, 7.5 mmol) were added ethyl glycolate (0.83 mL, 8.8 mmol), DBU (1.31 mL, 8.8 mmol), and ethanol (20 mL). This reaction mixture was stirred at 80 °C for 1 h. Additional DBU (3.0 mL, 20.0 mmol) was added and the reaction mixture was stirred under reflux overnight (12 h). After cooling, solvent was removed with a rotary evaporator, and the product mixture was redissolved in water and extracted with a mixture of ethyl acetate and THF. The organic layer was washed with brine, dried over MgSO₄, and concentrated with a rotary evaporator. Flash column chromatography on silica gel was used to purify the product by eluting with ethyl acetate/hexane (1/2), and a pure yellow solid was obtained (0.45 g, 2.0 mmol, 27 % yield); TLC R_f = 0.09 (EtOAc/Hexane : 1/4); ¹H-NMR (400 MHz, CDCl₃) δ, 7.82 (d, 1 H, J = 8.0 Hz), 7.09 (d, 1 H, J = 8.0 Hz), 5.04 (br, 2 H), 4.39 (q, 2 H, J = 7.2 Hz), 2.63 (s, 3 H), 1.40 (t, 3 H, J = 7.2 Hz); ¹³C-NMR (100 MHz, CDCl₃) δ, 161.70, 159.75, 159.12, 137.27, 129.30, 123.94, 118.57, 111.16, 60.41, 24.69, 14.46; MS (ESI), m/z = 221.1 (M+H)⁺.

3-(3-Methoxy-benzoylamino)-6-methyl-furo[2,3-*b*]pyridine-2-carboxylic acid ethyl

ester (3.40): To a solution of compound **3.34** (0.45 g, 2.0 mmol) in methylene chloride (20 mL) was added triethylamine (0.5 mL) and 3-methoxybenzoyl chloride (0.4 mL, 2.8 mmol) at 0 °C. This reaction mixture was stirred at room temperature for 3 h. The reaction mixture was diluted with water and saturated NaHCO₃, and extracted with methylene chloride. The organic layer was washed with brine and dried with MgSO₄, and concentrated with a rotary evaporator. Flash column chromatography on silica gel (ethyl acetate/hexane 1/3) was used to purify the product and it was further purified by crystallization with acetone to give the title compound as a white solid (0.65 g, 1.8 mmol, 92 % yield); TLC *R_f* = 0.18 (EtOAc/Hexane : 1/4); ¹H-NMR (400 MHz, CDCl₃) δ, 10.51 (s, 1 H), 8.89 (d, 1 H, *J* = 8.0 Hz), 7.54 (d, 1 H, *J* = 6.4 Hz), 7.51 (s, 1 H), 7.40 (t, 1 H, *J* = 8.0 Hz), 7.16 (d, 1 H, *J* = 8.4 Hz), 7.11 (dd, 1 H, *J* = 8.0 Hz, *J* = 1.6 Hz), 4.45 (q, 2 H, *J* = 7.2 Hz), 3.87 (s, 3 H), 2.64 (s, 3 H), 1.43 (t, 3 H, *J* = 7.2 Hz); ¹³C-NMR (100 MHz, CDCl₃) δ, 164.31, 162.04, 160.03, 159.60, 159.53, 137.29, 134.38, 130.40, 129.91, 128.00, 119.88, 119.23, 118.96, 112.66, 110.79, 61.61, 55.40, 24.51, 14.20; MS (ESI), *m/z* = 355.1 (M+H)⁺.

8-Chloro-6-(3-methoxy-phenyl)-2-methyl-9-oxa-1,5,7-triaza-fluorene (3.34): To a solution of compound **3.40** (0.65 g, 1.8 mmol) in methanol (20 mL) was added 28 % aqueous NH₃ (ca. 20 mL). After stirring at room temperature overnight (18 h), a sample of the reaction was analyzed by mass spectrometry. No reactant peak (*m/z* = 355.1) was detected and the peak (*m/z* = 326.1) of the product (**3.35**) was detected. The reaction mixture was concentrated to one-third of its initial volume with a rotary evaporator. To

this solution was added 2-propanol (10 mL) and 2 N NaOH (10 mL). After stirring under reflux for 5 h, the reaction mixture was cooled and analyzed by mass spectrometry. The peak ($m/z = 308.0$) of the product (**3.41**) was detected and there was no reactant peak ($m/z = 355.1$). The reaction mixture was neutralized with 2 N HCl and a white solid precipitated and was collected and dried in oven overnight. To the white solid was added POCl_3 (5 mL), and the reaction mixture was stirred at $100\text{ }^\circ\text{C}$ for 8 h. After cooling the reaction mixture, ice-water was slowly added, and the reaction mixture was neutralized with aqueous NaOH. The product mixture was extracted with methylene chloride, dried with MgSO_4 , and concentrated with a rotary evaporator. The title compound **3.34** (0.22 g, 0.68 mmol, 38 % yield) was purified with flash column chromatography on silica gel by eluting with ethyl acetate/hexane (1/5) and 10 % methylene chloride; TLC $R_f = 0.27$ (EtOAc/Hexane : 1/4); mp $197\text{ }^\circ\text{C}$; $^1\text{H-NMR}$ (400 MHz, CDCl_3) δ , 8.49 (d, 1 H, $J = 8.0$ Hz), 8.09 (dd, 1 H, $J = 7.8$ Hz, $J = 1.0$ Hz), 8.03 (t, 1 H, $J = 2.0$ Hz), 7.42-7.38 (m, 2 H), 7.03 (dd, 1 H, $J = 8.0$ Hz, $J = 2.4$ Hz), 3.93 (s, 3 H), 2.77 (s, 3 H); $^{13}\text{C-NMR}$ (100 MHz, CDCl_3) δ , 164.09, 162.87, 160.28, 159.97, 150.09, 142.89, 141.72, 137.79, 132.60, 129.64, 120.98, 117.20, 113.12, 111.70, 55.45, 25.06; MS(ESI) $m/z = 326.1$ ($\text{M}+\text{H}$) $^+$.

6-(3-Methoxy-phenyl)-2-methyl-8-morpholin-4-yl-9-oxa-1,5,7-triaza-fluorene (3.42):

To a solution of compound **3.34** (0.22 g, 0.68 mmol) in methanol (10 mL) were added morpholine (4 eq.) and three drops of acetic acid. The reaction mixture was stirred under reflux overnight (12 h). After cooling, methanol was removed with a rotary

evaporator. The product mixture was redissolved in water, and extracted with methylene chloride. The organic layer was washed with brine, dried with MgSO_4 , and concentrated with a rotary evaporator to give a white solid. It was further purified with flash column chromatography on silica gel by eluting with ethyl acetate/hexane (1/2) to give the title compound **3.42** (0.24 g, 0.64 mmol, 94 % yield) as a white solid; TLC R_f = 0.33 (EtOAc/Hexane : 1/1), R_f = 0.06 (EtOAc/Hexane : 1/4); mp 203 °C; $^1\text{H-NMR}$ (400 MHz, CDCl_3) δ , 8.44 (d, 1 H, J = 8.0 Hz), 8.05 (dt, 1 H, J = 8.0 Hz, J = 1.2 Hz), 8.01 (s, 1H), 7.39 (t, 1 H, J = 8.0 Hz), 7.29 (t, 1 H, J = 7.8 Hz), 7.00 (dq, 1 H, J = 8.1 Hz, J = 1.2 Hz), 4.18 (t, 4 H, J = 4.8 Hz), 3.92 (s, 3 H), 3.89 (t, 4 H, J = 4.8 Hz), 2.72 (s, 3 H); $^{13}\text{C-NMR}$ (100 MHz, CDCl_3) δ , 162.53, 159.94, 159.71, 159.22, 148.52, 147.42, 139.74, 132.88, 131.77, 129.27, 120.65, 120.00, 115.66, 113.36, 112.32, 66.86, 55.34, 45.62, 24.72; MS (ESI), m/z = 377.1 (M+H) $^+$.

3-(2-Methyl-8-morpholin-4-yl-9-oxa-1,5,7-triaza-fluoren-6-yl)-phenol (C601): To compound **3.42** (0.15 g, 0.40 mmol) was added 48 % HBr (5 mL) and acetic acid (5 mL). The reaction mixture was stirred under reflux for 48 h. After cooling, the acid solution was neutralized with aqueous NaOH. The product mixture was extracted with a mixture of ethyl acetate and THF. The organic layer was washed with brine, dried with MgSO_4 , and concentrated with a rotary evaporator. The product was purified with flash column chromatography on silica gel by eluting with ethyl acetate/hexane (1/1) to give the title compound **C601** (0.09 g, 0.25 mmol, 62 % yield) as a white solid; TLC R_f = 0.21 (EtOAc/Hexane : 1/1); mp > 250 °C; MS (ESI), m/z = 363.1 (M+H) $^+$.

5-(4-Chloro-phenyl)-3-(3-methoxy-benzoylamino)-thiophene-2-carboxylic acid ethyl

ester (3.44): To a solution of ethyl 3-amino-5-(4-chlorophenyl)thiophene-2-carboxylate (**3.43**) (0.89 g, 3.1 mmol) in anhydrous methylene chloride (20 mL) were added triethylamine (1 mL) and 3-methoxybenzoyl chloride (0.5 mL, 3.7 mmol) at 0 °C. This reaction mixture was stirred at room temperature for 4 h. The reaction mixture was diluted in water and the product mixture was extracted with methylene chloride. The organic layer was washed with brine, dried with MgSO₄, and concentrated with a rotary evaporator. The product was purified with flash column chromatography on silica gel by eluting with ethyl acetate/hexane (1/5) to give the title compound **3.44** (1.22 g, 2.9 mmol, 94 % yield); TLC *R_f* = 0.39 (EtOAc/Hexane : 1/4); ¹H-NMR (400 MHz, CDCl₃) δ, 11.19 (s, 1 H), 8.52 (s, 1 H), 7.64-7.54 (m, 4 H), 7.44-7.37 (m, 4 H), 7.11 (dd, 1 H, *J* = 8.0 Hz, *J* = 2.0 Hz), 4.39 (q, 2 H, *J* = 7.1 Hz), 3.89 (s, 3 H), 1.41 (t, 3 H, *J* = 7.2 Hz); ¹³C-NMR (100 MHz, CDCl₃) δ, 164.59, 164.10, 160.06, 148.26, 145.30, 135.14, 134.99, 131.72, 129.89, 129.25, 127.33, 119.09, 118.72, 118.36, 112.69, 109.89, 61.27, 55.43, 14.35; MS (ESI), *m/z* = 416.1 (M+H)⁺.

5-(4-Chloro-phenyl)-3-(3-methoxy-benzoylamino)-thiophene-2-carboxylic acid amide

(3.37): To a solution of compound **3.44** (0.15 g, 0.36 mmol) in methanol was added 1N NaOH (5 mL). This reaction mixture was stirred under reflux for 2 h, and it became homogeneous. The basic solution was neutralized with 1N HCl and a mixture of ethyl acetate and THF was used to extract the product. The organic layer was washed with

brine, dried with MgSO_4 , and concentrated with a rotary evaporator to give the corresponding carboxylic compound as a white solid (0.14 g, 0.36 mmol); MS (ESI), $m/z = 385.0$ (M-H^-). To this carboxylic compound was added methylene chloride (20 mL) and SOCl_2 (1 mL). This reaction mixture was stirred under reflux for 5 h. TLC showed that all of the polar compound was changed to a less polar one ($R_f = 0.72$ (EtOAc/Hexane : 1/1)). Solvent and the remaining SOCl_2 were removed with a rotary evaporator. Anhydrous THF (20 mL) was added. NH_4OH (1N, 5 mL) was added slowly at 0°C and then the reaction was stirred at room temperature for 3 h. The reaction mixture was diluted in water, and the product was extracted with a mixture of ethyl acetate and THF. The organic layer was washed with brine, dried with MgSO_4 , and concentrated with a rotary evaporator. The product was purified with flash column chromatography on silica gel by eluting with ethyl acetate/hexane (1/3) to give the title compound **3.37** (0.11 g, 0.28 mmol, 79 % yield); TLC $R_f = 0.36$ (EtOAc/Hexane : 1/4); $^1\text{H-NMR}$ (400 MHz, $\text{DMSO-}d_6$) δ , 12.40 (s, 1 H), 8.45 (s, 1 H), 7.86 (br, 2 H), 7.73 (d, 1 H, $J = 9.6$ Hz), 7.57-7.46 (m, 5 H), 7.23 (d, 1 H, $J = 8.0$ Hz), 3.86 (s, 3 H); $^{13}\text{C-NMR}$ (100 MHz, $\text{DMSO-}d_6$) δ , 165.69, 162.90, 159.58, 143.65, 143.47, 134.93, 133.67, 131.48, 130.26, 129.43, 127.36, 118.97, 118.23, 118.06, 112.84, 112.42, 55.29.

4-Chloro-6-(4-chloro-phenyl)-2-(3-methoxy-phenyl)-thieno[3,2-d]pyrimidine (3.36):

Compound **3.45** was prepared from **3.37** (0.65 g, 1.7 mmol) according to the same procedure as that for **3.41**. This compound was analyzed by mass spectrometry; MS (ESI), $m/z = 368.0$ (M+H^+), $m/z = 367.0$ (M-H^-). Compound **3.36** was directly prepared

from **3.45** according to the same procedure as that for **3.34**, and a colorless solid was obtained (0.48 g, 1.3 mmol, 76 % yield); TLC $R_f = 0.54$ (1/4 EtOAc/Hexane); This product was directly used for the next reaction without NMR characterization.

6-(4-Chloro-phenyl)-2-(3-methoxy-phenyl)-4-morpholin-4-yl-thieno[3,2-d]pyrimidine

(3.46): Compound **3.46** was prepared from **3.36** (0.48 g, 1.3 mmol) according to the same procedure as that for **3.42**. Compound **3.46** was obtained as a colorless solid (0.51 g, 1.2 mmol, 92% yield); TLC $R_f = 0.21$ (1/4 EtOAc/Hexane), $R_f = 0.60$ (1/1 EtOAc/Hexane); $^1\text{H-NMR}$ (400 MHz, CDCl_3) δ , 8.03 (d, 1 H, $J = 7.6$ Hz), 7.99 (s, 1 H), 7.58-7.34 (m, 6 H), 6.99 (dd, 1 H, $J = 8.2$ Hz, $J = 2.2$ Hz), 3.98 (t, 4 H, $J = 4.6$ Hz), 3.90 (s, 3 H), 3.85 (t, 4 H, $J = 4.6$ Hz); $^{13}\text{C-NMR}$ (100 MHz, CDCl_3) δ , 163.18, 160.24, 159.62, 157.64, 147.64, 139.83, 135.26, 131.30, 129.20, 129.16, 127.40, 120.98, 120.59, 115.73, 113.26, 112.47, 66.67, 55.28, 46.21.

3-[6-(4-Chloro-phenyl)-4-morpholin-4-yl-thieno[3,2-d]pyrimidin-2-yl]-phenol (C701):

Compound **C701** was prepared from **3.46** (0.18 g, 0.38 mmol) according to the same procedure as that for **C601**. Compound **C701** was obtained as a colorless solid (0.11 g, 0.26 mmol, 68% yield); TLC $R_f = 0.45$ (1/1 EtOAc/Hexane).

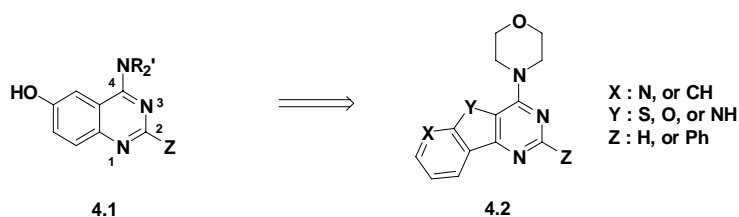
Chapter 4. Generating novel lead compounds

Novel compounds similar to PI103 were designed based on structure activity relationship (SAR) results, chemical property analysis, and knowledge obtained from Chapters 2 and 3. Furthermore, virtual database screening based on pharmacophore matching was employed to find active compounds having different core structures from **C401** and PI103.

4.1 SAR data-inspired approach

Recently PI103 was developed by Hayakawa *et al.* as a PI3 kinase p110 α inhibitor. In the course of their studies, quinazoline derivatives **4.1** were optimized by substituting the 2- and 4-positions with saturated six-membered rings and various phenol rings. These compounds were further developed into PI103 by changing the quinazoline structure to a tricyclic ring (**4.2**, Figure 4.1).

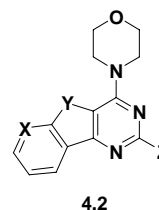
Figure 4.1 Core ring fragments used in the development of PI103 by Hayakawa *et al.*



SAR data presented in two papers^{180, 181} gave potentially valuable ideas for the development of more selective mTOR inhibitors (Tables 4.1 and 4.3). A phenyl ring at the Z-position did not significantly effect inhibition toward p110 α as IC₅₀ values for compounds **4.2_1** vs. **4.2_4** and **4.2_2** vs. **4.2_5** are similar. Compounds having an oxygen atom at the Y-position (**4.2_2** and **4.2_5**) are about 3 to 10 times more potent than equivalent structures having a sulfur atom (**4.2_1** and **4.2_4**). However, a nitrogen atom at the Y-position **4.2_3** greatly decreased the inhibition of p110 α , as no inhibition was observed at 30 μ M. Changing of N at the X-position of **4.2_1** to CH to give **4.2_6** caused a 2-fold decrease in potency. However, the same N to CH change in the phenyl-substituted **4.2_4** to give **4.2_7** resulted in total loss of activity at 30 μ M. The overall shapes of compound **4.2** and derivatives are almost identical. SAR studies indicate that the major binding components of these derivatives are the morpholine oxygen and the hydrophobic surface of the tricyclic ring.¹⁸¹ The literatue does not explain the greatly diminished inhibition by compounds **4.2_3** and **4.2_7**.

Table 4.1 Inhibition of p110 α by tricyclic derivatives (taken from ref ¹⁸¹)

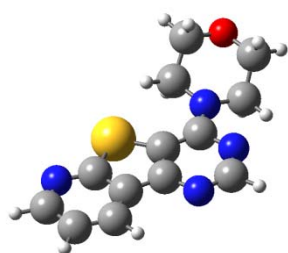
Compound 4.2	X	Y	Z	IC ₅₀ (μ M) p110 α
LY294002 ^a				0.63
4.2_1 ^a	N	S	H	1.4
4.2_2 ^a	N	O	H	0.56
4.2_3 ^a	N	NH	H	>30
4.2_4 ^a	N	S	Ph	1.7
4.2_5 ^a	N	O	Ph	0.16
4.2_6 ^b	CH	S	H	2.4
4.2_7 ^a	CH	S	Ph	>30

^aFree base^bHCl salt

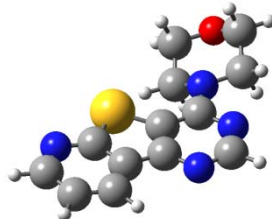
To further examine these observations, DFT calculations were performed with Gaussian 03W and GaussView3.09. Structures **4.2_1**, **4.2_2**, **4.2_3**, **4.2_4**, **4.2_5**, **4.2_6**, and **4.2_7** were optimized at the B3LYP/6-311G(d) level. Two possible conformations of each structure were examined; one having the morpholine ring slightly distorted clockwise from the plane of the tricyclic ring (R is added to the compound name) and the other having the morpholine ring slightly distorted counterclockwise from the plane of the tricyclic ring (P is added to the compound name) (Figure 4.2). For compounds in which Y = S or NH, distinct minima were obtained for each of the two different conformers. However, for compounds in which Y = O (**4.2_2** and **4.2_5**), only one conformation was obtained, having the morpholine ring in the plane of the tricyclic ring. Structure **4.2_2** was optimized by starting from conformations having the morpholine ring distorted clockwise and counterclockwise, but both gave the same planar structure.

The nonplanarity of the N-H compounds can be explained by the steric effect of the -CH₂- group of the morpholine ring. The nonplanarity of the sulfur compounds can be explained by the large size of the sulfur atom and resulting steric effect with the -CH₂- group of the morpholine ring. However, the steric contribution of the lone pair electrons on the oxygen atom is minimal due to the small size of the oxygen atom. The orientation of the morpholine ring in **4.2_2** or **4.2_5** is similar to the transition state for interconversion of the two conformers of the other compounds.

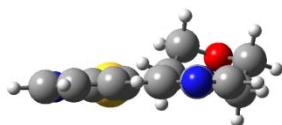
Figure 4.2 Optimized geometries of **4.2_1**, **4.2_2**, **4.2_3**, **4.2_6** by DFT calculation. Top and side mean top view and side view. The appendix R and P mean clockwise and counterclockwise distortions of morpholine ring from the tricyclic rings. Carbon, nitrogen, oxygen, sulfur, and hydrogen atoms are represented by gray, blue, oxygen, yellow, and white spheres with van der Waals radii. The names of more stable conformers are in red. Other optimized geometries of **4.2_4**, **4.2_5**, and **4.2_7** are included in the appendix.



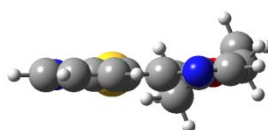
4.2_1_R (top)



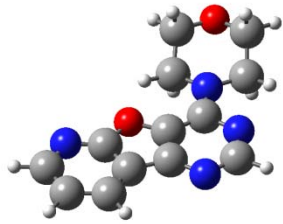
4.2_1_P (top)



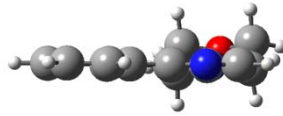
4.2_1_R (side)



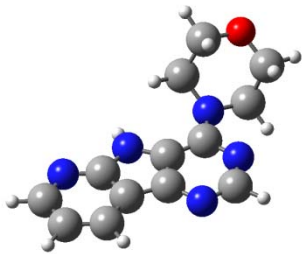
4.2_1_P (side)



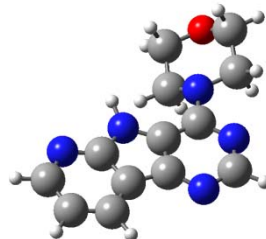
4.2_2 (top)



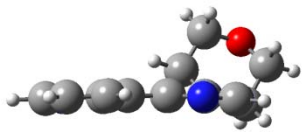
4.2_2 (side)



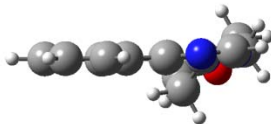
4.2_3_R (top)



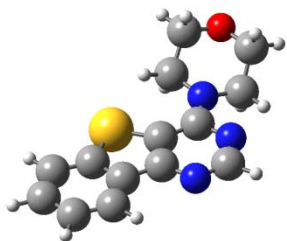
4.2_3_P (top)



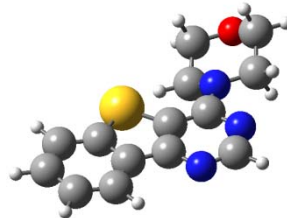
4.2_3_R (side)



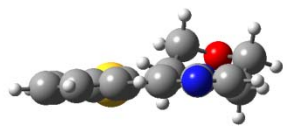
4.2_3_P (side)



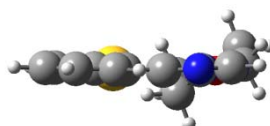
4.2_6_R (top)



4.2_6_P (top)



4.2_6_R (side)



4.2_6_P (side)

The free energies of activation for interconversion of R and P forms were determined from the relative energies of the minimum and the transition state structures (Table 4.2). The free energy difference between R and P conformers is small (0.24 ~ 0.43 kcal/mol). The R conformers of **4.2_1**, **4.2_4**, **4.2_6**, and **4.2_7** are more stable than the corresponding P conformers, while the P conformer of **4.2_3** is more stable. The free energies of activation for interconversion of P and R forms of all **4.2** compounds are very low (less than 2 kcal/mol); interconversion of conformers is thus very rapid for all compounds.

Table 4.2 The free energies of activation between R and P conformers of compounds in Table 4.1.

Compound 4.2	X	Y	Z	IC ₅₀ (μM) p110α	ΔG [‡] (TS-R) ^b	ΔG [‡] (TS-P) ^b	ΔG ^o (P-R) ^b
4.2_1	N	S	H	1.4	1.32	1.07	0.25
4.2_2	N	O	H	0.56		N/A	
4.2_3	N	NH	H	>30	1.19	1.62	-0.43
4.2_4	N	S	Ph	1.7	1.47	1.05	0.42
4.2_5	N	O	Ph	0.16		N/A	
4.2_6	C	S	H	2.4	1.34	1.10	0.24
4.2_7	C	S	Ph	>30	1.46	1.16	0.31

^a in Hartree

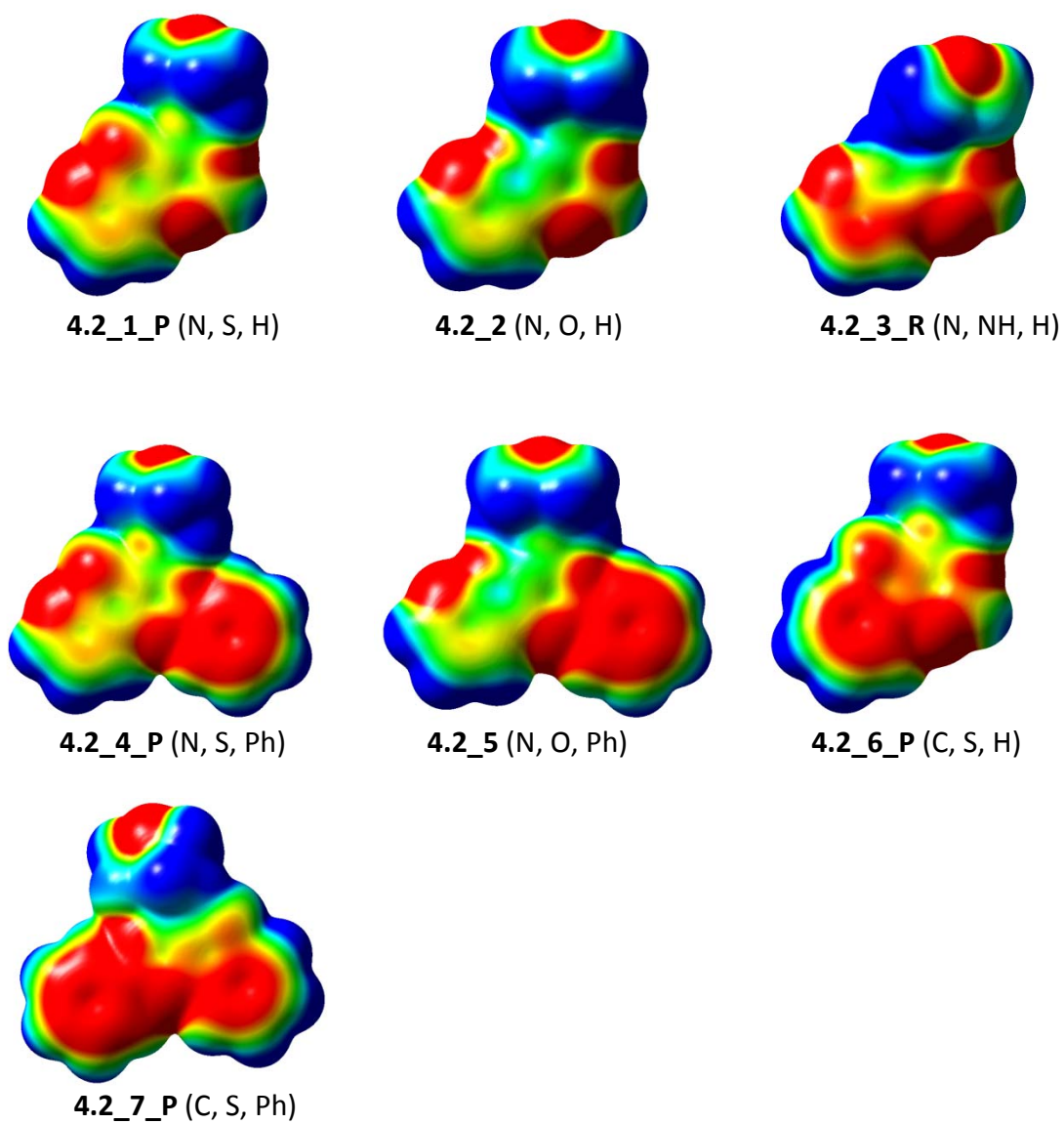
^b in kcal/mole

A possible explanation for the differences in inhibition between the compounds could be the electrostatic potential differences. Electrostatic differences were previously used to rationalize inhibition differences between compounds **II** and **III** in Chapter 2. The different atomic combination (N-S, N-O, N-NH, and C-S at X-Y-position) of

compounds **4.2** can cause the different electrostatic potentials of the tricyclic rings.

Charge densities of all **4.2** derivatives were calculated and electrostatic potentials were mapped to the calculated total densities (Figure 4.3).

Figure 4.3 Electrostatic potentials of **4.2** in Table 4.1. The combination of atoms at X-, Y-, and Z-positions is represented in brackets.



The results of electrostatic potentials showed that there is an interesting difference in **4.2_3** and **4.2_7** vs. the other compounds. In **4.2_3** and **4.2_7**, which exhibit no significant inhibition of p110 α at 30 μ M, the negative electrostatic potential is delocalized through the tricyclic rings. However, **4.2_1**, **4.2_2**, **4.2_4**, and **4.2_5**, which exhibit potent inhibition of p110 α , have the negative electrostatic potential concentrated on the X- and Y-positions with relatively neutral potentials distributed through the tricyclic rings. Furthermore, slight negative electrostatic potentials (orange color) are observed in the tricyclic rings of **4.2_1** and **4.2_4**, while approximately neutral potentials (green and yellow colors) are observed in **4.2_2** and **4.2_5** except at the X- and Y-positions. Thus the most potent inhibitors (**4.2_2** and **4.2_5**) have negative electrostatic potentials concentrated at the X and Y positions, while the less potent inhibitors have negative potential throughout the tricyclic ring system. The almost identical shapes of the different inhibitors suggest that the differences in inhibition properties may be a direct result of electrostatic differences.

These results contrast to those of compounds **II** and **III** in Chapter 2 (Table 2.1 and Figure 2.3). Compound **II**, with delocalized negative potential in the ring fragment, is potent against p110 α , while there is little inhibition by compound **III** (**C401**), with localized negative potential. This discrepancy may be rationalized by the flexible alignment in Figure 3.8. Although the ring fragments in compounds **II** and **III** and the tricyclic rings in **4.2** are similar, they do not fully overlap and may occupy different areas of the active site of PI3Kinase. Therefore, the upper part (in Figure 3.8) of the active site, occupied by the ring fragments of compounds **II** and **III**, may not be sensitive to the

negative potential, while the lower part (in Figure 3.8) of the active site, occupied by the tricyclic rings, may be more sensitive to the negative potential. While it is not clear why the compounds have different inhibition properties, the different electrostatic potential caused by the different atomic combinations of the X- and Y-positions may be one of the reasons.

Another SAR study shows a potential relationship between the conformation of the morpholine ring and inhibition of p110 α (Table 4.3). Compounds **4.1_1** and **4.1_3** having a hydroxyl group at the 6- and 5-positions, respectively, have very different inhibition properties ($IC_{50} = 1.3 \mu\text{M}$ vs. $>30 \mu\text{M}$, respectively). This different inhibition potency may be due to different interaction of the hydroxyl groups with active site amino acids, but may also be explained by the degree of planarity of the morpholine rings. To explore this possibility structures of **4.1_1** and **4.1_3** were optimized at the B3LYP/6-311G(d) level, omitting the phenyl group at the 2-position, since it does not affect the geometry of the morpholine ring. Both compounds have two possible conformations, differing in orientation of the morpholine ring (Figure 4.4). In compound **4.1_3** the hydrogen atom of the hydroxyl group interacts with the nitrogen atom of the morpholine ring. Due to this interaction and the steric effect of the hydroxyl group instead of a hydrogen atom at the 5-position, the morpholine ring of **4.1_3** is more twisted out of the plane of the bicyclic system in **4.1_1**. To examine the activation of energy for the conversion between two conformers, transition states of **4.1_1** and **4.1_3** were calculated at the B3LYP/6-311G(d) level, and the results are summarized in Table 4.4. The activation barriers of conversion between R and P forms in **4.1_3** is increased

(12 ~ 14 kcal/mole) as compared to those (ca. 1 kcal/mole) in **4.2s** and those (ca. 4 kcal/mole) in **4.1_1**. In addition, the quinazoline ring of **4.1_3** is twisted due to steric repulsion between the oxygen atom at the 5-position and -CH₂- group of the morpholine ring. Therefore, the morpholine ring might be localized to one of two forms, and only with high energy (such as high temperature) will interconversion occur. The steric effect of the hydroxyl group of **4.1_3** on the morpholine ring is significant, resulting in rotation of the morpholine ring out of the plane of the bicyclic system. Therefore, the dramatically decreased inhibition of **4.1_3** toward p110 α might result from rotation of the morpholine ring, causing the oxygen atom in the morpholine ring to be poorly positioned for H-bonding with the amide backbone (N-H) of Val in p110 α .

Figure 4.4 Optimized geometries of 4.1_1 and 4.1_3 by DFT calculation.

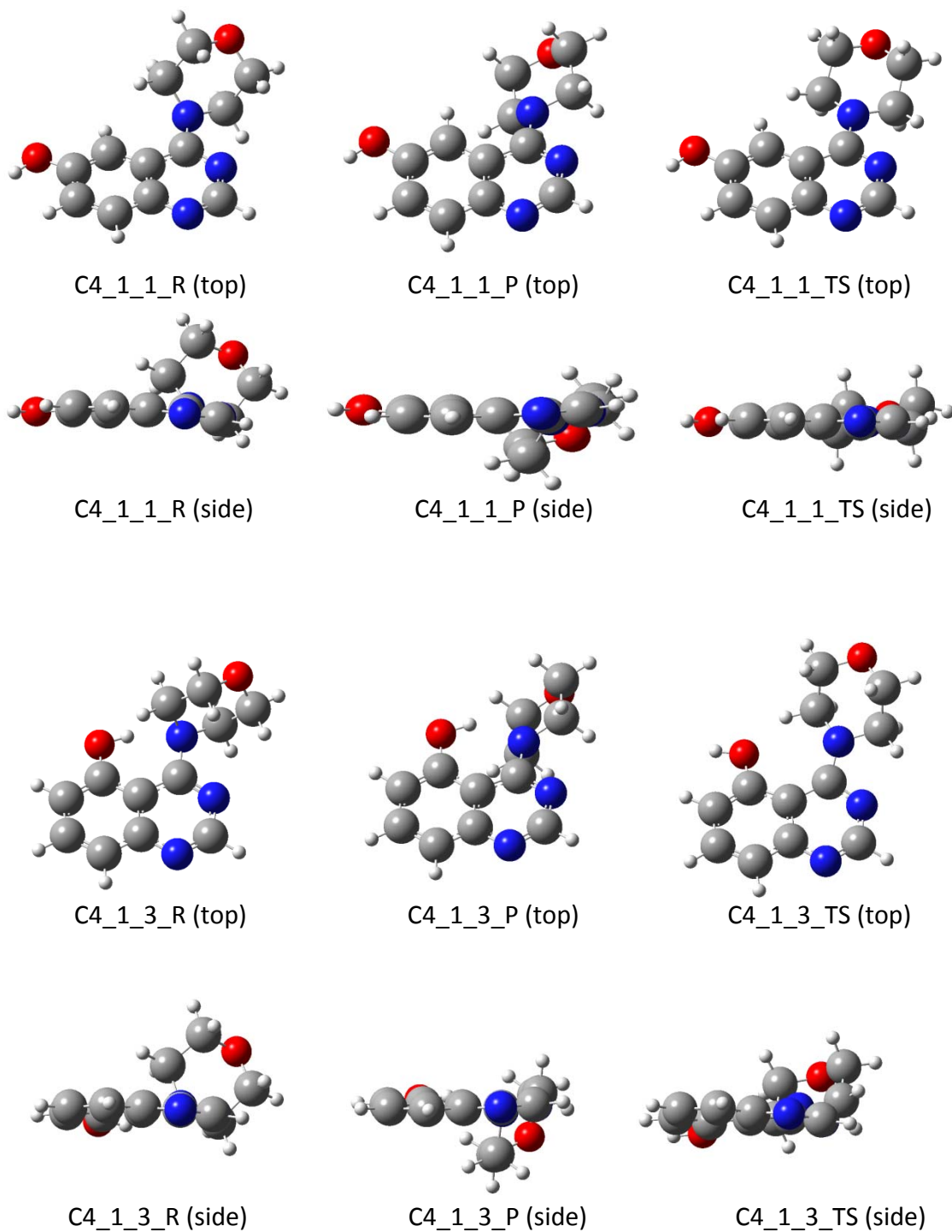


Table 4.3 Inhibition of p110 α by 4-morpholine-4-yl-2-phenyl-quinazolines (taken from ref ¹⁸⁰)

Compound 4.1	R	R'	IC ₅₀ (μ M) p110 α
4.1_1	6-OH	H	1.3
4.1_2	6-OH	3-OH	0.075
4.1_3	5-OH	H	>30
4.1_4	7-OH	H	9.8
4.1_5	6-OCH ₃	H	2.1
4.1_6	H	H	14
4.1_7	H	3-OH	0.056

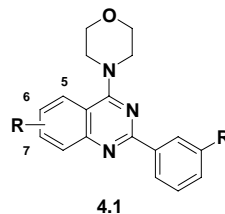


Table 4.4 The free energies of activation between R and P conformers of compounds **4.1_1** and **4.1_3**.

Compound 4.1	R	R'	IC ₅₀ (μ M) p110 α	$\Delta G^\ddagger(\text{TS-R})^b$	$\Delta G^\ddagger(\text{TS-P})^b$	$\Delta G^0(\text{P-R})^b$
4.1_1	6-OH	H	1.3	4.51	4.93	-0.43
4.1_3	5-OH	H	>30	12.62	14.59	-1.97

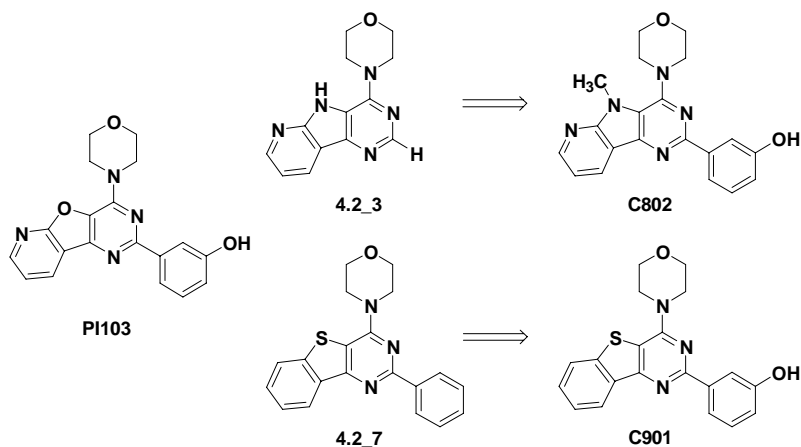
^b in kcal/mole

4.1.1 Design of novel lead compounds

Based on the results described in the previous chapters, we found that the phenolic oxygen and morpholine oxygen of PI103 and related compounds are critical components for the inhibition of mTOR and PI3Kinase. The importance of the phenolic oxygen for inhibition of p110 α is also examined in the above SAR data (Table 4.3). p110 α

Inhibition of compound **4.1_2** ($IC_{50} = 0.075 \mu\text{M}$), with a hydroxyl group at the 3-position of the phenyl ring, is dramatically increased as compared to compound **4.1_1** ($IC_{50} = 1.3 \mu\text{M}$), having no hydroxyl group. Therefore, in our designed compounds **C802**, **C803**, and **C901**, this phenol group is retained (Figure 4.5), although compounds lacking the phenolic hydroxyl have apparently not actually been tested against mTOR.¹⁸¹ The furan ring in PI103 is modified to a pyrrole ring in compound **C803**, which is expected to greatly decrease its potency against PI3Kinase, given the very weak inhibition of PI3 kinase by **4.2_3**. If inhibition of mTOR is not so effected by this O-to-NH substitution, compound **C803** could be a much more selective inhibitor of mTOR. Compound **C802**, with a 1-methyl-pyrrole ring, was also proposed, to examine the effect of rotation of the morpholine ring on the inhibition of mTOR. These designed compounds are expected to be much more potent inhibitors of PI3Kinase and mTOR than the **4.2_1** to **4.2_7** series, as the phenol group of PI103 greatly enhances potency against PI3Kinase ($IC_{50} = 5 \text{ nM}$). The N-CH₃ and N-H groups in compounds **C802** and **C803** are expected to result in greatly decreased inhibition of PI3Kinase based on the lack of inhibition of PI3Kinase by **4.2_3**. It is not clear how much the N-CH₃ or N-H group will affect the inhibition toward mTOR, as no inhibition results against mTOR have been reported for compounds having N at this position. Studies with compound **C401** and compound **II** (Table 2.1) suggest that mTOR may be much less sensitive to the heteroatom arrangement of the ring system than PI3Kinase. Thus, **C802**, **C803**, and **C901** were designed as potentially more selective inhibitors of mTOR.

Figure 4.5 Designed compounds **C802**, **C803**, and **C901**

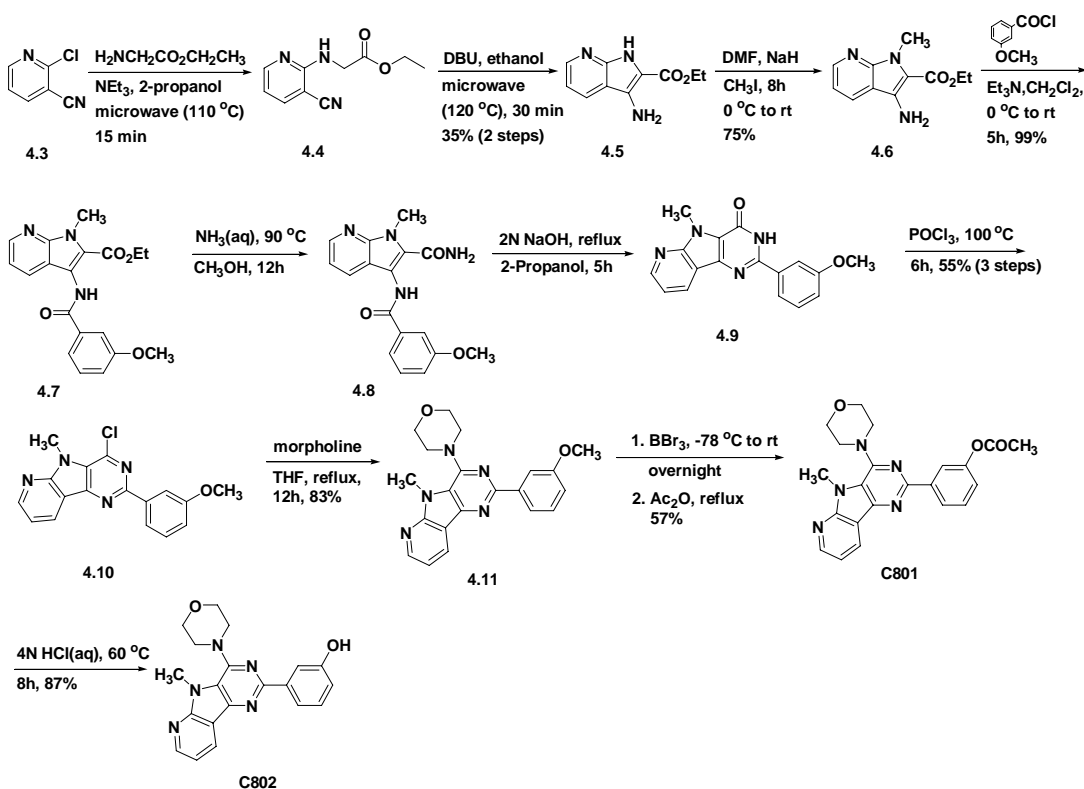


4.1.2 Synthesis of designed lead compounds

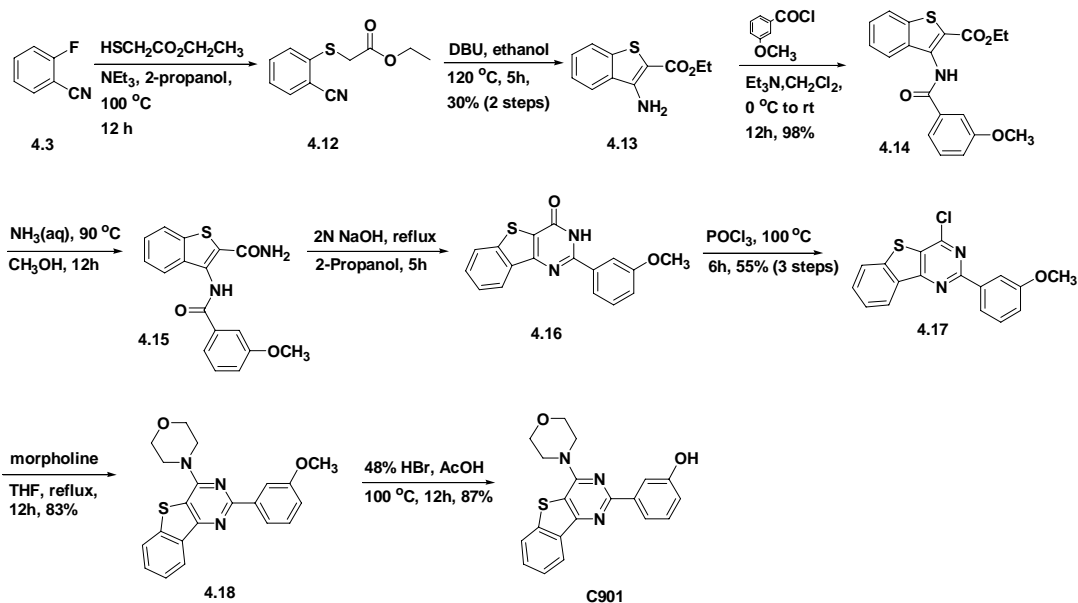
The syntheses of **C802** and **C901** were performed following the previously reported procedure for making PI103 with some modification (Schemes 4.1 and 4.2). Glycine ethyl ester was reacted with 2-chloro-3-pyridinecarbonitrile in a microwave reactor to afford compound **4.4**. The bicyclic acid ester **4.5** was formed from compound **4.4** in the presence of DBU and under heating by microwave. Compound **4.5** was also made directly from compound **4.3**, glycine ethyl ester, and potassium carbonate in DMSO under heating at 130 °C for 12 hours, and gave similar yield. Methylation of the pyrrole nitrogen was performed with sodium hydride as base and methyl iodide to obtain compound **4.6**. Acylation of the resulting product was achieved with 3-methoxybenzoyl chloride to give **4.7**. Attempted ammonolysis of compound **4.7** at room temperature gave only starting material. Therefore, a high-pressure stainless steel reactor was used with aqueous ammonia in methanol at 80 to 140 psi and heating at

about 90 °C. A mixture of compounds **4.8** and **4.9** was obtained and was confirmed by mass spectrometry. The resulting reaction mixture was further reacted with sodium hydroxide in 2-propanol at reflux to complete the conversion of **4.8** to **4.9**. Chlorination with phosphorous oxychloride gave the intermediate **4.10**, which was reacted with morpholine to form **4.11**. Demethylation of the methyl aryl ether followed by acylation was performed with boron tribromide followed by acetic anhydride to give **C801**. **C801** was further reacted with hydrochloric acid in water (4N) under mild heating (60 °C) to form the HCl salt of **C802**. **C803** was obtained from **4.11** by removal of both the O and N-methyl groups using conditions reported for making PI103.

Scheme 4.1 Synthesis of **C801** and **C802**



Scheme 4.2 Synthesis of C901



Ethyl thioglycolate was reacted with 2-fluorobenzonitrile to afford compound **4.12** followed by treating with DBU to afford the bicyclic acid ester **4.13**. The resulting product **4.13** was acylated with 3-methoxybenzoyl chloride to give **4.15**. Ammonolysis of compound **4.15** was performed with a high-pressure stainless steel reactor with aqueous ammonia in methanol at 90 °C. The resulting reaction mixture was further reacted with sodium hydroxide in 2-propanol at reflux to complete the conversion of **4.15** to **4.16**. Compound **4.17** was obtained by chlorination of **4.16** with phosphorous oxychloride, and chloro atom was substituted with morpholine to give compound **4.18**. Demethylation of the methyl aryl ether was performed with 48% hydrobromic acid to give the desired compound **C901**. The synthesized compounds are awaiting inhibition studies.

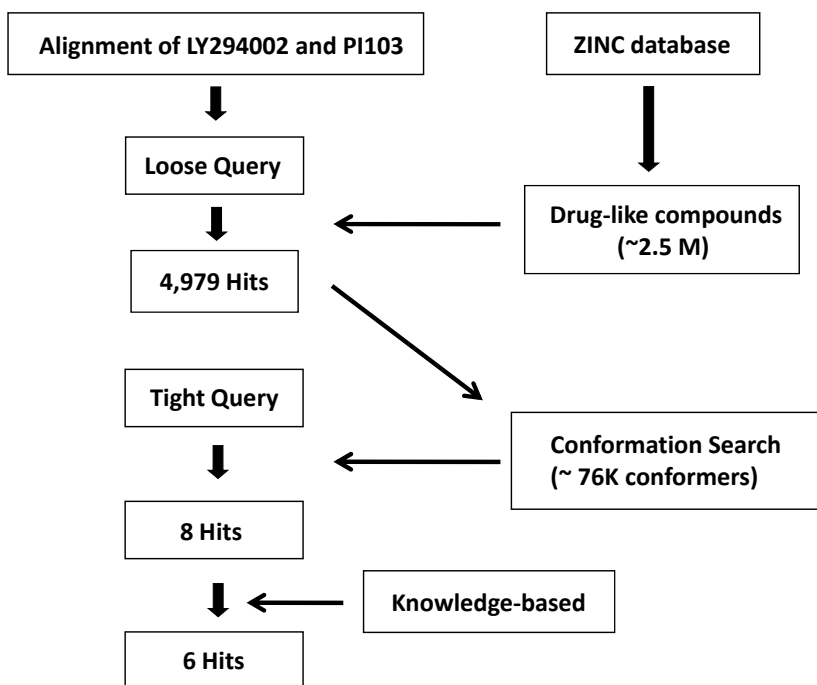
4.2 Virtual database screening approach

Virtual database screening was applied to search for novel lead compounds for inhibition of mTOR. **C401**, LY294002, PI103, and PI3-Kinase inhibitor 2 represent the major classes of known inhibitors of mTOR and PI3Ks. The goal of virtual screening was to find novel lead compounds for inhibition of mTOR having different core structures.

4.2.1 Pharmacophore searching

Pharmacophore searching was performed using the MOE Pharmacophore Application suite. The overall steps of pharmacophore searching are represented in Figure 4.6. “Drug-like” compounds (2,435,160), previously sorted in the ZINC database by the ‘Lipinski rule of five’,¹⁸⁷ were downloaded. Since many compound collections contain either undesirable compounds or compounds drawn in undesirable ways, compounds in the database were refined with the ‘wash’ command to remove salts and solvent, to deprotonate (or protonate) acids (or bases), and to add explicit hydrogen atoms.

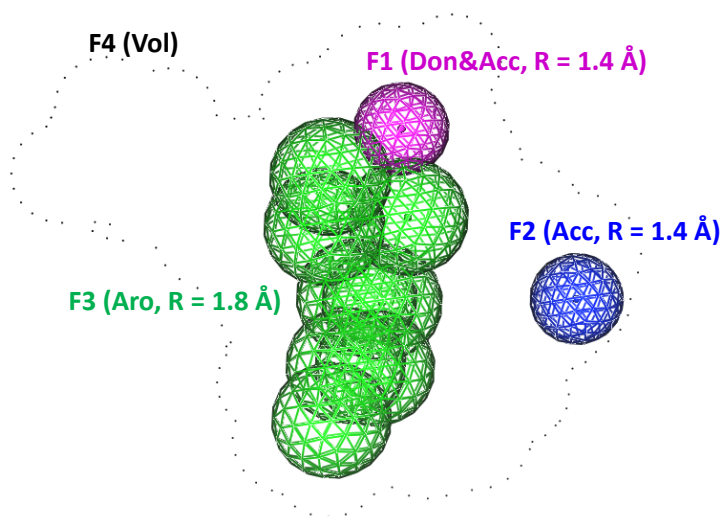
Figure 4.6 The flowchart of pharmacophore searching



An initial query was generated by examining the structural features from the alignment of PI103 and LY294002 in Chapter 3 (Figure 4.7). The radius (in angstroms) of the spherical volume for each of the features was set to be larger than the default value, in order to get as many hits as possible in the 'Loose Search' step. Each compound in the library may have many possible conformations, while calculating all the conformers of each compound takes a great deal of computational time. Therefore, by performing 'Loose searching', compounds lacking structural features matching the loose query could be rejected at the start. A search of the 'drug-like' compounds with the loose

query, led to 4,979 hits. All conformations of these hits were calculated, to consider the flexibility of ligands in the pharmacophore search, resulting in 76,369 conformers.

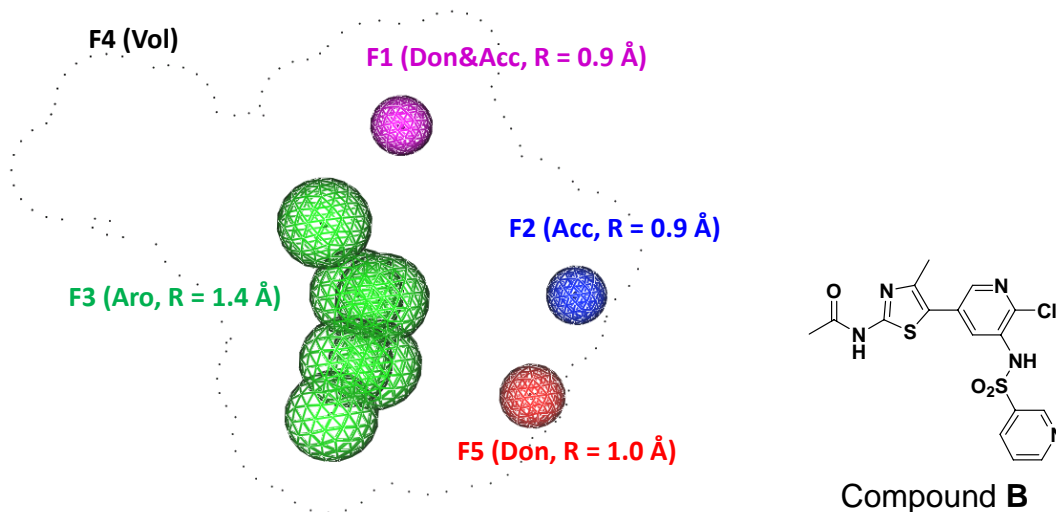
Figure 4.7 The loose query



To further refine these hits using ‘Tight Searching’, the initial “Loose Query” was tightened based on additional structural features of a potent but non-selective inhibitor (compound **B**, Figure 4.8) presented by AstraZeneca at a Keystone Symposium.¹⁸⁸ The crystal structure of the complex of this compound with PI3Kinase and mTOR was solved, but was not published in the PDB. It was presented at the symposium in a poster. Therefore, the binding mode of this compound was predicted by docking using MOE. The result showed that the sulfonyl group of the sulfonamide and the chlorine atom on the pyridine ring act as hydrogen bond acceptors with lys833, and the N atom of the

thiazole acts as an acceptor with val882. Additionally, the exocyclic NH of the acetamido group interacts with the carbonyl oxygen of the amide backbone of val882. The result of this docking study is consistent with the co-crystal structure shown in the AstraZeneca presentation. The hydrogen bond donor property of the acetamido (N-H) group (red sphere in Figure 4.8) in compound **B** was included as an additional structural feature in the 'Tight Query', and the query was further refined by decreasing the radius of each sphere of the 'Loose Query'.

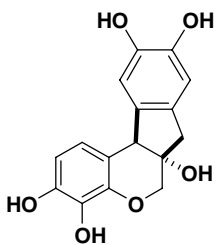
Figure 4.8 The structure of compound B and the refined tight query



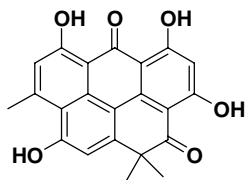
All of the conformers of initial hits from the "Loose Query" were searched through the 'Tight Query', and 8 hits were obtained. Spheres F1 and F2 were defined by

the carbonyl oxygen in the chromone ring of LY294002 or the phenolic hydroxyl group of PI103 and the morpholine oxygens of both. Previous results suggest that these groups are major tight binding factors to the active sites of PI3Kinase and mTOR, and the distance and rigidity between them may also be important for inhibition. Based on this knowledge, 6 compounds having rigidly linked groups matching spheres F1 and F2 were selected manually from the 8 hits obtained from the “Tight Query” (Figure 4.9).

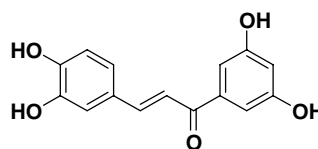
Figure 4.9 Hits from the pharmacophore search of the ZINC compound library



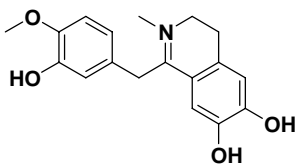
ZINC00155806 (Hit_1)



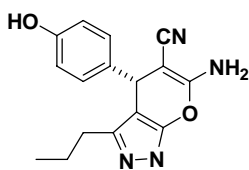
ZINC04017533 (Hit_2)



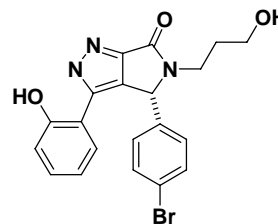
ZINC04099901 (Hit_3)



ZINC01559572 (Hit_4)



ZINC04599465 (Hit_5)

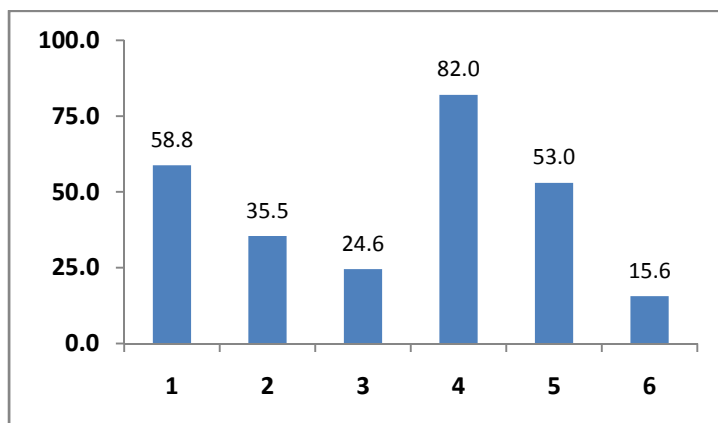


ZINC02210916 (Hit_6)

4.2.2 Bioassay of hits

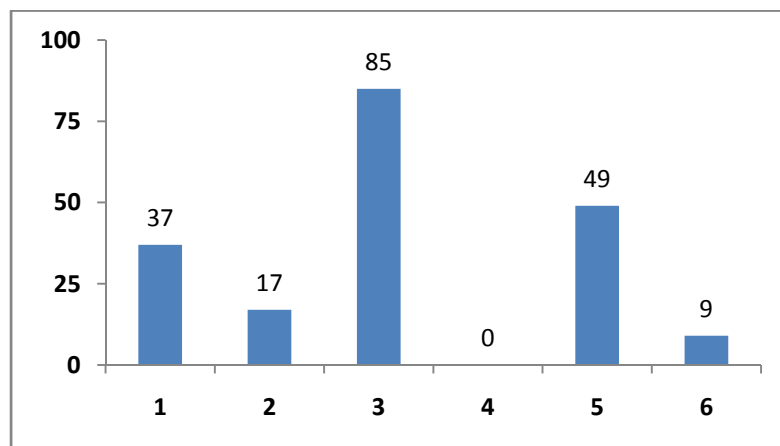
All 6 hits selected from the ZINC database screen are commercially available. They were tested against mTOR as described in chapter 2 at 10 μ M concentration. The results show that % inhibitions of **Hit_1**, **Hit_4**, and **Hit_5** at 10 μ M are 58.8%, 82.0% and 53.0%, respectively (Figure 4.10). These hits could be promising novel lead compounds for inhibition of the mTOR because these have totally different core fragments from those of conventional PI3Kinase and mTOR inhibitors such as LY294002, C401, and PI103. Furthermore, there have been no reports of these hits for inhibition of mTOR. In addition to **Hit_1**, **Hit_4**, and **Hit_5**, the other three hits (**Hit_2**, **Hit_3**, and **Hit_6**) are also active against mTOR, though with lower potency (35.5%, 24.6%, and 15.6%, respectively at 10 μ M) than **Hit_1**, **Hit_4**, and **Hit_5**. **Hit_4** was further tested against mTOR at low concentrations, and 74% and 51% inhibition were observed at 1 μ M and 0.1 μ M, respectively. The inhibition ability of **Hit_4** against mTOR is greater than those of LY294002 and **C401**.

Figure 4.10 % inhibition of mTOR at 10 μ M. Y-axis represents % inhibition of mTOR and X-axis represents hit number.



The 'Hit' compounds were also tested against PI3K α at 10 μ M (Figure 4.11). Because the pharmacophore queries, which were used for virtual screening, were generated from the non-selective inhibitors between PI3K α and mTOR, we can expect that the 'Hit' compounds might inhibit PI3Kinase with similar potency toward mTOR. The inhibition abilities of **Hit_1**, **Hit_2**, **Hit_5**, and **Hit_6** against PI3K α is similar to those against mTOR, but interestingly inhibition of PI3K α with **Hit_3**, which has low inhibition potency against mTOR (25% inhibition), is pretty high (85% inhibition). Furthermore, inhibition of mTOR with **Hit_4**, which is very potent against mTOR, was not observed at 10 μ M.

Figure 4.11 % inhibition of PI3K α at 10 μ M. Y-axis represents % inhibition of PI3K α and X-axis represents hit number.



The assay results confirm that our pharmacophore query is a useful predictive model for searching for lead compounds targeting mTOR and PI3K α . In this virtual screening, we obtained not only very potent selective inhibitor (**Hit_4**) of mTOR vs.

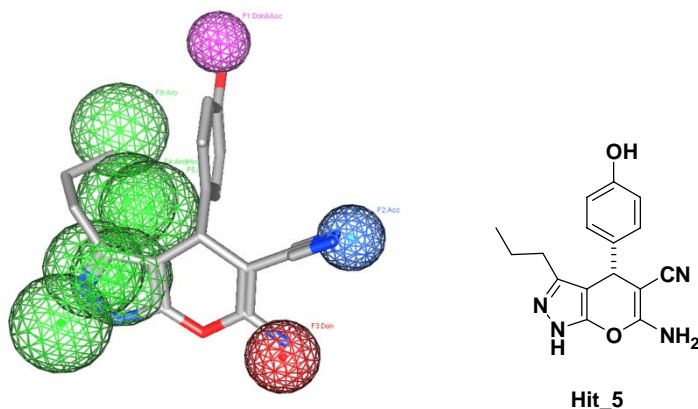
PI3K α , but also very potent selective inhibitor (**Hit_3**) of PI3K α vs. mTOR. These 'Hits' could be further developed for selective inhibition of mTOR, or PI3K α .

The pharmacophore query was further applied to other databases. The ZINC database mostly includes commercially available compounds, and thus the number and diversity of compounds is somewhat limited. Therefore, the much larger 'PubChem' library was searched against the same pharmacophore query by following the previous steps. From the 'PubChem' compound library, more than 22 million compounds were downloaded.¹⁸⁹ Again, salts and solvent were removed, acids were deprotonated, and bases protonated. Compounds were again rejected according to the filtering rules of Lipinski of no more than 5 hydrogen bond donors, no more than 10 hydrogen bond acceptors, molecular weight < 500, and log P < 5 to give about 10 million compounds. From the 'Loose Search' 40,480 hits were obtained and 880,000 conformers of them were obtained by calculation with MOE software. These hits were searched using the 'Tight Query' to obtain 235 hits. Finally, 27 compounds having rigidly linked groups positioning F1 and F2 were selected manually (See appendix for structures). These hits have not been tested against mTOR, as one of them (**Hit_1**) was already tested and many of them are not commercially available. However, any of these compounds found to inhibit mTOR could be potential novel lead compounds for the development of improved mTOR inhibitors.

4.2.3 Further strategies with hits from virtual screening

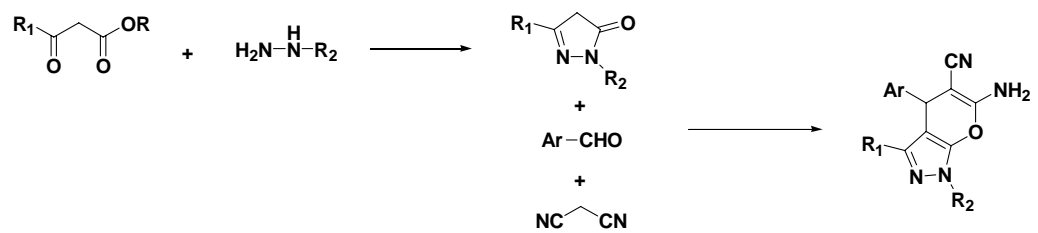
To develop further strategies based on hits from pharmacophore matching, **Hit_5** was mapped to the pharmacophore query (Figure 4.12). Based on this result of mapping, the phenolic oxygen and nitrile group of **Hit_5** occupy the positions of the carbonyl oxygen of the chromone ring and the morpholine oxygen of LY294002. An amine group of **Hit_5** overlaps with the F5 sphere generated from compound **B** (Figure 4.8). All of these functional groups may contribute to the binding to the active site of mTOR. The propyl group on the pyrazole ring is oriented toward the hydrophobic and aromatic sphere probes, and is a potential site for variation such as the introduction of aromatic groups. The pyrazole -NH- group can also be easily substituted with other functional groups. This pyrazole -NH- hydrogen atom is predicted to be oriented toward the area of Lys in mTOR and Trp in PI3Kinase. Thus variation of this position may provide an approach for increasing selectivity for mTOR. A similar structure to **Hit_5** was identified as an inhibitor of checkpoint kinase 1 (Chk1) ($IC_{50} = 20.4 \mu\text{M}$) by receptor-based virtual screening by Vernalis (R&D) Ltd,¹⁹⁰ though further development has not been reported. Variation of **Hit_5** could be an interesting future project for mTOR inhibitor design.

Figure 4.12 Overlap of **Hit_5** with the pharmacophore query



A synthetic procedure for **Hit_5** has been reported.¹⁹¹ Analogs of **Hit_5** (6-amino-5-cyano-4-aryl-1,4-dihydropyrano[2,3-c]pyrazoles) could be synthesized by a three-component reaction of an aromatic aldehyde, malononitrile, and 3-methyl-1-phenyl-2-pyrazolin-5-one (Scheme 4.2), as has been reported.¹⁹¹ By incorporating a diverse set of aromatic groups at the Ar position and by substituting R₁ and R₂ with aromatics and other groups, **Hit_5** could be further optimized for increased inhibition of mTOR.

Scheme 4.2 Schematic procedure for synthesis of **Hit_5** analogs identified by pharmacophore searching



4.3 Computational and Experimental details

DFT calculations

The Gaussian 03W program package (Revision-C.02) was used for geometry optimization and frequency calculations. Input files were generated using GaussView 3.09. This program was also used to generate Cubes for measuring total density and electrostatic potential surfaces. The initial structures of compounds **4.2s** were built using GaussView. The geometries were initially optimized at the RHF/6-31G(d) level. Transition states of **4.2_1**, **4.2_3**, **4.2_4**, **4.2_6**, and **4.2_7** were located with the Synchronous Transit-Guided Quasi-Newton (STQN) method^{192, 193} (using opt=QST2 option) at the RHF/6-31G(d) level. The required reactant (R conformers) and product (P conformers) structures as input were obtained from the optimized structures at the RHF/6-31G(d) level. After frequency calculations, the transition state of each compound was confirmed by the observation of one imaginary frequency. It was further confirmed by visualizing the vibration mode of the imaginary frequency with GaussView 3.09. The obtained transition state of each compound at the RHF/6-31G(d) level was further used to search the transition state of each compound at the B3LYP/6-311(d) level. Searching for the transition states of **4.2_4** and **4.2_7** at the B3LYP/6-311(d) level from the RHF/6-31G(d) structure gave the rotation of the phenyl ring instead of the morpholine ring as a transition state (confirmed by visualizing the vibrational mode of the imaginary frequency). Therefore, the optimized R and P conformers of **4.2_4** and **4.2_7** at the B3LYP/6-311G(d) level were used to locate the transition states at the same level. All

transition states of **4.2_1**, **4.2_3**, **4.2_4**, **4.2_6**, and **4.2_7** were obtained at the B3LYP/6-311G(d) level and were confirmed by frequency calculations with one imaginary frequency and by analysis of the vibrational mode of the imaginary frequency with GaussView 3.09. The electrostatic potentials of compounds **4.2s** were obtained by following the procedures in Chapter 2.

Locating the transition states of **4.1_1** and **4.1_3** with the STQN method gave unmeaningful results. Therefore, the geometry of the second step (it is the average structure of R and P forms) was taken from the output of Gaussian 03 calculation (with opt=QST2 option). With this geometry the transition state of **4.1_1** was located directly with 'calcall' option. The desired transition state was obtained at the RHF/6-31G(d) level and confirmed by frequency calculation and visualization. The calculation level was increased to the B3LYP/6-311G(d) level, and the final transition state was located and confirmed. The transition state of **4.1_3** was located by the same approach for **4.1_1**.

Pharmacophore searching

The preparation of the compound library for virtual screening was started by downloading 'drug-like' compounds, already sorted in the ZINC database according to the 'Lipinski rule of five'. Ten separate databases were built, and structures in the databases were refined by the 'wash' command. Partial charges of all compounds were calculated with the MMFF94x force field and the structures were minimized with an RMS gradient of 0.1. Structural features of compounds such as H-bond donor and acceptor, cation/anion, aromatic ring center, hydrophobic region, and metal ligator in

databases were pre-calculated with the polar-charged-hydrophobic (PCH) scheme in MOE.

To set up a pharmacophore query, the result of flexible alignment of LY294002 and PI103 was loaded to MOE. A 'Pharmacophore Query Editor' was used to assign queries based on the significant common features of LY294002 and PI103. The oxygen atoms in the chromone ring of LY294002 and in the phenol ring of PI103 was set to a H-bond donor and acceptor sphere (F1, Don&Acc) with 1.4 Å radius, and the oxygen atom in the morpholine rings of LY294002 and PI103 was set to a H-bond acceptor sphere (F2, Acc) with 1.4 Å radius. These two queries were assigned to be 'essential'. Eight aromatic spheres were assigned with 1.8 Å radius by examining the aromatic rings of LY294002 and PI103, and these were constrained to 'at least one'. An additional structure of ATP was used to set up volume constraint since it occupies more space than LY294002 and PI103. Volume was created by unionizing a group of spheres positioned at the centers of all atoms in LY294002, PI103, and ATP. The radii of spheres were set to the van der Waals radii of the atoms. An exterior volume constraint was chosen to not allow compounds to have atoms located outside of the volume. Partial match was enabled to specify the minimum number of features to be matched, and it was set to 'at least 4'.

The pre-calculated structures in the databases were searched with the pharmacophore query to give 4,979 hits. All conformations of these hits were searched and all conformers were minimized with default values to give 76,369 conformers of hits.

The initial pharmacophore query, named 'Loose query' was refined to 'Tight query'. The radii of F1 (Don&Acc), F2 (Acc), and aromatic spheres were shrank to 0.9 Å,

0.9 Å, and 1.4 Å respectively. Two aromatic spheres, which are not in the overlapped region between LY294002 and PI103, were removed to leave six spheres, and these were constrained to 'at least one'. One additional feature (F3, Don) from compound B was implemented. The radius of the sphere (F3, Don) was set to 1.0 Å, and it was also assigned to 'essential'. Partial match was allowed, and it was set to 'at least 5'.

All conformers of 4,979 initial hits were searched with the 'Tight query' to give 8 hits, and six of them were selected by examining the structures within the query.

3-Amino-1H-pyrrolo[2,3-b]pyridine-2-carboxylic acid ethyl ester (4.5): To a solution of 2-chloro-3-pyridinecarbonitrile (1.42 g, 10.0 mmol) in DMSO (20 mL) was added glycine ethyl ester hydrochloride (2.80 g, 19.9 mmol) and potassium bicarbonate (4.0 g, 40.0 mmol). The reaction mixture was stirred at 130 °C for 15 h. After cooling, the reaction mixture was diluted in water, and the product mixture was extracted with a mixture of ethyl acetate and THF. The organic layer was washed with brine, dried over MgSO₄, and concentrated with a rotary evaporator. The product was purified with flash column chromatography on silica gel by eluting with THF/hexane (1/5) to give the desired product **4.5** as a yellow-green solid (0.50 g, 2.44 mmol, 24.4% yield); TLC *R_f* = 0.21 (Hexane/EtOAc 1:1); mp 181 °C; ¹H-NMR (300 MHz, DMSO-*d*₆) δ, 11.37 (s, 1 H), 8.39 (d, 1 H, *J* = 4.8 Hz), 8.26 (d, 1 H, *J* = 8.1 Hz), 6.98 (dd, 1 H, *J* = 8.0 Hz, *J* = 4.8 Hz), 5.95 (s, 2 H), 4.32 (q, 2 H, *J* = 7.2 Hz), 1.31 (t, 3 H, *J* = 7.2 Hz); ¹³C-NMR (100 MHz, DMSO-*d*₆) δ, 162.50,

147.94, 147.46, 134.71, 129.95, 114.00, 111.61, 105.86, 59.48, 14.64; MS(ESI) $m/z = 206.1 (M+H)^+$.

3-Amino-1-methyl-1H-pyrrolo[2,3-*b*]pyridine-2-carboxylic acid ethyl ester (4.6): To a solution of **4.5** (1.45 g, 7.06 mmol) in dry DMF (20 mL) was slowly added 60% NaH (0.36 g, 8.50 mmol) at 0 °C. After 30 min, methyl iodide (0.53 mL, 8.49 mmol) was added to the reaction mixture at 0 °C. After another 30 min, the reaction mixture was allowed to warm to room temperature, and stirred for an additional 5 h. The product mixture was diluted in water and extracted with a mixture of ethyl acetate and THF. The organic layer was washed with saturated sodium thiosulfate solution and brine, dried with MgSO₄, and concentrated with a rotary evaporator. The product was purified with flash column chromatography on silica gel by eluting with ethyl acetate/hexane (1/4) to give the title product as a yellow solid (0.40 g, 1.82 mmol, 75% yield); TLC $R_f = 0.42$

(Hexane/EtOAc 1:1); ¹H-NMR (400 MHz, CDCl₃) δ , 8.40 (dd, 1 H, $J = 4.4$ Hz, $J = 1.6$ Hz), 7.81 (dd, 1 H, $J = 8.0$ Hz, $J = 1.6$ Hz), 6.88 (dd, 1 H, $J = 8.0$ Hz, $J = 4.8$ Hz), 4.98 (br, 1 H), 4.37 (q, 2 H, $J = 7.2$ Hz), 3.95 (s, 3 H), 1.39 (t, 3 H, $J = 7.2$ Hz); ¹³C-NMR (100 MHz, CDCl₃) δ , 163.19, 148.04, 147.73, 134.18, 127.97, 114.10, 110.93, 109.24, 60.00, 30.35, 14.42.

3-(3-Methoxy-benzoylamino)-1-methyl-1H-pyrrolo[2,3-*b*]pyridine-2-carboxylic acid ethyl ester (4.7): To a solution of **4.6** (0.78 g, 3.56 mmol) in dry methylene chloride (20 mL) was added triethylamine (1.4 mL, 10.0 mmol) at 0 °C. 3-methoxybenzoyl chloride (0.60 mL, 4.3 mmol) was slowly added to the solution at 0 °C. After 30 min, the reaction

mixture was allowed to warm to room temperature and stirred further for 5 h. The product mixture was diluted with water and saturated sodium bicarbonate, and extracted with methylene chloride. The organic layer was washed with brine, dried with MgSO_4 , and concentrated with a rotary evaporator. The product was purified with flash column chromatography on silica gel by eluting with ethyl acetate/hexane (1/4) to give the title compound **4.7** as a dim yellow solid (1.25 g, 3.54 mmol, 99% yield); TLC R_f = 0.45 (Hexane/EtOAc 1:1); mp 117 °C; $^1\text{H-NMR}$ (400 MHz, CDCl_3) δ , 10.65 (s, 1 H), 8.86 (dd, 1 H, J = 8.0 Hz, J = 1.6 Hz), 8.51 (dd, 1 H, J = 4.4 Hz, J = 1.6 Hz), 7.61-7.57 (m, 2 H), 7.43 (t, 1 H, J = 8.0 Hz), 7.11 (dd, 1 H, J = 8.2 Hz, J = 3.0 Hz), 4.50 (q, 2 H, J = 7.2 Hz), 4.12 (s, 3 H), 3.90 (s, 3 H), 1.46 (t, 3 H, J = 7.2 Hz); $^{13}\text{C-NMR}$ (100 MHz, CDCl_3) δ , 164.28, 163.51, 160.05, 148.23, 147.17, 135.61, 135.40, 129.82, 124.78, 119.20, 118.47, 116.17, 114.43, 112.65, 112.18, 61.47, 55.47, 31.03, 14.36; MS(ESI) m/z = 354.1 ($\text{M}+\text{H}$) $^+$.

8-Chloro-6-(3-methoxy-phenyl)-9-methyl-9H-1,5,7,9-tetraaza-fluorene (4.10):

Compound **4.7** (1.63 g, 4.61 mmol) was dissolved in a mixture of methanol (20 mL) and THF (20 mL), and the solution was transferred to a high pressure stainless steel reactor with a stirring bar. Ammonium hydroxide (ca. 10 mL) was added, and the reaction mixture was stirred at 90 °C under about 70 psi for 36 h. After cooling, ammonia gas was released, and the solvent was removed with a rotary evaporator. Mass spectrometry analysis showed that two amide products **4.8** and **4.9** were present, having two peaks (m/z = 325.1 and 307.1 ($\text{M}+\text{H}$) $^+$, respectively). The product mixture was redissolved in 2N NaOH (30 mL) and 2-propanol and stirred under reflux for 5 h. The presence of one

single cyclized amide product **4.9** was confirmed by mass spectrometry analysis. The basic solution was neutralized with 1N HCl, and a dim yellow solid was precipitated. This solid was collected by filtration, washed with water, and dried in an oven overnight (1.46 g, 4.77 mmol with some impurities). POCl₃ (5.0 mL) was slowly added to the dried solid, and the reaction mixture was stirred at 110 °C for 8 h. After cooling, ice water (10 mL) was added at 0 °C, and the acidic solution was neutralized with saturated sodium carbonate to precipitate the product as a yellow solid. The product was further purified with flash column chromatography on silica gel by eluting with ethyl acetate/hexane (1/3) to afford the title compound **4.10** (0.82 g, 2.52 mmol, 55% yield from **4.7**); TLC R_f = 0.48 (Hexane/EtOAc 1:1); mp 148 °C; ¹H-NMR (400 MHz, CDCl₃) δ, 8.72 (dd, 1 H, J = 4.8 Hz, J = 1.6 Hz), 8.65 (dd, 1 H, J = 8.0 Hz, J = 1.6 Hz), 8.11 (d, 1 H, J = 7.6 Hz), 8.06 (t, 1 H, J = 1.6 Hz), 7.40 (t, 1 H, J = 8.0 Hz), 7.31 (dd, 1 H, J = 7.8 Hz, J = 4.6 Hz), 7.00 (dd, 1 H, J = 7.6 Hz, J = 2.4 Hz), 4.29 (s, 3 H), 3.94 (s, 3 H); ¹³C-NMR (100 MHz, CDCl₃) δ, 159.94, 156.35, 152.98, 151.29, 146.54, 142.19, 138.51, 131.05, 129.52, 126.65, 120.55, 117.04, 116.36, 113.44, 112.73, 55.42, 30.00; MS(ESI) m/z = 325.1 (M+H)⁺.

6-(3-Methoxy-phenyl)-9-methyl-8-morpholin-4-yl-9H-1,5,7,9-tetraaza-fluorene (4.11):

To compound **4.10** (0.72 g, 2.22 mmol) in THF (40 mL) was added morpholine (4 eq.) and catalytic amount of acetic acid (3 drops). The reaction mixture was stirred under reflux for 8 h, and the reactant was completely consumed as indicated by TLC. The solvent was removed with a rotary evaporator, and the product mixture was diluted with water followed by extraction with a mixture of ethyl acetate and THF. The organic layer was

washed with brine, dried with MgSO_4 , and concentrated with a rotary evaporator. The product was purified with flash column chromatography by eluting with ethyl acetate/hexane (2/1) to yield the desired product (0.69 g, 1.84 mmol, 83% yield); TLC R_f = 0.30 (100% EtOAc); mp 162 °C; $^1\text{H-NMR}$ (400 MHz, CDCl_3) δ , 8.68-8.65 (m, 2 H), 8.16-8.12 (m, 2 H), 7.41 (t, 1 H, J = 7.8 Hz), 7.29 (dd, 1 H, J = 7.8 Hz, J = 5.0 Hz), 7.00 (dd, 1 H, J = 8.2 Hz, J = 2.6 Hz), 4.12 (s, 3 H), 3.99 (t, 4 H, J = 4.4 Hz), 3.94 (s, 3 H), 3.59 (t, 4 H, J = 4.4 Hz); $^{13}\text{C-NMR}$ (100 MHz, CDCl_3) δ , 159.84, 156.04, 154.08, 153.68, 149.85, 145.82, 140.12, 130.40, 129.38, 121.67, 120.44, 116.65, 115.36, 115.06, 113.06, 66.52, 55.37, 50.20, 30.62; MS(ESI) m/z = 375.2 ($\text{M}+\text{H}$) $^+$.

Acetic acid 3-(9-methyl-8-morpholin-4-yl-9H-1,5,7,9-tetraaza-fluoren-6-yl)-phenyl ester (C801): To a solution of **4.11** (0.13 g, 0.35 mmol) in dry methylene chloride (10 mL) was added boron tribromide (1 mL, 1.0 mmol) at -78 °C. After stirring 30 min at -78 °C, the reaction mixture was warmed to room temperature and stirred for 20 h. After cooling the reaction mixture to -78 °C again, 1 N HCl (1.5 mL) was added and stirred at room temperature for 30 min. The solvent was removed with a rotary evaporator. The reaction mixture was redissolved with water and neutralized with saturated NaHCO_3 . The product mixture was extracted with a mixture of THF and ethyl acetate. The organic layer was washed with brine, dried with MgSO_4 , and concentrated with a rotary evaporator. The crude product was dissolved in acetic anhydride (10 mL) and THF, and the reaction mixture was refluxed for 8 h. After cooling, the reaction mixture was diluted with water, and the product mixture was extracted with a mixture of THF and

ethyl acetate. The organic layer was washed with brine, dried over MgSO_4 , and concentrated with a rotary evaporator. The crude product was purified with flash column chromatography by eluting with ethyl acetate/hexane (1/1) to give the desired product **C801** as a colorless solid (0.08 g, 0.20 mmol, 57% yield); TLC R_f = 0.45 (100% EtOAc); mp 219 - 210 °C; $^1\text{H-NMR}$ (400 MHz, CDCl_3) δ , 8.68 (dd, 1 H, J = 4.8 Hz, J = 1.6 Hz), 8.64 (dd, 1 H, J = 7.6 Hz, J = 1.6 Hz), 8.44 (d, 1 H, J = 8.0 Hz), 8.27 (t, 1 H, J = 1.8 Hz), 7.50 (t, 1 H, J = 8.0 Hz), 7.30 (dd, 1 H, J = 8.0 Hz, J = 4.8 Hz), 7.17 (dd, 1 H, J = 8.0 Hz, J = 2.0 Hz), 4.12 (s, 3 H), 3.99 (t, 4 H, J = 4.6 Hz), 3.58 (t, 4 H, J = 4.6 Hz), 2.37 (s, 3 H); $^{13}\text{C-NMR}$ (100 MHz, CDCl_3) δ , 169.52, 155.20, 154.09, 153.68, 150.99, 149.91, 145.78, 140.38, 130.37, 129.27, 125.26, 122.59, 121.73, 120.87, 116.71, 114.99, 66.50, 50.22, 30.62, 21.22; MS(ESI) m/z = 404.2 ($\text{M}+\text{H}$) $^+$.

3-(9-Methyl-8-morpholin-4-yl-9H-1,5,7,9-tetraaza-fluoren-6-yl)-phenol (C802): To a solid compound of **C801** (13.2 mg, 0.033 mmol) was added 4N HCl (1 mL) and ethyl acetate (4 mL) at room temperature. The white solid turned yellow. The reaction mixture was stirred at 50 °C for 3 h. The solvent was removed by rotary evaporation. The product mixture was redissolved in ethyl acetate, and unreacted neutral compound was removed by ethyl acetate. It was repeated three times, and the HCl salt form of **C802** (13.1 mg, 0.033 mmol, 99% yield) was obtained. The HCl salt of **C802** was neutralized with saturated NaHCO_3 , and the neutral **C802** was extracted with a mixture of THF and ethyl acetate. The organic layer was washed with brine, dried over MgSO_4 , and concentrated by rotary evaporation. The product was further purified by a flash

column chromatography with ethyl acetate/hexane (2/1) to give the title compound **C802** (10 mg, 0.028 mmol, 85% yield); TLC R_f = 0.33 (100% EtOAc): mp 250 °C; $^1\text{H-NMR}$ (400 MHz, CDCl_3) δ , 8.68 (d, 1 H, J = 4.4 Hz), 8.65 (d, 1 H, J = 7.6 Hz), 8.12-8.09 (m, 2 H), 7.37 (t, 1 H, J = 7.8 Hz), 7.29 (t, 1 H, J = 7.8 Hz, J = 5.0 Hz), 6.94 (dd, 1 H, J = 8.0 Hz, J = 2.4 Hz), 5.94 (br, 1 H), 4.12 (s, 3 H), 3.98 (t, 4 H, J = 4.4 Hz), 3.59 (t, 4 H, J = 4.4 Hz); $^{13}\text{C-NMR}$ (100 MHz, CDCl_3) δ , 155.88, 154.12, 153.71, 149.91, 145.81, 140.32, 130.45, 129.73, 121.70, 120.47, 116.76, 116.62, 115.04, 114.62, 66.54, 50.21, 30.69; MS(ESI) m/z = 362.1 (M+H) $^+$.

Reference

1. Chiang, G. G.; Abraham, R. T., Targeting the mTOR signaling network in cancer. *Trends Mol. Med.* **2007**, *13* (10), 433-442.
2. Wan, X.; Helman, L. J., The biology behind mTOR inhibition in sarcoma. *Oncologist* **2007**, *12* (8), 1007-1018.
3. Guertin, D. A.; Sabatini, D. M., Defining the role of mTOR in cancer. *Cancer Cell* **2007**, *12* (1), 9-22.
4. Abraham, R. T.; Gibbons, J. J., The mammalian target of rapamycin signaling pathway: twists and turns in the road to cancer therapy. *Clin. Cancer Res.* **2007**, *13* (11), 3109-3114.
5. Yang, Q.; Guan, K. L., Expanding mTOR signaling. *Cell Res.* **2007**, *17* (8), 666-681.
6. Vezina, C.; Kudelski, A.; Sehgal, S. N., Rapamycin (AY-22,989), a new antifungal antibiotic. I. Taxonomy of the producing streptomycete and isolation of the active principle. *J. Antibiot.* **1975**, *28* (10), 721-726.
7. Sehgal, S. N.; Baker, H.; Vezina, C., Rapamycin (AY-22,989), a new antifungal antibiotic. II. Fermentation, isolation and characterization. *J. Antibiot.* **1975**, *28* (10), 727-732.
8. Georger, B.; Kerr, K.; Tang, C. B.; Fung, K. M.; Powell, B.; Sutton, L. N.; Phillips, P. C.; Janss, A. J., Antitumor activity of the rapamycin analog CCI-779 in human primitive neuroectodermal tumor/medulloblastoma models as single agent and in combination chemotherapy. *Cancer Res.* **2001**, *61* (4), 1527-1532.
9. Dudkin, L.; Dilling, M. B.; Cheshire, P. J.; Harwood, F. C.; Hollingshead, M.; Arbuck, S. G.; Travis, R.; Sausville, E. A.; Houghton, P. J., Biochemical correlates of mTOR inhibition by the rapamycin ester CCI-779 and tumor growth inhibition. *Clin. Cancer Res.* **2001**, *7* (6), 1758-1764.
10. Boulay, A.; Zumstein-Mecker, S.; Stephan, C.; Beuvink, I.; Zilbermann, F.; Haller, R.; Tobler, S.; Heusser, C.; O'Reilly, T.; Stolz, B.; Marti, A.; Thomas, G.; Lane, H. A.,

Antitumor efficacy of intermittent treatment schedules with the rapamycin derivative RAD001 correlates with prolonged inactivation of ribosomal protein S6 kinase 1 in peripheral blood mononuclear cells. *Cancer Res.* **2004**, *64* (1), 252-261.

11. Mabuchi, S.; Altomare, D. A.; Connolly, D. C.; Klein-Szanto, A.; Litwin, S.; Hoelzle, M. K.; Hensley, H. H.; Hamilton, T. C.; Testa, J. R., RAD001 (Everolimus) delays tumor onset and progression in a transgenic mouse model of ovarian cancer. *Cancer Res.* **2007**, *67* (6), 2408-2413.

12. Mabuchi, S.; Altomare, D. A.; Cheung, M.; Zhang, L.; Poulikakos, P. I.; Hensley, H. H.; Schilder, R. J.; Ozols, R. F.; Testa, J. R., RAD001 inhibits human ovarian cancer cell proliferation, enhances cisplatin-induced apoptosis, and prolongs survival in an ovarian cancer model. *Clin. Cancer Res.* **2007**, *13* (14), 4261-4270.

13. Mita, M.; Sankhala, K.; Abdel-Karim, I.; Mita, A.; Giles, F., Deforolimus (AP23573) a novel mTOR inhibitor in clinical development. *Expert Opin. Investig. Drugs.* **2008**, *17* (12), 1947-1954.

14. Rizzieri, D. A.; Feldman, E.; Dipersio, J. F.; Gabrail, N.; Stock, W.; Strair, R.; Rivera, V. M.; Albitar, M.; Bedrosian, C. L.; Giles, F. J., A phase 2 clinical trial of deforolimus (AP23573, MK-8669), a novel mammalian target of rapamycin inhibitor, in patients with relapsed or refractory hematologic malignancies. *Clin. Cancer Res.* **2008**, *14* (9), 2756-2762.

15. Choi, J.; Chen, J.; Schreiber, S. L.; Clardy, J., Structure of the FKBP12-rapamycin complex interacting with the binding domain of human FRAP. *Science* **1996**, *273* (5272), 239-242.

16. Bader, A. G.; Kang, S.; Zhao, L.; Vogt, P. K., Oncogenic PI3K deregulates transcription and translation. *Nat. Rev. Cancer* **2005**, *5* (12), 921-929.

17. Cantley, L. C., The phosphoinositide 3-kinase pathway. *Science* **2002**, *296* (5573), 1655-1657.

18. Engelman, J. A.; Luo, J.; Cantley, L. C., The evolution of phosphatidylinositol 3-kinases as regulators of growth and metabolism. *Nat. Rev. Genet.* **2006**, *7* (8), 606-619.

19. Jackson, S. P.; Schoenwaelder, S. M.; Goncalves, I.; Nesbitt, W. S.; Yap, C. L.; Wright, C. E.; Kenche, V.; Anderson, K. E.; Dopheide, S. M.; Yuan, Y.; Sturgeon, S. A.; Prabakaran, H.; Thompson, P. E.; Smith, G. D.; Shepherd, P. R.; Daniele, N.; Kulkarni, S.; Abbott, B.; Saylik, D.; Jones, C.; Lu, L.; Giuliano, S.; Hughan, S. C.; Angus, J. A.; Robertson, A. D.; Salem, H. H., PI 3-kinase p110beta: a new target for antithrombotic therapy. *Nat. Med.* **2005**, *11* (5), 507-514.
20. Barber, D. F.; Bartolome, A.; Hernandez, C.; Flores, J. M.; Redondo, C.; Fernandez-Arias, C.; Camps, M.; Ruckle, T.; Schwarz, M. K.; Rodriguez, S.; Martinez, A. C.; Balomenos, D.; Rommel, C.; Carrera, A. C., PI3Kgamma inhibition blocks glomerulonephritis and extends lifespan in a mouse model of systemic lupus. *Nat. Med.* **2005**, *11* (9), 933-935.
21. Camps, M.; Ruckle, T.; Ji, H.; Ardisson, V.; Rintelen, F.; Shaw, J.; Ferrandi, C.; Chabert, C.; Gillieron, C.; Francon, B.; Martin, T.; Gretener, D.; Perrin, D.; Leroy, D.; Vitte, P. A.; Hirsch, E.; Wymann, M. P.; Cirillo, R.; Schwarz, M. K.; Rommel, C., Blockade of PI3Kgamma suppresses joint inflammation and damage in mouse models of rheumatoid arthritis. *Nat. Med.* **2005**, *11* (9), 936-943.
22. Ruckle, T.; Schwarz, M. K.; Rommel, C., PI3Kgamma inhibition: towards an 'aspirin of the 21st century'? *Nat. Rev. Drug Discov.* **2006**, *5* (11), 903-918.
23. Okkenhaug, K.; Bilancio, A.; Farjot, G.; Priddle, H.; Sancho, S.; Peskett, E.; Pearce, W.; Meek, S. E.; Salpekar, A.; Waterfield, M. D.; Smith, A. J.; Vanhaesebroeck, B., Impaired B and T cell antigen receptor signaling in p110delta PI 3-kinase mutant mice. *Science* **2002**, *297* (5583), 1031-1034.
24. Hara, K.; Maruki, Y.; Long, X.; Yoshino, K.; Oshiro, N.; Hidayat, S.; Tokunaga, C.; Avruch, J.; Yonezawa, K., Raptor, a binding partner of target of rapamycin (TOR), mediates TOR action. *Cell* **2002**, *110* (2), 177-189.
25. Kim, D. H.; Sarbassov, D. D.; Ali, S. M.; King, J. E.; Latek, R. R.; Erdjument-Bromage, H.; Tempst, P.; Sabatini, D. M., mTOR interacts with raptor to form a nutrient-sensitive complex that signals to the cell growth machinery. *Cell* **2002**, *110* (2), 163-175.
26. Sarbassov, D. D.; Ali, S. M.; Kim, D. H.; Guertin, D. A.; Latek, R. R.; Erdjument-Bromage, H.; Tempst, P.; Sabatini, D. M., Rictor, a novel binding partner of mTOR, defines a rapamycin-insensitive and raptor-independent pathway that regulates the cytoskeleton. *Curr. Biol.* **2004**, *14* (14), 1296-1302.

27. Sarbassov, D. D.; Guertin, D. A.; Ali, S. M.; Sabatini, D. M., Phosphorylation and regulation of Akt/PKB by the rictor-mTOR complex. *Science* **2005**, *307* (5712), 1098-1101.
28. Kim, D. H.; Sarbassov, D. D.; Ali, S. M.; Latek, R. R.; Guntur, K. V.; Erdjument-Bromage, H.; Tempst, P.; Sabatini, D. M., GbetaL, a positive regulator of the rapamycin-sensitive pathway required for the nutrient-sensitive interaction between raptor and mTOR. *Mol. Cell* **2003**, *11* (4), 895-904.
29. Frias, M. A.; Thoreen, C. C.; Jaffe, J. D.; Schroder, W.; Sculley, T.; Carr, S. A.; Sabatini, D. M., mSin1 is necessary for Akt/PKB phosphorylation, and its isoforms define three distinct mTORC2s. *Curr. Biol.* **2006**, *16* (18), 1865-1870.
30. Jacinto, E.; Facchinetti, V.; Liu, D.; Soto, N.; Wei, S.; Jung, S. Y.; Huang, Q.; Qin, J.; Su, B., SIN1/MIP1 maintains rictor-mTOR complex integrity and regulates Akt phosphorylation and substrate specificity. *Cell* **2006**, *127* (1), 125-137.
31. Yang, Q.; Inoki, K.; Ikenoue, T.; Guan, K. L., Identification of Sin1 as an essential TORC2 component required for complex formation and kinase activity. *Genes Dev.* **2006**, *20* (20), 2820-2832.
32. Guertin, D. A.; Stevens, D. M.; Thoreen, C. C.; Burds, A. A.; Kalaany, N. Y.; Moffat, J.; Brown, M.; Fitzgerald, K. J.; Sabatini, D. M., Ablation in mice of the mTORC components raptor, rictor, or mLST8 reveals that mTORC2 is required for signaling to Akt-FOXO and PKCalpha, but not S6K1. *Dev. Cell* **2006**, *11* (6), 859-871.
33. Shiota, C.; Woo, J. T.; Lindner, J.; Shelton, K. D.; Magnuson, M. A., Multiallelic disruption of the rictor gene in mice reveals that mTOR complex 2 is essential for fetal growth and viability. *Dev. Cell* **2006**, *11* (4), 583-589.
34. Schroder, W. A.; Buck, M.; Cloonan, N.; Hancock, J. F.; Suhrbier, A.; Sculley, T.; Bushell, G., Human Sin1 contains Ras-binding and pleckstrin homology domains and suppresses Ras signalling. *Cell Signal* **2007**, *19* (6), 1279-1289.
35. Pearce, L. R.; Huang, X.; Boudeau, J.; Pawlowski, R.; Wullschleger, S.; Deak, M.; Ibrahim, A. F.; Gourlay, R.; Magnuson, M. A.; Alessi, D. R., Identification of Protor as a novel Rictor-binding component of mTOR complex-2. *Biochem. J.* **2007**, *405* (3), 513-522.

36. Dan, H. C.; Sun, M.; Yang, L.; Feldman, R. I.; Sui, X. M.; Ou, C. C.; Nellist, M.; Yeung, R. S.; Halley, D. J.; Nicosia, S. V.; Pledger, W. J.; Cheng, J. Q., Phosphatidylinositol 3-kinase/Akt pathway regulates tuberous sclerosis tumor suppressor complex by phosphorylation of tuberin. *J. Biol. Chem.* **2002**, *277* (38), 35364-35370.
37. Inoki, K.; Li, Y.; Zhu, T.; Wu, J.; Guan, K. L., TSC2 is phosphorylated and inhibited by Akt and suppresses mTOR signalling. *Nat. Cell Biol.* **2002**, *4* (9), 648-657.
38. Manning, B. D.; Tee, A. R.; Logsdon, M. N.; Blenis, J.; Cantley, L. C., Identification of the tuberous sclerosis complex-2 tumor suppressor gene product tuberin as a target of the phosphoinositide 3-kinase/akt pathway. *Mol. Cell* **2002**, *10* (1), 151-162.
39. Potter, C. J.; Pedraza, L. G.; Xu, T., Akt regulates growth by directly phosphorylating TSC2. *Nat. Cell Biol.* **2002**, *4* (9), 658-665.
40. Cantrell, D. A., Phosphoinositide 3-kinase signalling pathways. *J. Cell Sci.* **2001**, *114* (Pt 8), 1439-1445.
41. Vanhaesebroeck, B.; Alessi, D. R., The PI3K-PDK1 connection: more than just a road to PKB. *Biochem. J.* **2000**, *346* Pt 3, 561-576.
42. Belham, C.; Wu, S.; Avruch, J., Intracellular signalling: PDK1--a kinase at the hub of things. *Curr. Biol.* **1999**, *9* (3), R93-R96.
43. Toker, A.; Newton, A. C., Cellular signaling: pivoting around PDK-1. *Cell* **2000**, *103* (2), 185-188.
44. Vander Haar, E.; Lee, S. I.; Bandhakavi, S.; Griffin, T. J.; Kim, D. H., Insulin signalling to mTOR mediated by the Akt/PKB substrate PRAS40. *Nat. Cell Biol.* **2007**, *9* (3), 316-323.
45. Sancak, Y.; Thoreen, C. C.; Peterson, T. R.; Lindquist, R. A.; Kang, S. A.; Spooner, E.; Carr, S. A.; Sabatini, D. M., PRAS40 is an insulin-regulated inhibitor of the mTORC1 protein kinase. *Mol. Cell* **2007**, *25* (6), 903-915.

46. Kovacina, K. S.; Park, G. Y.; Bae, S. S.; Guzzetta, A. W.; Schaefer, E.; Birnbaum, M. J.; Roth, R. A., Identification of a proline-rich Akt substrate as a 14-3-3 binding partner. *J. Biol. Chem.* **2003**, *278* (12), 10189-10194.
47. Jacinto, E.; Loewith, R.; Schmidt, A.; Lin, S.; Ruegg, M. A.; Hall, A.; Hall, M. N., Mammalian TOR complex 2 controls the actin cytoskeleton and is rapamycin insensitive. *Nat. Cell Biol.* **2004**, *6* (11), 1122-1128.
48. Yokogami, K.; Wakisaka, S.; Avruch, J.; Reeves, S. A., Serine phosphorylation and maximal activation of STAT3 during CNTF signaling is mediated by the rapamycin target mTOR. *Curr. Biol.* **2000**, *10* (1), 47-50.
49. Castedo, M.; Ferri, K. F.; Blanco, J.; Roumier, T.; Larochette, N.; Barretina, J.; Amendola, A.; Nardacci, R.; Metivier, D.; Este, J. A.; Piacentini, M.; Kroemer, G., Human immunodeficiency virus 1 envelope glycoprotein complex-induced apoptosis involves mammalian target of rapamycin/FKBP12-rapamycin-associated protein-mediated p53 phosphorylation. *J. Exp. Med.* **2001**, *194* (8), 1097-1110.
50. Huang, J.; Manning, B. D., The TSC1-TSC2 complex: a molecular switchboard controlling cell growth. *Biochem. J.* **2008**, *412* (2), 179-190.
51. Consortium, E. C. T. S., Identification and characterization of the tuberous sclerosis gene on chromosome 16. *Cell* **1993**, *75* (7), 1305-1315.
52. Kandt, R. S.; Haines, J. L.; Smith, M.; Northrup, H.; Gardner, R. J.; Short, M. P.; Dumars, K.; Roach, E. S.; Steingold, S.; Wall, S.; et al., Linkage of an important gene locus for tuberous sclerosis to a chromosome 16 marker for polycystic kidney disease. *Nat. Genet.* **1992**, *2* (1), 37-41.
53. van Slegtenhorst, M.; de Hoogt, R.; Hermans, C.; Nellist, M.; Janssen, B.; Verhoef, S.; Lindhout, D.; van den Ouweland, A.; Halley, D.; Young, J.; Burley, M.; Jeremiah, S.; Woodward, K.; Nahmias, J.; Fox, M.; Ekong, R.; Osborne, J.; Wolfe, J.; Povey, S.; Snell, R. G.; Cheadle, J. P.; Jones, A. C.; Tachataki, M.; Ravine, D.; Sampson, J. R.; Reeve, M. P.; Richardson, P.; Wilmer, F.; Munro, C.; Hawkins, T. L.; Sepp, T.; Ali, J. B.; Ward, S.; Green, A. J.; Yates, J. R.; Kwiatkowska, J.; Henske, E. P.; Short, M. P.; Haines, J. H.; Jozwiak, S.; Kwiatkowski, D. J., Identification of the tuberous sclerosis gene TSC1 on chromosome 9q34. *Science* **1997**, *277* (5327), 805-808.

54. Jin, F.; Wienecke, R.; Xiao, G. H.; Maize, J. C., Jr.; DeClue, J. E.; Yeung, R. S., Suppression of tumorigenicity by the wild-type tuberous sclerosis 2 (Tsc2) gene and its C-terminal region. *Proc. Natl. Acad. Sci. USA* **1996**, *93* (17), 9154-9159.
55. Bai, X.; Ma, D.; Liu, A.; Shen, X.; Wang, Q. J.; Liu, Y.; Jiang, Y., Rheb activates mTOR by antagonizing its endogenous inhibitor, FKBP38. *Science* **2007**, *318* (5852), 977-980.
56. Cai, S. L.; Tee, A. R.; Short, J. D.; Bergeron, J. M.; Kim, J.; Shen, J.; Guo, R.; Johnson, C. L.; Kiguchi, K.; Walker, C. L., Activity of TSC2 is inhibited by AKT-mediated phosphorylation and membrane partitioning. *J. Cell Biol.* **2006**, *173* (2), 279-289.
57. Lee, D. F.; Kuo, H. P.; Chen, C. T.; Hsu, J. M.; Chou, C. K.; Wei, Y.; Sun, H. L.; Li, L. Y.; Ping, B.; Huang, W. C.; He, X.; Hung, J. Y.; Lai, C. C.; Ding, Q.; Su, J. L.; Yang, J. Y.; Sahin, A. A.; Hortobagyi, G. N.; Tsai, F. J.; Tsai, C. H.; Hung, M. C., IKK beta suppression of TSC1 links inflammation and tumor angiogenesis via the mTOR pathway. *Cell* **2007**, *130* (3), 440-455.
58. Inoki, K.; Zhu, T.; Guan, K. L., TSC2 mediates cellular energy response to control cell growth and survival. *Cell* **2003**, *115* (5), 577-590.
59. Brugarolas, J.; Lei, K.; Hurley, R. L.; Manning, B. D.; Reiling, J. H.; Hafen, E.; Witters, L. A.; Ellisen, L. W.; Kaelin, W. G., Jr., Regulation of mTOR function in response to hypoxia by REDD1 and the TSC1/TSC2 tumor suppressor complex. *Genes Dev.* **2004**, *18* (23), 2893-2904.
60. DeYoung, M. P.; Horak, P.; Sofer, A.; Sgroi, D.; Ellisen, L. W., Hypoxia regulates TSC1/2-mTOR signaling and tumor suppression through REDD1-mediated 14-3-3 shuttling. *Genes Dev.* **2008**, *22* (2), 239-251.
61. Jastrzebski, K.; Hannan, K. M.; Tchoubrieva, E. B.; Hannan, R. D.; Pearson, R. B., Coordinate regulation of ribosome biogenesis and function by the ribosomal protein S6 kinase, a key mediator of mTOR function. *Growth Factors* **2007**, *25* (4), 209-226.
62. Fingar, D. C.; Blenis, J., Target of rapamycin (TOR): an integrator of nutrient and growth factor signals and coordinator of cell growth and cell cycle progression. *Oncogene* **2004**, *23* (18), 3151-3171.

63. Fingar, D. C.; Salama, S.; Tsou, C.; Harlow, E.; Blenis, J., Mammalian cell size is controlled by mTOR and its downstream targets S6K1 and 4EBP1/eIF4E. *Genes Dev.* **2002**, *16* (12), 1472-1487.
64. Hannan, K. M.; Brandenburger, Y.; Jenkins, A.; Sharkey, K.; Cavanaugh, A.; Rothblum, L.; Moss, T.; Poortinga, G.; McArthur, G. A.; Pearson, R. B.; Hannan, R. D., mTOR-dependent regulation of ribosomal gene transcription requires S6K1 and is mediated by phosphorylation of the carboxy-terminal activation domain of the nucleolar transcription factor UBF. *Mol. Cell Biol.* **2003**, *23* (23), 8862-8877.
65. Hannan, K. M.; Thomas, G.; Pearson, R. B., Activation of S6K1 (p70 ribosomal protein S6 kinase 1) requires an initial calcium-dependent priming event involving formation of a high-molecular-mass signalling complex. *Biochem. J.* **2003**, *370* (Pt 2), 469-477.
66. Fingar, D. C.; Richardson, C. J.; Tee, A. R.; Cheatham, L.; Tsou, C.; Blenis, J., mTOR controls cell cycle progression through its cell growth effectors S6K1 and 4E-BP1/eukaryotic translation initiation factor 4E. *Mol. Cell Biol.* **2004**, *24* (1), 200-216.
67. Lane, H. A.; Fernandez, A.; Lamb, N. J.; Thomas, G., p70s6k function is essential for G1 progression. *Nature* **1993**, *363* (6425), 170-172.
68. Pende, M.; Kozma, S. C.; Jaquet, M.; Oorschot, V.; Burcelin, R.; Le Marchand-Brustel, Y.; Klumperman, J.; Thorens, B.; Thomas, G., Hypoinsulinaemia, glucose intolerance and diminished beta-cell size in S6K1-deficient mice. *Nature* **2000**, *408* (6815), 994-997.
69. Hanks, S. K.; Hunter, T., Protein kinases 6. The eukaryotic protein kinase superfamily: kinase (catalytic) domain structure and classification. *FASEB J.* **1995**, *9* (8), 576-596.
70. Akimoto, K.; Nakaya, M.; Yamanaka, T.; Tanaka, J.; Matsuda, S.; Weng, Q. P.; Avruch, J.; Ohno, S., Atypical protein kinase Clambda binds and regulates p70 S6 kinase. *Biochem. J.* **1998**, *335* (Pt 2), 417-424.
71. Romanelli, A.; Martin, K. A.; Toker, A.; Blenis, J., p70 S6 kinase is regulated by protein kinase Czeta and participates in a phosphoinositide 3-kinase-regulated signalling complex. *Mol. Cell Biol.* **1999**, *19* (4), 2921-2928.

72. Harrington, L. S.; Findlay, G. M.; Gray, A.; Tolkacheva, T.; Wigfield, S.; Rebholz, H.; Barnett, J.; Leslie, N. R.; Cheng, S.; Shepherd, P. R.; Gout, I.; Downes, C. P.; Lamb, R. F., The TSC1-2 tumor suppressor controls insulin-PI3K signaling via regulation of IRS proteins. *J. Cell Biol.* **2004**, *166* (2), 213-223.
73. Shah, O. J.; Hunter, T., Turnover of the active fraction of IRS1 involves raptor-mTOR- and S6K1-dependent serine phosphorylation in cell culture models of tuberous sclerosis. *Mol. Cell Biol.* **2006**, *26* (17), 6425-6434.
74. Shah, O. J.; Wang, Z.; Hunter, T., Inappropriate activation of the TSC/Rheb/mTOR/S6K cassette induces IRS1/2 depletion, insulin resistance, and cell survival deficiencies. *Curr. Biol.* **2004**, *14* (18), 1650-1656.
75. Anderson, W. M.; Grundholm, A.; Sells, B. H., Modification of ribosomal proteins during liver regeneration. *Biochem. Biophys. Res. Commun.* **1975**, *62* (3), 669-676.
76. Gressner, A. M.; Wool, I. G., The phosphorylation of liver ribosomal proteins in vivo. Evidence that only a single small subunit protein (S6) is phosphorylated. *J. Biol. Chem.* **1974**, *249* (21), 6917-6925.
77. Raught, B.; Peiretti, F.; Gingras, A. C.; Livingstone, M.; Shahbazian, D.; Mayeur, G. L.; Polakiewicz, R. D.; Sonenberg, N.; Hershey, J. W., Phosphorylation of eucaryotic translation initiation factor 4B Ser422 is modulated by S6 kinases. *EMBO J.* **2004**, *23* (8), 1761-1769.
78. Redpath, N. T.; Foulstone, E. J.; Proud, C. G., Regulation of translation elongation factor-2 by insulin via a rapamycin-sensitive signalling pathway. *EMBO J.* **1996**, *15* (9), 2291-2297.
79. Wilson, K. F.; Wu, W. J.; Cerione, R. A., Cdc42 stimulates RNA splicing via the S6 kinase and a novel S6 kinase target, the nuclear cap-binding complex. *J. Biol. Chem.* **2000**, *275* (48), 37307-37310.
80. Holz, M. K.; Ballif, B. A.; Gygi, S. P.; Blenis, J., mTOR and S6K1 mediate assembly of the translation preinitiation complex through dynamic protein interchange and ordered phosphorylation events. *Cell* **2005**, *123* (4), 569-580.

81. Holz, M. K.; Blenis, J., Identification of S6 kinase 1 as a novel mammalian target of rapamycin (mTOR)-phosphorylating kinase. *J. Biol. Chem.* **2005**, *280* (28), 26089-26093.
82. Zhang, C.; Comai, L.; Johnson, D. L., PTEN represses RNA Polymerase I transcription by disrupting the SL1 complex. *Mol. Cell Biol.* **2005**, *25* (16), 6899-6911.
83. Schmelzle, T.; Hall, M. N., TOR, a central controller of cell growth. *Cell* **2000**, *103* (2), 253-262.
84. Tee, A. R.; Proud, C. G., Caspase cleavage of initiation factor 4E-binding protein 1 yields a dominant inhibitor of cap-dependent translation and reveals a novel regulatory motif. *Mol. Cell Biol.* **2002**, *22* (6), 1674-1683.
85. Schalm, S. S.; Blenis, J., Identification of a conserved motif required for mTOR signaling. *Curr. Biol.* **2002**, *12* (8), 632-639.
86. Sonenberg, N., *mRNA 5' cap-binding protein eIF4E and control of cell growth*. Cold Spring Harbor Laboratory Press: Cold Spring Harbor, New York, 1996; p 249-269.
87. Rosner, M.; Hanneder, M.; Siegel, N.; Valli, A.; Fuchs, C.; Hengstschlager, M., The mTOR pathway and its role in human genetic diseases. *Mutat. Res.* **2008**, *659* (3), 284-292.
88. Tsang, C. K.; Qi, H.; Liu, L. F.; Zheng, X. F., Targeting mammalian target of rapamycin (mTOR) for health and diseases. *Drug Discov. Today* **2007**, *12* (3-4), 112-124.
89. Wei, C.; Amos, C. I.; Zhang, N.; Wang, X.; Rashid, A.; Walker, C. L.; Behringer, R. R.; Frazier, M. L., Suppression of Peutz-Jeghers polyposis by targeting mammalian target of rapamycin signaling. *Clin. Cancer Res.* **2008**, *14* (4), 1167-1171.
90. Corradetti, M. N.; Inoki, K.; Bardeesy, N.; DePinho, R. A.; Guan, K. L., Regulation of the TSC pathway by LKB1: evidence of a molecular link between tuberous sclerosis complex and Peutz-Jeghers syndrome. *Genes Dev.* **2004**, *18* (13), 1533-1538.

91. Shaw, R. J.; Bardeesy, N.; Manning, B. D.; Lopez, L.; Kosmatka, M.; DePinho, R. A.; Cantley, L. C., The LKB1 tumor suppressor negatively regulates mTOR signaling. *Cancer Cell* **2004**, *6* (1), 91-99.
92. Eng, C., PTEN: one gene, many syndromes. *Hum. Mutat.* **2003**, *22* (3), 183-198.
93. Orloff, M. S.; Eng, C., Genetic and phenotypic heterogeneity in the PTEN hamartoma tumour syndrome. *Oncogene* **2008**, *27* (41), 5387-5397.
94. Kaelin, W. G., Jr., The von Hippel-Lindau tumor suppressor gene and kidney cancer. *Clin. Cancer. Res.* **2004**, *10* (18 Pt 2), 6290S-6295S.
95. Johannessen, C. M.; Johnson, B. W.; Williams, S. M.; Chan, A. W.; Reczek, E. E.; Lynch, R. C.; Rioth, M. J.; McClatchey, A.; Ryeom, S.; Cichowski, K., TORC1 is essential for NF1-associated malignancies. *Curr. Biol.* **2008**, *18* (1), 56-62.
96. Johannessen, C. M.; Reczek, E. E.; James, M. F.; Brems, H.; Legius, E.; Cichowski, K., The NF1 tumor suppressor critically regulates TSC2 and mTOR. *Proc. Natl. Acad. Sci. USA* **2005**, *102* (24), 8573-8578.
97. Harvey, R. D.; Lonial, S., PI3 kinase/AKT pathway as a therapeutic target in multiple myeloma. *Future Oncol.* **2007**, *3* (6), 639-647.
98. Vogt, P. K.; Bader, A. G.; Kang, S., Phosphoinositide 3-kinase: from viral oncoprotein to drug target. *Virology* **2006**, *344* (1), 131-138.
99. Manning, B. D.; Cantley, L. C., AKT/PKB signaling: navigating downstream. *Cell* **2007**, *129* (7), 1261-1274.
100. Basso, A. D.; Mirza, A.; Liu, G.; Long, B. J.; Bishop, W. R.; Kirschmeier, P., The farnesyl transferase inhibitor (FTI) SCH66336 (lonafarnib) inhibits Rheb farnesylation and mTOR signaling. Role in FTI enhancement of taxane and tamoxifen anti-tumor activity. *J. Biol. Chem.* **2005**, *280* (35), 31101-31108.
101. Barlund, M.; Forozan, F.; Kononen, J.; Bubendorf, L.; Chen, Y.; Bittner, M. L.; Torhorst, J.; Haas, P.; Bucher, C.; Sauter, G.; Kallioniemi, O. P.; Kallioniemi, A., Detecting

activation of ribosomal protein S6 kinase by complementary DNA and tissue microarray analysis. *J. Natl. Cancer Inst.* **2000**, *92* (15), 1252-1259.

102. Folkman, J.; Klagsbrun, M., Angiogenic factors. *Science* **1987**, *235* (4787), 442-447.

103. Guba, M.; von Breitenbuch, P.; Steinbauer, M.; Koehl, G.; Flegel, S.; Hornung, M.; Bruns, C. J.; Zuelke, C.; Farkas, S.; Anthuber, M.; Jauch, K. W.; Geissler, E. K., Rapamycin inhibits primary and metastatic tumor growth by antiangiogenesis: involvement of vascular endothelial growth factor. *Nat. Med.* **2002**, *8* (2), 128-135.

104. Brugarolas, J., Renal-cell carcinoma - molecular pathways and therapies. *New Engl. J. Med.* **2007**, *356* (2), 185-187.

105. Hanna, S. C.; Heathcote, S. A.; Kim, W. Y., mTOR pathway in renal cell carcinoma. *Expert Rev. Anticancer Ther.* **2008**, *8* (2), 283-292.

106. Lu, K. H.; Wu, W.; Dave, B.; Slomovitz, B. M.; Burke, T. W.; Munsell, M. F.; Broaddus, R. R.; Walker, C. L., Loss of tuberous sclerosis complex-2 function and activation of mammalian target of rapamycin signaling in endometrial carcinoma. *Clin. Cancer Res.* **2008**, *14* (9), 2543-2550.

107. Li, X.; Alafuzoff, I.; Soininen, H.; Winblad, B.; Pei, J. J., Levels of mTOR and its downstream targets 4E-BP1, eEF2, and eEF2 kinase in relationships with tau in Alzheimer's disease brain. *FEBS J.* **2005**, *272* (16), 4211-4220.

108. Berger, Z.; Ravikumar, B.; Menzies, F. M.; Oroz, L. G.; Underwood, B. R.; Pangalos, M. N.; Schmitt, I.; Wullner, U.; Evert, B. O.; O'Kane, C. J.; Rubinsztein, D. C., Rapamycin alleviates toxicity of different aggregate-prone proteins. *Hum. Mol. Genet.* **2006**, *15* (3), 433-442.

109. Saltiel, A. R.; Kahn, C. R., Insulin signalling and the regulation of glucose and lipid metabolism. *Nature* **2001**, *414* (6865), 799-806.

110. Briaud, I.; Dickson, L. M.; Lingohr, M. K.; McCuaig, J. F.; Lawrence, J. C.; Rhodes, C. J., Insulin receptor substrate-2 proteasomal degradation mediated by a mammalian target of rapamycin (mTOR)-induced negative feedback down-regulates protein kinase B-mediated signaling pathway in beta-cells. *J. Biol. Chem.* **2005**, *280* (3), 2282-2293.

111. McMullen, J. R.; Sherwood, M. C.; Tarnavski, O.; Zhang, L.; Dorfman, A. L.; Shioi, T.; Izumo, S., Inhibition of mTOR signaling with rapamycin regresses established cardiac hypertrophy induced by pressure overload. *Circulation* **2004**, *109* (24), 3050-3055.
112. Holzenberger, M.; Dupont, J.; Ducos, B.; Leneuve, P.; Geloën, A.; Even, P. C.; Cervera, P.; Le Bouc, Y., IGF-1 receptor regulates lifespan and resistance to oxidative stress in mice. *Nature* **2003**, *421* (6919), 182-187.
113. Jorgensen, W. L., The many roles of computation in drug discovery. *Science* **2004**, *303* (5665), 1813-1818.
114. Kuntz, I. D., Structure-based strategies for drug design and discovery. *Science* **1992**, *257* (5073), 1078-1082.
115. Karplus, M.; Petsko, G. A., Molecular dynamics simulations in biology. *Nature* **1990**, *347* (6294), 631-639.
116. Jorgensen, W. L.; Tirado-Rives, J., Molecular modeling of organic and biomolecular systems using BOSS and MCPRO. *J. Comput. Chem.* **2005**, *26* (16), 1689-1700.
117. Akamatsu, M., Current state and perspectives of 3D-QSAR. *Curr. Top. Med. Chem.* **2002**, *2* (12), 1381-1394.
118. Bacilieri, M.; Moro, S., Ligand-based drug design methodologies in drug discovery process: an overview. *Curr. Drug Discov. Technol.* **2006**, *3* (3), 155-165.
119. McInnes, C., Virtual screening strategies in drug discovery. *Curr. Opin. Chem. Biol.* **2007**, *11* (5), 494-502.
120. Wold, S.; Ruhe, A.; Wold, H.; Dunn, W. J., The collinearity problem in linear-regression - the partial least-squares (PLS) approach to generalized inverses. *SIAM J. Sci. Stat. Comp.* **1984**, *5* (3), 735-743.
121. Geladi, P.; Kowalski, B. R., Partial least-squares regression - a tutorial. *Anal. Chim. Acta.* **1986**, *185*, 1-17.

122. Cramer, R. D., Bc(def) parameters .1. intrinsic dimensionality of intermolecular interactions in the liquid-state. *J. Am. Chem. Soc.* **1980**, *102* (6), 1837-1849.
123. Cramer, R. D., Bc(def) parameters .2. empirical structure-based scheme for the prediction of some physical-properties. *J. Am. Chem. Soc.* **1980**, *102* (6), 1849-1859.
124. Booker, L. B.; Goldberg, D. E.; Holland, J. H., Classifier systems and genetic algorithms. *Artif. Intell.* **1989**, *40* (1-3), 235-282.
125. Holland, J. H., Genetic algorithms. *Sci. Am.* **1992**, *267* (1), 66-72.
126. Breiman, L.; Friedman, J.; Olshen, R.; Stone, C., *Classification and regression trees*. Wadsworth, 1984.
127. Chothia, C.; Lesk, A. M., The relation between the divergence of sequence and structure in proteins. *EMBO J.* **1986**, *5* (4), 823-826.
128. Fiser, A.; Feig, M.; Brooks, C. L., 3rd; Sali, A., Evolution and physics in comparative protein structure modeling. *Acc. Chem. Res.* **2002**, *35* (6), 413-421.
129. *Molecular Operating Environment (MOE), 2008.10*, Chemical Computing Group, Inc.: Montreal, 2008.
130. Pearson, W. R., Effective protein sequence comparison. In *Method Enzymol*, 1996; Vol. 266, pp 227-258.
131. Needleman, S. B.; Wunsch, C. D., A General method applicable to search for similarities in amino acid sequence of 2 proteins. *J. Mol. Biol.* **1970**, *48* (3), 443-453.
132. Mount, D. W., *Bioinformatics: sequence and genome analysis* 2nd ed.; Cold Spring Harbor Laboratory Press: Cold Spring Harbor, NY, 2004.
133. Gotoh, O., Optimal alignment between groups of sequences and its application to multiple sequence alignment. *Comput. Appl. Biosci.* **1993**, *9* (3), 361-370.

134. Hirosawa, M.; Totoki, Y.; Hoshida, M.; Ishikawa, M., Comprehensive study on iterative algorithms of multiple sequence alignment. *Comput. Appl. Biosci.* **1995**, *11* (1), 13-18.
135. Building Homology Models. *Manual of Molecular Operating Environment (MOE)*, 2008. 10.
136. Okur, A.; Roe, D. R.; Cui, G. L.; Hornak, V.; Simmerling, C., Improving convergence of replica-exchange simulations through coupling to a high-temperature structure reservoir. *J. Chem. Theory Comp.* **2007**, *3* (2), 557-568.
137. Okur, A.; Wickstrom, L.; Layten, M.; Geney, R.; Song, K.; Hornak, V.; Simmerling, C., Improved efficiency of replica exchange simulations through use of a hybrid explicit/implicit solvation model. *J. Chem. Theory Comp.* **2006**, *2* (2), 420-433.
138. Roitberg, A. E.; Okur, A.; Simmerling, C., Coupling of replica exchange simulations to a non-Boltzmann structure reservoir. *J. Phys. Chem. B* **2007**, *111* (10), 2415-2418.
139. Labute, P.; Williams, C.; Feher, M.; Sourial, E.; Schmidt, J. M., Flexible alignment of small molecules. *J. Med. Chem.* **2001**, *44* (10), 1483-1490.
140. Lemmen, C.; Lengauer, T., Computational methods for the structural alignment of molecules. *J. Comput. Aided Mol. Des.* **2000**, *14* (3), 215-232.
141. Martin, Y. C.; Bures, M. G.; Danaher, E. A.; DeLazzer, J.; Lico, I.; Pavlik, P. A., A fast new approach to pharmacophore mapping and its application to dopaminergic and benzodiazepine agonists. *J. Comput. Aided Mol. Des.* **1993**, *7* (1), 83-102.
142. Miller, M. D.; Sheridan, R. P.; Kearsley, S. K., SQ: a program for rapidly producing pharmacophorically relevant molecular superpositions. *J. Med. Chem.* **1999**, *42* (9), 1505-1514.
143. Good, A., Structure-based virtual screening protocols. *Curr. Opin. Drug Discov. Devel.* **2001**, *4* (3), 301-307.
144. Lyne, P. D., Structure-based virtual screening: an overview. *Drug Discov. Today* **2002**, *7* (20), 1047-1055.

145. Eckert, H.; Bajorath, J., Molecular similarity analysis in virtual screening: foundations, limitations and novel approaches. *Drug Discov. Today* **2007**, *12* (5-6), 225-233.
146. Willett, P., Similarity-based virtual screening using 2D fingerprints. *Drug Discov. Today* **2006**, *11* (23-24), 1046-1053.
147. Langer, T.; Wolber, G., Pharmacophore definition and 3D searches. *Drug Discov. Today: Technologies* **2004**, *1* (3), 203-207.
148. Pharmacophore discovery and 3D database search. *Manual of Molecular Operating Environment (MOE)*, 2008. 10.
149. Vlahos, C. J.; Matter, W. F.; Hui, K. Y.; Brown, R. F., A specific inhibitor of phosphatidylinositol 3-kinase, 2-(4-morpholinyl)-8-phenyl-4H-1-benzopyran-4-one (LY294002). *J. Biol. Chem.* **1994**, *269* (7), 5241-5248.
150. Hardcastle, I. R.; Cockcroft, X.; Curtin, N. J.; El-Murr, M. D.; Leahy, J. J.; Stockley, M.; Golding, B. T.; Rigoreau, L.; Richardson, C.; Smith, G. C.; Griffin, R. J., Discovery of potent chromen-4-one inhibitors of the DNA-dependent protein kinase (DNA-PK) using a small-molecule library approach. *J. Med. Chem.* **2005**, *48* (24), 7829-7846.
151. Di Braccio, M.; Roma, G.; Leoncini, G.; Poggi, M., Pyran derivatives XIX. (Dialkylamino) substituted 1-benzopyranones and naphthopyranones with platelet antiaggregating activity. *Farmaco* **1995**, *50* (10), 703-711.
152. Guram, A. S.; Rennels, R. A.; Buchwald, S. L., A simple catalytic method for the conversion of aryl bromides to arylamines. *Angew. Chem. Int. Ed. Engl.* **1995**, *34* (12), 1348-1350.
153. Louie, J.; Driver, M. S.; Hamann, B. C.; Hartwig, J. F., Palladium-catalyzed amination of aryl triflates and importance of triflate addition rate. *J. Org. Chem.* **1997**, *62* (5), 1268-1273.
154. Louie, J.; Hartwig, J. F., Palladium-catalyzed synthesis of arylamines from aryl halides - mechanistic studies lead to coupling in the absence of Tin reagents. *Tetrahedron Lett.* **1995**, *36* (21), 3609-3612.

155. Walker, E. H.; Pacold, M. E.; Perisic, O.; Stephens, L.; Hawkins, P. T.; Wymann, M. P.; Williams, R. L., Structural determinants of phosphoinositide 3-kinase inhibition by wortmannin, LY294002, quercetin, myricetin, and staurosporine. *Mol. Cell* **2000**, *6* (4), 909-919.
156. Walker, E. H.; Perisic, O.; Ried, C.; Stephens, L.; Williams, R. L., Structural insights into phosphoinositide 3-kinase catalysis and signalling. *Nature* **1999**, *402* (6759), 313-320.
157. Abraham, R. T., PI 3-kinase related kinases: 'big' players in stress-induced signaling pathways. *DNA Repair (Amst)* **2004**, *3* (8-9), 883-887.
158. Griffin, R. J.; Fontana, G.; Golding, B. T.; Guiard, S.; Hardcastle, I. R.; Leahy, J. J.; Martin, N.; Richardson, C.; Rigoreau, L.; Stockley, M.; Smith, G. C., Selective benzopyranone and pyrimido[2,1-a]isoquinolin-4-one inhibitors of DNA-dependent protein kinase: synthesis, structure-activity studies, and radiosensitization of a human tumor cell line in vitro. *J. Med. Chem.* **2005**, *48* (2), 569-585.
159. Hohenberg, P.; Kohn, W., Inhomogeneous electron gas. *Phys. Rev. B* **1964**, *136* (3B), B864-B871.
160. Kohn, W.; Sham, L. J., Self-consistent equations including exchange and correlation effects. *Phys. Rev.* **1965**, *140* (4A), A1133-A1138.
161. Frisch, M. J. T., G. W.; Schlegel, H. B.; Scuseria, G. E.; Robb, M. A.; Cheeseman, J. R.; Montgomery, Jr., J. A.; Vreven, T.; Kudin, K. N.; Burant, J. C.; Millam, J. M.; Iyengar, S. S.; Tomasi, J.; Barone, V.; Mennucci, B.; Cossi, M.; Scalmani, G.; Rega, N.; Petersson, G. A.; Nakatsuji, H.; Hada, M.; Ehara, M.; Toyota, K.; Fukuda, R.; Hasegawa, J.; Ishida, M.; Nakajima, T.; Honda, Y.; Kitao, O.; Nakai, H.; Klene, M.; Li, X.; Knox, J. E.; Hratchian, H. P.; Cross, J. B.; Bakken, V.; Adamo, C.; Jaramillo, J.; Gomperts, R.; Stratmann, R. E.; Yazyev, O.; Austin, A. J.; Cammi, R.; Pomelli, C.; Ochterski, J. W.; Ayala, P. Y.; Morokuma, K.; Voth, G. A.; Salvador, P.; Dannenberg, J. J.; Zakrzewski, V. G.; Dapprich, S.; Daniels, A. D.; Strain, M. C.; Farkas, O.; Malick, D. K.; Rabuck, A. D.; Raghavachari, K.; Foresman, J. B.; Ortiz, J. V.; Cui, Q.; Baboul, A. G.; Clifford, S.; Cioslowski, J.; Stefanov, B. B.; Liu, G.; Liashenko, A.; Piskorz, P.; Komaromi, I.; Martin, R. L.; Fox, D. J.; Keith, T.; Al-Laham, M. A.; Peng, C. Y.; Nanayakkara, A.; Challacombe, M.; Gill, P. M. W.; Johnson, B.; Chen, W.; Wong, M. W.; Gonzalez, C.; and Pople, J. A.; *Gaussian 03, Revision C.02*, Gaussian, Inc., Wallingford, CT, 2004.

162. Dennington II, R.; Keith, T.; Millam, J.; Eppinnett, K.; Hovell, W. L.; Gilliland, R. *GaussView, Version 3.09*, Semichem, Inc., Shawnee Mission, KS, 2003.
163. Schlegel, H. B., Optimization of equilibrium geometries and transition structures. *J. Comp. Chem.* **1982**, *3* (2), 214-218.
164. Becke, A. D., Density-functional thermochemistry .3. The role of exact exchange. *J. Chem. Phys.* **1993**, *98* (7), 5648-5652.
165. Lee, C. T.; Yang, W. T.; Parr, R. G., Development of the Colle-Salvetti Correlation-Energy Formula into a Functional of the Electron-Density. *Phys Rev B* **1988**, *37* (2), 785-789.
166. Csizmadia, L. G., In *Theory and practice of MO calculation on organic molecules: Progress in theoretical organic chemistry*, Elsevier: Amsterdam, The Netherlands, 1976; Vol. 1, p 239.
167. Johnson, B. G.; Gill, P. M. W.; Pople, J. A.; Fox, D. J., Computing molecular electrostatic potentials with the prism algorithm. *Chem. Phys. Lett.* **1993**, *206* (1-4), 239-246.
168. Besler, B. H.; Merz, K. M.; Kollman, P. A., Atomic charges derived from semiempirical methods. *J. Comp. Chem.* **1990**, *11* (4), 431-439.
169. Singh, U. C.; Kollman, P. A., An approach to computing electrostatic charges for molecules. *J. Comp. Chem.* **1984**, *5* (2), 129-145.
170. Alaimo, P. J.; Knight, Z. A.; Shokat, K. M., Targeting the gatekeeper residue in phosphoinositide 3-kinases. *Bioorg. Med. Chem.* **2005**, *13* (8), 2825-2836.
171. Huang, C. H.; Mandelker, D.; Schmidt-Kittler, O.; Samuels, Y.; Velculescu, V. E.; Kinzler, K. W.; Vogelstein, B.; Gabelli, S. B.; Amzel, L. M., The structure of a human p110alpha/p85alpha complex elucidates the effects of oncogenic PI3Kalpha mutations. *Science* **2007**, *318* (5857), 1744-1748.
172. Lee, J. Y.; Engelman, J. A.; Cantley, L. C., Biochemistry. PI3K charges ahead. *Science* **2007**, *317* (5835), 206-207.

173. Estel, L.; Marsais, F.; Queguiner, G., Metalation/ SRN1 coupling in heterocyclic synthesis - a convenient methodology for ring functionalization. *J. Org. Chem.* **1988**, *53* (12), 2740-2744.
174. Miyaura, N.; Suzuki, A., Stereoselective synthesis of arylated (E)-alkenes by the reaction of alk-1-enylboranes with aryl halides in the presence of palladium catalyst. *Chem. Comm.* **1979**, (19), 866-867.
175. Miyaura, N.; Suzuki, A., Palladium-catalyzed cross-coupling reactions of organoboron compounds. *Chem. Rev.* **1995**, *95* (7), 2457-2483.
176. Miyaura, N.; Yamada, K.; Suzuki, A., New stereospecific cross-coupling by the palladium-catalyzed reaction of 1-alkenylboranes with 1-alkenyl or 1-alkynyl halides. *Tetrahedron Lett.* **1979**, (36), 3437-3440.
177. Heck, R. F.; Nolley, J. P., Palladium-catalyzed vinylic hydrogen substitution reactions with aryl, benzyl, and styryl halides. *J. Org. Chem.* **1972**, *37* (14), 2320-&.
178. Brois, S. J.; Pilot, J. F.; Barnum, H. W., A new pathway to unsymmetrical disulfides. The thiol-induced fragmentation of sulfenyl thiocarbonates. *J. Am. Chem. Soc.* **1970**, *92* (26), 7629-7631.
179. Brenner, E.; Baldwin, R. M.; Tamagnan, G., Asymmetric synthesis of (+)-(S,S)-reboxetine via a new (S)-2-(hydroxymethyl)morpholine preparation. *Org. Lett.* **2005**, *7* (5), 937-939.
180. Hayakawa, M.; Kaizawa, H.; Moritomo, H.; Koizumi, T.; Ohishi, T.; Okada, M.; Ohta, M.; Tsukamoto, S.; Parker, P.; Workman, P.; Waterfield, M., Synthesis and biological evaluation of 4-morpholino-2-phenylquinazolines and related derivatives as novel PI3 kinase p110alpha inhibitors. *Bioorg. Med. Chem.* **2006**, *14* (20), 6847-6858.
181. Hayakawa, M.; Kaizawa, H.; Moritomo, H.; Koizumi, T.; Ohishi, T.; Yamano, M.; Okada, M.; Ohta, M.; Tsukamoto, S.; Raynaud, F. I.; Workman, P.; Waterfield, M. D.; Parker, P., Synthesis and biological evaluation of pyrido[3',2':4,5]furo[3,2-d]pyrimidine derivatives as novel PI3 kinase p110alpha inhibitors. *Bioorg. Med. Chem. Lett.* **2007**, *17* (9), 2438-2442.

182. Knight, Z. A.; Gonzalez, B.; Feldman, M. E.; Zunder, E. R.; Goldenberg, D. D.; Williams, O.; Loewith, R.; Stokoe, D.; Balla, A.; Toth, B.; Balla, T.; Weiss, W. A.; Williams, R. L.; Shokat, K. M., A pharmacological map of the PI3-K family defines a role for p110alpha in insulin signaling. *Cell* **2006**, *125* (4), 733-747.
183. Chook, Y. M.; Blobel, G., Structure of the nuclear transport complex karyopherin-beta2-Ran x GppNHp. *Nature* **1999**, *399* (6733), 230-237.
184. Turner, J. A., Regiospecific electrophilic substitution of aminopyridines - ortho lithiation of 2, 3, and 4-(pivaloylamino) pyridines. *J. Org. Chem.* **1983**, *48* (20), 3401-3408.
185. Bethge, L.; Jarikote, D. V.; Seitz, O., New cyanine dyes as base surrogates in PNA: forced intercalation probes (FIT-probes) for homogeneous SNP detection. *Bioorg. Med. Chem.* **2008**, *16* (1), 114-125.
186. Lainton, J. A.; Allen, M. C.; Burton, M.; Cameron, S.; Edwards, T. R.; Harden, G.; Hogg, R.; Leung, W.; Miller, S.; Morrish, J. J.; Rooke, S. M.; Wendt, B., Design and synthesis of a diverse morpholine template library. *J. Comb. Chem.* **2003**, *5* (4), 400-407.
187. Lipinski, C. A.; Lombardo, F.; Dominy, B. W.; Feeney, P. J., Experimental and computational approaches to estimate solubility and permeability in drug discovery and development settings. *Adv. Drug Del. Rev.* **1997**, *23* (1-3), 3-25.
188. Cosulich, S. C.; Griffen, E. J., New thiazole pyridine sulfonamides as orally bioavailable highly potent PI3 kinase inhibitors. In *Keyston Symposia on Molecular and Cellular Biology*, Santa Fe, New Mexico, Feb. 15-20, 2007.
189. <http://pubchem.ncbi.nlm.nih.gov/>.
190. Foloppe, N.; Fisher, L. M.; Howes, R.; Potter, A.; Robertson, A. G.; Surgenor, A. E., Identification of chemically diverse Chk1 inhibitors by receptor-based virtual screening. *Bioorg. Med. Chem.* **2006**, *14* (14), 4792-802.
191. Shi, D.; Mou, J.; Zhuang, Q.; Niu, L.; Wu, N.; Wang, X., Three-component one-pot synthesis of 1,4-dihydropyrano[2,3-c]pyrazole derivatives in aqueous media *Syn. Comm.* **2004**, *34* (24), 4557-4563.

192. Peng, C. Y.; Ayala, P. Y.; Schlegel, H. B.; Frisch, M. J., Using redundant internal coordinates to optimize equilibrium geometries and transition states. *J. Comp. Chem.* **1996**, *17* (1), 49-56.

193. Peng, C. Y.; Schlegel, H. B., Combining synchronous transit and quasi-newton methods to find transition states. *Israel J. Chem.* **1993**, *33* (449), 449-454.

Appendix 1. The full sequence alignment of mTOR, DNA-PK, ATM, ATR, PI3K α , PI3K γ

mTOR	-----	-----	-----	-----	-----
DNA-PK	MAGSGAGVRC	SLLRLQETLS	AADRCGAALA	GHQLIRGLGQ	ECVLSSSPAV
ATM	-----	-----	-----	-----	-----
ATR	-----	-----	-----	-----	-----
PI3Kalpha	-----	-----	-----	-----	-----
PI3Kgamma	-----	-----	-----	-----	-----
mTOR	-----	-----	-----	-----	-----
DNA-PK	LALQTSLVFS	RDFGLLVFVR	KSLNSIEFRE	CREEILKFLC	IFLEKMGQKI
ATM	-----	-----	-----	-----	-----
ATR	-----	-----	-----	-----	-----
PI3Kalpha	-----	-----	-----	-----	-----
PI3Kgamma	-----	-----	-----	-----	-----
mTOR	-----	-----	-----	-----	-----
DNA-PK	APYSVEIKNT	CTSVYTKDRA	AKCKIPALDL	LIKLLQTFRS	SRLMDEFKIG
ATM	-----	-----	-----	-----	-----
ATR	-----	-----	-----	-----	-----
PI3Kalpha	-----	-----	-----	-----	-----
PI3Kgamma	-----	-----	-----	-----	-----
mTOR	-----	-----	-----	-----	-----
DNA-PK	ELFSKFYGEL	ALKKKIPDTV	LEKVYELLGL	LGEVHPSEMI	NNAENLFRAF
ATM	-----	-----	-----	-----	-----
ATR	-----	-----	-----	-----	-----
PI3Kalpha	-----	-----	-----	-----	-----
PI3Kgamma	-----	-----	-----	-----	-----
mTOR	-----	-----	-----	-----	-----
DNA-PK	LGELKTQMTS	AVREPKLPVL	AGCLKGLSSL	LCNFTKSMEE	DPQTSREIFN
ATM	-----	-----	-----	-----	-----
ATR	-----	-----	-----	-----	-----
PI3Kalpha	-----	-----	-----	-----	-----
PI3Kgamma	-----	-----	-----	-----	-----
mTOR	-----	-----	-----	-----	-----
DNA-PK	FVLKAIRPQI	DLKRYAVPSA	GLRLFALHAS	QFSTCLLDNY	VSLFEVLLKW
ATM	-----	-----	-----	-----	-----
ATR	-----	-----	-----	-----	-----
PI3Kalpha	-----	-----	-----	-----	-----
PI3Kgamma	-----	-----	-----	-----	-----
mTOR	-----	-----	-----	-----	-----
DNA-PK	CAHTNVELKK	AALSALESFL	KQVSNMVAKN	AEMHKKNLQY	FMEQFYGIIR
ATM	-----	-----	-----	-----	-----
ATR	-----	-----	-----	-----	-----
PI3Kalpha	-----	-----	-----	-----	-----
PI3Kgamma	-----	-----	-----	-----	-----

mTOR	-----	-----	-----	-----	-----
DNA-PK	NVDSNNKELS	IAIRGYGLFA	GPCKVINAKD	VDFMYVELIQ	RCKQMFLTQT
ATM	-----	-----	-----	MSLVLNDLLI	CCRQL---EH
ATR	-----	-----	-----	-----	-----
PI3Kalpha	-----	-----	-----	-----	-----
PI3Kgamma	-----	-----	-----	-----	-----
mTOR	-----	-----	-----	-----	-----
DNA-PK	DTGDDRVIQM	PSFLQSVASV	LLYLDTVPEV	YTPVLEHLVV	MQIDSFPQYS
ATM	DRATERKKEV	EKFKRLIRD-	-----PET	----IKHL--	---D---RHS
ATR	-----	-----	-----	-----	-----
PI3Kalpha	-----	-----	-----	-----	-----
PI3Kgamma	-----	-----	-----	-----	-----
mTOR	-----	-----	-----	-----	-----
DNA-PK	PKMQLVCCRA	IVKVFLALAA	KGPVLRNCIS	TVVHQGLIRI	CSKPVVLPKG
ATM	DSKQ-----	--GKYLNWDA	VFRFLQKYIQ	KETE--CLRI	-AKPNV---S
ATR	-----	-----	-----	-----	-----
PI3Kalpha	-----	-----	-----	-----	-----
PI3Kgamma	-----	-----	-----	-----	-----
mTOR	-----	-----	-----	-----	-----
DNA-PK	PESESEDHRA	SGEVRTGKWK	VPTYKDYVDL	FRHLLSSDQM	MDSILADEAF
ATM	ASTQASRQKK	MQEISS---L	VKYFIKCANR	RAPRLKCQEL	LNYIM-D---
ATR	-----	-----	-----	-----	-----
PI3Kalpha	-----	-----	-----	-----	-----
PI3Kgamma	-----	-----	-----	-----	-----
mTOR	-----	-----	-----	-----	-----
DNA-PK	FSVNSSSESL	NHLLYDEFVK	SVLKIVEKLD	LTLEIQTVGE	QENGDEAPGV
ATM	-TVKDSS---	NGAIYG-ADC	SNILLKDILS	VRKYWCEISQ	QQ-----
ATR	-----	-----MGE	HGLELASMIP	ALRELGSATP	EE-----
PI3Kalpha	-----	-----	-----	-----	-----
PI3Kgamma	-----	-----	-----	-----	-----
mTOR	-----	-----	-----	-----	-----
DNA-PK	WMIPTSDPAA	NLHPAKPKDF	SAFINLVEFC	REILPEKQAE	FFEPWVYSFS
ATM	WLELFS--VY	FRLYLKPS--	-----QDV	HRVLVARI--	-----IHAVT
ATR	-----Y	NTVVQKPRQI	-----LCQFI	DRILTD----	-----VNVVA
PI3Kalpha	-----	-----	-----	-----	-----
PI3Kgamma	-----	-----	-----	-----	-----
mTOR	-----	-----	-----	-----	-----
DNA-PK	YELILQSTRL	PLISGFYKLL	SITVRNAKKI	KYFEGVSPKS	LKHSPEDPEK
ATM	KGCCSQTDG-	-LNSKFLDFF	SKAIQCARQE	K-----SSSG	LNHIL----A
ATR	VELVKKTDSQ	PTSVMLLDFI	QHIMKSSPLM	F-----VNVS	GSHEA----K
PI3Kalpha	-----	-----	-----	-----	-----
PI3Kgamma	-----	-----	-----	-----	-----
mTOR	-----	-----	-----	-----	-----
DNA-PK	YSCFALFVKF	GKEVAVKMKQ	YKDELLASCL	TFLLSLPHNI	IELDVRAYVP
ATM	ALTIF-LKTL	AVNFRIRVCE	LGDEILPTLL	-YIWT-QHRL	NDSLKEVIIE
ATR	GSCIE-FSNW	IITRLLRIAA	-----TPSC-	-----HLL	HKKICEVICIS
PI3Kalpha	-----	-----	-----	-----	-----
PI3Kgamma	-----	-----	-----	-----	-----

mTOR	-----	-----	-----	-----	-----
DNA-PK	ALQMA-FKLG	LSYTPLAEVG	LNALLEEWSIY	IDRHVMQPY	KDIL-PCLDG
ATM	LFQLQIYIHH	PKGAKTQEK	AYESTKW-RS	ILYNLYDLLV	NEIS-HIGSR
ATR	LL----FLFK	SKSPAIFGVL	TKEL----LQ	LFEDLVYLHR	RNVMGHAVEW
PI3Kalpha	-----	-----	-----	-----	-----
PI3Kgamma	-----	-----	-----	-----	-----
mTOR	-----	-----	-----	-----MLGTG	PAAATTAATT
DNA-PK	YLKTSALSD-	ETKNNWEVSA	LSRAAQKGFN	KVVLKHLKKT	KNLSSNEAIS
ATM	GKYSSGFRNI	AVKENL-IEL	MADICHQVFN	EDT-RSLEIS	QSYTTTQRES
ATR	PVVMRSRFLS-	QLDEH--MGY	LQSAPLQLMS	MQNLEFIEVT	LLMVLTRIIA
PI3Kalpha	-----	-----	-----	-----	-----
PI3Kgamma	-----	-----	-----	-----	-----
mTOR	SS--NVSVLQ	QFASGLKSRN	EETRAKAAKE	---LQHYVTM	ELREMSQEES
DNA-PK	LEEIRIRVVQ	MLGSLGGQIN	KNLLTVTSSD	E--MMKSYVA	WDREKRLSFA
ATM	SD-YSVPCKR	KKIELGWEVI	KDHLQKSQND	FDLVPWLQIA	TQLISKYPAS
ATR	-----IVFFR	RQELLLWQIG	CVLLEYGSPK	---IKSLAIS	FLTELFQLGG
PI3Kalpha	-----	-----	-----	-----	-----
PI3Kgamma	-----	-----	-----	-----	-----
mTOR	TRF--YDQ--	-LNHHIFELV	S-SSDANERK	GGILAI---A	SLIGVEGGNA
DNA-PK	VPFREMKPVI	FLDVFLPRVT	ELALTASDRQ	TKVAACELLH	SMVMFMLGKA
ATM	LPNCELSP--	-LLMILSPLL	P-QQRHGERT	PYVLR---L	TEVALCQDKR
ATR	LP---AQP--	-ASTFFSSFL	ELLKHLVEMD	TDQLKL---Y	EEPLSKLIK-
PI3Kalpha	-----	-----	-----	-----	-----
PI3Kgamma	-----	-----	-----	-----	-----
mTOR	TRIGRFANY-	--LRNLLPSN	DPVME-MA-	-----SKAI-	-----
DNA-PK	TQMPEGGQGA	PPMYQLYKRT	FPVLLR-LAC	DVDQVTRQLY	EPLVMQLIHW
ATM	SNLESSQKS-	-DLLKLWNKI	WCITFRGIS-	-----SEKI-	-----
ATR	TLFPFEAEA-	-----YRNI	EPVYLN-ML-	-----LEKL-	--CVM-----
PI3Kalpha	-----	-----	-----	-----	-----
PI3Kgamma	-----	-----	-----	-----	-----
mTOR	-----	GRLAMAGDTF	TAEYVEFE--	-----VK	RALEW-----
DNA-PK	FTNNKKFESQ	DTVALLEAIL	DGIVDPVDST	LRDFCGRCIR	EFLKWSIKQI
ATM	-----QA	ENFGLLGAI	QGSLVEVD--	-----R	EFWKL-----
ATR	-----FEDG	VLMRLKSDLL	KAALCHL---	-----LQ	YFLKF-----
PI3Kalpha	-----	-----	-----	-----	-----
PI3Kgamma	-----	-----	-----	-----	-----
mTOR	LGADRNEGRR	HA AVLVLREL	AISVPTFFFQ	--QVQPFDFN	IFVAVWDPK-
DNA-PK	TPQQQEKSPV	NTKSLFKRLY	SLALHPNAFK	RLGASLAFNN	IYREFREEE-
ATM	FTGSACRPSC	PAVCCLTAL	TTSIVPGAVK	-MGIEQNMCE	VNRSFSLKE-
ATR	VPAGYESALQ	VRKVYVRNIC	KALLDVLGIE	-VDAEYLLGP	LYAALKMESM
PI3Kalpha	-----	-----	-----	-----	-----
PI3Kgamma	-----	-----	-----	-----	-----
mTOR	QAIREGAVAA	LRACLI----	-LTTQREP--	-----	-----
DNA-PK	SLVEQFVFEA	LVIYMESLAL	AHADEKSLGT	IQQCCDAIDH	LCRIIEKKHV
ATM	SIMKWLLFYQ	LEGDLE----	-NSTEVPP--	ILH--SNFPH	L--VLEKILV
ATR	EIIIEIQCQT	QQENLSS---	-NSDGISP--	-----	-----
PI3Kalpha	-----	-----	-----	-----	-----
PI3Kgamma	-----	-----	-----	-----	-----

mTOR	-----KEMQK	PQWYRHTF--	-----	EEAEKGFDET	LAKEKGM---
DNA-PK	SLNKAKKRRL	PRGFPPSASL	CLLDLVKWLL	AHCGRPQTEC	RHKSIELFYK
ATM	SLTM-KNCKA	AMNFFQSVPE	C-----	EHHQKDKEEL	SFSEVEELFL
ATR	-----KRRRL	SSSLNPS---	-----	KRAPKQTEEI	--KHVDM---
PI3Kalpha	-----	-----	-----	-----	-----
PI3Kgamma	-----	-----	-----	-----	-----
mTOR	-----NRD	DRIH--GALL	ILNELVRISS	MEGERLREEM	EEITQQQLVH
DNA-PK	FVPLLPGNRS	PNLWLKDVVK	EEGVSFLINT	FEGGGCGQPS	GILAQPTLLY
ATM	QTTTF---DKM	DFL---TIVR	ECGIEKHQSS	I-GFSVHQNL	KESLDRCLLG
ATR	-----NQK	SILW--SALK	QKAESLQIS-	LEYSGLKNPV	IEMLEGIADV
PI3Kalpha	-----	-----	-----	-----	-----
PI3Kgamma	-----	-----	-----	-----	-----
mTOR	DKY---CKD-	-----LMG	FGTKPRHIT-	-PFTSFQAVQ	PQOSNALVGL
DNA-PK	LRGPFSLQAT	LCWLDLLAA	LECYNTFIGE	RTVGALQVLG	TEAQSSLLKA
ATM	LSEQL-LNNY	SSEITNSETL	VRCSRLLVG-	-VLGCYCYMG	VIAEEEEAYKS
ATR	LQ----LTA-	-----LCT	VHCSHQNMN-	--CRTFKDCQ	HKSKKKPSVV
PI3Kalpha	-----	-----	-----	-----	-----
PI3Kgamma	-----	-----	-----	-----	-----
mTOR	LGYSSHQGLM	-----GF	GTSPSPAKST	LVESRCCRDL	MEEKFDQVCQ
DNA-PK	VAFFLESIAM	HDIIAAEKCF	GTGAAGNRTS	PQEGERYNYS	KCTVVVRIME
ATM	ELFQKANSLM	-----QCA	GESITLTKNK	TNEEFRIKSL	R-NMMQLCTR
ATR	ITWMSLD---	-----F	YTKVLKSCRS	LLESVQKLDL	E-ATIDKVVK
PI3Kalpha	-----	-----	-----	-----	-----
PI3Kgamma	-----	-----	-----	-----	-----
mTOR	WVLKCRN-SK	N-----SL	IQMTILNLLP	R-----	-----LA
DNA-PK	FTTTLLNTSP	EGWKLLKKDL	CNTHLMRVLV	QTLCEPASIG	FNIGDVQVMA
ATM	CLSNCTKKSP	N-----KI	ASGFFLRLLT	SKL-----	-----MN
ATR	IYDALIYMQV	N-----SS	FEDHILEDLC	GMLSLP----	-----WIYS
PI3Kalpha	-----	-----	-----	-----	-----
PI3Kgamma	-----	-----	-----	-----	-----
mTOR	AFRPSAFTDT	QYLQ-DTMNH	VLSCVKKEK-	-----	-----ERTAA-
DNA-PK	HLPDVCVNLM	KALKMSPYKD	ILETHLREKI	TAQSIEELCA	VNLYGPDAQV
ATM	DIADICKSLA	SFIK-KPF--	--DRGEVES-	-----	-----MEDDTN-
ATR	HSDDGCLKLT	TFAA-NLLT-	-LSCRISDS-	-----	-----YSPQAQ-
PI3Kalpha	-----	-----	-----	-----	-----
PI3Kgamma	-----	-----	-----	-----	-----
mTOR	--FQALGLLS	VAVRS-----	EFKVYLPRVL	DII-----	-----
DNA-PK	DRSRLAAVVS	ACKQLHRAGL	LHNILPSQST	DLHHSVGTTEL	LSLVYKGIAP
ATM	--GNLMEVED	QSSMN-----	LFNDYPDSSV	SDANEPGES-	-----
ATR	--SRCVFLLT	LFPRR-----	IFLEWRTAVY	NWALQSSHEV	I-----
PI3Kalpha	-----	-----	-----	-----	-----
PI3Kgamma	-----	-----	-----	-----	-----
mTOR	---RAALPPK	DFAHKRQKAM	Q-----	-VDATVFTCI	S-----ML
DNA-PK	GDERQCLPSL	DLSCQLASG	LLELAFAFGG	LCERLVSLLL	NPAVLSTASL
ATM	---QSTIGAI	NPLAEEYLSK	Q-DLLF----	-LDMLKFLCL	C-----V
ATR	--RASCVSGF	FILLQQQNS-	-----	-CNRVPKILI	D-----K
PI3Kalpha	-----	-----	-----	-----	-----
PI3Kgamma	-----	-----	-----	-----	-----

mTOR	ARAMGPGIQQ	DIKE-----	---LLEPMLA	VG-----L	SPALTAVLYD	
DNA-PK	GSSQGSVIHF	SHGEYFYSLF	SETINTELLK	NLDLAVLELM	QSSVDNTKMV	
ATM	TTAQTNTVSF	RAAD-----	---IRRKLLM	LID-----	SSTLEPTKSL	
ATR	VKDDSDIVKK	EFAS-----	---ILGQLVC	TLH--GMFYL	TSSLTEPFSE	
PI3Kalpha	-----	-----	-----	-----	-----	
PI3Kgamma	-----	-----	-----	-----	-----	
mTOR	LSRQIPQL--	-KKDI--QDG	L-LKMLSLVL	MH-----	---KPL----	
DNA-PK	SAVLNGMLDQ	SFRERANQKH	QGLKLATTIL	QHWKCDSSW	AKDSPLETKM	
ATM	HLHMYLML--	-LKELPGEEY	P-LPMEDVLE	LL-----	---KPLSN--	
ATR	HGHVDLFC--	-RNLKATSQH	E-CSSSQLKA	SV---C----	---KPF----	
PI3Kalpha	-----	-----	-----	-----	-----	
PI3Kgamma	-----	-----	-----	-----	-----	
mTOR	-----RHP	GMPKGL----	AH-----	QLASPGLTTL	PEASDVGSIT	
DNA-PK	AVLALLAKIL	QIDSSVSFNT	SHGSFPEVFT	TYISLLADTK	LDLHLKGQAV	
ATM	-VCSLYRRDQ	DVCKTILNHV	LH-----	VVK	NLGQSNMDE	NTRDAQGQFL
ATR	-LFLLKKKIP	SPVKLAFIDN	LH-----	HLCKHLDFRE	DETDVKAVLG	
PI3Kalpha	-----	-----	-----	-----	-----	
PI3Kgamma	-----	-----	-----	-----	-----	
mTOR	LALRTLGSFE	----FE----	GHSLTQF---	-----	-----VRHCA	
DNA-PK	TLLPFFTSLT	GGSLLEELRRV	LEQLIVAHFP	MQSREFPPGT	PRFNNYVDCM	
ATM	TVIGAFWHLT	----KE-RKY	IFSVRMA---	-----	-----LVNCL	
ATR	TLLNLMEDPD	----KD----	---VRVA---	-----	-----FSGNI	
PI3Kalpha	-----	-----	-----	-----	-----	
PI3Kgamma	-----	-----	-----	-----	-----	
mTOR	DHFLNSEHKE	IR-----	MEA	ARTCSR----	---LLTPSIH	LISGHAHVVS
DNA-PK	KKFLDALELS	QSPMLLELMT	EVLCREQQHV	MEELFQSSFR	RIARRGSCVT	
ATM	KTLLEADPYS	KW-----	AIL	NVMGKDFP--	---VNEVFTQ	FLADNHQVR
ATR	KHILES LDSE	DG-----	FIK	ELFVLR----	---MKEAYTH	AQISRNNELK
PI3Kalpha	-----	-----	-----	-----	-----	-----
PI3Kgamma	-----	-----	-----	-----	-----	-----
mTOR	QT-AVQVVAD	VLSK-----	L	LVVGITDPDP	DIR---YCVL	ASLDERFDAH
DNA-PK	QVGLLESVYE	MFRKDDPRLS	FTRQSFVDRS	LLTLLWHCSL	DALREFFSTI	
ATM	ML-AAESINR	LFQD-----	-TKGD--SSR	LLK---ALPL	KLQQTAFENA	
ATR	DT-LILTTGD	IGRA-----	-AKGDLVPFA	LLHLL-HCLL	SKSASVSGAA	
PI3Kalpha	-----	-----	-----	-----	-----	-----
PI3Kgamma	-----	-----	-----	-----	-----	-----
mTOR	LAQA-ENLQA	LFVAL-NDQV	FEI---REL	AICTVGR LSS	MNP-----	
DNA-PK	VVDAIDVLKS	RFTKL-NEST	FDTQITKKMG	YKILDVMYS	RLPKDDVHAK	
ATM	YLKAQEGMRE	MSHSAENPET	LDEIYNRKS	VLLTLIAVVL	S	CSP---ICEK
ATR	YTEIRALVAA	KSVKL---QS	FFSQY-KKPI	CQFLVESLHS	SQ-----	
PI3Kalpha	-----	-----	-----	-----	-----	-----
PI3Kgamma	-----	-----	-----	-----	-----	-----
mTOR	-----AFV-	-----MPFLR	KMLIQILTEL	EHSIGI----	-----RIKEQ	
DNA-PK	ESKINQVFHG	SCITEGNETL	KTLIKLCYDA	F TENMAGENQ	LLERRRLYHC	
ATM	QA----LFAL	CKSVKENGLE	PHLVKKVLEK	VSETFG----	---YRRLEDF	
ATR	-----	-----MTALP	NTPCQNA-DV	RKQDVA----	-----HQREM	
PI3Kalpha	-----	-----	-----	-----	-----	-----
PI3Kgamma	-----	-----	-----	-----	-----	-----

mTOR	SARM--LGHL	V-----	-----SNAP-	-RLIR-PYME	PILKA--LIL
DNA-PK	AAYNCAISVI	CCVFNELKFY	QGFLFSEKPE	KNLLIFENLI	DLKRRYNFPV
ATM	MASH--LDYL	VLEWLNLDQT	E-YNLSSFPP	-ILLNYTNIE	DFYRS---CY
ATR	ALNT--LSEI	A-----	-----	-NVFDFPDLN	RFLTR---TL
PI3Kalpha	-----	-----	-----	-----	-----
PI3Kgamma	-----	-----	-----	-----	-----
mTOR	KLKDPDPDPN	PGV--INNVL	ATIGE-----	---LAQVSGL	EMRKWVDELF
DNA-PK	EVEVPMERKK	KYI-EIRKEA	REAANGDSDG	PSYMSSLSYL	ADSTLSEEMS
ATM	KVLIPHLVIR	SHFDEVKSIA	NQIQE-----	-DWKSLLTDC	FPKILVNILP
ATR	QVLLPDLAAK	ASP-AASALI	RTLKG-----	-----QLNVN	RREILINNFK
PI3Kalpha	-----	-----	-----	-----	-----
PI3Kgamma	-----	-----	-----	-----	-----
mTOR	IIIMDMLQDS	SLLAKRQVAL	WTLGQLVAST	-----	GYVVEPYRK-
DNA-PK	QFDFSTGVQS	YSYSSQDPRP	ATGRFRRREQ	RDPTVHDDVL	ELEMDELNRH
ATM	YFAYEGTRDS	GMAQQRETAT	KVYDMLKSEN	-----LL	GKQIDHLFIS
ATR	YI-FSHLVCS	---CSKDELE	RALHYLKNET	-----	EIELGSLLRQ
PI3Kalpha	-----	-----	-----	-----	-----
PI3Kgamma	-----	-----	-----	-----	-----
mTOR	-----YPTLL	EVLLNFLKTE	QNQGTRREAI	RVLGLL----	GALDPYKHKV
DNA-PK	ECMAPLTALV	KHMHRSLGPP	QGEEDSVPRD	-LPSWMKFLH	GKLGNIIVPL
ATM	N----LPEIV	VELLMTLHEP	ANSSASQSTD	-LCDFS----	GDLDPAPNPP
ATR	D----FQGLH	NELLLRIGEH	YQQVFNGLSI	-LASFA----	SSDDPYQGPR
PI3Kalpha	-----	-----	-----	-----	-----
PI3Kgamma	-----	-----	-----	-----	-----
mTOR	NI-----	----GMIDQS	RDASAVSLSE	SKSSQDSSD-	---YSTSEM-
DNA-PK	NIRLFLAKLV	INTEEVFRPY	AKHWLSPLLQ	LAASENNGGE	GIHYMVVEIV
ATM	HF---PSHVI	KATFAYISNC	HKTCLKSILE	ILSKSPDS--	---YQKILL-
ATR	DI---ISP--	----ELMADY	LQPKLLGILA	-----	---FFNMQL-
PI3Kalpha	-----	-----	-----	-----	-----
PI3Kgamma	-----	-----	-----	-----	-----
mTOR	-----LV	NMGNLPLDEF	YPAVSMVALM	-RIFRDQ-SL	SHHHTMVVQA
DNA-PK	ATILSWTGLA	TPTGVPKDEV	LANRLLNFLM	KHVFHPKRAV	FRHNLEIIKT
ATM	-----AI	CEQAAETNNV	YKKHRILKIY	-HLFVSL-LL	KDIKSGLGGA
ATR	-----LS	SSVGIE-DKK	MALNSLMSLM	-KLMGPK-HV	SSVRVKMMTT
PI3Kalpha	-----	-----	-----	-----	-----
PI3Kgamma	-----	-----	-----	-----	-----
mTOR	ITFIFK----	-----	-----SLGLK	----CVQFLP	QVMPTFL---
DNA-PK	LVECWKDCLS	IPYRLIFEKF	SG--KDPNSK	DNSVGIQLLG	IVMANDLPPY
ATM	WAFVLRDVIY	TLIH-YINQR	PSCIMDVSLR	SFSLCCDLLS	QVCQTAVT-Y
ATR	LRTGLR----	-----FKDDF	P----ELCCR	AWDCFVRCLD	HACLGSL---
PI3Kalpha	-----	-----	-----	-----	-----
PI3Kgamma	-----	-----	-----	-----	-----
mTOR	-----N	VIRVCDGAIR	EFLFQQL---	-GMLVSFVKS	HIRPYMDEIV
DNA-PK	DPQCGIQSSE	YFQALVNNMS	FVRYKEYVYAA	AAEVLGLILR	YVMERKNILE
ATM	---CKDALEN	HLHVIVGTLI	PLVYEQV-EV	QKQVLDLLKY	LVIDNKDN-E
ATR	-----	LSHVIV-ALL	PLIHIQP---	-KETAAIFHY	LIIENRDAVQ
PI3Kalpha	-----	-----	-----	-----	-----
PI3Kgamma	-----	-----	-----	-----	-----

mTOR	TLMREF--WV	M---NTSIQS	TIIL-LIEQI	VVA-----	-LGGEFKLYL
DNA-PK	ESLCELVAKQ	LKQHQNTMED	KFIV-CLNKV	TKSFPPLADR	FMNAVFFLL-
ATM	NLYITI--KL	LDPFPDHVVF	KDLR-ITQOK	IKY-----	-SRGPFSL-
ATR	DFLHEI--YF	L---PDHPEL	KKIKAVLQEY	RKE-----	-TSESTDLQ-
PI3Kalpha	-----	-----	-----	-----	-----
PI3Kgamma	-----	-----	-----	-----	-----
mTOR	PQLIPHMLRV	FMHDNSP-GR	IVSIKLLA--	-----AIQ	LFGANLDDY-
DNA-PK	-PKFHGVLKT	LCLEVVL-CR	VEGMELEYFQ	LK-SKD-FVQ	VMRHRDDERQ
ATM	-EEINHFLSV	SVYDALPLTR	LEGLKDLRRQ	LELHKDQMVD	IMRASQDNPQ
ATR	-TTLQLSMKA	IQHENVD-VR	IHALTSLKET	L--YKN-QEK	LIKYATDS--
PI3Kalpha	-----	-----	-----	-----	-----
PI3Kgamma	-----	-----	-----	-----	-----
mTOR	---LHLLLPP	IVKLFDAPEA	PL--PSRKAA	LETVDRLTES	L-----
DNA-PK	KVCLDIIYKM	MPKLPVELR	ELLNPVVEFV	SHPSTTCREQ	MYNILMWIHD
ATM	D---GIMVKL	VVNLQLSKM	AINHTGEKEV	LEAVGSCLGE	VGPI-----
ATR	----ETVEPI	ISQLVTVLLK	GC-QDANSQA	RLLCGECLGE	LGAIIDPG-RL
PI3Kalpha	-----	-----	-----	-----	-----
PI3Kgamma	-----	-----	-----	-----	-----
mTOR	DFTDYASR--	----IIHPIV	RT-----LD	QSPELR----	-----STA
DNA-PK	NYRDPESSETD	NDSQEIFKLA	KDVLIQGLID	ENPGLQLIIR	NFWSHETRLP
ATM	DFSTIAIQHS	KDA-SYTKAL	K-----LF	EDKELQ----	--W---TFIM
ATR	DFSTTETQ-G	KDF-TFVTGV	ED-----SS	FAYGLLMEL-	-----TRAY
PI3Kalpha	-----	-----	-----	-----	-----
PI3Kgamma	-----	-----	-----	-----	-----
mTOR	MDTLSSLVFQ	LGK---KYQI	-FIPMVNKVL	VR-----	-----HR--
DNA-PK	SNTLDRLLAL	NSLYSPKIEV	HFLSLATNFL	LEMTSMSPDY	PNPMFEHPLS
ATM	LTYLNNTLVE	DCV---KVRS	AAVTCLKNIL	ATKTG-----	-----HSF-
ATR	LAYADNSRAQ	DSA---AYAI	QELLSIYDCR	EMETN-GPG-	-----HQL-
PI3Kalpha	-----	-----	-----	-----	-----
PI3Kgamma	-----	-----	-----	-----	-----
mTOR	-----	-----INHQR	YDVLICRIVK	GYTLADEEED	PLIYQHRMLR
DNA-PK	ECEFQEYTTID	SDWR-FRSTV	LTPMFVETQA	SQGTLQTRTQ	EGSLSARWPV
ATM	-----	--WE-IYKMT	TDPMLAYLQP	FRTSRKKFLE	VPRFDKENPF
ATR	-----	--WRRFPEHV	REILEPHLNT	RYKSSQKSTD	WSGVKKPIYL
PI3Kalpha	-----	-----	-----	-----	-----
PI3Kgamma	-----	-----	-----	-----	-----
mTOR	SGQ-----	-----	GDALA-----	-----	-----
DNA-PK	AGQIRATQQQ	HDFTLTQTAD	GRSSFDWLTG	SSTDPLVDHT	SPSSDSLFA
ATM	EGL-----	-----	DDINL-WI--	----PL----	-----
ATR	SKL-----	-----	GSNFAEW---	-----	-----
PI3Kalpha	-----	-----	-----	-----	-----
PI3Kgamma	-----	-----	-----	-----	-----
mTOR	-----	-----S	GPVETGPMKK	LHVSTINLQK	---AWGAARR
DNA-PK	HKRSERLQRA	PLKSVGPDFG	KKRGLPGDE	VDNKVKAAG	RTDLLRLRRR
ATM	---SE-----	-----NHDIW	IKTLTCAFLD	SGGTKCEILQ	---LLKPMCE
ATR	-----	-----SASWA	GYLITKVRHD	LASKIFTCCS	I--MMKHDFK
PI3Kalpha	-----	-----	-----MPPRP	SSGELWGIH-	---LMPP--R
PI3Kgamma	-----	-----	-----	-----	-----

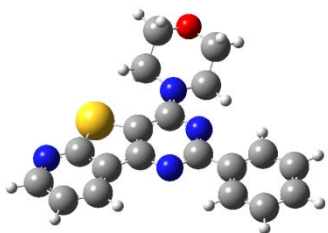
mTOR	VSKDDWLEWL	RRLSLELLKD	SSSPSLRSCW	A-----	-----
DNA-PK	FMRDQEKLSL	MYARKGVAEQ	KREKEIKSEL	KMKQDAQVVL	YRSYRHGDLP
ATM	VKTDFCQTVL	PYLIHDILLQ	DTNESWRNLL	STH--VQGFF	TSCLRH----
ATR	VTIYLLPHIL	VYVLLGCNQE	DQQEVYAEIM	AV-----	---LKHDD--
PI3Kalpha	ILVECLLPNG	MIVTLECLRE	ATLVTIKHEL	F-----	-----
PI3Kgamma	-----	-----	-----	-----	-----
mTOR	-LAQAYNPMA	RDLFNAAFV-	-----SCWSE	LNEDQQDEL-	-IRSIE----
DNA-PK	DIQIKHSSLI	TPLQAVAQRD	PIIAKQLFSS	LFSGILKEMD	KFKTLSEKNN
ATM	FSQTSRSTTP	ANLDSESEH-	-----FFRCC	LDKKSQRTM-	-LAVVDYMRR
ATR	QHTINTQDIA	SDLCQLSTQ-	-----TVFSM	LDHLTQWARH	KFQALKAEK-
PI3Kalpha	-KEARKYPLH	QLLQDESS--	-----YIFVS	VTQEAEREE-	-----
PI3Kgamma	-----	-----	-----	-----	-----
mTOR	-----	-----L	ALTSQDIAEV	TQTLLN--LA	EFMEHSDKGP
DNA-PK	ITQKLLQDFN	RFLNNTTFSFF	PPFVSCIQDI	SCQHAA--LL	SLDPAAVSAG
ATM	--QKRPSSTG	IF-NDAF-WL	DLNYLEVAKV	AQSCAAHFTA	LLYAEIYADK
ATR	-----	-----C	PHSKSNRNKV	DSMVST--VD	YEDYQSVTRF
PI3Kalpha	-----	-----F	FDETRRLCDL	RLFQPF--LK	VIEPVGNREE
PI3Kgamma	-----	-----	-----	-----	-----ASEET
mTOR	LPLRDDNGIV	LLGERAAKCR	AYAKALHYKE	LEFQKGPTPA	IL--ESLISI
DNA-PK	CLASLQQPVG	IRLLEEALLR	LLPAELPAKR	VRGKARLPPD	VLRWVELAKL
ATM	KSMDDQEKRS	LAFEEGSQST	TIS-SLSEKS	KEETGISLQD	L-----LLEI
ATR	LDLIPQDTLA	VASFRSKAYT	RAVMHFESFI	TEKKQNIQEH	L---GFLQKL
PI3Kalpha	KILNREIGFA	IGMPVCEFDM	VKDPEVQDFR	RNILNVCKEA	V----DLRDL
PI3Kgamma	LAFQRQLNAL	IGYDVTDVSN	VHDDELEFTR	RRLVTPRMAE	V-----
mTOR	NNKLQQPEAA	AGVLEYAMKH	FGELEIQATW	YEKLHEWEDA	LVAYD-----
DNA-PK	YRSIGEYDVL	RGIFTSEIGT	K-QITQSALL	AEARSDYSEA	AKQYDEALNK
ATM	YRSIGEPDSL	YGCGGKMLQ	P-ITRLRT--	YEHEAMWGKA	LVTYD-----
ATR	YAAMHEPDGV	AGVSAIRKAE	P-SLKEQILE	HESLGLLRDA	TACYD-----
PI3Kalpha	--NSPHSRAM	YVYPPHVESS	P-ELPKHI--	YNKLDRGQII	VVIWVIV---
PI3Kgamma	---AGRDPKL	YAMHPWVTSK	P--LPEYL--	LKKITNNCVF	IVIHR-----
mTOR	-----KKMD	TNKDD----P	ELMLGRMRCL	EALGEWGQLH	QQCCEKWTLV
DNA-PK	QDWVDGEPTE	AEKDFWELAS	LDCYNHLAEW	KSLEYCSTAS	IDS-ENPPDL
ATM	-----LE	TAIPS----S	TRQAGIIQAL	QNLGLCHILS	VYL-KGLDYE
ATR	-----RAIQ	LEPDQ----I	IHYHGVVKSM	LGLGQLSTVI	TQV-NGVHAN
PI3Kalpha	-----SPNN	DKQKY----T	LKINHDCVPE	QVIAEAIRKK	TRS-MLLSSE
PI3Kgamma	-----	STTSQ----T	IKVSADDTPG	TILQSFFTKM	AKK-KSLMDI
mTOR	NDETQAKMAR	-----MAAAA	AWGLGQWDSM	EEYTTCMI-PR	DTHDGAFYRA
DNA-PK	NKIWSEPFYQ	ETYLPMIRS	KLKLLLQGEA	DQSLLTTF-ID	KAMHGELQKA
ATM	NKDWCPELEE	-----LHYQA	AWRNMQWDHC	TSVSKEV-EG	TSYHESLYNA
ATR	RSEWTDELNT	-----YRVEA	AWKLSQWDLV	ENYLAADGKS	TTWSVRLGQL
PI3Kalpha	QLKLCVLEYQ	GKYI-LKVCG	CDEYFLEKYP	LSQYKYI-RS	CIMLGRMPNL
PI3Kgamma	PESQNERDFV	-----LRVCG	RDEYLVGETP	IKNFQWV-RQ	CLKNGEEIHL
mTOR	VLALH-QDLF	SLAQ---QCI	D--KARDLLD	----AELTAM	AGESYSRAYG
DNA-PK	ILELHYSQEL	SLLYLLQDDV	D--RAKYIIQ	NGIQSFMQNY	SSIDVLLHQ5
ATM	LQSLR-DREF	STFY---ESL	K--YARVKEV	----EEMCKR	SLESVYSLYP
ATR	LLSAK-KRDI	TAFY---DSL	KLVRAEQIVP	----LSAASF	ERGSYQRGYE
PI3Kalpha	KM-----MAK	ESLY---SQL	P--MDCFTMP	----SYSRRI	STATPYMNGE
PI3Kgamma	VL-----DTPP	DPAL---DEV	R--KEEWPLV	DDC-TGVTGY	HEQLTIHGKD

mTOR	AMVS---CHM	LSELEEVIQY	KLVPERRE--	-----IIRQI	WVERLQGCQR
DNA-PK	RLTKLQSVQA	LTEIQEFISF	ISKQGNLSSQ	VPLKRLLNLT-	WTNRYPDAKM
ATM	TLSR---LQA	IGELESIGEL	FSRSVTHRQL	S--EVYIK--	WQKHSQLLKD
ATR	YIVR---LHM	LCELEHSIKP	LFQHSPGDSS	Q--EDSLN--	WVARLEMTQN
PI3Kalpha	TSTK-----S	LWVINRALRI	KILCATYV--	-----NLN--	IRDIDKIYVR
PI3Kgamma	HESVF--TVS	LWDCDRKFRV	KIRGIDIP--	-----VLP--	RTADLTVFVE
mTOR	I-VEDWQKIL	MVRSLVVS--	-----PHEDM	RTWL-----	-----KYA-S
DNA-PK	DPMNIWDDII	TNRCFFLSKI	EEKLTPLPED	NSMNVDDQGD	PSDRMEVQ-E
ATM	SDFSQEPIM	ALRTVILE--	-----ILMEK	EMDN-----	-----SQR-E
ATR	S-YRAKEPIL	ALRRALLS--	-----LNKR	PDYN-----	-----EMVGE
PI3Kalpha	TGIYHGGEPL	CDNVNTQR--	-----VPCSN	PRWN-----	-----EWL-N
PI3Kgamma	ANIQYGGQVL	CQRRTSPK--	-----PFTEE	VLWN-----	-----VWL-E
mTOR	L--CGKSGRL	ALAHKTLVLL	LGVDPSRQLD	HPLPTVHPQV	TYAYMKNMWK
DNA-PK	Q--EEDISSL	IRSCFKSMKM	KMIDSARKQN	N-----	FSLAMKLL-K
ATM	CIKDILTKHL	VELSILARTF	KNTQLPER--	-----	---AIFQI-K
ATR	C--WLQSARV	ARKAGHHQTA	YN-----	-----	---ALLNA-G
PI3Kalpha	Y--DIYIPDL	PRAARCLSI	CS-----	-----	---VKGR-K
PI3Kgamma	F--SIKIKDL	PKGALLNLQI	YCGKAP----	-----	---ALSGK-T
mTOR	SARKIDAFQH	MQHFBVQTMQQ	QAQHAIATED	QQH-KQELHK	LMARCFLKLG
DNA-PK	ELHKESKTRD	-DWLVSQVQS	YCRLSHCRSR	SQGCSEQVLT	VLKTVSLLDE
ATM	QYNSVSCG--	---VSEWQLE	EAQVFWAKKE	Q---SLALSI	LKQMIKKLDA
ATR	ESR-----	---LAELYVE	RAKWLWSKGD	V---HQALIV	LQKGVLCFP
PI3Kalpha	GAK-----	-----EE	HCPLAWGN--	-----INL	FDYDTLTVSG
PI3Kgamma	SAEMPSP---	-----ESKGG	AQLLYYVN--	-----LLL	IDHRFLLRHG
mTOR	EWQLNLQGIN	ESTI-PKVLQ	YYSAA---TE	HDRSWYKAHW	AWAVMNFVAV
DNA-PK	NNVSSYLSKN	ILAF-RDQNI	LLGTTYRIIA	NALSSEPACL	AEIEEDKARR
ATM	SCAANNPSLK	-LTY-TECLR	VCGNW---LA	ETCLENPAVI	MQTYLEKAVE
ATR	ENETPPEGKN	MLIH-GRAML	LVGRF---ME	ETANFESNAI	MKKYKD---V
PI3Kalpha	KMALNLWPVP	-HGL-EDLLN	PIGVT---G	SNPNKETPC-	LELEFDWFSS
PI3Kgamma	EYVLHMWQLS	GKGEDQGSFN	ADKLT---SA	TNPDKENSMS	ISILLDNYCH
mTOR	LHYKHQNQAR	DEKKK---LR	HASGANITNA	TTAATTAATA	TTTAS-----
DNA-PK	ILELSGSSSE	DSEKVIAGLY	QRAFQHLSEA	VQAAEEEAQP	PSWSCGPAAG
ATM	VAGNYDGESS	DELR-----N	GKMKAFSLA	RFSDTQYQR-	-----
ATR	TACLPEWE--	-----	-----	-----	-----
PI3Kalpha	VVKFPDMSVI	EEH-----	----ANWSVS	REAGFSYSH-	-----
PI3Kgamma	PIALPKHRPT	PDP-----	-----	-----	-----
mTOR	-TEGSNSESE	AESTEN-SPT	PSPLQKKVTE	DLSKTLMLYT	VPAVQGFRRS
DNA-PK	VIDAYMTLAD	FCDQQL--RK	EEENASVIDS	AELQA---YP	ALVVEKMLKA
ATM	-IENYMKSSSE	FENKQALLKR	AKEEVGLLRE	HKIQTN-RYT	-VKVQRELEL
ATR	--DGHFYLA	YYDKLM--PM	VTDNKMEKQG	DLIR-----	-YIVLHFGRS
PI3Kalpha	--AGLSNRLA	RDNELR-END	KEQLKAISTR	DPLS-----	-EITEQEKDF
PI3Kgamma	--EGDRVRAE	MPNQLR----	-KQLEAIIAT	DPLN-----	-PLTAEDKEL
mTOR	ISLSRGNNLQ	DTLRVLTWLF	D-YGHPW-DV	NEALVEGVKA	IQIDTW-LQV
DNA-PK	LKLNSNEARL	KFPRLLQIIE	R-YPEETLSL	MTKEISSVPC	WQFISW-ISH
ATM	DELALRALKE	DRKRFLCKAV	ENYIN---CL	LSGEEHDMWV	FRLCSLWLEN
ATR	LQYGNQFIYQ	SMPRMLTLWL	D-Y-----GT	KAYEWKAG-	-RSDRV-QMR
PI3Kalpha	LWSHRHYCVT	I-PEILPKLL	L-----SV	KWNSRDEVA-	-QMYCL----
PI3Kgamma	LWHFRYESLK	D-PKAYPKLF	S-----SV	KWGQOEIVA-	-KTYQL-LAK

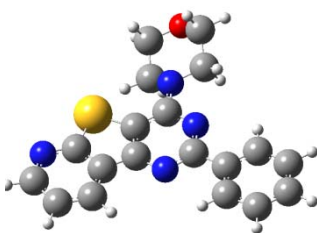
mTOR	IPQLIARIDT	PRPLVGRLIH	QLLTDIGRYH	PQALIYPLTV	ASKSTTT-AR
DNA-PK	---MVALLDK	DQAVAVQHSV	EEITD---NY	PQAIVYPFII	SSE-SYS-FK
ATM	-----SGVSE	VNGMMKRDGM	KIPTY---KF	LPLMYQLAAR	MG--TKM-MG
ATR	-----NDLGK	INKVITEHTN	YLAPY---QF	LTAFSQLISR	IC-----HS
PI3Kalpha	-----VKD	WPPIKPEQAM	ELLDC---NY	PDPMVRGFAV	RC--LEKYLT
PI3Kgamma	-----REVWD	QSALDVGLTM	QLLDC---NF	SDENVRAIAV	QK--LES-LE
mTOR	HNAANKILKN	MCEHSNTLVQ	QAMMVSEELI	RVAILWHEMW	HEGLEEASRL
DNA-PK	DTSTGHKNKE	FVARIKSKLD	QGGVIQDFIN	ALDQLSNP--	-ELLFKDWSN
ATM	GLGFHEVLNN	LISRISMDHP	HHTLF--IIL	ALANANRD--	-EFLTKP-EV
ATR	HDEVFVVLME	IIAKVFLAYP	QQAMW--MMT	AVSKSSYP--	-----
PI3Kalpha	DDKLSQYLIQ	LVQVLKYEQY	LDNLLVRFLL	KKALTNQR--	-----
PI3Kgamma	DDDVLYHYLLQ	LVQAVKFEPY	HDSALARFLL	KRGLRNKR--	-----
mTOR	YFGERNVKGM	FEVLEPLHAM	MERGPQTLKE	TSFNQAYGRD	LME-AQEWCR
DNA-PK	DVRAELAKTP	VNKKNIEKMY	ERMYAALGD-	-PKAPGLGAF	RRKFIQTFGK
ATM	ARRSRITKNV	PKQSSQLDED	RTEAANRII-	-CTIRSRRPQ	MVR---SVEA
ATR	-MRVNRCKEI	LNKAIHMKKS	LEKFV-----	-GDATRLTDK	LLE---LCNK
PI3Kalpha	-IGHFFFWHL	KSEM-HNKTV	SQRFGLLLE-	-SYCRACGMY	LKH----LNR
PI3Kgamma	-IGHFLFWFL	RSEIAQSRHY	QORFAVILE-	-AYLRGCGTA	MLH---DFTQ
mTOR	KYMKS-----	GNVKDLTQAW	--DLYYHVFR	RISKQLPQLT	SLELQ---YV
DNA-PK	EFDKHFQKGG	SKLLRMKLSL	FNDITNMLLL	KMNKDSKPPG	NLKECSPWMS
ATM	LCDAY-----	IILANLDA--	--TQWKTQRK	GINIPADQPI	TKLKN---LE
ATR	PVDGS-----	SSTLSMS---	--THFKMLKK	LVEEAT--FS	EILIP---LQ
PI3Kalpha	QVEAM-----	EKLINLT---	--DILK-QER	KDETQKVQMK	FLVEQ---MR
PI3Kgamma	QVQVI-----	DMLQKVITI--	--DIKLSLAE	KYDVSSQVIS	QLKQK---LE
mTOR	SPKLLMCRDL	ELAVPGTYDP	N-QPI-----I	RIQSIAPSLQ	VITSKQRPRK
DNA-PK	DFKVEFLRN-	ELEIPGQYDG	RGKPLPEYHV	RIAGFDERVT	VMASLRRPKR
ATM	DVVVPTMEI-	KVDHTGEYGN	L-----V	TIQSFKAEFR	LAGGVNLPKI
ATR	SVMIPTLPS-	ILGTHANHAS	H-EPFPGHWA	YIAGFDDMVE	ILASLQKPKK
PI3Kalpha	RPDFMDALQ-	GLLSPLNPAH	Q-----	LGNLRLKECR	IMSSAKRPLW
PI3Kgamma	NLQNLNLPQ-	SFRVPYDPGL	K-----	AGALVIEKCK	VMASKKKPLW
mTOR	LTLM-----G	SNG---HEFV	FLLKGHEDLR	QDERVMQLFG	LVNTLLANDP
DNA-PK	IIIR-----G	HDE---REHP	FLVKGGEDLR	QDQVEQLFQ	VMNGILAQDS
ATM	IDCV-----G	SDG---KERR	QLVKGRDDL	QDAVMQOVFQ	MCNTLLQRNT
ATR	ISLK-----G	SDG---KFYI	MMCKPKDDL	KDCRLMEFNS	LINKCLRKDA
PI3Kalpha	LNWE--NPDI	MSELLFQNNE	IIFKNGDDL	QDMLTLQIIR	IMENIWQNQG
PI3Kgamma	LEFKCADPTA	LSN---ETIG	IIFKHGDDL	QDMLLILQILR	IMESIWETES
mTOR	TSLRKNLSIQ	RYAVIPLSTN	SGLIGWVPHC	DTLHALIR-D	YREKKKILLN
DNA-PK	ACSQRALQLR	TYSVVPMTSR	LGLIEWLENT	VTLKDLLLNT	MSQEEKAAYL
ATM	ETRKRKLTIC	TYKVVPLSQR	SGVLEWCTGT	VPIGEFLV-N	NEDGAHKRYR
ATR	ESRRRELHIR	TYAVIPLNDE	CGIIEWVNNT	AGLRPIL--T	KLYKEKGVYM
PI3Kalpha	L----DLRML	PYGCLSIGDC	VGLIEVVRNS	HTIMQIQC-K	GGLKGALQFN
PI3Kgamma	L----DLCLL	PYGCISTGDK	IGMIEIVKDA	TTIAKIQ--Q	STVGNTGAFK
mTOR	IEH-RIMLRM	APD-----	-----	YDHLTLMQKV	EVFEHAVNNT
DNA-PK	SDP-RAPPCE	YKDWLTKMSG	KHDVGAYMLM	YKGANRTETV	TSFRKRESKV
ATM	PNDFAFQCC	KK-----	-----MME	VQKKSFEELY	EVFMDVCQNF
ATR	TGK-ELRQCM	LP-----	-----	-KSAALSEKL	KVFREFLLPR
PI3Kalpha	SHT-----	-----	-----	-----	-----
PI3Kgamma	DEV-----	-----	-----	-----	-----

mTOR	AGDDLAKLLW	LKSPSSEVWF	DRRTNYTRSL	AVMSMVGYIL	GLGDRHPSNL
DNA-PK	PADLLKRAFV	RMSTSPEAFL	ALRSHFASSH	ALICISHWIL	GIGDRHLNNF
ATM	Q-PVFRYFCM	EKFLDPAIWF	EKRLAYTRSV	ATSSIVGYIL	GLGDRHVQNI
ATR	HPPIFHEWFL	RTFPDPTSWY	SSRSAYCRST	AVMSMVGYIL	GLGDRHGENI
PI3Kalpha	----LHQWLK	DKN-KGEIYD	AAIDLFTRSC	AGYCVATFIL	GIGDRHNSNI
PI3Kgamma	----LSHWLK	EKCPIEEKFQ	AAVERFVYSC	AGYCVATFVL	GIGDRHNDNI
mTOR	MLDRLSGKIL	HIDFGDCFEV	AMTREKF-PE	KIPFRLTRML	TNAMEVTGLD
DNA-PK	MVAMETGGVI	GIDFGHAFGS	ATQFLPV-PE	LMPFRLTRQF	INLMLPMKET
ATM	LINEQSAELV	HIDLGVAFEQ	GKI-LPT-PE	TVPFRLTRDI	VDGMGITGVE
ATR	LFDSLGTGECV	HVDFNCLFNK	GET-FEV-PE	IVPFRLTHNM	VNGMGPMGTE
PI3Kalpha	MVKD-DGQLF	HIDFGHFLDH	KKKKFGYKRE	RVPFVLTQDF	LIVISKGAQE
PI3Kgamma	MISE-TGNLF	HIDFGHILGN	YKSFLGINKE	RVPFVLTPDF	LFVMGTSGKK
mTOR	-----GNY	RITCHTVMEV	LREHKDSVMA	VLEAFVYDPL	LNWRLMDTNT
DNA-PK	-----GLM	YSIMVHALRA	FRSDPGLLTN	TMDVFVKEPS	FDWKNFEQKM
ATM	-----GVF	RRCCEKTMEV	MRNSQETLLT	IVEVLLYDPL	FDWTMNPLKA
ATR	-----GLF	RRACEVTMRL	MRDQREPLMS	VLKTFLHDPL	VEWSKPVKGH
PI3Kalpha	CTKTREFERF	QEMCYKAYLA	IRQHANLFIN	LFSMMLGSGM	PELQSFDDIA
PI3Kgamma	--TSLHFQKF	QDVCVKAYLA	LRHHTNLLII	LFSMMLMTGM	PQLTSKEDIE
mTOR	KGNKRSRTRT	DSYSAGQSVE	ILDGVELGEP	AHKKTGTTVP	ESIHSFIGDG
DNA-PK	L-KKGGSWIQ	EINVAEKNWY	PRQKICYAKR	KLAPANPAVI	TCDELLLGH-
ATM	L-----	-----	YLQQRPEDET	ELHPTLNADD	QECKRNLS-
ATR	S-----	-----	KAPLNETGEV	V-----N	EKAKTHVLD-
PI3Kalpha	Y-----	-----	IRKTLALDKT	E-----Q	EALEYFMKQ-
PI3Kgamma	Y-----	-----	IRDALTVGKS	E-----E	DAKKYFLDQ-
mTOR	LVKPEALNKK	AIQIINRVR-	DKLTGRDFSH	DDTLDVPTQV	ELLIKQATSH
DNA-PK	--EKAPAFRD	YVAVARGSKD	HNIRAQEPE-	-SGLSEETQV	KCLMDQATDP
ATM	--IDQSFDKV	AERVLMLRQ-	EKLKGVEEG-	-TVLSVGGQV	NLLIQQAIDP
ATR	--IEQ-RLQG	VIKTRNRVT-	GLPLSIE---	-----GHV	HYLIQEATDE
PI3Kalpha	--MNDAAHGG	WTTKMDWIF-	HTIKQHALN-	-----	-----
PI3Kgamma	--IEVCRDKG	WTVQFNWFL-	HLVLGI----	-----	-----
mTOR	ENLCQCYIGW	CPFW			
DNA-PK	NILGRTWEGW	EPWM			
ATM	KNLSRFLPGW	KAWV			
ATR	NLLCQMYLGW	TPYM			
PI3Kalpha	-----	----			
PI3Kgamma	-----	----			

Appendix 2. Optimized geometries of 4.2_4, 4.2_5, and 4.2_7



4.2_4_R (top)



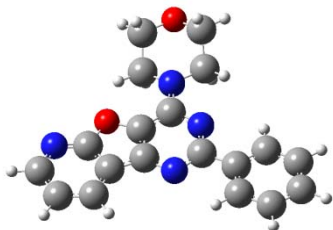
4.2_4_P (top)



4.2_4_R (side)



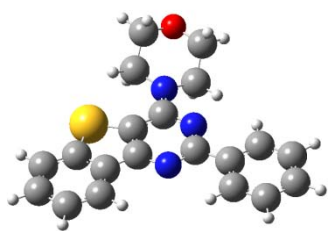
4.2_4_P (side)



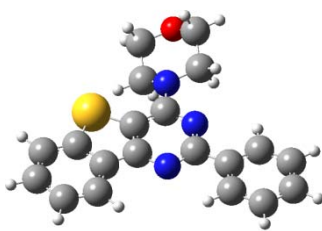
4.2_5 (side)



4.2_5 (side)



4.2_7_R (top)



4.2_7_P (top)

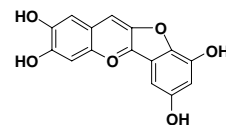
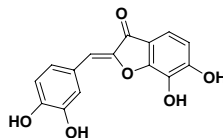
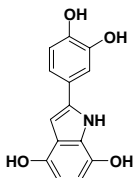
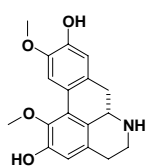
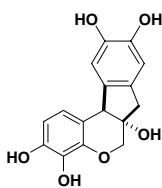


4.2_7_R (side)

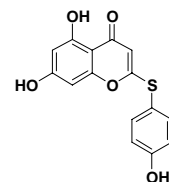
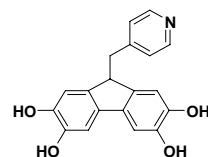
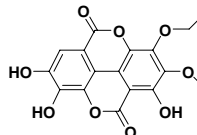
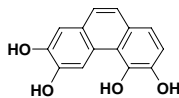
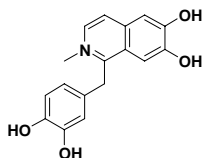
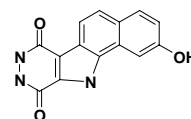
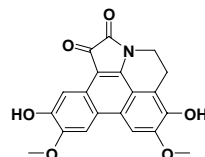
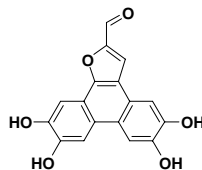
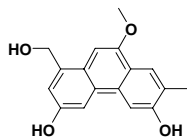
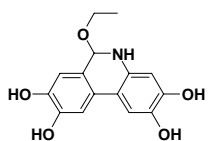
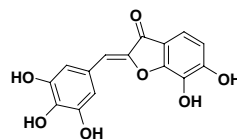
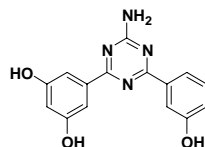
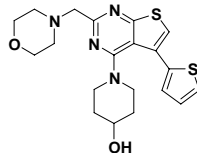
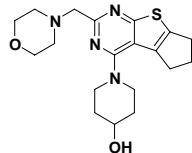
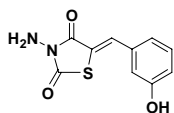
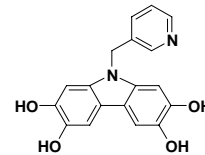
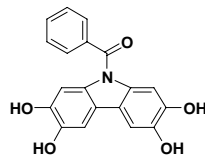
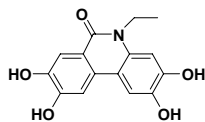
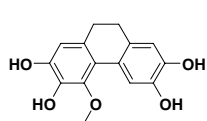
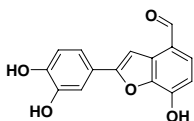


4.2_7_P (side)

Appendix 3. Hits from the pharmacophore search of the 'PubChem' compound library



ZINC00155806 (Hit_1)



Appendix 4. NMR peaks

